Formation of Calcium Naphthenate in Water/Oil Systems, Naphthenic Acid Chemistry and Emulsion Stability

by

Trond Erik Havre

Thesis Submitted in Partial Fulfilment of the Requirements for the Degree of

DOKTOR INGENIØR

Department of Chemical Engineering
Norwegian University of Science and Technology
Trondheim, October 2002

Preface

This thesis is submitted in partial fulfilment of the requirements for the degree of dr.ing. at the Norwegian University of Science and Technology. It consists of six papers that are based on work performed at Statoil R&D Centre from January 2000 to October 2002. In addition, some of the experiments were performed at the University of Bergen in February 2001.

I finished my sivilingeniør degree, at the Department of Chemical Engineering, NTNU, in December 1999. In January 2000, I joined the research programme FLUCHA II (Fluid Characterisation at Elevated Temperatures and Pressures). The programme is supervised by Professor Johan Sjöblom, and is a joint event between Statoil R&D Centre and Ugelstad Laboratory, Department of Chemical Engineering at NTNU in Trondheim. FLUCHA II is financed by The Research Council of Norway, Statoil, Norsk Hydro, TotalFinaElf and ABB. The sponsors have acted as a reference group by evaluating the programme progress twice a year. The project has involved three doctoral students and one post doc.

Parts of the work contained in this thesis were presented at the 2nd International Conference of Petroleum and Gas Phase Beaviour and Fouling in Copenhagen, Denmark in August 2000 and at the 3rd International Conference on Petroleum Phase Behavior and Fouling in New Orleans, USA in March 2002.

Acknowledgements

I would like to express my gratitude to:

Abstract

In recent years the production of crude oils with high amounts of naphthenic acids has increased. Certain problems are related to this type of crudes and a better understanding of the chemistry of the naphthenic acids is therefore of interest.

Synthetic model naphthenic acids, as well as commercial mixtures and crude oil naphthenic acids have been utilized to study the chemistry of naphthenic acids. Partitioning of naphthenic acids between oil and water and the dissociation equilibria in water have been studied in addition to their interfacial tension and micellisation behaviour.

A method for studying the precipitation of calcium naphthenate particles by means of near infrared spectroscopy was presented. It was shown that the method gives information about the induction period and about the rate of reaction for particle growth. Solubility products can also be estimated.

Near infrared spectroscopy were also utilized to study the ability of naphthenic acids and other amphiphiles to disintegrate asphaltene particles. It was shown that the structure of the naphthenic acids is important and that a commercial mixture of different surfactants had the best disintegration effect. The technique is applicable for screening the efficiency of various additives as disaggregation chemicals.

Emulsion stability was studied by means of Langmuir technique, critical electric field and bottle tests. The Langmuir study showed that the presence of Ca^{2+}-ions at elevated pH gave rise to stable naphthenate monolayers. Oil/water emulsions stabilized with different carboxylic acids were investigated at different pH-levels and water-contents. It was demonstrated that water/oil emulsions could be stabilized by a combination of multilayer (D-phase) and asphaltene particles. Critical electric field was used to determine the emulsion stability of these systems and it was shown that a combination of 60% asphaltene particles and 40% D-phase gave the stablest w/o-emulsions. This investigation verifies the importance of D-phase stabilization in combination with asphaltene particles in systems with acidic heavy crude oil (including bitumen) and water.

List of Papers

I. Havre, T. E., Ese, M.-H., Sjöblom, J. and Blokhus, A. M., *Langmuir Films of Naphthenic Acids at Different pH and Electrolyte Concentrations*, Colloid Polym Sci, **280**(7) (2002) 647-652.

II. Auflem, I. H., Havre, T. E. and Sjöblom, J. *Near-IR Study on the Dispersive Effects of Amphiphiles and Naphthenic Acids on Asphaltenes in Model Heptane-Toluene Mixtures*, Colloid Polym Sci, **280**(8) (2002) 695-700.

III. Havre, T. E. and Sjöblom, J., *Emulsion stabilization by means of Combined Surfactant Multilayer (D-phase) and Asphaltene Particles*, Colloids Surf A, Accepted, 2002.

IV. Havre, T. E., Sjöblom, J. and Vindstad, J. E., *Oil/Water- Partitioning and Interfacial Behaviour of Naphthenic Acids*, J Dispersion Sci Technol, Submitted, 2002.

V. Havre, T. E., *Near Infrared Spectroscopy as a Method for Studying Formation of Calcium Naphthenate*, Colloid Polym Sci, Submitted, 2002.

VI. Sjöblom, J., Aske, N., Auflem, I. H., Brandal, Ø., Havre, T. E., Sæther, Ø., Westvik, A., Johnsen E. E. and Kallevik, H., *Our Current Understanding of Water-in-Crude Oil Emulsions, Recent Characterization*, Techniques and High Pressure Performance, Adv Colloid Interface Sci, Special Issue: A Collection of Invited Papers in Honour of Professor J.Th.G. Overbeek on the Occasion of his 90th Birthday, in press, 2002.

Additional publications

VII.   Sjöblom, J., Johnsen, E. E., Westvik, A., Bergflødt, L., Auflem, I. H., Havre, T. E. and Kallevik, H.: *"Colloid Chemistry in Sub Sea Petroleum and Gas Processing."* Presented at: "The 2nd International Conference on Petroleum and Gas Phase Behaviour and Fouling", Copenhagen, Denmark, August 27-31, 2000.

VIII.   Sjöblom, J., Kallevik, H., Aske, N., Auflem, I. H., Havre, T. E., Sæther, Ø. and Orr, R.: *"Recent Development in the Understanding of the Stability and Destabilization of Water-in-Crude Oil Emulsions."* Presented at: "The 3rd International Conference on Petroleum Phase Behavior and Fouling", New Orleans, USA, March 10-14, 2002.

Contents

Paper I-VI are enclosed and separated by grey sheets.

1   Introduction

In recent years there has been an increase in the production of acidic crude oils with high amounts of naphthenic acids [1, 2]. Certain problems are related to this type of crudes and a better understanding of the chemistry of the naphthenic acids is therefore of great interest.

The corrosive properties of naphthenic acids have been known for a long time. The mechanism of this process takes place in an oil environment and is not clarified in detail [3-6]. Because the naphthenic acids and their soaps are surface/interfacially active they will accumulate at w/o interfaces and stabilize colloidal structures [7-9]. The worst scenario from an operational point of view is the stabilization of water-in-oil emulsions, which can cause problems in the separation process [10]. The naphthenic acids can affect the emulsion stability directly or through interactions with other crude oil components. Due to the hydrophilic acid group, the lower molecular weight naphthenic acids have a high water solubility compared to other crude oil components. The presence of naphthenic acids in the wastewater can cause significant environmental problems [11].

Under certain conditions, the naphthenic acids will form metallic soaps with metal ions in the produced water. These metallic soaps, mainly calcium naphthenates, are neither soluble in water nor oil, and due to their density they will accumulate at the oil-water interface in separators. They may also precipitate in other parts of the process. The formation of naphthenate deposit will cause operational problems with shutdown periods, during which thorough cleaning must take place.

With this background, it is evident that a better understanding of the chemistry of naphthenic acids is needed. Although the corresponding paraffinic fatty acids are very well characterized with regard to association and micellization in water, phase equilibrium, formation of lyotropic liquid crystals and microemulsions, monomolecular film properties, etc. [12-24], little information is available for naphthenic acids.

This thesis focuses on the basic chemistry of naphthenic acids, their impact on emulsion stability and naphthenate formation.

2   Naphthenic Acid Chemistry

2.1   Origin and Structure

Naphthenic acids are classified as carboxylic monoacids of the general formula RCOOH, where R represents any cycloaliphatic structure. Generally, the term "naphthenic acid" is used to account for all carboxylic acids present in crude oil, including acyclic and aromatic acids. Nearly all crude oils contain some naphthenic acids. Heavy crudes from geologically young formations have the highest acid content while paraffinic crudes usually have low acid content [25]. Naphthenic acids are known to be produced during the in-reservoir biodegradation of petroleum hydrocarbons [26], and they are considered to be a class of biological markers, closely linked to the maturity and the biodegradation level of the oil fields [2].

The naphthenic acids are complicated mixtures. Many different methods and analytical techniques have been used for analyzing these acids [9, 27-32]. An overview shows them to be C_{10}-C_{50} compounds with 0-6 fused saturated rings and with the carboxylic acid group apparently attached to a ring with a short side chain [33]. The distribution of carbon number and ring content varies with crude oil source and distillate fraction. Naphthenic acids with similar total acid number (TAN) and average molecular weight can have significantly different profiles [34]. Examples of structures of naphthenic acids that may be found in crude oils are given in Figure 2.1.
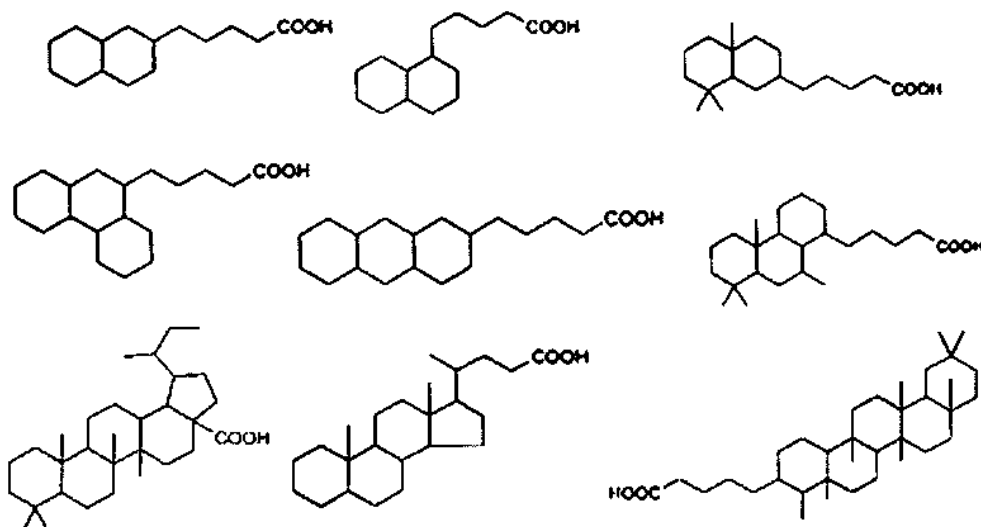

Figure 2.1   Examples of structures of naphthenic acids that may be found in crude oils.

Roussis and Lawlor [35] have published the distribution of naphthenic acids in a crude oil from the Norwegian continental shelf. This is reproduced in Figure 2.2. z=0 correponds to fully saturated (aliphatic) acid, z=-2 to one-ring naphthenic acids, z=-4 to two-ring naphthenic acids etc.
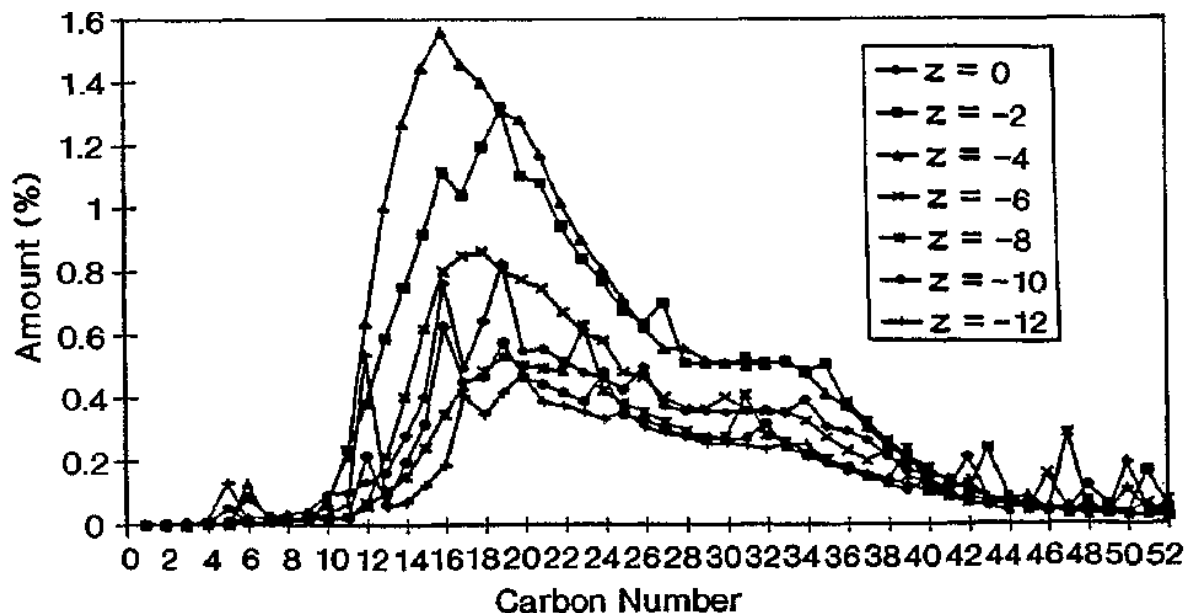

Figure 2.2 Molar amount of naphthenic acids with different number of carbons for a crude oil from the Norwegian continental shelf. z=0 indicates no ring, z=-2 one ring, z=-4 two rings etc. [35].

2.2 Equilibria in water/oil/naphthenic acid systems

In a system that consists of naphthenic acids in combination with a water phase and an oil phase, several equilibria will be involved. The two terms believed to be most important at low pH is the partitioning of undissociated acid between the phases and the dissociation of carboxylic acid in the water phase. At higher pH formation of micelles in the water phase and reversed micelles in the oil phase is believed to be of importance. Other equilibria involved in the system are dimerisation in both water and oil and formation of different metal soaps. As a consequence of the amphiphilic nature of the carboxylic acid, they will prefer the oil-water interface. Hence, equilibria of adsorption and desorption at the interface are established.

The monomeric form of the naphthenic acids will be distributed between the hydrocarbon and the water phase according to Equation 1, where HA_o and HA_w represent undissociated naphthenic acid in the oil and water phase, respectively.

$$HA_o \leftrightharpoons HA_w \qquad\qquad (2.1)$$

This equilibrium can be described in terms of a partition coefficient, given by Equation 2.2.

$$K_{wo} = \frac{[HA]_w}{[HA]_o} \qquad\qquad (2.2)$$

The acid will dissociate in the water phase according to Equation 2.3, with equilibrium constant given in Equation 2.4.

$$HA_w \leftrightharpoons A_w^- + H^+ \qquad\qquad (2.3)$$

$$K_a = \frac{[A^-]_w \cdot [H^+]}{[HA]_w} \qquad\qquad (2.4)$$

Dimerization of carboxylic acids has been the subject for several studies. Goodman [36] found that fatty acids of chain length 14C and below had monomer-dimer equilibrium in the oil phase (*n*-heptane) and no association in the aqueous phase. The relative amount of dimers in aqueous solution tends to increase with an increase in alkyl chain length according to Suzuki [37]. Takeda *et al.* [38] found that the dimerization in the hydrocarbon phase increased with increasing concentration. Somasundaran *et al.* [39] determined the dimerization constant of oleate in aqueous solution of 6E-3 (mol dm^{-3})$^{-1}$ at pH=11.4. Mukerjee [40] studied association of long chain fatty acid anions in water. It was found that the association involves only two anions. The formation of trimers and higher is negligible. The dimerisation increases progressively with increasing chain length up to palmitate (C16). However, stearate, oleate and linoleate have dimerisation constants at the same order as palmitate. Mukerjee also concluded that dimerisation of undissociated acid is less significant than dimerisation of dissociated acid.

Other equilibra will also exist and influence the system. Formation of metal soaps can be of importance if divalent metal ions are present in the aqueous phase. In addition,

formation of micelles and reverse micelles can occur at higher pH. The micellisation can be treated as a pseudophase phenomenon, i.e.

$$nM \leftrightarrows M_n \qquad (2.5)$$

where M is a monomeric fatty acid or carboxylate molecule. The corresponding equilibrium constant is given by:

$$K_{mic} = \frac{[M_n]}{[M]^n} \qquad (2.6)$$

The micellisation must be accounted for when the total concentration exceeds the critical micelle concentration. Figure 2.3 shows how the complexity of the system increases when going from a system involving only monomer equilibria, at low pH, to a system, at higher pH, with micellisation involved.
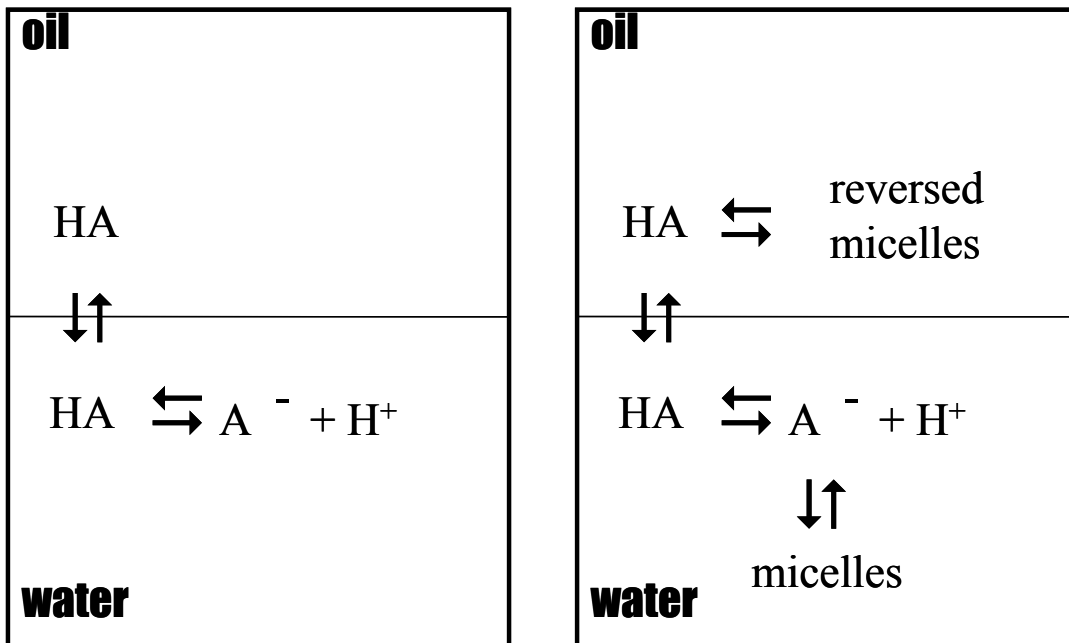
Figure 2.3 Equilibria in water/oil/naphthenic acid systems. Left) Low pH. Right) high pH with formation of micelles and reversed micelles.

According to Leo *et al.* [41] association becomes significant even at low concentration with long chain fatty acids. Even though one works with concentration below the critical micelle concentration (CMC), association in the water phase cannot be completely eliminated. Formation of micelles is described in detail in Chapter 2.4 (page 7).

2.3 Interfacial Activity of Naphthenic Acids

In addition to the equilibria discussed earlier, equilibria involving adsorption and desorption of amphiphiles at the oil/water interface will be established. The presence of amphiphilic carboxylic acids in a water/hydrocarbon system will lower the interfacial tension. The dissociated and associated form of the acid molecules will have different interfacial properties. Several studies have been performed in assessing the pH dependence on interfacial tension in oil/water/carboxylic acid-systems [42-50]. The interfacial activity for surfactants in crude oil has also been studied by several authors [8, 10, 51, 52]. Generally, a marked decrease in interfacial tension as the pH of the water phase increases has been observed. The interfacial tension will continue to decrease after complete ionization. Danielli [44] have explained this by use of the Donnan equilibrium.

Rudin and Wasan [47, 48] studied the mechanism for lowering of interfacial tension in alkali and acidic oil systems. They related the lowering of interfacial tension to dissociation of acid molecules, and they also considered the presence of unionized acids at the interface. They argue that the interfacial tension vs. pH goes through an ultra low minimum due to simultaneous adsorption of ionized and unionized acids. They also consider how formation of micelles influenced the amount of surfactants at the interface.

The fact that interfacial tension decreases at high pH for acidic crude oils is used in enhanced oil recovery. Alkaline solutions can be injected into the reservoir in order to lower capillary forces and thereby facilitate oil recovery [48].

The bulk concentration of surface-active species is in equilibrium with the concentration at the oil/water interface according to Equation 8 and 9.

$$A_w^- \leftrightarrows A_{int}^- \tag{2.7}$$

$$HA_o \leftrightarrows HA_{int} \leftrightarrows HA_w \tag{2.8}$$

where A_{int}^- and HA_{int} are the concentration of ionised and unionised naphthenic acid at the interface.

The pH at the interface, pH_{int}, can be related to the bulk phase pH_{bulk}, by assuming a Boltzmann distribution of the counterions in the electrical double-layer, i.e.

$$\text{pH}_{int} = \text{pH}_{bulk} + \frac{e\psi}{2.3kT} \qquad\qquad (2.9)$$

were e is the electronic charge, ψ is the surface potential, k is the Boltzmann constant, and T is the temperature [45]. Hence, for a given bulk pH the interfacial pH will be lower and the fraction of dissociated acid at the interface will therefore be lower than the fraction of dissociated acid in the bulk phases.

The concentration of the surfactants at the interface is related to the bulk concentration if the effect of the counterions in the electrical double layer is accounted for. Hence, the total amount of the different acid forms in the bulk phases will govern the amount of each form at the oil/water interface. The interfacial concentration is related to the interfacial tension, since the dissociated acids are more interfacially active than the undissociated form.

2.4 Micelle formation

Naphthenic acids and naphthenates are amphiphilic molecules, were the carboxylic acid group represents the hydrophilic part and the carbon moiety represents the hydrophobic part. Molecules of this nature may form micelles in the water phase. The micelles are aggregates of molecules where the oil-soluble, hydrophobic part of the molecules are directed into the centre of the micelles, while the water-soluble, hydrophilic part is directed towards the water phase. The aggregation process is driven by an increase in entropy [53]. When a hydrocarbon chain is put in contact with water, the water molecules close to the chain will order themselves leading to reduced entropy compared to bulk water. The entropy will increase if the hydrocarbon chains are removed from contact with the water into the micelles.

A crucial parameter for surfactant association and for the formation of different kind of structures is the molecular packing parameter, MPP, defined by Equation (2.10) [17].

$$MPP = \frac{V}{a \cdot l} \qquad\qquad (2.10)$$

Here, V is the volume of the surfactant, a is the head-group area (topological) and l is the length of the almost extended hydrocarbon chain. Restrictions with regard to geometries of aggregates will occur depending on the topology of the area of the end group and volume of the hydrocarbon chain. Possible aggregate shapes expected for different values of MPP are shown in Figure 2.4 [17].
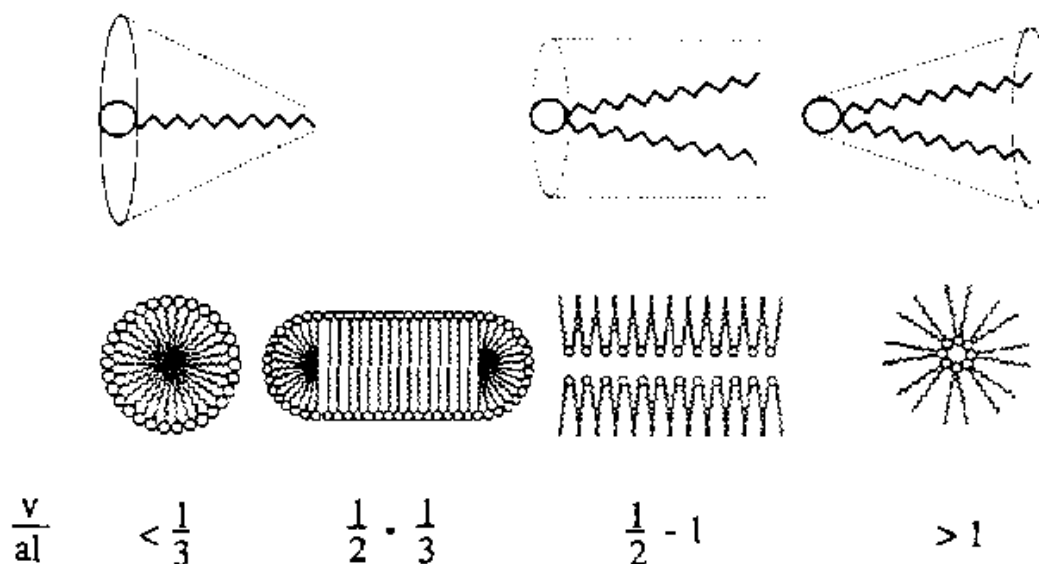

Figure 2.4 Schematic diagram of possible aggregate shapes expected for different geometries of the surfactant molecule according to MPP=v/al criteria [17].

When MPP≤1/3 spherical aggregates with a large area will form. When the value of MPP is between 1/3 and 1/2, rod-shaped aggregates are most probable, while lamellar structures are formed for $1/2 \leq MPP \leq 1$. For MPP>1 reverse structures with the hydrocarbon chain directed outwards occur.

For charged surfactants, the tendency will be to form spherical micelles, due to a strong electrostatic repulsion between the head-groups. In a system consisting of a naphthenic acid, RH and a naphthenic salt, RNa, the ratio, RH/RNa, will determine the geometry formed. Normally by varying RH/RNa (in water), at high enough pH, one will have micelles, liquid crystals and reversed structures [54].

The formation of micelles occurs when the concentration of the micelle-forming species is above a certain concentration known as the critical micelle concentration (CMC). The CMC is often determined by measuring the surface tension at different concentration of surfactant. Upon addition of surfactant to a water solution, the surface tension decreases until CMC is reached. Above this concentration, surfactants that are added will form

micelles and the concentration of monomeric surfactant will remain practically constant, resulting in a constant surface tension. CMC can also be determined by measuring other physiochemical properties that changes over the CMC; such as electric conductivity, refractive index, x-ray diffraction or viscosity [55].

The CMC-value gives a first basis in understanding the intermolecular interactions in aqueous solutions of surfactants. For paraffinic fatty acid salts with sufficiently long alkyl chains a distinct CMC is normally observed. At the same time the paraffinic alkyl chains do not have any severe packing constraint. On the other hand pharmaceutical surfactants with condensed ring structures are known to have a step-wise association in water and a weak CMC is resulting. These molecules have restrictions in their packing, and ordinary spherical micellar structures do not emerge. The difference in the molecular packing is also reflected in the aggregation numbers. For the paraffinic fatty acid salts the micelles can contain up to 100 monomers, which is considerably higher than for the monomers with large condensed ring structures. The logarithm of CMC often varies linearly with the size of the hydrophobic part of surfactants [17, 56]. In an aqueous solution of carboxylic acids, there will be mixed micelles composed of ionised and unionised acid molecules. The pH will determine the amount of the different forms. Theander and Pugh [57] showed that the CMC increases with pH over the pH range 7-12 in a solution of sodium oleate.

2.5 Phase Equilibria

As the concentration of "naphthenic acid / naphthenates" increases beyond the CMC, eventually, different types of liquid crystalline phases will result. Per today, no detailed and complete phase equilibria of a "sodium naphthenate / naphthenic acid / water / oil" system have been published. Horváth-Szabó and co-workers have published qualitative phase equilibria of sodium naphthenates in aqueous solution [54] and "sodium naphthenates / toluene / water" systems [58]. One of the most important findings of these investigations is that liquid crystals can be present over a large range of compositions in sodium naphthenate / water / toluene mixtures. The effect on the phase equilibria on adding heptane to a "sodium naphthenate / toluene / water"-systems have also been studied [59] in addition to the presence of sodium naphthenate liquid crystals at oil/water interfaces [60].

It is our opinion that the phase equilibria in the system water/sodium hexadecanoate (NaC16)/hexadecanoic acid (HC16) at 70°C is representative also for naphthenic acid

based systems. The phase diagram of this system has been published by Skurtveit *et al.* [16] and is given in Figure 2.5.
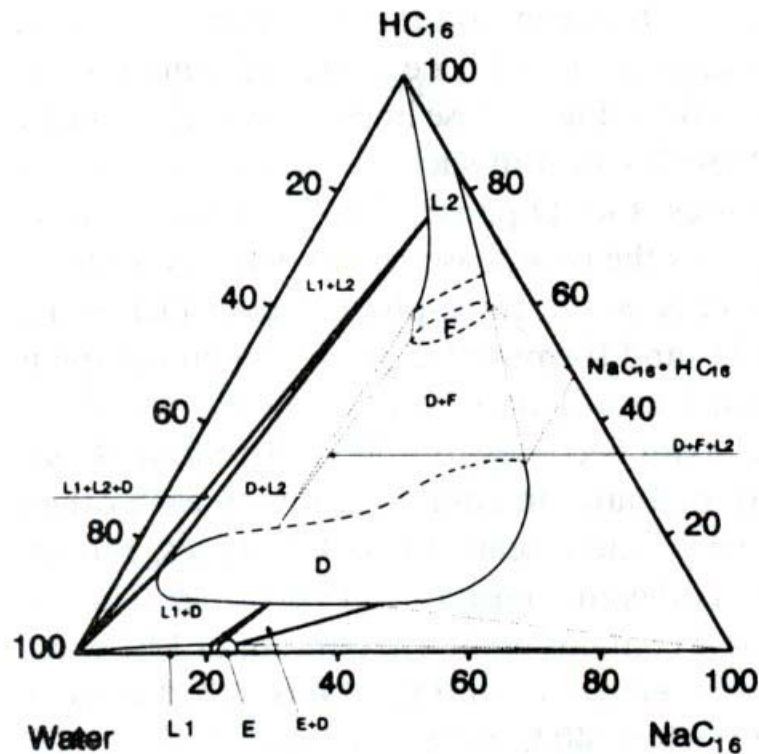

Figure 2.5 Phase equillibria in the system water/hexadecanoic acid (HC16)/sodium hexadecanoate (NaC16) at 70°C . The diagram is expressed in weight percent [16].

In this system, existence of 4 or 5 isotropic phases can be observed. These are a micellar L_1-phase (with ordinary micelles), a hexagonal liquid crystalline E-phase (with long rods in an aqueous environment), a lamellar liquid crystalline D-phase (with a bilayer structure) and a reversed solution phase L_2 (with reversed micelles). It is questionable if a F-phase with a reverse hexagonal structure exists.

The importance of phase equilibria in water/oil/stabilizer systems were first linked with emulsion stability by Professor Friberg. He documented the importance of the existence of a lamellar liquid crystal (D-phase) and a corresponding increase in emulsion stability [61-64]. The basic idea is to cover the emulsion droplets with a multiple layer of surfactant/water to enhance the rigidity of the interfacial w/o-layer. In this way a barrier against coalescence is built up.

The importance of the stabilization of water/oil emulsions, due to the D-phase has been documented for the phase diagram in Figure 2.5 [16]. It is noticeable that an upper limit

of phase equilibria including the D-phase, seems to be HC16/NaC16 ≈ 85/15, and a lower limit is HC16/NaC16 ≈ 15/85. Hence, it can be claimed that in an equivalent naphthenic acid-based system, a D-phase can exist for ratios of naphthenic acid to sodium naphthenate ~ 0.1 to 6. It is sufficient to have only 10% of a naphthenate salt to obtain the D-phase.

In order to find the best additives for emulsion breaking in the oil industry, a detailed understanding of the mechanism responsible for the formation of kinetically stable emulsions is an advantage. It is evident that the investigation of the phase behaviour, beyond its theoretical importance, can support the development of efficient separation methodologies, if the phase diagram is mapped together with the emulsion stability. Phase behaviour investigations, in certain cases, can help eliminate the need for emulsion breakers in industrial processes since a small change in the composition can lead to a dramatic change in the separation efficiency [59].

Phase diagrams usually represents equilibrium systems, while in industrial processes the components are usually in a non-equilibrium state. Studies of non-equilibria systems can be useful for industrial purposes. However, an understanding of the equilibria system is necessary as a starting point for understanding the non-equilibria phase behaviour [59].

3 Crude Oil Composition and State

3.1 Composition

Crude oil is a complex mixture of gaseous, liquid and solid hydrocarbons with small quantities of organic compounds containing sulphur, oxygen, nitrogen, and trace amounts of metallic constituents [65]. The hydrocarbons in a light distillate of petroleum can be divided into three types: alkanes (paraffins), cycloalkanes (naphthenes) and aromatics. Heteroatoms tend to concentrate in the higher molecular weight proportion of the crude oil. The crude oil composition may vary widely from one oil field to another. Due to the large number of isomers, a determination of the molecular composition of crude oil is not possible. Hence, analysis of crude oil properties and structure is done on fractions, consisting of large number of different molecule structures. Four fractions, defined by polarity and solubility, are readily used. These fractions are known as the SARA-fractions, i.e. saturates, aromatics, resins and asphaltenes.

Asphaltenes are defined by solubility characteristics, i.e. they are insoluble in *n*-heptane or *n*-pentane and are soluble in toluene [65]. They are generally composed of polyaromatic nuclei carrying aliphatic chains and rings and a number of heteroatoms, including sulphur, oxygen, nitrogen and metals such as vanadium, nickel and iron. These heteroelements account for a variety of polar groups, such as aldehyde, carbonyl, carboxylic acid, amine and amide [66-68]. The average molecular weight of asphaltene molecules is difficult to measure due to their tendency to self-aggregate. However, molecular weights in the range 500-2000 g mole^{-1} are believed to be reasonable [69]. Figure 3.1 shows the structure of a hypothetical asphaltene monomer molecule [70]. The sizes of asphaltene monomers have been reported to be in the range 12-24 Å [65, 71].
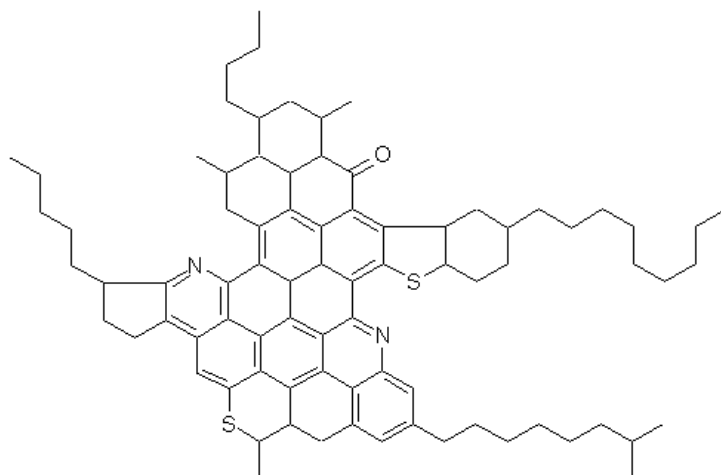
Figure 3.1 Hypothetical asphaltene molecule [70].

Saturates account for the alkanes (paraffins) and cycloalkanes (naphthenes) in the crude oil and are generally the lightest fraction of crude oil. Wax is a sub-class of the saturates, consisting primarily of straight-chain alkanes, mainly ranging from C_{20} to C_{30}. Wax precipitates as a particulate solid at low temperatures, and is known to affect emulsion stability properties of crude oil systems [69].

The aromatic fraction contains molecules with aromatic or condensed aromatic rings. Representatives of which are benzene, naphthalene, phenanthrene as well as higher condensed ring systems and their derivates. Polar, higher molecular weight aromatics may fall in the resin or asphaltene fraction [65].

Resins are readily defined as soluble in *n*-heptane or *n*-pentane but insoluble in liquid propane [65]. They contain various polar groups, often containing heteroatoms such as nitrogen, oxygen and sulphur. Since resins are defined by solubility, overlap to the aromatic fraction will occur. The resins are similar to the asphaltenes but have a higher H/C ratio, indicating less aromaticity and they generally have a lower molar mass. Naphthenic acids are a part of the resin fraction. The naphthenic acids have been described in detail in Chapter 2 (page 2).

Crude oil can be fractionated into the SARA-fractions by first precipitating the asphaltenes in *n*-pentane. The remaining fractions can then be separated by their polarity with high pressure liquid chromatography (HPLC) as described by Aske *et al.* [72].

3.2 Structure

The structure of crude oil is closely related to the state of the asphaltene fraction, i.e. the form in which the asphaltene molecules exist in the hydrocarbon solution. Asphaltenes exists in a monomeric form in aromatic solvents in dilute concentration. However, in most hydrocarbon solutions the asphaltenes tend to self-associate into particles or micelles. The asphaltene monomers are believed to be held together by charge transfer, hydrogen bonds and van der Waal forces [65].

Pressure, temperature, aromaticity and polarity of the asphaltenes and the surrounding solution are all parameters that will affect the aggregation of asphaltenes and thus the state of the crude oil.

Resins are essential in dissolving the asphaltenes in the crude oil. They are thought to attach to the asphaltene aggregates with their polar groups and stretch their aliphatic groups outward, thereby stabilizing the asphaltenes against aggregation. This is illustrated in Figure 3.2 [73].
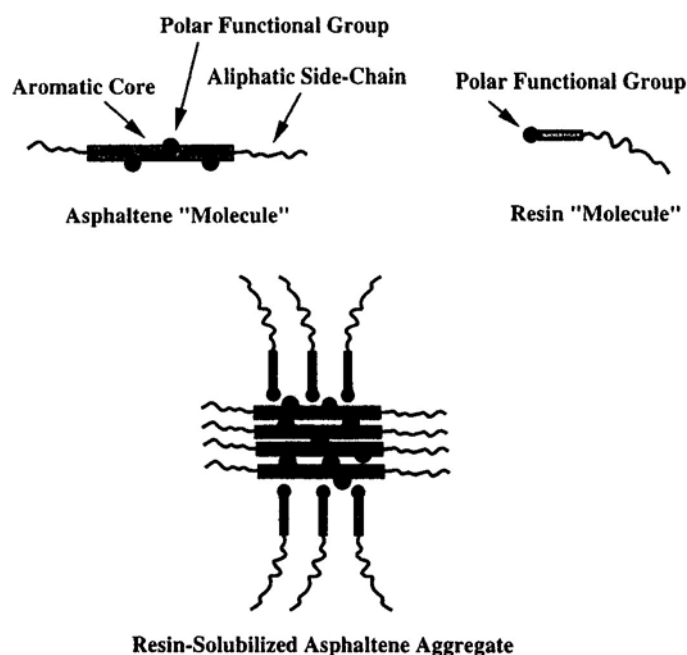

Figure 3.2 Stabilization of asphaltene aggregates by interactions with resins [73].

Other amphiphiles can also disintegrate asphaltene particles in the same way as resins. Gonzalez and Middea [74] studied the peptization of asphaltenes in aliphatic solvents by various oil-soluble amphiphiles. They showed that the effectiveness of amphiphiles on

asphaltene stabilization was influenced by the interactions between the polar headgroups of the amphiphiles and polar groups on the asphaltene molecules. However, their results also indicated that other interactions could be of importance. For example, the π–electrons of the aromatic portions of the asphaltenes may act as electron donors for hydrogen bonds with hydroxyl groups of the amphiphiles. In 1994, Chang and Fogler [75, 76] discussed the stabilization of asphaltenes in aliphatic solvents using alkylbenzene-derived amphiphiles. The results supported earlier suggestions of a hydrogen-bonding effect or possible acid–base interactions between the amphiphile headgroups and polar groups on the asphaltenes, and also showed that the length of the alkyl tail of the amphiphiles was of significance. They also found that in some cases the asphaltenes and the amphiphiles (*p*-dodecylbnzenesulfonic acid) could associate into large electronic conjugated complexes. It has been shown by Östlund *et al.* [77] that the effectiveness of naphthenic acids to disperse asphaltenes depends on the type of asphaltenes.

In Paper II [78] the disintegration of asphaltene aggregates by various amphiphiles was studied by means of near infrared spectroscopy.

4 Emulsions

The concept of emulsions has been defined by IUPAC as a dispersion of droplets of one liquid in another one with which it is incompletely miscible. In emulsions the droplets often exceed the usual limits for colloids in size [79].

Emulsions of oil-droplets in a continuous water-phase are termed oil-in-water emulsions (o/w), while emulsions made up of droplets of water in a continuous oil-phase are termed water-in-oil emulsion (w/o). In petroleum industry, emulsions of the latter type are most common. In addition to the usual emulsion types, multiple emulsions of for instance oil droplets dispersed in water droplets that in turn are dispersed in a continuous oil phase (o/w/o) can occur. The size of the water droplets in a crude oil emulsion can be up to 100 μm, which is large compared to the common definition of the upper limit of colloidal size (1 μm) [80]. The emulsion formation is a result of the co-production of water from the oil reservoir. During processing, pressure gradients over chokes and valves introduce sufficiently high mechanical energy input to disperse water as droplets in the oil phase [81]. An efficient separation of water-in-crude oil emulsions is of importance in order to reduce processing costs and increase the quality of the crude oil. Emulsions of the o/w type can exist in the produced water, causing environmental problems.

All emulsions, except microemulsions are thermodynamically unstable. The presence of different types of stabilizers can however make an emulsion stable for a considerably long time. Components that can work as stabilizers in petroleum industry are asphaltenes, resinous substances, naphthenic acids, finely divided carbonate scale, silica, clays, metal sulphates, metal sulphides and chemical additives [80]. These components stabilize emulsions by adsorbing at the o/w interface creating a steric or electrostatic repulsion between droplets that hinders coalescence.

Asphaltenes are known to be the dominant contributor in stabilizing water in crude oil emulsions [82]. The primary mechanism of stabilization is through the formation of a cross-linked three-dimensional network with high mechanical rigidity at the oil water interfaces. This film also consists of resins. Ese *et al.* [83] used atomic force microscopy images in addition to Langmuir studies to explain the interactions of asphaltenes and resins at an oil/water interface. The interactions between asphaltenes and resins and its importance for emulsion stabilization have also been studied by others [73, 84]. The asphaltenes are believed to accumulate at the oil/water interface as illustrated in Figure 4.1 [85].
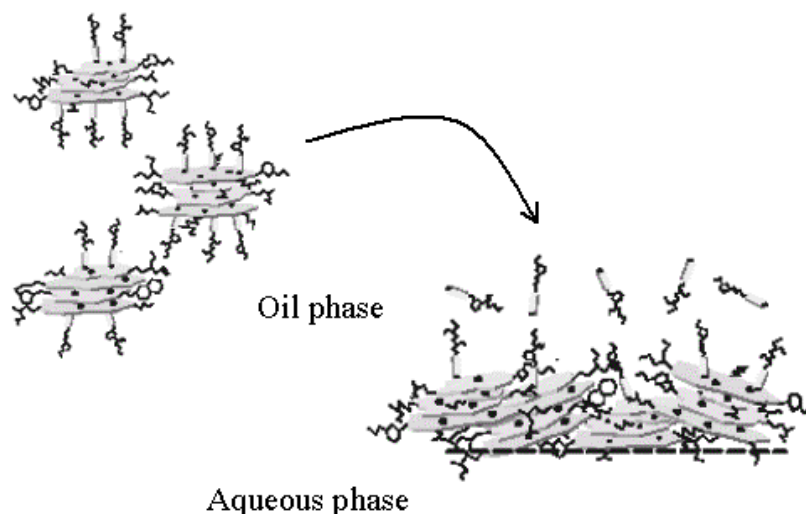
Figure 4.1 Accumulation of asphaltene aggregates at the oil/water interface [85].

The interactions between the different crude oil components will be crucial for the formation of stabile emulsions. In Paper II [78] it is described how naphthenic acids and other amphiphilic molecules can disperse the asphaltenes into the solution and hinder them from stabilizing emulsions.

Naphthenic acids are surface active and will influence the stability of crude oil emulsions [1, 10, 51]. Alkali soaps were among the first compounds used to stabilize emulsions [86]. The pH together with the solubility will be sensitive variables for the ability of naphthenic acid monomers to stabilize emulsions [87]. As the pH of the water phase increases, the acids become ionized and can thus stabilize oil in water emulsions by an electrostatic repulsion between droplets.

Emulsions can be stabilized by formation of a stable monolayer of surfactants that sterically hinders coalescence. The Langmuir technique can be used to study the ability of surfactants to form such a monolayer. This technique is described in Chapter 6.1 (page 24). In Paper I [88] this technique was employed in order to study monolayers of naphthenic acids and naphthenates.

The presence of a surfactant multilayer (D-phase) can be efficient in stabilizing droplets and hinder coalescence through a sterical mechanism. The phase behaviour of naphthenic acids/naphthenates is described in Chapter 2.5 (page 9). In Paper III [89],

we showed that a multilayer (D-phase) of carboxylic acids/carboxylates together with asphaltene particles can stabilize emulsions in a combined mechanism.

The break-up of emulsions basically involves three mechanisms; i.e. flocculation, sedimentation (or creaming) and coalescence. Sedimentation is favoured by large droplet sizes, high differences in density and low viscosity of the continuous phase. While coalescence is the complete association of two bubbles into one, flocculation is a reversible formation of droplet clusters with virtually no change in the total oil/water interface area. Formation of flocculates will increase the sedimentation rate and eventually, coalescence will occur. The mechanisms are illustrated in Figure 4.2.
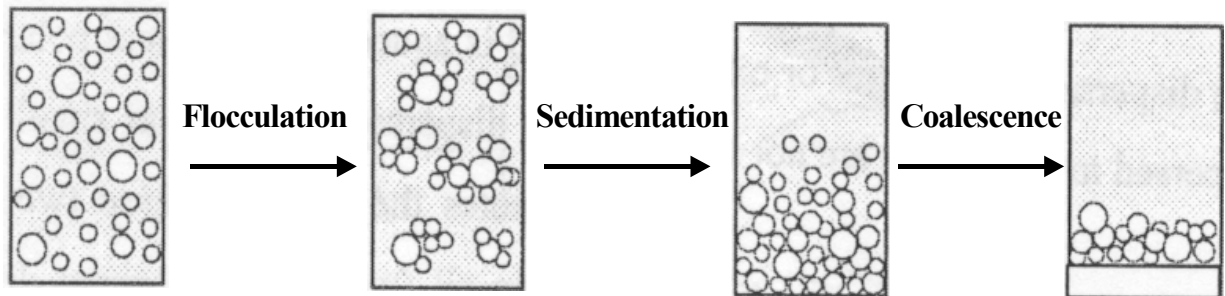

Figure 4.2 Emulsion separation by flocculation, sedimentation, and coalescence.

5   Formation of Calcium Naphthenate

Under certain conditions, the naphthenic acids present in acidic crude oil will precipitate with Ca^{2+}-ions that are present in the co-produced water and form calcium naphthenate and, to a lesser extent, other metal naphthenates. This precipitation accumulates predominantly in oil/water separators and de-salters, but naphthenates can also deposit in the tube and pipelines. Calcium naphthenate deposit from an oil/water separator are shown in Figure 5.1.

Figure 5.1 Calcium naphthenate deposit (right picture) collected from an o/w-separator. The outlet of the separator (left picture) is located at the o/w-interface. [Pictures, by courtesy of Statoil ASA]

The literature have been lacking on information about the formation of calcium naphthenate in crude oil production facilities. However, recently several reports regarding the subject have been published [1, 2, 90-92].

5.1 Mechanism and Inhibition

When the crude oil is being processed offshore the pressure decreases. This leads to degassing of carbon dioxide from the formation water and hence an increase in pH. When the pH of the water increases, the concentration of dissociated acid also increases, which in turn favours the formation of calcium naphthenate. Calcium naphthenate is neither soluble in water nor oil. Having a density lower than water and higher than the oil phase, accumulation of voluminous particles at the oil/water interface in separators may result. This will lead to costly shutdown periods in which thorough cleaning must take place.

Addition of acid will keep the pH low and thereby avoid naphthenate formation. However, such addition is costly, it will increase corrosion problems and it is environmentally unfavourable. Use of special additives, such as demulsifiers or dispersants, have given encouraging results, but an additive which works well with one crude can be inefficient with another [2]. Naphthenates are often found to co-precipitate with scale. Goldszal *et al.* [1] have studied the inhibition of naphthenate and scale in deep-offshore fields. They found that if naphthenates are present at the oil water interface, small amounts of minerals (~5wt%) can induce precipitation. To inhibit naphthenate formation it is necessary to destabilize or prevent emulsions from being formed, disperse the naphthenates to avoid accumulation, and to prevent formation of scale. Some additives where found to be efficient in terms of demulsification and naphthenate deposit prevention. Poggesi *et al.* [91] have reported on multifunctional chemicals that have proved useful as inhibitors for naphthenate formation.

Gallup *et al.* [90] reported on the formation of "metallic soap sludge" in an Indonesian field. The greenish-brown sludge accumulates in onshore oil storage tanks. The sludge consists of metallic soaps with bicarbonate complexation, closely related to naphthenate deposits.

The deposition of insoluble metal soaps can also be a problem in paper industry. Deposits that can be formed as multivalent metal ions react with fatty or resin acids at pH>6 [93, 94]. Stenius and co-workers [95-100] have studied the phase behaviour and micellisation of sodium abietate and oleate as model compounds for resins and fatty acid soaps, respectively.

For calcium naphthenate to precipitate it is expected that the naphthenic acids must be present in the Ca^{2+}-containing water phase at its dissociated form. The concentration of the dissociated acid and the solubility of the corresponding calcium soap are thus interesting parameters for an understanding of when naphthenate deposits are formed. In Paper IV [101], pK_a and partitioning constants for several naphthenic acids were determined. Solubility products for some carboxylic acids were estimated in Paper V [102]. In addition to information about the different equilibria in water/oil/naphthenic acid systems, knowledge of the kinetics of precipitation and accumulation is necessary. A method for studying the formation and growth of calcium naphthenate particles were presented in Paper V. The total oil/water interfacial area as well as the agitation during production may be important variables for naphthenate deposit to form.

5.2 Crystallization Theory

The theory for crystallization is described by Mullin [103]. A brief description is given below.

The first step in a crystallization process is the nucleation. While secondary crystallization is induced by already present crystals, primary crystallization occurs either spontaneous (homogeneous) or is induced by foreign particles (heterogeneous).

A period of time elapses between the achievement of supersaturation and the appearance of crystals. This time lag, generally referred to as an "induction period", is influenced by the supersaturation, state of agitation, presence of impurities viscosity etc. The induction period, t_{ind}, can be considered as made up of several parts defined by Equation 5.1.

$$t_{ind} = t_r + t_n + t_g \qquad (5.1)$$

Where t_r is the "relaxation time" required for the system to achieve a quasi-steady-state distribution of molecular clusters, t_n is the time necessary to form a stable nucleus and t_g is the time needed for the particle to grow to a detectable size. The nucleation time depends mainly on temperature, supersaturation and the interfacial tension between the solution and the solid formed.

The rate of nucleation, J, i.e. the number of nuclei formed per unit time per unit volume, can be expressed as:

$$J = A \cdot \exp\left(\frac{16\pi r \gamma^3 v^2}{3k^3 T^3 (\ln S)^2}\right) \qquad (5.2)$$

were A is a constant, r is the particle radius, γ is the interfacial tension, v is the molecular volume, k is the Boltzmann constant, T is the temperature and S is the supersaturation. For systems involving sparingly soluble salts, the supersaturation, S, can be defined as the ratio of the ion concentration product, Q, to the solubility product, K_{sp}. For a calcium naphthenate system this will be according to Equation 5.3.

$$S = \frac{[Ca^{2+}] \cdot [A^-]^2}{[Ca^{2+}]_{eq} \cdot [A^-]^2_{eq}} = \frac{Q}{K_{sp}} \qquad (5.3)$$

were $[Ca^{2+}]$ and $[A^-]$ are the actual concentration of calcium ions and dissociated acid respectively. $[Ca^{2+}]_{eq}$ and $[A^-]_{eq}$ are the concentrations in an aqueous solution in equilibrium with the solid salt.

The induction period cannot be regarded as a fundamental property since it is affected by many external parameters. By assuming that it is inverse proportional to the rate of nucleation, information about the nucleation process can be extracted. The induction period will then depend on the supersaturation according to Equation 5.4.

$$\log t_{ind} \propto \frac{\gamma^3}{T^3 (\log S)^2} \qquad (5.4)$$

Hence, a plot of log t_{ind} versus (log S)$^{-2}$ will give a straight line with a slope dependent on the temperature and the interfacial tension.

The induction period is followed by a period where the particles grow. In order to understand the kinetics of this process, several different mechanisms are proposed. The surface energy theories claim that the shape the growing crystals assume is the one with a minimum surface area. The diffusion theories presume that matter is deposited at the surface due to the concentration gradient between the bulk solution and at the surface. Adsorption layer theories assume that the crystals grow by a layer-by-layer adsorption process.

Burton, Cabrera end Frank have proposed a relationship between the growth rate and the supersaturation, i.e. the BCF-relationship, given by Equation 5.5.

$$R = A(S-1)^2 \tanh\left(\frac{B}{S-1}\right) \qquad (5.5)$$

were R is the rate of crystallization, S is the supersaturation and A and B are complex temperature dependent constants. At low supersaturations the rate of reaction is proportional with $(S-1)^2$, while at high supersaturations it is proportional with $(S-1)$. Other models end up with a similar result. Due to the complexity of the crystallization processes, empirical models as given in Equation 5.6, are readily used [104].

$$R = k(S-1)^n \qquad (5.6)$$

were k is a constant and n is the effective order of crystallization.

Agglomeration of particles can occur in a crystallization process. The rate of agglomeration will depend on the number of particles, the stirring speed and the ability of the particles to be stable towards agglomeration upon collision. For calcium naphthenate particles to be stable against agglomeration, the ratio of acid to calcium may be of importance. Precipitation phenomena of calcium oleate in aqueous solution have been studied by Matijević et al. [105]. It was shown that a ratio of oleate ions to Ca^{2+} of 2:1 gave solutions with the highest turbidity. Excess of any of the two ions led to formation of small particles that were stable towards agglomeration due to electrostatic stabilization. Small particles will contribute less to the turbidity. Precipitation phenomena of colloidal laureate soap particles with different cations were studied by Young et al. [106]. They came to the same conclusion regarding particles of calcium and copper laureate. For thallium and lanthanum laureate the systems were influenced by formation of complex ions. With this background, It is likely that agglomeration of particles will be most prominent in systems were the ratio of Ca^{2+} to dissociated acid is 1:2. However, high electrolyte concentration in the water will decrease the particles ability to be electrostatically stabilized towards agglomeration.

Ostwald ripening will also influence the particle sizes. Ostwald ripening is the process in which small particles dissolves and the solute deposit subsequently on the larger particles. The driving force of this process is the lowering of the total surface energy.

6 Techniques

Different analytical techniques have been utilized in this doctoral work. An outline of the most important ones are given in this chapter.

6.1 Langmuir Films

A central property for emulsion stabilization is the formation of a w/o film that is stable against coalescence. Film formation of naphthenic acids can be studied by the Langmuir technique. The technique is used in order to characterize monolayer properties of surface-active materials. The objective is to get information about how the molecules pack in a monolayer, i.e. how much area each molecule requires and how the molecules interact with each other. A stable monolayer indicates the ability of the surfactant to stabilize emulsions. Børve [107] found a strong correlation between the ability of different crude oil fractions to stabilize w/o emulsions, and the properties of the films formed by the different fractions at the air/water interface

In order to perform a Langmuir experiment the amphiphilic molecules must be spread on a water surface. Since many film-forming substances do not spread well by themselves, it is normal to use a spreading solvent. This spreading solvent must have the ability to disperse the film-forming molecules so that they are in a monomeric form at the water surface. For this to happen, the spreading coefficient of the solvent on the bulk phase must be positive. The spreading solvent must evaporate completely within a reasonably short time (15 minutes), and it must have sufficient solvency power so that the volume of solvent needed to produce a film does not become too large. The application of the spreading-solvent to the surface is usually accomplished by allowing small drops to fall from a syringe, held a few millimeters above the surface [108].

The Langmuir instrumentation consists of a shallow rectangular trough in which a liquid sub-phase is added until a meniscus appears above the rim. Two moving barriers are placed at the edges of the through. The monolayer is deposited between the barriers and by moving the barriers the area of the water-air surface is changed.

When the available area for the monolayer is large the distance between adjacent molecules is large and their interactions are weak. The monolayer can then be regarded as a two-dimensional gas. Under these conditions the monolayer has little effect on the surface tension of water. If the available surface area of the monolayer is reduced by a

barrier system, the molecules start to exert a repulsive effect on each other. This two-dimensional analogue of a pressure is called surface pressure, Π, and is given by Equation 6.1.

$$\Pi = \gamma - \gamma_0 \qquad\qquad (6.1)$$

where γ is the surface tension in absence of a monolayer and γ_0 the surface tension with the monolayer present. The surface pressure is measured with a Wilhelmy plate partially immersed in the water sub-phase. The Wilhelmy plate is hanging on a balance and the surface pressure is calculated from the force that works on the plate due to surface tension [109].

An important indicator of the monolayer properties of an amphiphilic material is given by measuring the surface pressure as a function of the area of water surface available to each molecule. This is carried out at constant temperature and is known as a surface pressure - area isotherm. Usually an isotherm is recorded by compressing the film (reducing the area with the barriers) at a constant rate while continuously monitoring the surface pressure [109]. An example of such isotherm is shown in Figure 6.1 [110]. The diagram is not intended to represent that observed for any particular substance, but shows most of the features observed for long chain compounds.
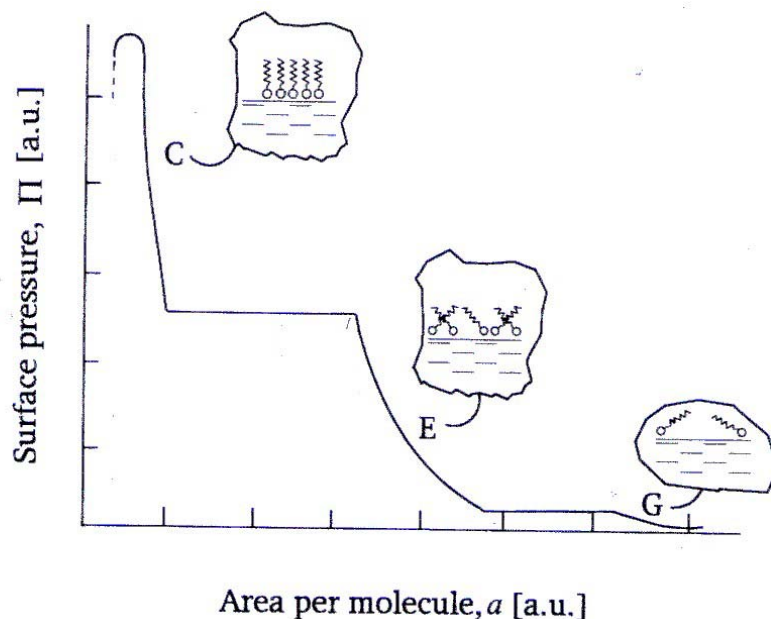

Figure 6.1 Surface pressure–area isotherm for a hypothetical long chain organic compund [110].

When the monolayer is compressed it can pass through several different phases, which are identified as discontinuities in the isotherm [110]. At first, when the molecules are far apart, little or no interactions exist between the molecules and the monolayer is in a gaseous state (G). As the available area is reduced, the monolayer can undergo a phase transition to the liquid-expanded state (E). In this state the molecules start to interact with each other. The hydrocarbon chains are in a random rather than in a regular orientation. Upon further compression, condensed phases (C) may appear. There may be more than one of these and the emergence of each condensed phase can be accompanied by constant pressure regions in the surface pressure-area plot. In the condensed phase, the molecules are closely packed and are oriented with the hydrocarbon chain pointing away from the water surface. If the monolayer is further compressed, a collapse of the condense monolayer into a multilayer will eventually take place as illustrated in Figure 6.2 [110].
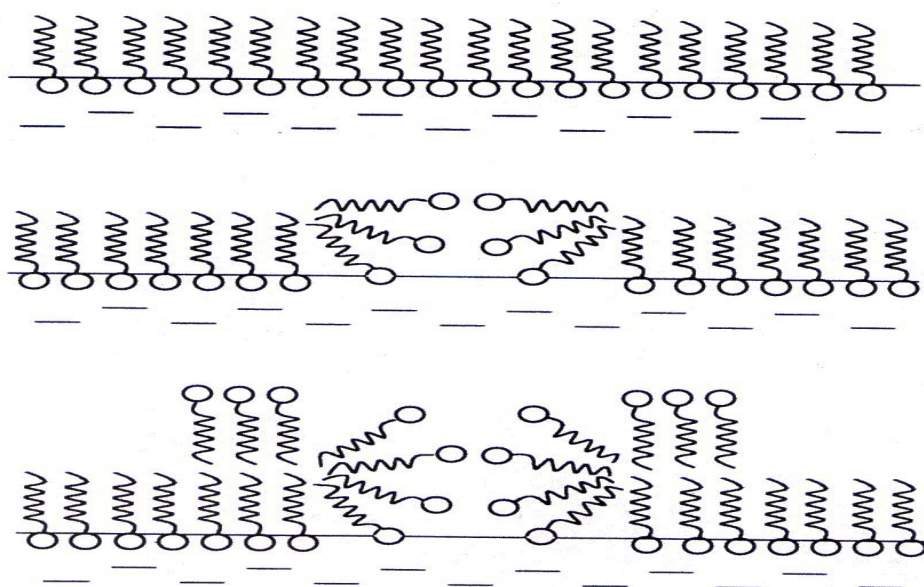

Figure 6.2 Collapse of a monolayer [110].

The phase behaviour of the monolayer is mainly determined by the physical and chemical properties of the amphiphile, the subphase temperature and the subphase composition. For example, various monolayer states exist depending on the length and structure of the hydrocarbon chain length and the magnitude of other cohesive and repulsive forces existing between head groups. An increase in the chain length increases the attraction between molecules. On the other hand, if an ionisable amphiphile is used, the ionisation of the head groups induces repulsive forces between the molecules [110].

In order to investigate the stability of the monolayers, the area loss at constant surface pressure can be measured. This is done by compressing the film to a surface pressure of for example 10 mN m^{-1}. The area of the monolayer is changed in order to keep the surface pressure at this value. The results are normally presented as a plot of A/A_0 versus time t, where A_0 is the area of the monolayer after compression to constant surface pressure and A is the area of the monolayer at time t. If the monolayer is stable, the area, A, will remain about constant. Rearrangement of the molecules, dissolution of the film into the sub-phase or evaporation will lead to a decrease in the area. Higher surface pressure leads to faster area loss [108].

6.2 Near Infrared Spectroscopy

Over the last 30 years near infrared spectroscopy (NIR) has been increasingly used as an analytical tool, particularly by the food and agricultural industries, but also by textile, polymer and petroleum industry. The increasing popularity is due to four principal advantages of the method; efficiency, simplicity, multiciplicity of analysis from a single spectrum, and the non-consumption of the samples. The rapid development of advanced and user-friendly software for multivariate analysis further enhance the usability of NIR [69]. Optical fibers can be used to carry the light from the light source to the point of measurement and back to the light detector. This makes NIR applicable in many processes, for example in high-pressure environments [111].

When light is sent through a chemical sample not all light will be transmitted. This can be accounted for by two distinct mechanisms; electronic absorption by the different molecules and scattering from particles or aggregates. Due to the light scattering, the near infrared spectra will display a baseline elevation that is dependent on the size and number of the particles. Hence, by monitoring the baseline elevation, the growth of particles can be followed. In this doctoral thesis, NIR have been utilized to measure disintegration of asphaltenes in Paper II [78] and the growth of calcium naphthenate particles in Paper V [102].

Light scattering in the near-infrared region is described in detail by Mullins [112] and Kerker [113]; a brief description is given below.

The light scattering can be divided into two groups: wavelength-independent scattering, where the size of the particles is large compared to the wavelength of the light, and wavelength-dependent scattering, where the particles are of comparable sizes to or smaller than the wavelength of the light. The latter group contains the case of $r/\lambda \leq 0.05$,

where λ is the wavelength of light and r the particle radius. At this, so-called Rayleigh condition, the particle is so small that the electromagnetic field it experiences is uniform over the particle. By also assuming that the particles are slightly lossy and dielectric, an expression for the scattering cross section of a particle is given by Equation 6.2.

$$\sigma_{sc} = \frac{2^7 \pi^5}{3} \frac{r^6}{\lambda^4} \left(\frac{n^2 - 1}{n^2 + 2} \right)^2 \tag{6.2}$$

where r is the particle radius, λ the wavelength of the incident light and n is the ratio of the discrete phase to the continuous phase index of refraction. In the absence of multiple scattering, and in the Rayleigh limit ($r/\lambda \leq 0.05$), fewer, but larger spheres are much more efficient scatterers than the same mass of smaller particles.

Within the Rayleigh limit, the light extinction can be considered a sum of the absorbance and scattering contribution, represented by the particle cross-sections.

$$\sigma_{tot} = \sigma_{sc} + \sigma_{abs} \tag{6.3}$$

where σ_{tot}, σ_{sc} and σ_{abs} are the total, scattering and absorption cross sections, respectively. The absorption cross section scales with r^3, while the scattering cross section scales with r^6. Hence, the change in the total cross section as a result of particle growth will be governed by the scattering contribution.

The optical density, OD, is given by:

$$OD = \log\left(\frac{I_0}{I} \right) = 0.434 N \sigma_{tot} \tag{6.4}$$

where I and I_0 are the intensities of the transmitted and incident light respectively and N is the number of particles in the total cross section σ_{tot}.

The measured optical density is thus a combination of absorption and scattering contributions. The effect of multiple scattering is not accounted for in this equation. Absence of multiple scattering implies that radiation scattered by a single particle proceeds directly to the detector without any further scattering encounters. In case of multiple scattering, the scattering and absorption cannot be treated separately.

Conditions for single scattering can usually be attained by working with dilute systems and with small volumes.

Figure 6.3 demonstrates the effect of particle size on NIR spectra. The spectra are taken at different time during growth of calcium naphthenate particles in water. The increasing optical density due to increasing particle size is clearly seen for wavelengths were the absorption from the surrounding media is low, for example around 1280 nm.
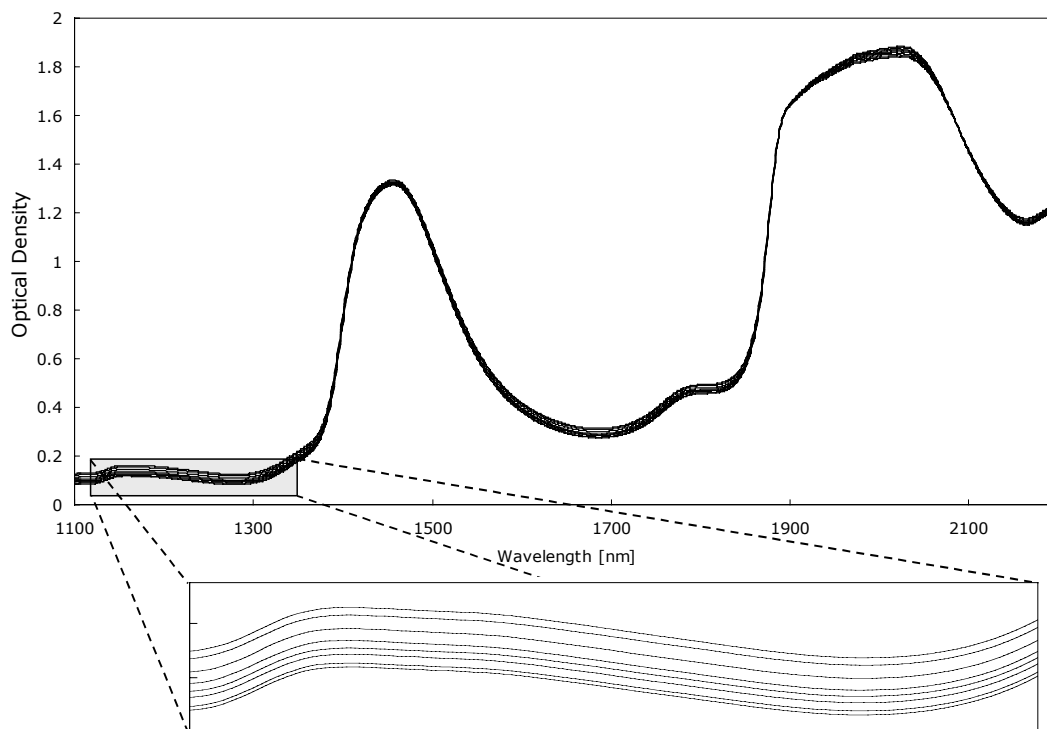

Figure 6.3 Baseline elevation in NIR-spectra due to increased scattering as a result of growth of calcium naphthenate particles in water. The optical density at wavelength with low absorption from surrounding media (~1280nm) increases when the particle sizes increases.

Several authors report on the use of NIR for determination of particle sizes, often in combination with multivariate analysis [114-117].

6.3   Critical Electric Field

Electrocoalescence is commonly used for demulsification in the petroleum industry. Water is separated from the emulsion by applying a electric field of 1-10 kV/cm to cause flocculation and coalescence of water droplets in a continuous oil phase [118]. This

principle can be applied to evaluate the different levels of emulsion stability in different systems.

In the critical electric field technique, an increasing electric field is applied to an emulsion and the current that passes through the sample is continuously measured. When the voltage is increased (but below the critical value) the droplets undergo a flocculation and as a result "a bridge of droplets" is formed between the electrodes. E_{crit} is defined as the electric field necessary to achieve a sudden increase in the current. This increase is due to breakdown of the emulsion droplets and a formation of a continuous water-channel between the electrodes. Figure 6.4 [69] demonstrates the effect on the water droplets when the electric field is increased over an emulsion.
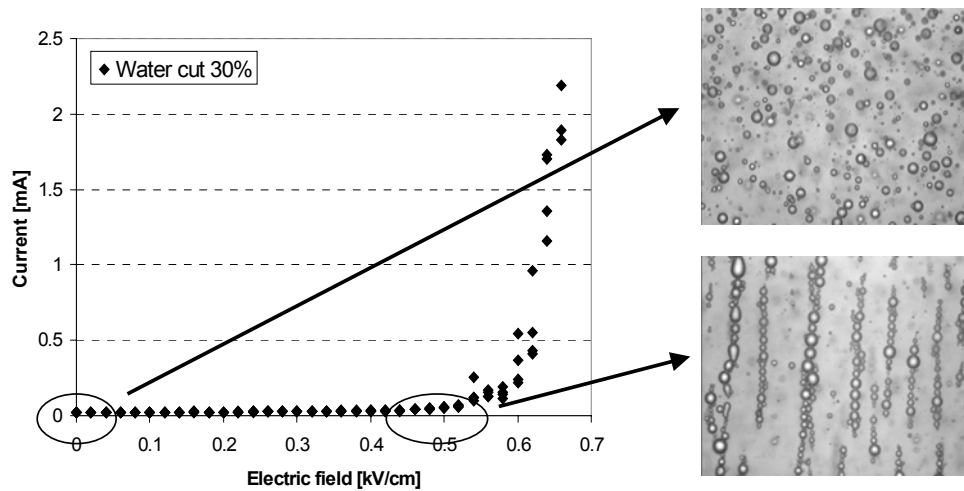

Figure 6.4 Emulsion droplets in an increasing electric field [69].

The mechanism behind the breakdown is believed to be an ion-transport between the aqueous droplets over the protecting membrane. Hence the critical electric field will reflect the resistance towards coalescence of the interfacial structures.

In Paper III [89], an electric field cell was used for the determination of emulsion stability. The method is similar to the one employed by Aske *et al.* [119] and Kallevik *et al.* [120]. The cell for determining the critical electric field is depicted schematically in Figure 6.5. It consists of a Teflon plate with a hole in the centre (r = 5 mm), and a brass plate on each side. The distance between the plates is 0.5 mm, and the upper brass plate has holes for sample injection. The system is held together with isolating Plexiglas plates. The brass plates are connected to a computer-controlled power supply (Agilent Model 6634B) that can deliver a maximum of 100 V DC. The cell can be placed in a heating

cabinet if elevated temperatures are desired. The emulsion samples are injected into the cell and the power supply is starting at 0 V and increased by steps of for example 1V every other second, corresponding to an increase in the electric field of 0.01 kV cm^{-1} s^{-1}. The electric field required to break the emulsions, $E_{critical}$, is recorded when a sudden increase in the current through the sample is seen.
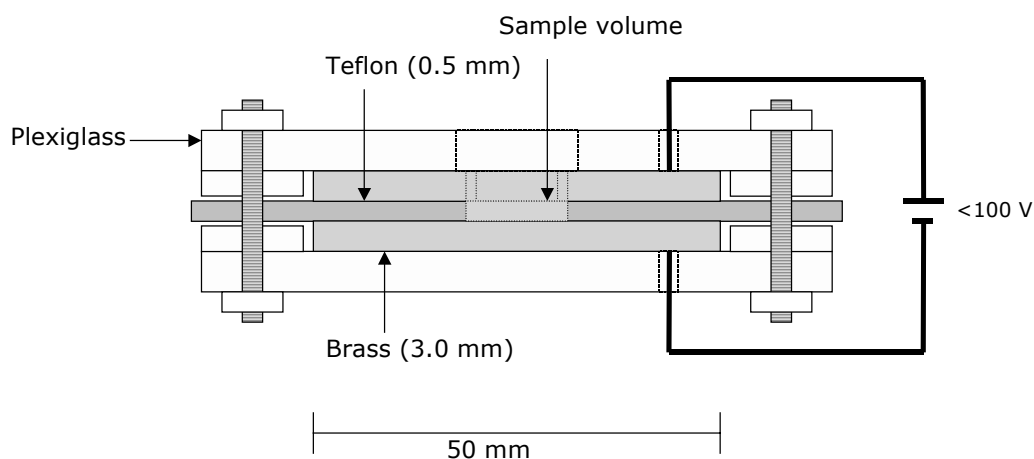

Figure 6.5 Electric field cell for emulsion stability measurements.

6.4 LC/MS

Liquid chromatography/mass spectrometry (LC/MS) has been used to determine the concentration of naphthenic acid in an aqueous phase in Paper IV [101]. The samples go through a LC column were the molecules are separated on the basis of their polarity. A mass spectrometer is then utilized to determine the ratio of mass to charge (m/z) for the various naphthenic acid species.

Liquid chromatography is a fundamental separation technique in the life sciences and related fields of chemistry. Unlike gas chromatography, which is unsuitable for non-volatile and thermally fragile molecules, liquid chromatography can safely separate a wide range of organic compounds, from small-molecule drug metabolites to peptides and proteins [121].

After the LC separation, a mass spectrometer is used as detector. In addition to signal strength, they generate mass spectral data that can provide valuable information about the molecular weight, structure, identity, quantity, and purity of a sample. Mass spectrometers work by ionising molecules and then sorting and identifying the ions

according to their mass-to-charge (m/z) ratios. Two key components in this process are the ion source, which generates the ions, and the mass analyser, which sorts the ions. Different types of ion sources and mass analysers are used for different analyses [121].

LC/MS was used to determine the concentration of different carboxylic acids in water in Paper IV. The advantages of the method are that the analysis can be performed directly on water and that the sample consumption is small. The latter is important due to use of costly special synthesized naphthenic acids.

7 Main Results

This chapter summarises the main results from the papers presented in this thesis.

In Paper I we report on a Langmuir study of naphthenic acids at different pH-levels and electrolyte concentrations. The formation of stable films was seen when cations were present in the bulk phase at elevated pH. In Paper II the interactions between asphaltenes and various surfactants, including synthetic and natural naphthenic acids were studied. The ability of the different amphiphiles to disintegrate asphaltene particles in model heptane-toluene mixtures was documented with the use of near infrared spectroscopy. Emulsion stabilization was the topic of Paper III. Stabilization of emulsions by combined surfactant multilayer (D-phase) and asphaltene particles was reported. In addition, the ability of carboxylic acids to stabilize water-continuous emulsions at different pH-levels and water-cuts was investigated. In Paper IV the oil/water-partitioning and interfacial behaviour of naphthenic acids were investigated. Near infrared spectroscopy was presented as a tool for studying the formation and growth of calcium naphthenate particles in Paper V.

Paper VI is a review article about the stabilization mechanism of crude oil emulsions. Crude oil components that are important for the emulsion stability are described. Techniques for describing these components as well as oil/water interfaces, for pressures ranging from ambient to high, are presented along with recent results.

Paper I

A central property for emulsion stabilization is the formation of a w/o film that is stable towards coalescence. Film formation of naphthenic acids can be studied by Langmuir technique. The technique, described in Chapter 6.1 (page 24), is used in order to characterize monolayer properties of surface-active materials. The objective is to get information about how the molecules pack in a monolayer, i.e. how much area each molecule requires and how the molecules interact with each other. The stability of the monolayer and how the pH and electrolyte concentration affect this stability can also be discovered. A stable monolayer indicates the ability of the surfactant to stabilize emulsion droplets towards coalescence.

In Paper I, Fluka naphthenic acid (a commercial mixture), 5β(H)-cholanoic acid (**1**) and 1-naphthalenepentanoic acid, decahydro- (9CI) (**2**) (Chiron AS) have been used in a Langmuir study [88].
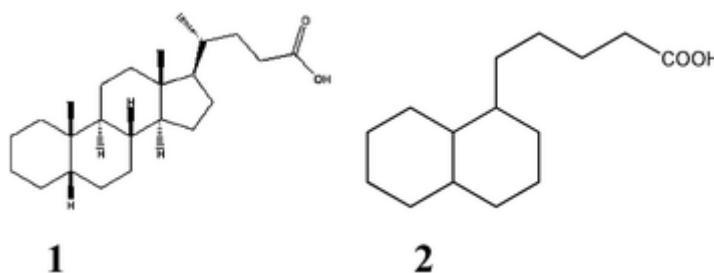
Scheme 7.1: Naphthenic acids used in Langmuir study.

1-naphthalenepentanoic acid, decahydro- (**2**) rapidly dissolves into the bulk phase and, hence, no stable films are formed. Acidifying the subphase or addition of cations does not influence this situation.

5β(H)-cholanoic acid (**1**) and Fluka naphthenic acid form stable films when cations are present in the aqueous sub phase. The stability isotherm for 5β(H)-cholanoic acid is given in Figure 7.1. The results are expressed as A/A_0 versus time, t, where A_0 is the area of the monolayer after compression to constant surface pressure (10 mN/m) and A is the area of the monolayer at time t. At lower pH, the addition of metal ions will have less effect since the naphthenic acid is not protolyzed and naphthenates will not be formed. The divalent calcium ions have a more stabilizing effect on the film than the sodium ions.
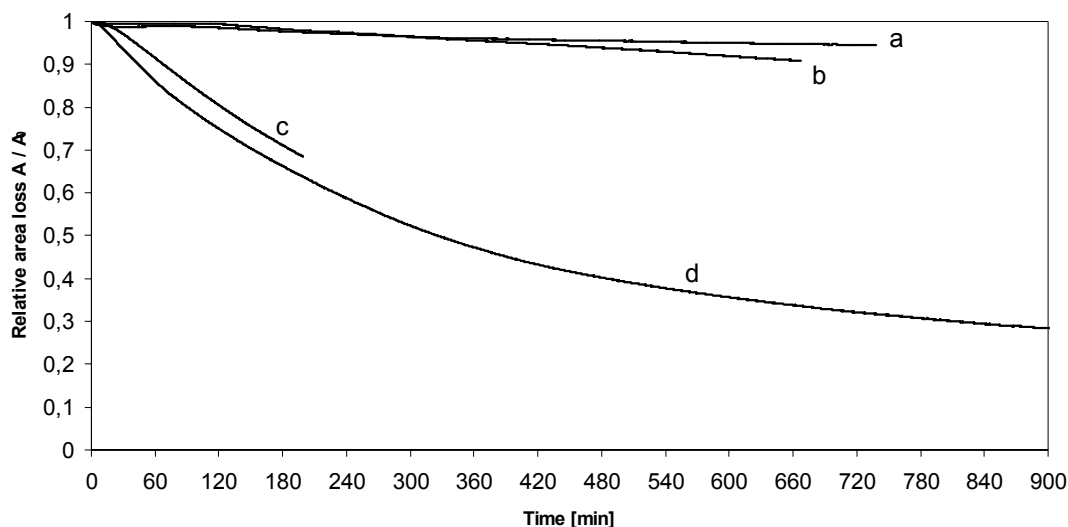
Figure 7.1 Stability isotherms (surface pressure of 10 mN/m) for 5β(H)-cholanoic acid at a pH 5.6, [Ca^{2+}]=0.01 M, b pH 7.0, [Na^{+}]=0.1 M, c pH 3.1, [Na^{+}]=0.1 M and d pH 5.6, pure water.

Pressure-area isotherms for different pH values, at a fixed sodium ion concentration of 0.1 M, are given in Figure 7.2. As the pH increases, the film tends to tolerate a higher pressure before collapse. This is an indication of more stable films due to naphthenate formation. The figure shows that the pressure increase sets in at different areas per molecule at the different pH values. At pH 3.0 the film properties are dominated by the fact that this film has a low long-term stability (Figure 7.1, curve c). The reason for this is that the molecules are in an undissociated form and will not be stabilized by Na^{+} ions.
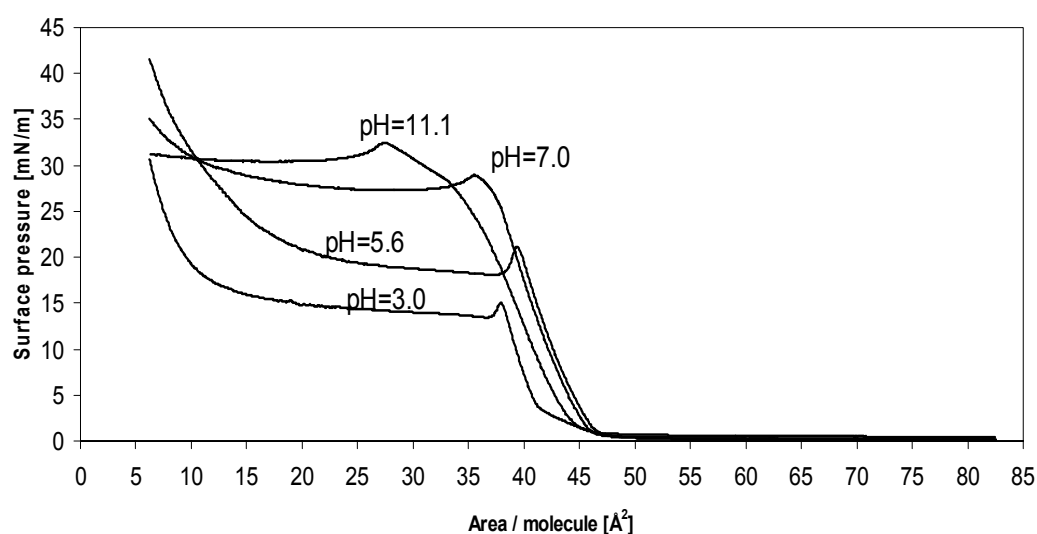

Figure 7.2 Pressure–area isotherms for 5β(H)-cholanoic acid at [Na^{+}]=0.1 and pH 11.1, 7.0, 5.6 and 3.0.

Joos [122, 123] has suggested that the collapse pressure, $\pi_{c,m}$, of a mixed miscible monolayer may be evaluated from the collapse pressures, $\pi_{c,1}$ and $\pi_{c,2}$, of the separate components according to Equation 7.1.

$$X_1 \exp\left[\frac{(\pi_{c,m} - \pi_{c,1})\omega_1}{kT}\right] + X_2 \exp\left[\frac{(\pi_{c,m} - \pi_{c,2})\omega_2}{kT}\right] = 1 \tag{7.1}$$

X_1 and X_2 are the mole fractions in the monolayer of component 1 and 2 respectively and ω_1 and ω_2 are their partial molecular area. The activity coefficients are neglected, and it is assumed that equilibrium exist between the molecules in the monolayer and in the collapsed phase. The acidity constant, K_a^s, in the monolayer can be defined according to Equation 6.2.

$$K_a^s = \frac{X_{ZH}}{X_{ZNa}[\text{H}^+]} \tag{7.2}$$

Here X_{ZH} and X_{ZNa} represent the mole fractions in the monolayer of naphthenic acid and sodium naphthenate, respectively. [H$^+$] refers to the bulk concentration of H$^+$ ions. Due to the electrical double layer, the concentration of H$^+$ at the surface will be higher than in the bulk. The pK_a^s-value will thus be higher than an ordinary pK_a.

If it is assumed that the partial molecular area of the undissociated and the soap form of the acid is the same ($\omega_{ZH} = \omega_{ZNa} = \omega$), Equations 7.1 and 7.2 can be rewritten as

$$\pi_{c,m} = -\frac{kT}{\omega}\ln\left[\frac{[\text{H}^+]}{K_a^s + [\text{H}^+]}\exp\left(\frac{-\pi_{c,ZH}\omega}{kT}\right) + \frac{K_a^s}{K_a^s + [\text{H}^+]}\exp\left(\frac{-\pi_{c,ZNa}\omega}{kT}\right)\right] \tag{7.3}$$

This equation gives the collapse pressure of the monolayer as a function of the H$^+$ concentration or the pH of the bulk phase, provided the collapse pressures of the acid form and the soap form are known. It is seen that the surface dissociation constant, K_a^s, can be evaluated from such experiments.

A plot of a curve according to Equation 7.3 and the experimental points from Figure 7.2 are shown in Figure 7.3. The fitting of the theoretical curve to the experimental values gives a pK_a^s of 5.65 for 5β(H)-cholanoic acid. The barrier speed and the composition of the subphase will probably influence the determination of pK_a^s.
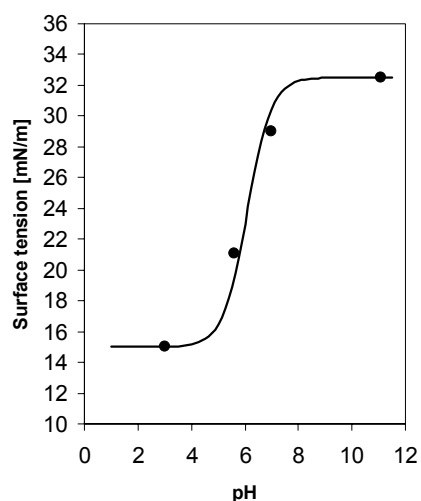
Figure 7.3 Collapse pressure of a 5β(H)-cholanoic acid monolayer as a function of pH.
Points: **experiment;** *full line:* **calculated according to Equation 7.3. ω=46Å^2, T=293K, pK$_a^s$=5.65, $\pi_{c,ZH}$=15, $\pi_{c,ZNa}$=32.5.**

Critical micelle concentrations (CMC) were determined for some naphthenic acids in Paper I. CMC-values of additional naphthenic acids were reported in Paper III [89]. The main results from both these studies are given in the description of Paper III, page 41.

Paper II

Asphaltenes are known to be the dominant contributor in stabilizing water in crude oil emulsions [82]. How the asphaltenes interacts with other crude oil components are thus of great interest.

In Paper II, the dispersive effects of naphthenic acids and other amphiphilic molecules on asphaltenes in model heptane-toluene mixtures were studied. Near infrared spectroscopy (NIR) was used to follow the disintegration of the asphaltene aggregates as a function of time and chemical additive concentration. The use of NIR as a method to study particle sizes is described in Chapter 6.2 (page 27).

Different chemicals with different functional groups were employed in the experiments. The structures of the naphthenic acids are given in Scheme 7.2. In addition to these acids, two commercial blends, Fluka and Crude Naphthenic Acid (CNA), as well as acids extracted from a crude oil, were used. Fatty alcohols, fatty amines and a commercial inhibitor, designed to inhibit asphaltene precipitation, were also used in the study.

CHOL   **2C4**   **C42**
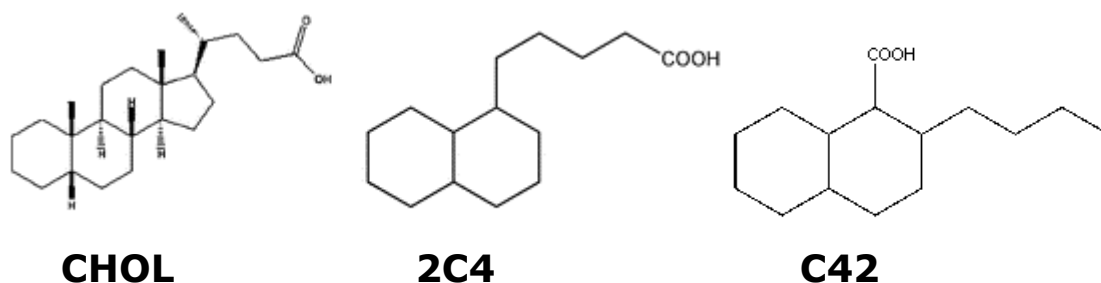
Scheme 7.2: Structures of naphthenic acids used in asphaltene disintegration study.

The experiments were performed by continuously measuring the change in scattering at a wavelength of 1600 nm, upon addition of various chemicals, in a solution of asphaltenes in heptane/toluene (70/30 by volume). At this aromatic/paraffinic ratio, the asphaltenes is expected to form rather large aggregates. Hence, any effect on the size ought to be easily detected.

In Figure 7.4, the effect of different concentrations of a polydisperse naphthenic acid on the aggregate sizes is shown. The results indicate a clear decrease in scattering as a function of time after the acid was introduced, i.e. the aggregate sizes decrease. Faster disaggregation is seen as the concentration of added naphthenic acid is increased.
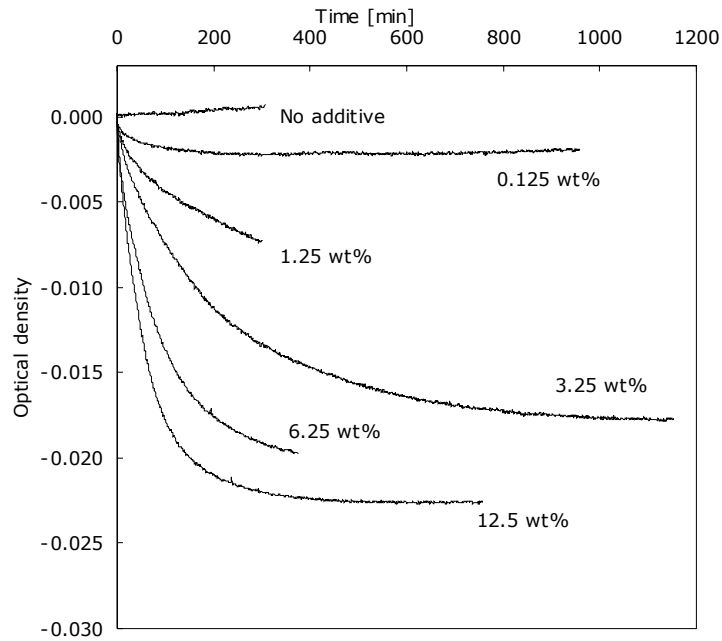
Figure 7.4 NIR scattering measurements at 1600 nm for 0.125 wt% asphaltenes in a 70/30 by volume *n*-heptane/toluene mixture with crude naphthenic acid (CNA) added in various concentrations.

The relative optical density versus time for toluene/*n*-heptane/asphaltene mixtures with various naphthenic acids are plotted in Figure 7.5.
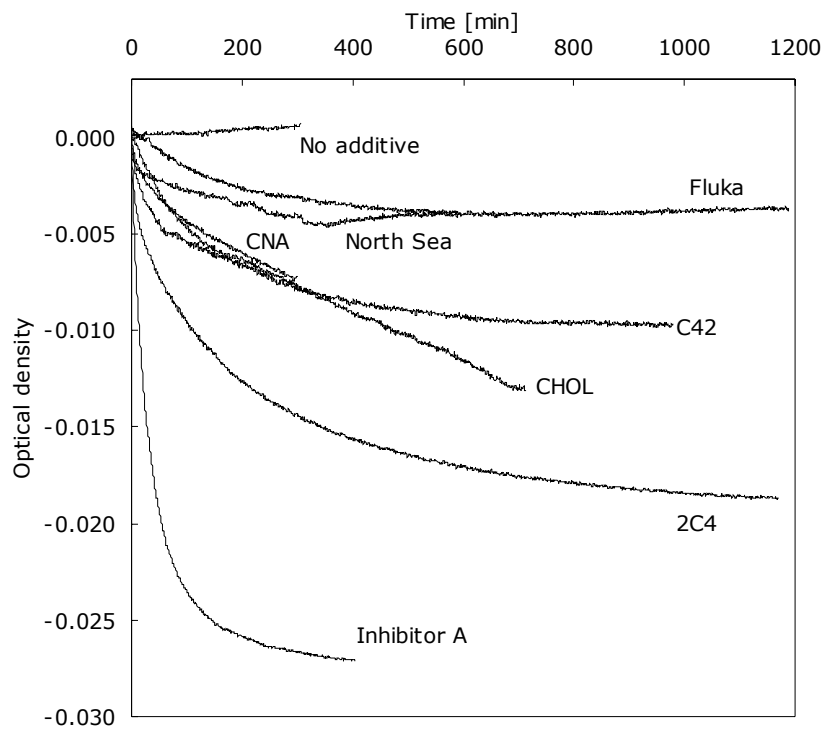

Figure 7.5 NIR scattering measurements at 1600 nm for 0.125 wt% asphaltenes in a 70/30 *n*-heptane/toluene mixture with 1.25 wt% of various naphthenic acids added.

The commercial Fluka naphthenic acid and the naphthenic acid extracted from a North Sea crude seem to affect the state of the asphaltenes only to a minor extent. CNA is most efficient of these polydisperse naphthenic acids. A comparison between 2C4, C42 and CHOL (Scheme 7.2) shows these species to be somewhat more efficient than the previous group. Especially, the 2C4 molecule has a very efficient breakdown to start with and also attains a low final value. It is interesting to see that the molecular structure affects the results to this extent.

The other amphiphiles showed a varying effect on the disintegration of the asphaltenes. In all cases the most efficient treatment was obtained by Inhibitor A, the commercial mixture.

Alkylbenzenesulfonic acid was shown to associate with the asphaltenes and create aggregates of increased sizes. This is in accordance with the results obtained by Chang and Fogler [75] in a UV/Vis spectroscopic study. They suggested that asphaltenes and dodecylbenzenesulfonic acid could associate into large electronic conjugated complexes.

The conclusions of this paper are that NIR spectroscopy is a powerful method for following the disintegration of asphaltene aggregates upon addition of chemicals. The NIR technique, which is very fast and accurate, is hence a good choice for the initial screening of large numbers of chemicals for asphaltene inhibition. The results show that additives that are efficient in replacing hydrogen bonds, possess dispersive power and can serve as inhibitors.

Paper III

Emulsions constitute a major problem in crude oil production offshore. In this paper the CMC-values of some naphthenic acids were obtained and the influence of different carboxylic acids on emulsion stability were investigated. It was shown that water-in-oil emulsions can be stabilized by a combined mechanism of multilayer and asphaltene particle stabilization.

Critical micelle concentration at high pH

The theory behind micellisation is described in Chapter 2.4, page 7. Critical micelle concentrations (CMC) were determined for some naphthenic acids in Paper I [88] and additional CMC-values were reported in this paper. The determined CMC-values and the area/molecule at the water surface are given in Table 7.1.

Table 7.1 CMC and area per molecule for different carboxylic acids at high pH (11.0-11.5).

Carboxylic acid		pH	CMC [mol dm^{-3}]	Area/molecule [Å^2]
[C7a1]	4-heptylbenzoic acid	11.5	1.7E-2	31
[C51]	*trans*-4-*n*-pentylcyclohexanecarboxylic acid	11.5	6.7E-2	35
[2C4]	1-naphthalenepentanoic acid, decahydro-	11.0	2E-4	52
[CNA]	CNA 160-170 Corn van der Locke	11.3	2.7E-4	71
[Fluka]	Fluka Naphthenic Acid	11.3	8E-4	61

CMC-values for the sodium *n*-alkanoates were collected from Mukerjee and Mysels [55] and compared with CMC-values for the naphthenates. Figure 7.6 shows the molecular weight (of the acidic forms) versus log[CMC]. It should be noted that the values from Mukerjee and Mystels [55] are for pure aqueous solution while the other are for pH>11. It is well known that the logarithm of CMC often vary linearly with the size of the hydrophobic part of surfactants [17, 56].
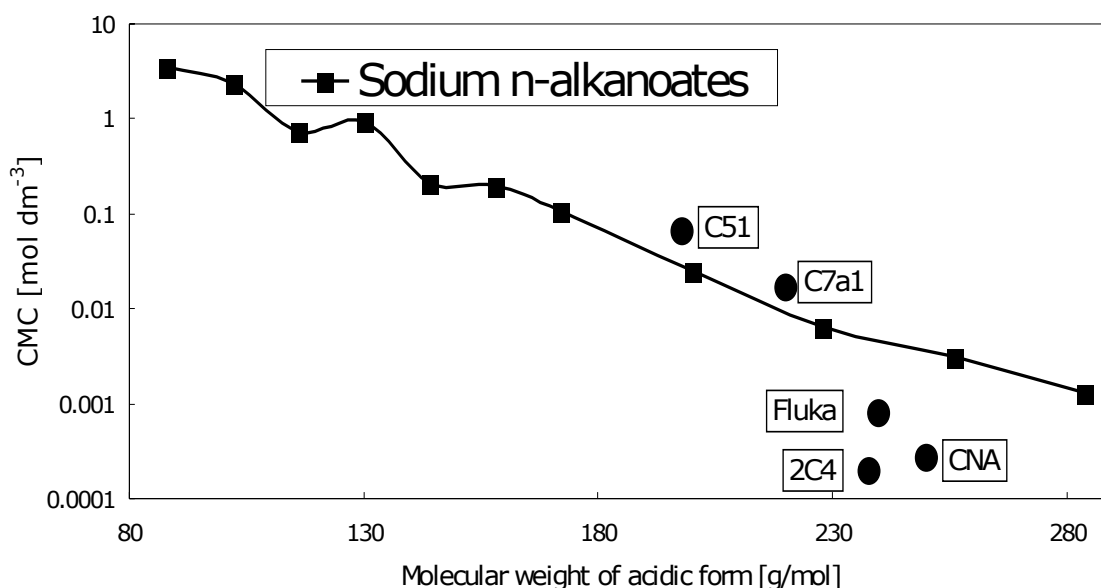
Figure 7.6 CMC-values for different carboxylates as a function of the molecular weight of the acidic form. The squares connected with a line are literature values for sodium *n*-alkanoates. The abbreviations used for the other points (circles) are explained in Table 7.1.

The naphthenates from the commercial mixtures of naphthenic acids (CNA and Fluka) and 2C4 have lower CMC-values than straight chain carboxylates with similar molecular weight. Characteristic for the structures of C51 and C7a1 is that they have the acid group connected directly to a condensed and an aromatic ring respectively. These two acids have CMCs that are higher than corresponding *n*-alkanoates.

The CMC-measurements reveal that the naphthenic acid salts behave as micelle-forming surfactants at appropriate pH values.

The area per molecule given in Table 7.1 reveals that the naphthenic acids tested occupy between 31-71 $Å^2$/molecule. Ovalles *et al.* [52] have reported values for the area per molecule for naturally occurring naphthenic acids at an interface between water and toluene, finding 113–152 $Å^2$/molecule for different fractions. For these systems (at full dissociation) a strong electrostatic repulsion is dominant, which is explaining the large area demands at high pH. In a system consisting of a naphthenic acid, RH and a naphthenic salt, RNa, the ratio, RNa/RH, will determine what kind of structure to occur. Normally by varying RNa/RH (in water), at high enough pH, one will have micelles, liquid crystals and reversed structures [54]. For emulsion stabilization, the occurrence of a lamellar liquid crystalline D-phase will be crucial.

Oil in Water Emulsions

The emulsion stability of systems containing paraffinic, aromatic or naphthenic acid (~1wt%), water and heptane/toluene were investigated at different pH-levels. High pH (around 11) gave rise to o/w emulsions that were stable for several days. The drop size distribution of these emulsions was narrow with drop sizes in the range 9-24 nm. A decrease in pH reduced the emulsion stability significantly. High molecular weight acids seem to have a slightly better stabilizing effect on the emulsions.

Combined D-phase and Asphaltene Particle Stabilization

It is our opinion that the phase equilibria in the system water/sodium hexadecanoate (NaC16)/hexadecanoic acid (HC16) at 70°C is representative also for naphthenic acid based systems. This diagram is given and explained in Chapter 2.5, page 9. In this diagram, the importance of the stabilization of water/oil emulsions, due to the D-phase has been documented [16].

In order to evaluate the different levels of emulsion stability in different systems, the critical electric field technique can be applied. This technique is explained in Chapter 6.3, page 29. The critical electric field will reflect the resistance towards coalescence of the interfacial structures and thus serve as a parameter for emulsion stability.

The competition between D-phase stabilization and asphaltene-particle stabilization of water/oil emulsions was investigated using the following experiments. A hexadecanoic acid / sodium hexadecanoate D-phase was prepared based on the equilibria in Figure 2.5 (page 10). A dichloromethane solution, containing dissolved asphaltenes, was mixed with the D-phase and the solvent was evaporated. After 24 hours there was clear evidence of asphaltene particles present in the D-phase. This D-phase, modified with different amount of asphaltenes, was used to stabilize w/o-emulsions at 70°C. The emulsions were prepared from 55.7 wt% n-decane, 32.7 wt% 0.5M NaCl and 11.7 wt% asphaltene modified D-phase. In order to measure the emulsion stability, the $E_{critical}$ was determined. The result is shown in Figure 7.7.
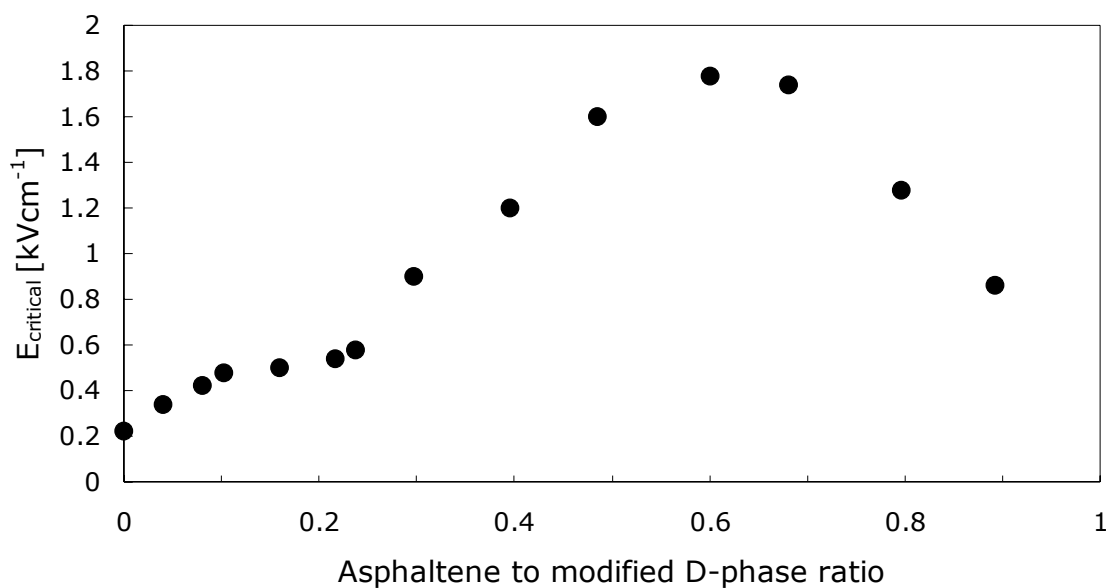
Figure 7.7 Emulsion stability, represented by the critical electric field, E_{crit}, as a function of different asphaltene fractions of the modified D-phase (by weight).

Obviously, the addition of asphaltene particles can enhance the w/o-emulsion stability from the case with just a D-phase present. However, too high amount of asphaltene particles will give a destabilization. A ratio of 0.6, i.e. 60 wt% particles and 40 wt% D-phase seems to be optimal. The mechanism is most likely that these nano-particles are dispersed in the surfactant multilayer of the D-phase, giving further protection towards coalescence. The experiment in Figure 7.7 is very important in visualizing different mechanisms behind emulsion stability in crude oils with high amounts of asphaltenes and naphthenic acids. Representatives to these are heavy crudes, and bitumens.

Paper IV

An understanding of the equilibria involved in a water/oil/naphthenic acid system is important in order to understand the different problems naphthenic acids causes in crude oil production. In Paper IV the dissociation and partitioning equilibria, in addition the interfacially behaviour of the naphthenic acids at different pH have been studied. Equilibira in water/oil/naphthenic acid systems are described in Chapter 2.2 (page 3).

A crude oil from the Norwegian continental shelf, with an acid content of 2 wt%, was used to study the partitioning and acidic constants of the naphthenic acids. The crude oil samples were mixed with an equal amount of water with different pH-values. The samples was agitated for at least 24 hours, separated and the concentrations of the naphthenic acids in the water phase were determined with GC/MS. The naphthenic acids in the crude oil used, were extracted by an ion exchange method [124] and then analyzed by GC/MS. With this technique it was possible to determine the content of some of the naphthenic acid structures defined by size and number of double bound equivalents. It was assumed that each double bound equivalent corresponded to one ring rather than one double bond since the olefins are unstable and, consequently, not present in crude oils [27].

The total concentration of naphthenic acid in the water phase can be expressed as a function of the total concentration of acid, pH, the partitioning constant, K_{wo} and the acidic constant, K_a. By fitting this expression to experimental determined points (concentration of acid in water at different pH), the equilibria constants can be determined. pK_a–values for C10-C16 naphthenic acids with one, two, or three saturated rings were determined to 4.9±0.1 at 25°C. Water-soluble paraffinic carboxylic acids have pK_a-values ranging from 4.8 to 4.9 [125]. Cyclohexanecarboxylic acid are reported to have $pK_a=4.91$ [126]. Hence, the crude oil naphthenic acids have pK_a-values in the same order as the water-soluble aliphatic acids.

The partitioning constants for the crude oil naphthenic acids are shown in Figure 7.8. The logarithm of the determined partition coefficients varies linearly versus the number of methyl groups in the naphthenic acid molecules. This is in accordance with findings of Reinsel *et al.* [127] who have studied the partitioning of acetic, propionic and butyric acids between crude oil and water. The naphthenic acids with three rings are apparently more hydrophilic than acids with one or two rings.
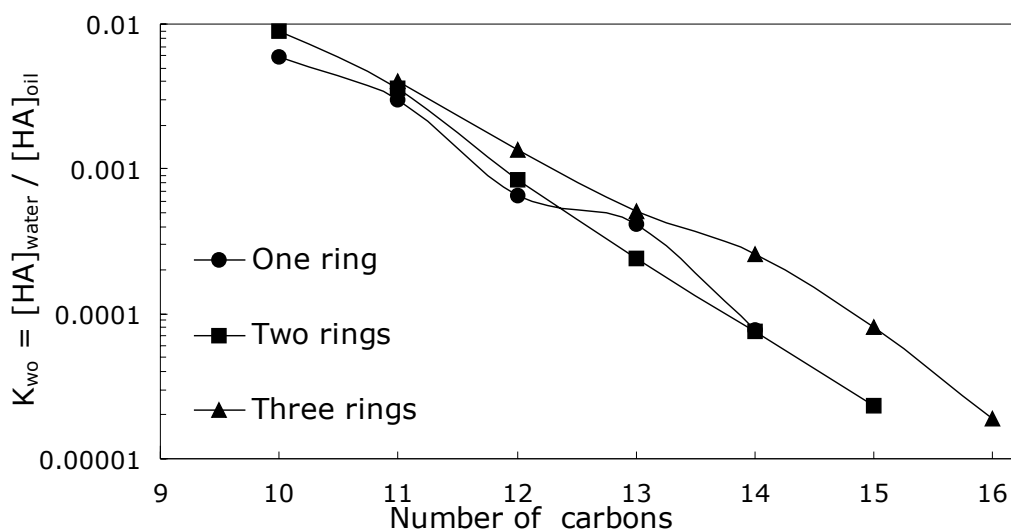
Figure 7.8 Partitioning constants, K_{wo}, for naphthenic acids with one, two and three rings and different numbers of methyl groups.

Different synthetic or commercially available carboxylic acids were added to a mixture of *n*-heptane and toluene (50:50 by volume). Water with different pH was added. The mixtures were stirred for 24 hours, separated by centrifugation and the naphthenic acid content in the water phase was analyzed by LC/MS. At higher pH the collected water samples were diluted prior to LC/MS analysis. The experimentally determined concentrations of the different acids in water at different pH were fitted to the theoretical expression in the same way as for the crude oil naphthenic acids. Figure 7.9 gives the experimental points and the fitted model-line for C41a1. For C41a1, the model gives a good fit to the experimental points.
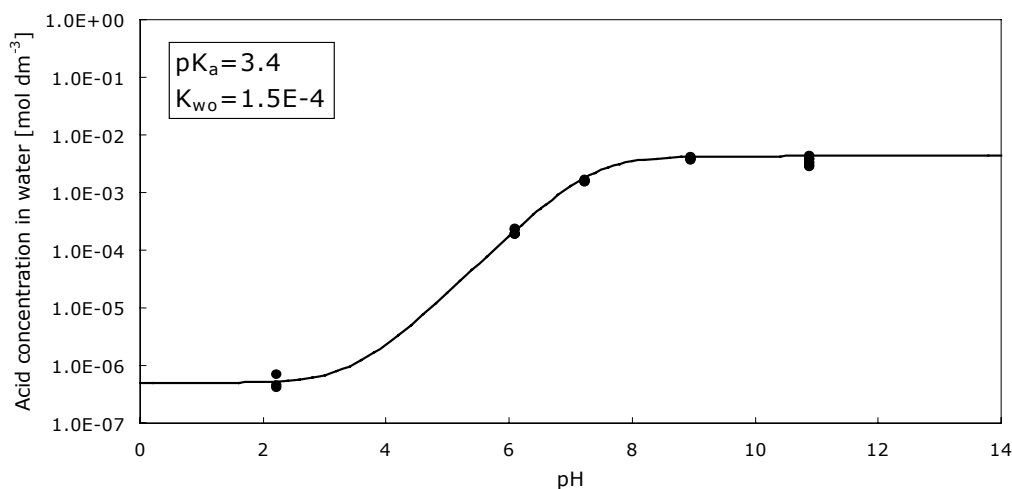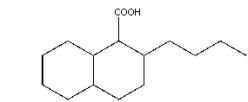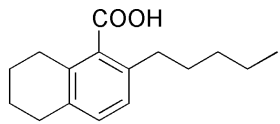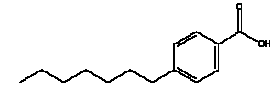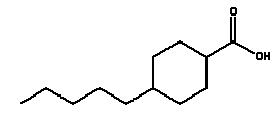

Figure 7.9   pH versus total concentration of C41a1 in the water phase. The theoretical model (line) is fitted to the experimental points.

C42, C7a1 and C51 were investigated at a higher acid concentration than C41a1. For these acids, the experimental determined points at pH 2, 6 and 7 were used. The model could not describe the concentrations at pH 9 and 11. It is believed that the reason for the deviation between the model and the experimental points at high pH is the formation of micelles and reversed micelles. These processes will enhance the complexity of the system, and a detailed investigation is needed in order to map all the equilibria. Partitioning experiments were performed at pH 9 with variable total acid concentration. The results from this study showed that the relative deviation from the model decreased with decreasing total acid concentration. This indicates that in dilute solutions, it is sufficient to account for the dissociation and partitioning of undissociated acid monomers in order to get a good description of the system, also at higher pH. The values for K_{wo} and pK_a for the carboxylic acids are given in Table 7.2.

Table 7.2 Partitioning and acidic constants for naphthenic acid model compounds

Shortname	Structure	Concentration [mol dm^{-3} water]	pK_a	K_{wo}
[C42]		3.0E-2	4.9	3.0E-5
[C41a1]		3.3E-3	3.4	1.5E-4
[C7a1]		3.3E-2	5.0	1.2E-4
[C51]		3.3E-2	5.1	8.0E-5

The K_{wo}-values are of the same order as the crude oil naphthenic acid for C42 and C7a1. For C41a1 the determined value of K_{wo} (1.5E-4) is higher than determined for crude oil naphthenic acids with two rings (2.3E-5). This is reasonable since the aromatic ring causes the molecule to be more hydrophilic. The K_{wo}-value for C51 is lower than for crude oil acids with the same number of carbon atoms. This may be explained by the fact that the structure of C51 differs from the crude oil naphthenic acids in that the acid group is attached directly to the ring. Analyses of crude oil naphthenic acids have indicated that the carboxylic acid group generally is attached to a ring with a short side

chain [33]. The pK_a for the acids C41a1 and C7a1 was determined as 3.4 and 5.0, respectively. For C7a1, being an aromatic acid, a value of 5.0 is unexpectedly high and probably not a correct pK_a-value. The reason for this high value might be that other equilibria are of importance also at lower pH values for this acid. The saturated C51 and C42 have pK_a-values in the same order as the crude oil naphthenic acids.

Interfacial activity of naphthenic acids

The interfacial tension between water and different hydrocarbon phases were investigated for several different naphthenic acids. Interfacial tension between heptane/toluene (50:50 by volume), containing 5.3E-5M of different naphthenic acids, and water are plotted as a function of pH in Figure 7.10. The volume of water was equal to the volume of hydrocarbon phase.
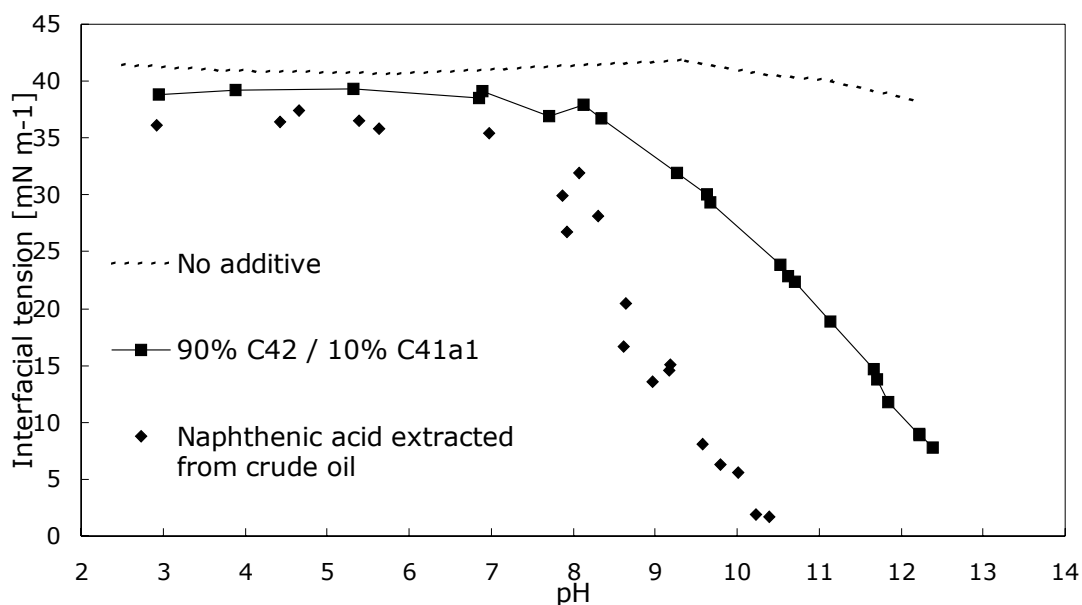

Figure 7.10 Interfacial tension between heptane/toluene, containing 5.3E-5M of different naphthenic acids, and water as a function of pH. Structures for C42 and C41a1 are given in Table 7.2.

At low pH the molecules at the oil/water interface will be unionized giving rise to a interfacial tension, γ_1. At high pH the interface will consist of dissociated acid molecules and it is seen from Figure 7.10 that the interfacial tension approach a value close to 0 for full dissociation. If it is assumed that the lowering of interfacial tension is directly related to ionization, the amounts of dissociated and undissociated acid at the interface are equal when the interfacial tension is equal to ½ γ_1. For C42 this occurs at pH=10.4. . It is assumed that the presence of 10% C41a1 do not cause a significant different interfacial

behaviour than if 100% was 2C4. Micellisation will most likely not occur in this dilute system (5.3E-5 mol acid / dm^3 water) and it can be shown that the concentration of ionised and unionised C42 will be equal in the bulk phases at pH=pK_a+pK_{wo}=9.4. Hence, in order to have equal amounts of the two acid forms at the interface, the concentration of dissociated acid must dominate over the concentration of undissociated acid in the bulk phases. This fact can be explained in term of the electrical double-layer. The pH close to the oil/water interface will be less than the bulk pH.

The reduction in interfacial tension sets in at a lower pH for the crude oil naphthenic acid. This is believed to be due to the presence of low molecular weight naphthenic acid that dissociates at the interface at lower pH.

Paper V

In Paper V, near infrared spectroscopy (NIR) was introduced as a method to study the formation of calcium naphthenate particles at elevated pH.

Naphthenic or fatty acids were dissolved in water at high pH (11.2-11.5). Upon addition of Ca^{2+}-solution the nucleation period and particle growth was monitored. The near infrared spectra experience a baseline elevation due to the formation and growth of calcium naphthenate particles. The use of NIR to detect particles sizes is explained in Chapter 6.2 (page 27).

Figure 7.11 shows the square root of the optical density (OD) at 1280 nm vs. time for experiments with a naphthenic acid labelled 1a1C4. The structure of 1a1C4 is given in the same figure.
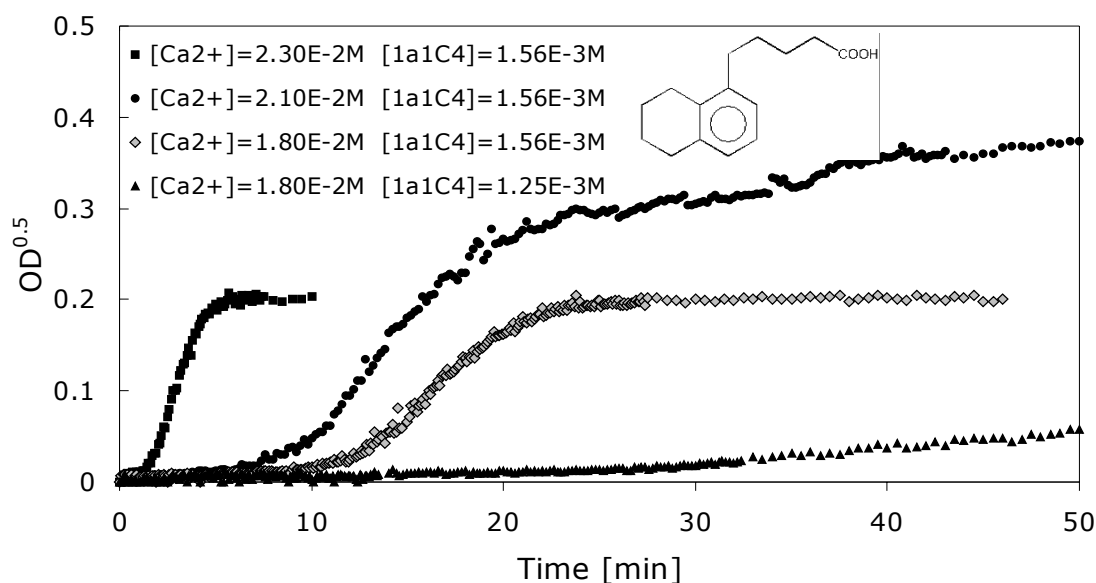
Figure 7.11 (Optical density)$^{0.5}$ at 1280 nm vs. time for different concentration of Ca^{2+} and 1a1C4.

The reason for plotting the square root of OD is that OD depends on radii[6] or volume[2] of the particles. Hence, change in the square root of OD can serve as a measurement of change in the total volume of precipitate. The square root of OD is directly proportional to the particle volume in systems consisting of a constant number of monodisperse particles. In the systems investigated, with polydisperse particles, the larger particles will govern the resulting OD since they contribute much more to OD than the small particles.

The number of particles is also unknown. Nevertheless, the curves give a good qualitative description of the calcium naphthenate formation.

Induction period

The induction period is the period where nucleation and growth of nuclei to a detectable size occurs. By assuming that the induction period is inverse proportional to the rate of nucleation, information about the nucleation process can be extracted. The induction period will then depend on the supersaturation according to Equation 7.4.

$$\log t_{ind} \propto \frac{\gamma^3}{T^3 (\log S)^2} \qquad (7.4)$$

In Figure 7.12, the logarithm of the induction period for systems consisting of 1a1C4 is plotted versus $(\log S)^{-2}$.
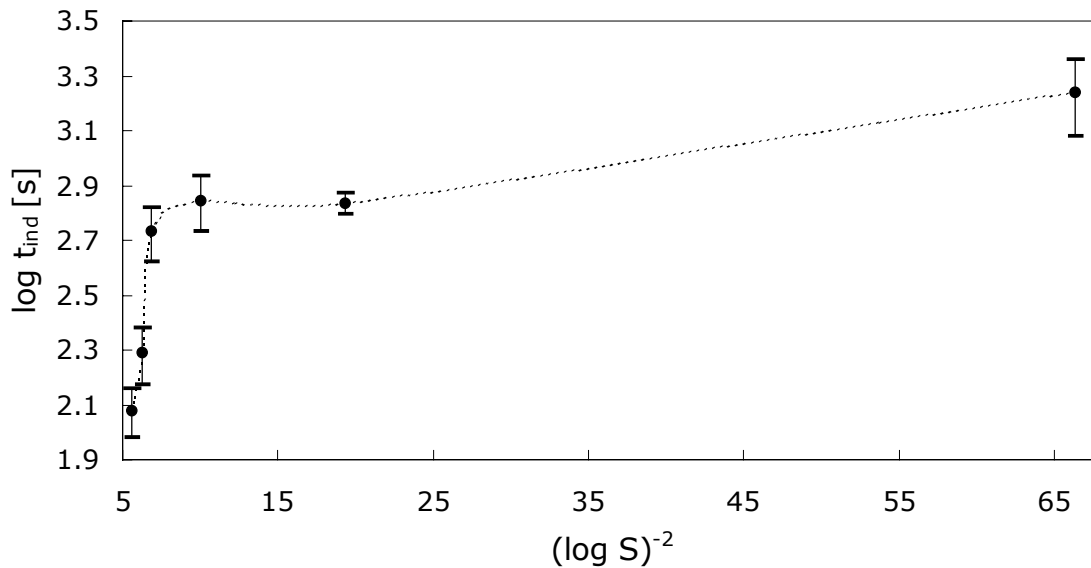
Figure 7.12 The logarithm of the induction period as a function of $(\log S)^{-2}$ for 1a1C4.

For ideal homogeneous nucleation, the plot would give a straight line according to Equation 7.4. At high supersaturations (to the left in the figure) log t_{ind} depends linearly on $(\log S)^{-2}$. A sudden decrease in the slope of the curve is then seen when approaching lower levels of supersaturation. This indicates a change in the interfacial tension between the solid and the water. The change in the curve at $(\log S)^{-2} \sim 10$ is most likely due to a transition from heterogeneous to homogeneous nucleation. At high supersaturation, the

nucleation is homogeneous and at lower supersaturation the nucleation becomes heterogeneous. The reason for this is that the concentration of impurities, leading to heterogeneous nucleation, will be constant in the system independently of the supersaturation. Since the rate of homogeneous nucleation is lower for lower supersaturations, the heterogeneous nucleation process will dominate.

The NIR-technique presented here can measure induction periods when it lasts for a certain time. When the induction period is less than about 5 seconds, difficulties arise. The mixing time of the solutions with the reactants can in this case be comparable with or exceed the measured induction period. In the experiments performed here, 10-20 seconds were allowed for the addition of calcium to the solution with carboxylic acid. In this case, if the induction period is determined to a value under 30s, the uncertainty will be large. If the Ca^{2+}-solution is added too fast, there is a chance that high local concentration of Ca^{2+} can initiate the precipitation.

Growth period

For all the systems investigated, higher concentration of acid and calcium ions led to an increase in the slope of the OD versus time curves after the induction period, representing an increase in the rate of reaction. In Figure 7.13, the slope of $OD^{0.5}$ versus time, representing the rate of crystallization, is plotted as a function of $(S-1)^2$ for 1a1C4. S is the supersaturation defined by Equation 5.3 (page 21).
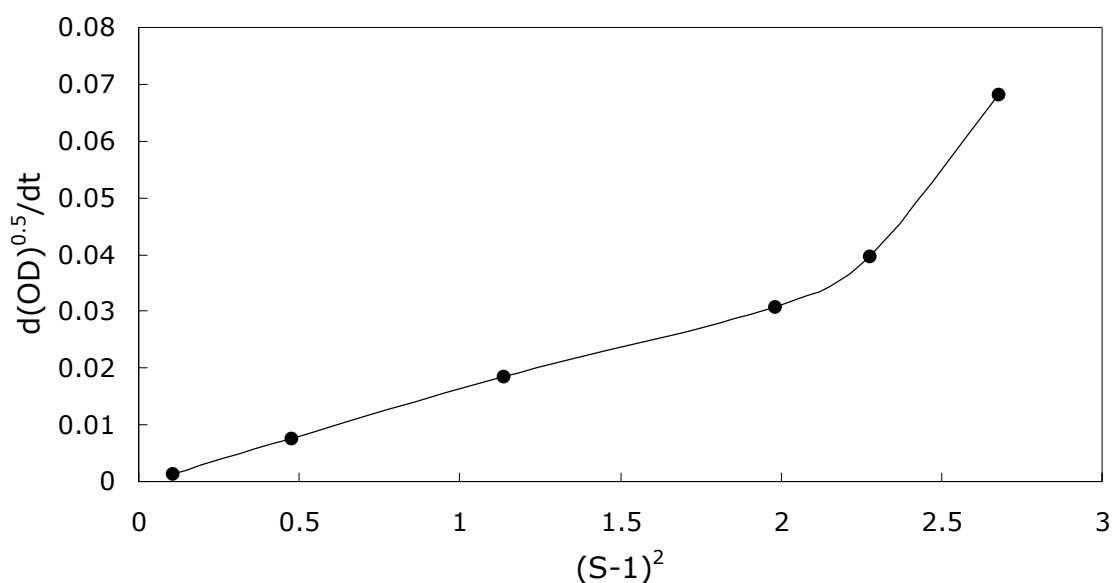

Figure 7.13 d($OD^{0.5}$)/dt versus $(S-1)^2$ for 1a1C4.

A linear relationship is seen for the lower supersaturations. The slope of the curve increases for higher supersaturations. The increase in the slope occurs at the same supersaturation level (S~1.4) as were the dependence of log t_{ind} versus (log S)$^{-2}$ changes in Figure 7.12. It was suggested that a transition from heterogeneous to homogeneous nucleation occurred at S~1.4. If the nucleation process is heterogeneous the number of nucleus will be considerable lower than if homogeneous nucleation occurs.

For the other carboxylic acids tested (Table 7.3), $dOD^{0.5}/dt$ depended on $(S-1)^n$, were n is in the range 0.2-0.5. This means that the change in $dOD^{0.5}/dt$ at higher levels of supersaturation was less than for lower levels of supersaturation. This is the opposite of what was found for the naphthenic acid, labelled 1a1C4 (Figure 7.13).

Independently of whether a transition from heterogeneous to homogeneous nucleation occurs, the number of particles is expected to be higher for higher levels of supersaturations. The reason for this is that supersaturation affects the nucleation rate more than the growth rate [128]. This fact can affect the resulting $dOD^{0.5}/dt$ in different ways.

The sizes of the particles are more important than the number for the response in OD. For a given value of $dOD^{0.5}/dt$, the actual crystallization rate will be higher for systems with a large number of small particles than for a system consisting of a less number of large particles. It is therefore expected that when going from a system were the number of particles are low, to a system with a large number of particles, the dependency of $dOD^{0.5}/dt$ on (S-1) would decrease. Evidence for the formation of smaller particles at high supersaturation can be found by studying Figure 7.11. The curve with the highest supersaturation (to the left) reaches a final OD lower than expected. The final value increases with supersaturation for the other experiments. This indicates that even if the experiment with highest supersaturation yield the highest amount of solid material, the particles are small and therefore their scattering efficiency is bad.

The presence of a large number of small particles, rather than a small number of large particles can also lead to an increased effect in $dOD^{0.5}/dt$. The rate of agglomeration will obviously depend on the number of particles. When particles agglomerate, OD will increase even though the volume of precipitated material remains constant. Ostwald ripening may also be of importance. Ostwald ripening is the process in which small particles dissolve and the solute deposits subsequently on the larger particles. The driving force of this process is the lowering of the total surface energy. The total surface area increases with decreasing number of particles. It is expected that this will increase
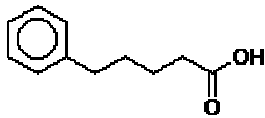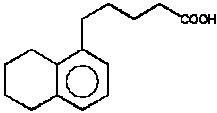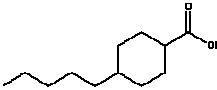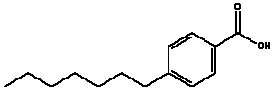
the rate of crystallization for the smaller particles. In all cases, the results may be influenced by the fact that the largest particles will govern the resulting OD. Different influence of the mechanisms may explain the different behaviour of $dOD^{0.5}/dt$ versus supersaturation for 1a1C4 and the other acids.

The particles tendency to agglomerate upon collision may be affected by the ratio of Ca^{2+} to naphthenic acid. An excess of one of the component may lead to an electrostatically stabilization that it sufficient to prevent the particles from agglomeration. However, this mechanism was not prominent enough to explain the results obtained in this study.

Estimation of solubility products

As the amount of Ca^{2+} and carboxylic acid is decreased, the response on the NIR-measurements will eventually become zero. The concentration at which this happens can be used to estimate the solubility products, K_{sp}, for the different calcium soaps. The solubility products were found by extrapolating a curve of $dOD^{0.5}/dt$ versus the ion concentration product to $dOD^{0.5}/dt=0$. The K_{sp}-values are given in Table 7.3 and are plotted versus the molecular weight of the acidic form in Figure 7.14.

Table 7.3 Solubility products for the calcium salt of different carboxylic acids. (Detailed information of the acids is given in Table 1)

Shortname	Chemical structure	K_{sp} [mol^3 dm^{-3}]
[a1C4]		6.1E-8
[1a1C4]		2.8E-8
[C51]		2.2E-9
[C7a1]		1.2E-10
[C16]	$CH_3(CH_2)_{14}COOH$	6.4E-13
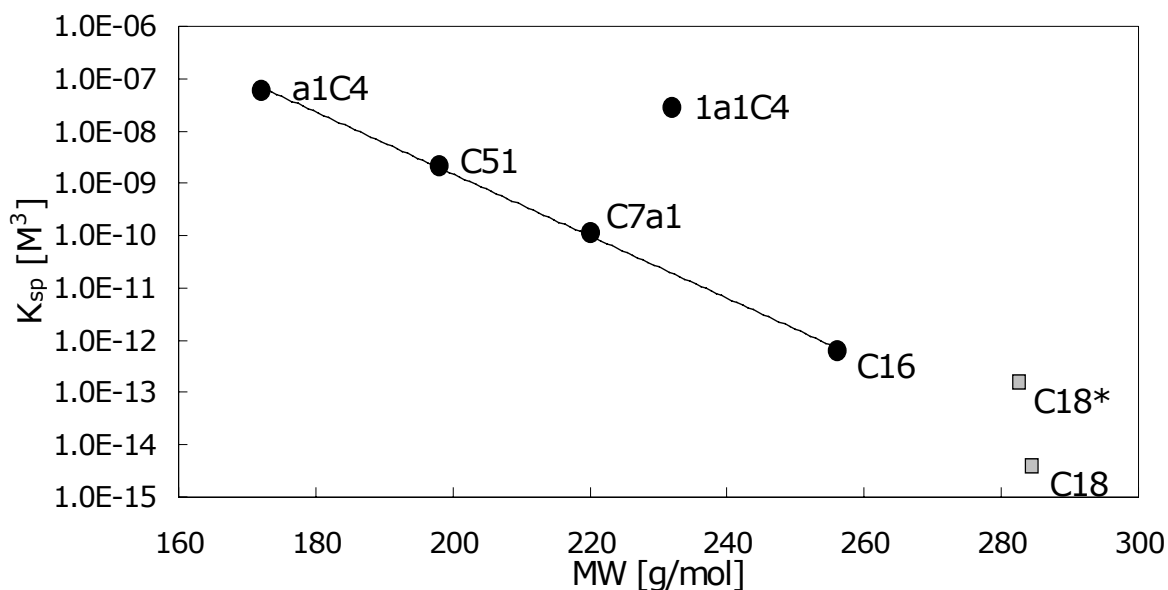
Figure 7.14 Solubility products for different carboxylic acids. Values for calcium stearate (C18) and calcium oleate (C18*) are from Beneventi *et al.* [129]. The other abbreviations are explained in Table 7.3.

A method for studying the precipitation of calcium naphthenate in an aqueous phase was presented in Paper V. It is shown that the induction period can be determined. Information about the rate of reaction for particle growth can be obtained. However its qualitative value is uncertain. This is because the number of particles and the total amount of precipitate is not known at a given time. In addition the larger particles will govern the resulting scattering contribution. The rate of nucleation versus the rate of growth, agglomeration, particles sizes and Ostwald ripening will influence the results. Solubility products can also be estimated. Although the method has some quantitative limitations, it is obvious that it has a qualitative advantage, for example to study the efficiency of different calcium naphthenate inhibitors.

8   Concluding Remarks

The main focus of this thesis has been to increase the understanding of acidic crudes, formation of calcium naphthenate deposits and the emulsion behaviour in these systems.

The equilibria involved in a water/oil/naphthenic acid system have been investigated and it was found that the naphthenic acids in crude oil have pK_a-values around 4.9. Naphthenic acids tend to form micelles at higher pH. Due to the many equilibria involved in a water/oil/naphthenic acid system, especially at high pH, the results from this study only gives a first basic in understanding the chemistry. A more in-detail study of the different equilibria involved is of great interest for further work.

The results obtained in this doctoral work clearly indicate that the naphthenic acids are of importance in the formation of undesirable emulsions in crude oil production offshore. The naphthenic acids will stabilize water-continuous emulsions electrostatically at higher pH. It was shown that a multilayer of carboxylic acids can stabilize w/o emulsions in a combined mechanism with asphaltenes. A combination of 60% asphaltene particles and 40% D-phase gave the most stable w/o-emulsions. This investigation verifies the importance of D-phase stabilization in combination with asphaltene particles in systems with acidic heavy crude oil (including bitumen) and water. Stable monolayers of calcium naphthenate are formed when the pH is sufficiently high. This monolayer can stabilize water droplets against coalescence. Since asphaltenes are the dominant contributor to emulsion stability in crude oil systems, the ability of the naphthenic acids to disintegrate asphaltenes in solution will be important for the emulsion stability. The disintegration effect of several different naphthenic acids and other amphiphiles were investigated.

The formation of calcium naphthenates in crude oil equipment is a potential threat to offshore production of acidic crudes. The ability to know at which conditions formation of naphthenate deposits can occur is of great importance in order to avoid costly shutdown periods. It is shown that near infrared spectroscopy can be used as a method to get a first basic description of the formation mechanism. The method can also be used to estimate solubility products.

References

1. Goldszal, A., Hurtevent, C. and Rousseau, G. *Scale and Naphthenate Inhibition in Deep-Offshore Fields*. in *SPE Oilfield Scale Symposium,* SPE74661 1-11. 2002. Aberdeen, UK.

2. Rousseau, G., Zhou, H. and Hurtevent, C. *Calcium carbonate and naphthenate mixed scale in deep-offshore fields*. in *SPE Oilfield Scale Symposium,* SPE68307 1-8. 2001. Aberdeen, UK.

3. Slavcheva, E., Shone, B. and Turnbull, A., *Review of naphthenic acid corrosion in oil refining*, Br Corros J, **34**(2) (1999) 125-131.

4. Babaian-Kibala, E., *Phosphate Ester Inhibitors Solve Naphthenic Acid Corrosion Problems*, Oil Gas J, **92**(9) (1994) 31-35.

5. Babaian-Kibala, E., Craig, H. L., Rusk, G. L., Blanchard, K. V., Rose, T. J., Uehlein, B. L., Quinter, R. C. and Summers, M. A., *Naphthenic Acid Corrosion in Refinery Settings*, Mater Performance, **32**(4) (1993) 50-55.

6. Piehl, R. L., *Naphthenic Acid Corrosion in Crude Distillation Units*, Mater Performance, **27**(1) (1988) 37-43.

7. Sjöblom, J., Johnsen, E. E., Westvik, A., Bergflødt, L., Auflem, I. H., Havre, T. E. and Kallevik, H. *Colloid Chemistry in Sub Sea Petroleum and Gas Processing*. in *The 2nd International Conference on Petroleum and Gas Phase Behaviour and Fouling,* 2000, August 27-31. Copenhagen, Denmark.

8. Márquez, M. L. *Interfacial activity of of native acids in heavy crude oil*. in *AICHE Spring National Meeting, Session T6005,* 99sp 56d 1999, March 14-18. Houston, Texas.

9. Acevedo, S., Escobar, G., Ranaudo, M. A., Khazen, J., Borges, B., Pereira, J. C. and Méndez, B., *Isolation and characterization of low and high molecular weight acidic compounds from Cerro Negro extraheavy crude oil. Role of these acids in the interfacial properties of the crude oil emulsions*, Energy Fuels, **13**(2) (1999) 333-335.

10. Pathak, A. K. and Kumar, T. *Study of Indigenous Crude Oil Emulsions and their Stability*. in *Proceedings of PETROTECH-95, Technology trends in oil industry,* 217-224. 1995. New Dehli.

11. Rogers, V. V., Wickstrom, M., Liber, K. and MacKinnon, M. D., *Acute and subchronic mammalian toxicity of naphthenic acids from oil sands tailings*, Toxicol Sci, **66**(2) (2002) 347-355.

12. Friman, R. and Stenius, P., *Association equilibria and micelle formation of fatty acid sodium salts. V. Investigation of branched chain salts by vapour pressure osmometry*, Acta Chem Scand Ser A, **A32**(4) (1978) 289-296.

13. Stenius, P., *Association equilibria and micelle formation of fatty acid sodium salts. II. An investigation of straight-chain salts by vapour pressure osmometry*, Acta Chem Scand, **27**(9) (1973) 3435-3451.

14. Stenius, P., *Association equilibria and micelle formation of fatty acid sodium salts. III. The Association of sodium butyrate at 40° in 3M Na(Cl)*, Acta Chem Scand, **27**(9) (1973) 3452-3466.

15. Stenius, P., *Association equilibria and micelle formation of fatty acid sodium salts. I. A survey of potentiometric measurements on salts with 2-6 carbon atoms at high ionic strength*, Acta Chem Scand, **25**(6) (1971) 2232-2250.

16. Skurtveit, R., Sjöblom, J. and Høiland, H., *Emulsions under elevated temperature and pressure conditions. I. The model system water-hexadecanoic acid-sodium hexadecanoate-decane at 70°C*, J Colloid Interface Sci, **133**(2) (1989) 395-403.

17. Sjöblom, J., Lindberg, R. and Friberg, S. E., *Microemulsions - phase equilibria characterization, structures, applications and chemical reactions*, Adv Colloid Interface Sci, **65** (1996) 125-287.

18. Gillberg, G., Lehtinen, H. and Friberg, S., *NMR and IR investigation of the conditions determining the stability of microemulsions*, J Colloid Interface Sci, **33**(1) (1970) 40-53.

19. Friberg, S. E., Mandell, L. and Ekwall, P., *Solutions of alkali soaps and water in fatty acids. III. Ir and N. M. R. investigations*, Kolloid Z Z Polym, **233**(1-2) (1969) 955-962.

20. Lindman, B. and Wennerstroem, H., *Micelles. Amphiphile aggregation in aqueous solution*, Top Curr Chem, **87** (1980) 1-83.

21. Wennerström, H. and Lindman, B., *Micelles. Physical chemistry of surfactant association*, Phys Rev, **52**(1) (1979) 1-86.

22. Ekwall, P., Danielsson, I. and Stenius, P. *Aggregation in surfactant systems*. in *MTP Int Rev Sci Phys Chem Ser 1, 7* 97-145. 1972. London: Butterworths.

23. Ekwall, P., *Composition, properties, and structures of liquid crystalline phases in systems of amphiphilic compounds*, in *Adv Liq Cryst*, G.H. Brown, Editor. 1975, Academic Press: New York. p. 1-142.

24. Ekwall, P., Mandell, L. and Fontell, K., *Solubilization in micelles and mesophases and the transition from normal to reversed structures*, Mol Cryst Liquid Cryst, **8** (1969) 157-213.

25. Brient, J. A., Wessner, P. J. and Doyle, M. N., *Naphthenic Acids*, in *Encyclopedia of Chemical Technology*, Kirk-Othmer, Editor. 1995, John Wiley & Sons: New York. p. 1017-1029.

26. Meredith, W., Kelland, S.-J. and Jones, D. M., *Influence of biodegradation on crude oil acidity and carboxylic acid composition*, Org Geochem, **31**(11) (2000) 1059-1073.

27. Fan, T.-P., *Characterization of Naphthenic Acids in Petroleum by Fast-Atom-Bombardment Mass-Spectrometry*, Energy Fuels, **5**(3) (1991) 371-375.

28. Hsu, C. S., Dechert, G. J., Robbins, W. K. and Fukuda, E. K., *Naphthenic Acids in Crude Oil Characterized by Mass Spectrometry*, Energy Fuels, **14** (2000) 217-223.

29. Koike, L., Reboucas, L. M. C., Reis, F. d. A., Marsaioli, A. J., Richnow, H. H. and Michaelis, W., *Naphthenic acids from crude oils of Campos Basin*, Org Geochem, **18**(6) (1992) 851-860.

30. Tomczyk, N. A., Winans, R. E., Shinn, J. H. and Robinson, R. C., *On the nature and origin of acidic species in petroleum. 1. Detailed acid type distribution in a California crude oil*, Energy Fuels, **15**(6) (2001) 1498-1504.

31. Qian, K., Robbins, W. K., Hughey, C. A., Cooper, H. J., Rodgers, R. P. and Marshall, A. G., *Resolution and identification of elemental compositions for more than 3000 crude acids in*

heavy petroleum by negative-ion microelectrospray high-field Fourier Transform ion cyclotron resonance mass spectrometry, Energy Fuels, **15**(6) (2001) 1505-1511.

32. Headley, J. V., Peru, K. M., McMartin, D. W. and Winkler, M., *Determination of dissolved naphthenic acids in natural waters by using negative-ion electrospray mass spectrometry*, J AOAC Int, **85**(1) (2002) 182-187.

33. Robbins, W. K., *Challenges in the characterization of naphthenic acids in petroleum*, Prepr - Am Chem Soc, Div Pet Chem, **43**(1) (1998) 137-140.

34. Brient, J. A., *Commercial utility of naphthenic acids recovered from petroleum distillates*, Prepr - Am Chem Soc, Div Pet Chem, **43**(1) (1998) 131-133.

35. Roussis, S. G. and Lawlor, L. J., *Direct determination of acid distributions in crudes and crude fractions,* Exxonmobil Research and Engineering Company, Patent: WO0248698, USA, 2002.

36. Goodman, D. S., *The Distribution of Fatty Acids between n-Heptane and Aqueous Phosphate Buffer*, J Am Chem Soc, **80** (1958) 3887-3892.

37. Suzuki, K., Taniguchi, Y. and Watanabe, T., *Effect of pressure on the dimerization of carboxylic acids in aqueous solution*, J Phys Chem, **77**(15) (1973) 1918-1922.

38. Takeda, K., Yamashita, H. and Akiyama, M., *Dimerization of some carboxylic acids in organic phases*, Solvent Extr Ion Exch, **5**(1) (1987) 29-53.

39. Somasundaran, P., Ananthapadmanabhan, K. P. and Ivanov, J. B., *Dimerization of Oleate in Aqueous Solutions*, J Colloid Interface Sci, **99**(1) (1984) 128-135.

40. Mukerjee, P., *Dimerization of Anions of Long-Chain Fatty Acids in Aqueous Solutions and the Hydrophobic Properties of the Acids*, J Phys Chem, **69** (1965) 2821.

41. Leo, A., Hansch, C. and Elkins, D., *Partition Coefficients and Their Uses*, Chem Rev, **71** (1971) 525-616.

42. Hartridge, H. and Peters, R. A., *Interfacial Tension and Hydrogen-Ion Concentration*, Proc R Soc A, **101** (1922) 348-367.

43. Peters, R. A., *Interfacial Tension and Hydrogen-ion Concentration*, Proc Roy Soc A, **131** (1931) 140-154.

44. Danielli, J. F., *The Relations between Surface pH, Ion Concentrations and Interfacial Tension*, Proc R Soc A, **122** (1937) 155-174.

45. Cratin, P. D., *Mathematical modelling of some pH-dependent surface and interfacial properties of stearic acid*, J Dispersion Sci Technol, **14**(5) (1993) 559-602.

46. Cratin, P. D., *Surface and Interfacial Dissociation Constants, Apparent vs. Absolute*, Colloids Surf, A, **89**(2/3) (1994) 103-108.

47. Rudin, J. and Wasan, D. T., *Mechanism of lowering interfacial tension in alkali/acidic systems. 2. Theoretical studies*, Colloids Surf, **68** (1992) 81-94.

48. Rudin, J. and Wasan, D. T., *Mechanism of lowering interfacial tension in alkali/acidic oil systems. 1. Experimental studies*, Colloids Surf, **68** (1992) 67-79.

49. Standal, S. H., Blokhus, A. M., Haavik, J., Skauge, A. and Barth, T., *Partion Coefficients and Interfacial Activity for Polar Components in Oil/Water Model Systems*, J Colloid Interface Sci, **212** (1999) 33-41.

50. Spildo, K. and Høiland, H., *Interfacial Properties and Partitioning of 4-Heptylbenzoic Acid between Decane and Water*, J Colloid Interface Sci, **209** (1999) 99-108.

51. Strassner, J. E., *Effect of pH on Interfacial Films and Stability of Crude Oil-Water Emulsions*, J Pet Technol, **20**(3) (1968) 303-312.

52. Ovalles, C., Carcia, M. d. C., Lujano, D., Aular, W., Barmúdez, R. and Cotte, E., *Structural/interfacial activity relationships and thermal stability studies of Cerro Negro crude oil and its acid, basic and neutral fractions*, Fuel, **77**(3) (1998) 121-126.

53. Skurtveit, R., *Surfactant Phase Behaviour and Aggregation in Microemulsions in Relation to Emulsion Stability*, doctoral thesis, Department of Chemistry, University of Bergen, 1992, Bergen.

54. Horváth-Szabó, G., Czarnecki, J. and Masliyah, J., *Liquid Crystals in Aqueous Solutions of Sodium Naphthenates*, J Colloid Interface Sci, **236** (2001) 233-241.

55. Mukerjee, P. and Mysels, K. J., *Critical Micelle Concentration of Aqueous Surfactant Systems*. NSRDS-NBS. Vol. 36. 1971, Washington.

56. Gu, T. and Sjöblom, J., *Surfactant structure and its relation to the Krafft point, cloud point and micellization: Some empirical relationships*, Colloids Surf, **64**(1) (1992) 39-46.

57. Theander, K. and Pugh, R.-J., *The influence of pH and temperature on the equilibrium and dynamic surface tension of aqueous solutions of sodium oleate.*, J Colloid Interface Sci, **239**(1) (2001) 209-216.

58. Horváth-Szabó, G., Masliyah, J. and Czarnecki, J., *Phase Behavior of Sodium Naphthenates, Toluene and Water*, J Colloid Interface Sci, **242** (2001) 247-254.

59. Horváth-Szabó, G., Masliyah, J. and Czarnecki, J., *Emulsion Stability Based on Phase Behavior in Sodium Naphthenates Containing Systems: Gels with a High Organic Solvent Content*, J Colloid Interface Sci, (2002) Accepted.

60. Horváth-Szabó, G., Czarnecki, J. and Masliyah, J., *Sandwich Structures at Oil-Water Interfaces under Alkaline Conditions*, J Colloid Interface Sci, **253**(2) (2002) 427-434.

61. Friberg, S., Mandell, L. and Larsson, M., *Medomorphous Phases, a Factor of Importance for the Properties of Emulsions*, J Colloid Interface Sci, **29** (1969) 155-161.

62. Friberg, S., *Liquid Crystalline Phases in Emulsions*, J Colloid Interface Sci, **37** (1971) 291-295.

63. Friberg, S., Jansson, P. O. and Cedreberg, E., *Surfactant Association Structure and Emulsion Stability*, J Colloid Interface Sci, **55** (1976) 614-623.

64. Friberg, S. and Solans, C., *Surfactant Association Structures and the Stability of Emulsions and Foams*, Langmuir, **2** (1986) 121.

65. Speight, J. G., *The chemistry and technology of petroleum*. 1999, New York.: Marcel Dekker.

66. Dickie, J. P. and Yen, T. F., *Macrostructures of the Asphaltic Fractions by Various Instrumental Methods*, Anal. Chem, **39** (1967) 1847-1852.

67. Mitchell, D. L. and Speight, J. G., *The solubility of asphaltenes in hydrocarbon solvents*, Fuel, **52** (1973) 149-152.

68. Strausz, O. P., Mojelsky, T. W. and Lown, E. M., *The molecular structure of asphaltene: an unfolding story*, Fuel, **71** (1992) 1355-1363.

69.   Aske, N., *Characterisation of Crude Oil Components, Asphaltene Aggregation and Emulsion Stability by means of Near Infrared Spectroscopy and Multivariate Analysis*, doctoral thesis, Department of Chemical Engineering, Norwegian University of Science and Technology, 2002, Trondheim.

70.   Kallevik, H., *Characterisation of Crude Oil and Model Oil Emulsions by means of Near Infrared Spectroscopy and Multivariate Analysis*, doctoral thesis, Department of Chemistry, University of Bergen, 1999, Bergen.

71.   Groenzin, H. and Mullins, O. C., *Molecular Size and Structure of Asphaltenes from Various Sources*, Energy Fuels, **14**(3) (2000) 677-684.

72.   Aske, N., Kallevik, H. and Sjöblom, J., *Determination of Saturate, Aromatic, Resin and Asphaltenic (SARA) Components in Crude Oils by Means of Infrared and Near-Infraared Spectroscopy*, Energy Fuels, **15**(5) (2001) 1304-1312.

73.   McLean, J. D. and Kilpatrick, P. K., *Effect of Asphaltenes Solvency on Stability of Water-in-Crude-Oil Emulsions*, J Colloid Interface Sci, **189** (1997) 242-253.

74.   Gonzalez, G. and Moreira, M. B. C., *The wettability of mineral surfaces containing adsorbed asphaltenes*, Colloids Surf, **58**(3) (1991) 293-302.

75.   Chang, C.-L. and Fogler, S. H., *Stabilization of Asphaltenes in Aliphatic Solvents Using Alkylbenzene-Derived Amphiphiles. 2. Study of the Asphaltene-Amphiphile Interactions and Structures Using Fourier Transform Infrared Spectroscopy and Small-Angel X-ray Scattering Techniques*, Langmuir, **10** (1994) 1758-1766.

76.   Chang, C.-L. and Fogler, S. H., *Stabilization of Asphaltenes in Aliphatic Solvents Using Alkylbenzene-Derived Amphiphiles. 1. Effect of the Chemical Structure of Amphiphiles on the Asphaltenes Stabilization*, Langmuir, **10** (1994) 1749-1757.

77.   Östlund, J.-A., Nydén, M., Auflem, I. H. and Sjöblom, J., *Interactions between asphaltenes and naphthenic acids*, Energy Fuel, (2002) Accepted.

78.   Auflem, I. H., Havre, T. E. and Sjöblom, J., *Near-IR study on the dispersive effects of amphiphiles and naphthenic acids on asphaltenes in model heptane-toluene mixtures*, Colloid Polym Sci, **280**(8) (2002) 695-700.

79.   Israelachvili, J., *The Science and Applications of Emulsions -an Overview*, Colloids Surf A, **91** (1994) 1-8.

80.   Schramm, L. L., *Emulsions, Fundamentals and Applications in the Petroleum Industry*. Advances in Chemistry Ser. Vol. 231. 1992, Washington DC: American Chemical Society.

81.   Sjöblom, J., Johnsen, E. E., Westvik, A., Ese, M.-H., Djuve, J., Auflem, I. H. and Kallevik, H., *Demulsifiers in the Oil Industry*, in *Encyclopedic Handbook of Emulsion Technology*, J. Sjøblom, Editor. 2000, Marcel Dekker Inc: New York. p. 595-619.

82.   Kilpatrick, P. K. and Spiecker, P. M., *Asphaltene Emulsions*, in *Encyclopedic Handbook of Emulsion Technology*, J. Sjöblom, Editor. 2001, Marcel Dekker, Inc.: New York. p. 707-730.

83.   Ese, M.-H., Sjöblom, J., Djuve, J. and Pugh, R., *An atomic force microscopy study of asphaltenes on mica surfaces. Influence of added resins and demulsifiers*, Colloid Polym Sci, **278**(6) (2000) 532-538.

84. McLean, J. D. and Kilpatrick, P. K., *Effects of asphaltene aggregation in model heptane-toluene mixtures on stability of water-in-oil emulsions*, J Colloid Interface Sci, **196**(1) (1997) 23-34.

85. Spiecker, P. M., *The Impact of Asphaltene Chemistry and Solvation on Emulsion and Interfacial Film Formation*, Ph. D. thesis, Department of Chemical Engineering, North Carolina State University, 2001, Raleigh.

86. Pickett, J. M. and Ellway, K. A., *Gels in soap stabilized emulsions*, J Pharm Pharmacol, **28**(8) (1976) 625-628.

87. Mendez, Z., Anton, R. E. and Salager, J.-L., *Surfactant-oil-water systems near the affinity inversion. Part XI . pH sensitive emulsions containing carboxylic acids.*, J Dispersion Sci Technol, **20**(30) (1999) 883-892.

88. Havre, T. E., Ese, M.-H., Sjöblom, J. and Blokhus, A. M., *Langmuir Films of Naphthenic Acids at Different pHs and Electrolyte Concentrations*, Colloid Polym Sci, **280**(7) (2002) 647-652.

89. Havre, T. E. and Sjöblom, J., *Emulsion Stabilization by means of Combined Surfactant Multilayer (D-phase) and Asphaltene Particles*, Colloids Surf A, (2002) Accepted.

90. Gallup, D. L., Smith, P. C., Chipponeri, J., Abuyazid, A. and Mulyono, D. *Formation & Mitigation of "Metallic Soap" Sludge, Attaka, Indonesia Field*. in *SPE International Conference on Health, Safety and Environment in Oil and Gas Exploration and Production,* SPE73960 1-16. 2002. Kuala Lumpur, Malaysia.

91. Poggesi, G., Hurtevent, C. and Buchart, D. *Multifunctional Chemicals for West African Deep Offshore fields*. in *SPE Oilfield Scale Symposium,* SPE74649 1-6. 2002. Aberdeen, UK.

92. Vindstad, J. E., Bye, A. S., Grande, K. V., Hustad, B. M., Hustvedt, E. and Nergård, B. *Fighting Naphthenate Deposition at the Statoil-Operated Heidrun Field*. in *5th SPE Oilfield Scale Symposium,* SPE80375 2003. Aberdeen, UK.

93. Allen, L. H., Sennett, P. S., Lapointe, C. L., Truitt, R. E. and Sithole, B. B., *Pitch deposition in newsprint mills using certain kaolin pigments*, Tappi Journal, **81**(7) (1998) 137-138.

94. Allen, L. H., *The importance of pH in controlling metal-soap deposition*, Tappi J, **71**(1) (1988) 61-64.

95. Ström, G., Stenius, P., Lindström, M. and Ödberg, L., *Surface chemical aspects of the behavior of soaps in pulp washing*, Nord Pulp Pap Res J, **5**(1) (1990) 44-51.

96. Lindström, M., Ödberg, L. and Stenius, P., *Resin and fatty acids in kraft pulp washing: physical state, colloid stability and washability*, Nord Pulp Pap Res J, **3**(2) (1988) 100-106.

97. Ödberg, L., Forsberg, S., McBride, G., Persson, M., Stenius, P. and Ström, G., *Surfactant behavior of wood resin components. Part 2. Solubilization in micelles of rosin and fatty acids*, Sven Papperstidn, **88**(12) (1985) R118-R125.

98. Stenius, P., Palonen, H., Ström, G. and Ödberg, L., *Micelle formation and phase equilibria of surface-active components of wood*, in *Surfactants Solution, (Proc Int Symp), 4th*, K.L. Mittal and B. Lindman, Editors. 1984, Plenum: New York, USA. p. 153-174.

99. Palonen, H. and Stenius, P., *Liquid crystalline phase behaviour of pitch components*, in *Ekman-Days 1981, Int. Symp. Wood Pulping Chem.* 1981, SPCI: Stocholm, Sweden. p. 100-102.

References

100. Palonen, H., Stenius, P. and Ström, G., *Surfactant behavior of wood resin components. The solubility of rosin and fatty acid soaps in water and in salt solutions*, Sven Papperstidn, **85**(12) (1982) R93-R99.

101. Havre, T. E., Sjöblom, J. and Vindstad, J. E., *Oil/water- Partitioning and Interfacial Behavior of Naphthenic Acids*, J Dispersion Sci Technol, (2002) Submitted.

102. Havre, T. E., *Near Infrared Spectroscopy as a Method for Studying Formation of Calcium Naphthenate*, Colloid Polym Sci (2002) Submitted.

103. Mullin, J. W., *Crystallization*. Fourth ed. 2001, Oxford: Butterworth-Heinemann.

104. Wu, W. and Nancollas, G. H., *The dissolution and growth of sparingly soluble inorganic salts: A kinetics and surface energy approach.*, Pure Appl Chem,, **70**(10) (1998) 1867-1872.

105. Matijevic, E., Leja, J. and Nemeth, R., *Precipitation phenomena of heavy metal soaps in aqueous solutions. I. Calcium oleate*, J Colloid Interface Sci, **22**(5) (1966) 419-429.

106. Young, S. L. and Matijevic, E., *Precipitation phenomena of heavy metal soaps in aqueous solutions. III. Metal laurates*, J Colloid Interface Sci, **61**(2) (1977) 287-301.

107. Børve, K. G. N., *Monolayer properties of interfacially active crude oil fractions and model systems*, doctoral thesis, Department of Chemistry, University of Bergen, 1991, Bergen.

108. Ese, M.-H., *Langmuir Film Properties of Indigenous Crude Oil Components. Influence of Demulsifiers*, doctoral thesis, Department of Chemistry, University of Bergen, 1999, Bergen.

109. KSV-Instuments-Ltd, *Langmuir and Langmuir-Blodgett Films : What and how?* Application note #107. 2000, Helsinki, Finland.

110. Petty, M. C., *Langmuir Blodgett Films : an introduction*. 1996, Cambridge: Cambridge University Press.

111. Aske, N., Kallevik, H., Johnsen, E. E. and Sjöblom, J., *Asphaltene Aggregation from Crude Oils and Model Systems Studied by High Pressure NIR Spectroscopy*, Energy Fuels, **16**(5) (2002) 1287-1295.

112. Mullins, O. C., *Asphaltenes in Crude Oil: Absorbers and/or Scatters in the Near-Infrared Region?*, Analytical Chemistry, **62** (1990) 508-514.

113. Kerker, M., *The Scattering of Light and Other Electromagnetic Radiation*. Physical Chemistry. A Series of Monographs, ed. E.M. Loebl. Vol. 16. 1969, New York: Academic Press. 666.

114. Gossen, P. D., MacGregor, J. F. and Pelton, R. H., *Composition and Particle Diameter for Styrene-Methyl Methacrylate Copolymer Latex using UV and NIR Spectroscopy*, Appl Spectrosc, **47**(11) (1993) 1852-1870.

115. Pasikatan, M. C., Steele, J. L., Spillman, C. K. and Haque, E., *Near infrared reflectance spectroscopy for online particle size analysis of powders and ground materials*, J Near Infrared Spectrosc, **9**(3) (2001) 153-164.

116. Frake, P., Gill, I., Luscombe, C. N., Rudd, D. R., Waterhouse, J. and Jayasorriya, U. A., *Near-infrared mass median particle size determination of lactose monohydrate, evaluating several chemometric approaches*, Analyst, **123**(10) (1998) 2043-2046.

117. Santos, A. F., Lima, E. L. and Pinto, J. C., *In-line evalution of average particle size in styrene suspension polymerizations using near-infrared spectroscopy*, J Appl Polym Sci, **70** (1998) 1737-1745.

118. Chen, T. Y., Mohammed, R. A., Bailey, A. I., Luckham, P. F. and Taylor, S. E., *Dewatering of crude oil emulsions 4. Emulsion resolution by the application of an electric field*, Colloids Surf A, **83** (1994) 273-284.

119. Aske, N., Kallevik, H. and Sjöblom, J., *Water-in-Crude Oil Emulsion Stability Studied by Critical Electric Field Measurements. Correlation to Physico-Chemical Parameters and Near Infrared Spectroscopy*, J Pet Sci Eng, **36** (2002) 1-17.

120. Kallevik, H., Kvalheim, O. M. and Sjöblom, J., *Quantitative determination of asphaltenes and resins in solution by means of near-infrared spectroscopy. Correlations to emulsion stability.*, J Colloid Interface Sci, **225**(2) (2000) 494-504.

121. Agilent-Technologies, *Basics of LC/MS*. Publication number: 5988-2045EN. 2001, USA.

122. Joos, P., *Theory on the collapse pressure of mixed insoluble monolayers with miscible components*, Bull Soc Chim Belg, **78**(3-4) (1969) 207-217.

123. Joos, P., Ruyssen, R., Minones Trillo, J., Garcia Fernandez, S. and Sanz Pedrero, P., *Collapse pressure of mixed surface layers of cholesterol and lecithin with bile acids*, J Chim Phys Physicochim Biol, **66**(10) (1969) 1665-1669.

124. Mediaas, H., Ardø, B. A., Grande, K., Hustad, B. M., Rasch, A., Rueslåtten, H. and Vindstad, J. E. *A Method for Selective Isolation of Naphthenic Acids from Crude Oils and Other Organic Solvents*. in *5th SPE Oilfield Scale Symposium,* SPE80404 2003. Aberdeen, UK.

125. Aylward, G. and Findlay, T., *SI Chemical Data*. 3rd ed. 1994, Singapore: John Wiley & Sons.

126. Lide, D. R., *CRC Handbook of Chemistry and Physics*. 81st ed. 2000-2001, Boca Raton: CRC Press LLC.

127. Reinsel, M. A., Borkowski, J. J. and Sears, J. T., *Partition coefficients for acetic, propionic, and butyric acids in a crude oil/water system*, J Chem. Eng Data, **39**(3) (1994) 513-516.

128. Andreassen, J.-P., *Growth and Aggregation Phenomena in Precipitation of Calcium Carbonate*, doctoral thesis, Department of Chemical Engineering, Norwegian University of Science and Technology, 2001, Trondheim.

129. Beneventi, D., Carré, B. and Gandini, A., *Precipitation and solubility of calcium soaps in basic aqueous media*, J Colloid Interface Sci, **237** (2001) 142-144.

Paper I

Paper I is not included due to copyright.

Paper II

Paper II is not included due to copyright.

Paper III

Emulsion stabilization by means of combined surfactant multilayer (D-phase) and asphaltene particles

Trond Erik Havre, Johan Sjöblom*

Ugelstad Laboratory, Department of Chemical Engineering, Norwegian University of Sciences and Technology (NTNU), 7491 Trondheim, Norway

Abstract

The emulsion stability of systems containing paraffinic, aromatic or naphthenic acid, water and heptane/toluene was investigated at different pH. High pH (around 11) gave rise to o/w emulsions with high stability. A decrease in pH reduced the emulsion stability significantly. In order to prepare stable w/o emulsions, D-phase samples were used. In addition to the multilayer stabilization, asphaltene nano-particles were mixed with the D-phase samples and used as stabilizers. It was shown that a combination of 60% asphaltene particles and 40% D-phase gave the most stable w/o-emulsions. All w/o-emulsion stabilities were evaluated by means of critical electric fields (E_{crit}). This investigation verifies the importance of D-phase stabilization in combination with asphaltene particles in systems with acidic heavy crude oil (including bitumen) and water.
© 2003 Elsevier B.V. All rights reserved.

Keywords: Emulsion stabilization; Naphthenic acids; Asphaltene particle; Lamellar liquid crystals; Electrocoale-scence

1. Introduction

Emulsions are a major problem in crude oil production offshore. In recent years an ever-increasing production of acidic crude oils with high amounts of naphthenic acids is taking place [1,2]. Since the naphthenic acids and their soaps are surface/interfacially active they will accumulate at w/o interfaces where they can stabilize colloidal structures [3–6]. An increased basic understanding of how naphthenic acids contributes to emulsion stability in crude oil systems is, hence, of great interest.

Naphthenic acids are classified as monobasic carboxylic acids of the general formula RCOOH, where R represents a cycloaliphatic structure. The term "naphthenic acid" is generally used to account for all carboxylic acids present in crude oil, including acyclic and aromatic acids [7]. These naphthenic acids show a polydispersity in size and structure [3,6,8–12]. The smallest molecules are readily dissolved in the aqueous phase at pH 5, while the larger molecules are preferably oil-soluble. Most of these homologues are dissolved in an aqueous phase at elevated pH [4,13,14].

Alkali soaps were among the first compounds used to stabilize emulsions [15]. The pH together with the solubility will be sensitive variables for the ability of naphthenic acid monomers to stabilize emulsions [16]. As the pH of the water phase increases, the acids become ionized and can thus stabilize oil in water emulsions by an electrostatic repulsion between droplets.

---

* Corresponding author
E-mail address: johsj@chemeng.ntnu.no (J. Sjöblom).

Literature reports a multitude of pH effects on acidic crude oil/water systems. Strassner [17] studied crude oil emulsions at different pH-values and found that a Venezuelian crude oil inverted from oil- to water-continuous at pH~10.5. Pathak and Kumar [18] also studied emulsion stability in crude oil systems. They found that crude oils with high content of naphthenic and fatty acids gave stable emulsions. Goldszal et al. [19] found that emulsions with much higher stability were observed at higher pH-values for water in acidic crude emulsions. Addition of Ca^{2+} or Na^+-ions led to destabilization of the emulsions, except in one case, were addition of Ca^{2+} at high pH gave a stabilizing effect.

In crude oils there are also other components that will influence the emulsion properties, for instance resins, asphaltenes and waxes. Asphaltenes are defined by solubility characteristics, i.e. they are insoluble in *n*-heptane or *n*-pentane and are soluble in toluene [20]. They are generally composed of polyaromatic nuclei carrying aliphatic chains and rings and a number of heteroatoms, including sulfur, oxygen, nitrogen and metals such as vanadium, nickel and iron. These heteroelements account for a variety of polar groups, such as aldehyde, carbonyl, carboxylic acid, amine and amide [21–23].

Asphaltenes are known to be the dominant contributor in stabilizing water in crude oil emulsions [24]. The primary mechanism of stabilization is through the formation of a cross-linked three-dimensional network with high mechanical rigidity at the oil water interfaces. This film also consists of resins, which are molecules similar to the asphaltenes, containing various polar groups as the asphaltenes do, yet are soluble in *n*-heptane or *n*-pentane but insoluble in liquid propane [20]. Several authors have studied the interactions between asphaltenes and resins and its importance for emulsion stabilization [25,26].

Professor Stig E. Friberg was a pioneer in linking the importance of phase equilibria in water/oil/ surfactant systems with emulsion stability. He documented very clearly the importance of the existence of a lamellar liquid crystal (a so-called D-phase) and a corresponding increase in emulsion stability [27–30]. The basic idea is to cover the emulsion droplets with a multiple layer of surfactant/water to enhance the rigidity of the interfacial w/o-layer. In this way a barrier against coalescence is build up.

In this paper we report on a combination of two stabilizing mechanisms for water-in-oil emulsions. These are particle-stabilization and multilayer stabilization (D-phase stabilization). The reason for this is that in acidic crude oils and crude oils with high amounts of both resins and asphaltenes both mechanisms may impact the final stability. In acidic crudes the pH has been documented to be of paramount importance for the stability and for the inversion. Obviously the mixture of ionized naphthenates and naphthenic acids is crucial for w/o stability. From phase diagram studies we know that a lamellar D phase is formed under such conditions in systems containing water/oil/surfactant (or mixtures of surfactants). However, in normal crude oil systems the asphaltene aggregation is known to be crucial for the stability of the w/o emulsions. Hence it is tempting to suggest that in many acidic crude oil systems a combination of these mechanisms would be of importance.

2. Experimental

2.1. Chemicals

All the chemicals were used as supplied. The following chemicals were delivered from Merck: dichloromethane (p.a.), *n*-decane (>95%), toluene (p.a.), *n*-heptane (p.a.), buffer solution ready for use, pH 7.00 ± 0.02, phosphate, traceable to SRM of NIST, NaCl (p.a.), $CaCl_2 \cdot 2H_2O$ (p.a.) and NaOH (p.a.). Information for the carboxylic acids used is given in Table 1.
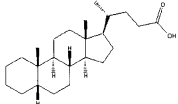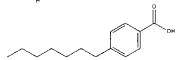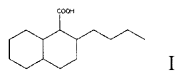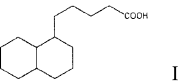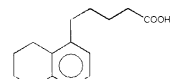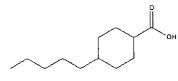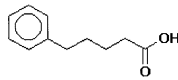
The asphaltenes were precipitated from a French crude oil by gently mixing crude oil and *n*-heptane (1 g:40 ml) at room temperature for 12 h. The mixture was then filtrated through a micro-filter (pore diameter 0.45 μm) to separate the asphaltenes from the diluted crude oil. The filtrate was then washed in *n*-heptane with constant stirring for 1 h before being filtrated and dried under a N_2 atmosphere to constant weight.

2.2. Methods

2.2.1. Bottle tests

The emulsions used in the bottle test were mixed, using an Ultra Turrax T25 rotor emulsifier at 9500 rpm for 30 s. All fluids and emulsions were kept at

Table 1
Carboxylic acids

Name	MW [g/mol]	Chemical structure	Source	Purity [wt%]
[CHOL] 5-β(H)-cholanoic acid	362		Chiron AS	> 99
[C7a1] 4-heptylbenzoic acid	220		Acros Organics	> 99
[C42] 1-naphthalenoic acid, decahydro-2-buthyl	238	I	Chiron AS	> 90
[2C4] 1-naphthalenepentanoic acid, decahydro	238	II	Chiron AS	> 90
[1a1C4] 1-Naptalenepentanoic acid, 5,6,7,8-tetrahydro-	232		University of Bergen	> 99
[C51] trans-4-n-Pentylcyclohexanecarboxylic acid	198		TCI	> 99
[a1C4] 5-phenylpentanoic acid	172		University of Bergen	> 99
Crude Naphthenic Acid 160-170	250[*]	Mixture	Corn van der Locke	-
Fluka Naphthenic Acid	240[*]	Mixture	Fluka	-
[C12] n-dodecanoic acid	200	$CH_3(CH_2)_{10}COOH$	Fluka	> 99.5
[C13] n-tridecanoic acid	214	$CH_3(CH_2)_{11}COOH$	Fluka	> 99.7
[C14] n-tetradecanoic acid	228	$CH_3(CH_2)_{12}COOH$	Fluka	> 99.5
[C15] n-pentadecanoic acid	242	$CH_3(CH_2)_{13}COOH$	Fluka	> 99.5
[C16] n-hexadecanoic acid	256	$CH_3(CH_2)_{14}COOH$	Fluka	> 99
[C17] n-heptadecanoic acid	270	$CH_3(CH_2)_{15}COOH$	Fluka	> 99
[C18] n-oktadecanoic acid	284	$CH_3(CH_2)_{16}COOH$	Merck	> 99

[I] Up to 10 wt% unsaturated bonds in cyclic part of molecular structure
[II] Up to 30 wt% unsaturated bonds in cyclic part of molecular structure
[*] Average value

70 °C in a water bath. The separation was carried out in graduated cylinders (12 ml).

2.2.2. Determination of emulsion type

The type of emulsion, oil/water or water/oil, was determined by measuring the electrical resistance through the emulsion. High resistance indicated oil-continuous, while low resistance indicated water-continuous emulsions.

2.2.3. Drop video monitoring (DVM)

A method based on video microscopy was used to determine the droplet size distribution (DSD) in the emulsions. The emulsions were gently pulled through

a vertical flow cell by use of a liquid chromatography pump. In some cases dilution was necessary; however, this is not believed to change the DSD significantly. A series of images were captured of the flowing emulsion, and an image analysis PC based tool was used to count and measure the droplets.

2.2.4. Determination of critical micelle concentration (CMC)

Surface tension measurements were performed by the ring method using a Du Noüy ring connected to a KSV Sigma 70 computer-controlled tensiometer. The surface tension could be determined to within 1 mN m^{-1}. The pH for the water solutions in the CMC-study was controlled by addition of NaOH.

2.2.5. Determination of critical electric field

The critical electric field, E_{crit}, was used as a measurement on water/oil emulsion stability. In this technique, an increasingly electric field is applied to the emulsion and the current that passes through the sample is continuously measured. E_{crit} is defined as the electric field necessary to achieve a sudden increase in the current. This increase is due to breakdown of the emulsion droplets and a formation of a continuous water-channel between the electrodes (Fig. 1, [31]).

The cell for determining the critical electric field is depicted schematically in Fig. 2. It consists of a Teflon plate with a hole in the center (r = 5 mm), and a brass

plate on each side. The distance between the plates is 0.5 mm, and the upper brass plate has holes for sample injection. The system is held together with isolating Plexiglas plates. The brass plates were connected to a computer-controlled power supply (Agilent Model 6634B) that can deliver a maximum of 100 V DC. The cell was placed in a heating cabinet at 70 °C.

The samples were emulsified using an Ultra Turrax T25 rotor emulsifier at 24 500 rpm for 15 s. The emulsion samples were then injected into the cell and the power supply was starting at 0 V and increasing by steps of 1 V every other second, corresponding to an increase in the electric field of 0.01 kV cm^{-1} s^{-1}.

The electric field required to break the emulsions, E_{crit}, were recorded when a sudden increase in the current through the sample was seen.

3. Results and discussion

3.1. CMC-determination in water

Normally a determination of CMC gives a first basis of understanding the intermolecular interactions in aqueous solutions of surfactants. For paraffinic fatty acid salts with sufficiently long alkyl chains a distinct CMC is normally observed. The driving force for micellization is normally considered to be a strong attractive hydrophobic interaction between the hydro-

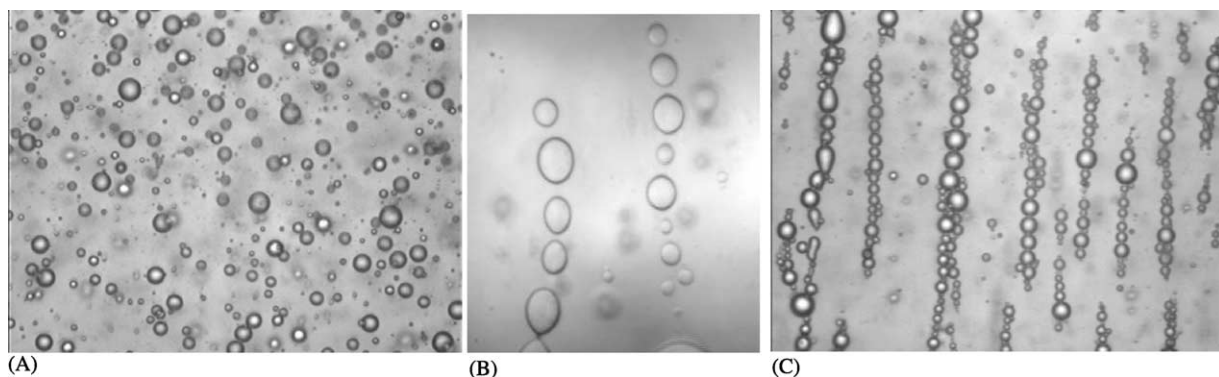(A)   (B)   (C)

Fig. 1. Illustration of how emulsions behave under the influence of an applied field [31]. (a) When no field is applied the water droplets are distributed according to Stokes law of sedimentation and Brownian motion. In addition, some degree of droplet flocculation may be present. (b) As the field increases the water droplets line up between the electrodes due to polarization of the droplets. (c) Finally the applied electric field is so high that the droplets coalesce, resulting in a water-continuous bridge between the electrodes. The ions of the water phase contribute to a sudden increase in the conductivity. The emulsion stability is hence defined as the strength of the field when the conductivity suddenly rises.
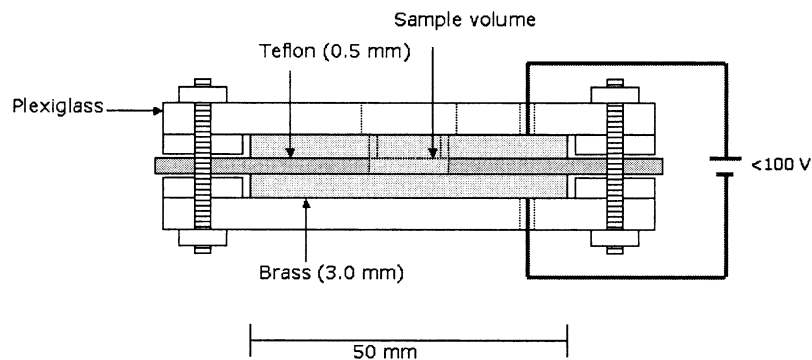
Fig. 2. The cell for determining critical electric field.

carbon chains. At the same time the paraffinic alkyl chains have no severe packing constraint. On the other hand pharmaceutical surfactants with condensed ring structures are known to have a step-wise association in water and a less well-defined CMC. Obviously these molecules have restrictions in their packing, and ordinary spherical micellar structures do not emerge. The difference in the molecular packing is also reflected in the aggregation numbers. For the paraffinic fatty acid salts the micelles can contain up to 100 monomers, which is considerably higher than for the monomers with large condensed ring structures. The interesting thing with naphthenates is to compare the structures and see to what extent they follow an association tendency as ordinary paraffinic homologues, or when a stacking of monomers will set in.

The critical micelle concentration (CMC) for some naphthenic acids at pH > 11 have recently been reported by Havre et al. [32]. In this paper, CMC-values for additional acids are reported. The results are given in Table 2. The area/molecule is determined from Gibbs' adsorption equation.

Both the commercial mixtures had distinct CMC-values. The two commercial mixtures have a mean molecular weight of 240 and 250 g mol^{-1}, respectively, while 2C4 has a molecular weight of 238 g mol^{-1}. These three acids have CMC-values of the same order of magnitude. All structures are presented in Table 1.

Values for the sodium *n*-alkanoates were collected from Mukerjee and Mysels [33] and compared with CMC-values for the naphthenates. Fig. 3 shows the molecular weight (of the acidic forms) versus log CMC. It should be noted that the values from Mukerjee and Mystels are for pure aqueous solution while the other are for pH > 11. It is well known that the logharitm of CMC often vary linearly with the size of the hydrophobic part of surfactants [34,35]. It is interesting to see whether naphthenates with different ring-structures follow the same trend.

The naphthenates from the commercial mixtures of naphthenic acids (CNA and Fluka) and 2C4 have lower CMC-values than straight chain carboxylates with similar molecular weight, Characteristic of the

Table 2
CMC and area per molecule for different carboxylic acids at high pH

	Carboxylic acid	pH	CMC (mol dm^{-3})	Area/molecule (Å^2)
[C7a1]	4-Heptylbenzoic acid	11.5	1.7E−2	31
[C51]	*trans*-4-*n*-Pentylcyclohexanecarboxylic Acid	11.5	6.7E−2	35
[CNA]	CNA 160–170 Corn van der Locke	11.3	2.7E−4	71
[2C4]	1-Naphthalenepentanoic acid, decahydro [32]	11.0	2E−4	52
[Fluka]	Fluka naphthenic acid [32]	11.3	8E−4	61

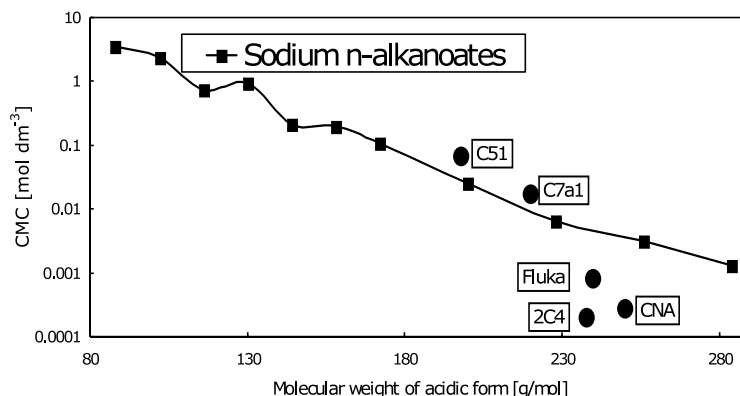Values for 2C4 and Fluka are from Havre et al. [32].

Fig. 3. CMC-values for different carboxylates as a function of the molecular weight of the acidic form. The squares connected with a line are literature values for sodium *n*-alkanoates. The abbreviations used for the other points (circles) are explained in Table 2.

structures of C51 and C7a1 are that they have the acid group connected directly to a condensed and an aromatic ring, respectively. These two acids have CMCs that are higher than corresponding *n*-alkanoates.

The CMC-measurements reveal that the naphthenic acid salts behave as micelle-forming surfactants at appropriate pH values. For this kind of surfactants, the molecular packing parameter, MPP, can be defined.

$$MPP = \frac{V}{a \cdot l} \tag{1}$$

Here, V is the topological volume of the surfactant, a is the head-group area (topological) and l is the length of the almost extended hydrocarbon chain. For micelle-forming surfactant (spherical aggregates) in water, the MPP is about 1/3. For lamellar aggregates (and microemulsions) MPP obtains a value of

approximately 1, while oil-continuous structures, like reversed micelles, have a MPP > 1 [36].

As for ordinary fatty acids we can predict a high solubility and the formation of ordinary micelles at high pH, i.e. the MPP is obtaining values around 1/3 for the ordinary naphthenates in water at high pH.

The area per molecule given in Table 2 reveals that the naphthenic acids tested occupy between 31 and 71 Å^2 per molecule. Ovalles et al. [37] have reported values for the area per molecule for naturally occurring naphthenic acids at an interface between water and toluene. They found 113–152 Å^2 per molecule for different fractions. For these systems (at full dissociation) a strong electrostatic repulsion is dominant, which is explaining the large area demands at high pH.

In a system consisting of a naphthenic acid, RCOOH and a naphthenic salt, RCOO$^-$, the ratio,

Table 3
Outline of experiments

pH	Water cut (vol%)	Carboxylic acids	Emulsion stability
> 11.5	30, 70	C12, C13, …, C18, CHOL, C7a1, 1a1C4 and C42	Stable emulsions, several days required for separation
> 5.6 (Distilled water)	30, 70	C13, C15, C18, CHOL, C7a1	Unstable emulsion, separation within a minute
7.0	10.0	C12	Unstable emulsion, separation within seconds
	19.8, 30.0, 70.0, 84.0, 93.5	C12	Fig. 4
	30	C18, CHOL, C7a1	Unstable emulsion, separation within few minutes
	30	C13	Some stability, separation within 2 hours
	70	C12, C18, CHOL, C7a1	Fig. 5

All emulsions were determined to be water-continuos (o/w).

RCOO⁻/RCOOH, will determine what kind of structure to occur. Normally by varying RCOO⁻/RCOOH (in water), at high enough pH, one will have micelles, liquid crystals and reversed structures [38]. For emulsion stabilization, the occurrence of a lamellar liquid crystalline D-phase will be most crucial.

3.2. Oil in water emulsions

The emulsion stability of systems containing carboxylic acid, water and heptane/toluene (50/50 by volume) was investigated at different pH. The acid concentration was always 0.0293 M (∼1 wt.%) of the oil phase and this resulted in water-continuous emulsions for all the experiments. Abbreviations used for the different acids are given in Table 1, while an outline of the experiments performed is given in Table 3.

At high pH (∼11.5), and 30 or 70 vol% water, all the carboxylic acid tested gave emulsions that were stable for several days. The DSD was measured using a drop video monitoring technique (DVM). This was done for the emulsions stabilized by C13, C15, C18, C42, 1a1C4, C7a1 and CHOL. The water-cut was 30 vol%; for 1a1C4 and CHOL additional DSDs were determined at 70 vol% water. There were no major differences in the DSDs. An example of a DSD (70 vol% water and CHOL as stabilizer) is given in Fig. 4. The figure reveals that the DSD is narrow and that the oil droplets have diameters from 9 to 24 μm. Addition of Ca^{2+}-solution destabilizes these emulsions.
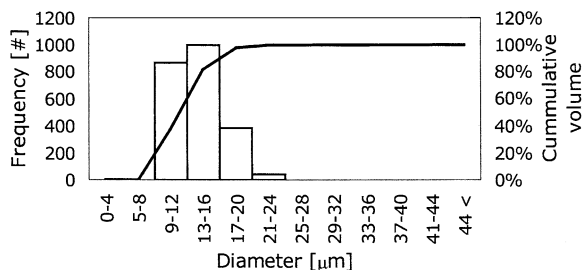

Fig. 4. Typical drop size distribution for water/oil emulsions at pH > 11. The bars show the frequency of droplets with diameters in the given intervals, while the curve shows the cumulative volume%. The DSD shown is for an emulsion consisting of 70 vol% water and stabilized by 5β(H)-cholanoic acid.

The emulsions were also destabilized upon reduction in pH. At pH 5.6 the o/w-emulsions separated within 1 min. At pH 7 the emulsions preserved some stability and the effect of water-cut and type of carboxylic acid was investigated at this pH.

The amount of water was varied for emulsions stabilized by dodecanoic acid at pH 7. Increased ratio of water resulted in decreased emulsion stability. No inversion was seen for a water-cut exceeding 10 vol%. The amount of separated oil is plotted as a function of time for different water-cuts in Fig. 5. When 10 vol% water was used, the emulsion was not stable enough for a separation curve to be recorded.

Fig. 6 gives the amount of oil separated as a function of time for different carboxylic acids at pH 7.0. The water-cut was 70 vol%. High molecular weight acids
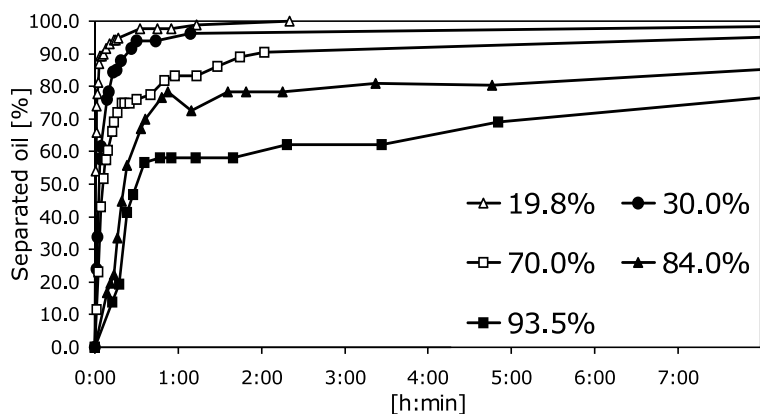

Fig. 5. Amount of oil separated from emulsions stabilized by dodecanoic acid, with different water contents, as a function of time at pH 7.
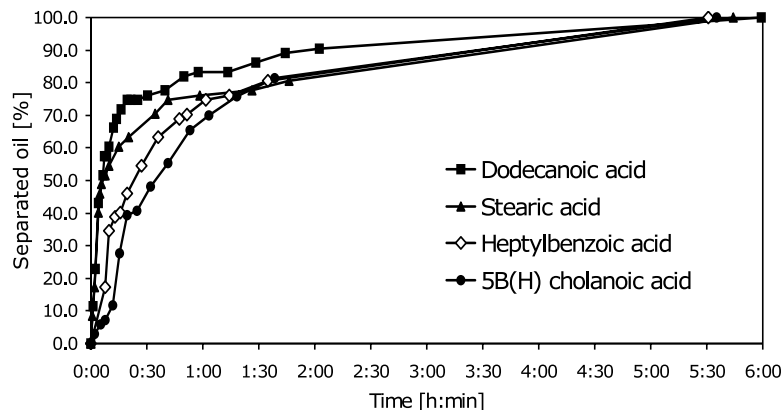
Fig. 6. Amount of oil separated from emulsions, with different carboxylic acids, as a function of time. Oil phase: *n*-heptane/toluene (50/50 by volume), pH 7, water content: 70 vol%, and acid concentration: 0.0293 M of oil phase.

seem to have a slightly better stabilizing effect on the emulsions. All the emulsions were separated within 6 h.

In these experiments, the concentration of carboxylic acid has not exceeded ∼1 wt.% of the oil phase. Different pH-values, water-cuts and carboxylic acid structures have not resulted in any stable oil-continuous emulsion. The pH is a very sensitive variable regarding the stability of the oil/water emulsions. This is obviously due to the dissociation of carboxylic acids at higher pH, which creates an electrostatic stabilizing effect. The results show that the emulsions have a drastically increase in stability somewhere between pH 7 and 11.5. Even though these carboxylic acids have a pK_a around 5, the undissociated forms of the acids are preferably oil-soluble. This means that the dissociated form of the acid will be dominant only at higher pH-values [39]. With low concentration of the fatty acid the occurrence of multilayers is not likely and a higher pH will give more dissociated acid, which favors the stabilization of the o/w emulsions. With a higher concentration of the carboxylic acid, multilayers may form and the relation between emulsion stability and pH is more complex. Here the ratio between the acid and its salt are of major importance in order to give the emulsions with the highest stability.

3.3. Combined D-phase and particle stabilization

As per today, no detailed and complete phase equilibria of a naphthenic acid (different pH)/water/oil or

sodium naphthenate/naphthenic acid/water/oil have been published. Horváth-Szabó has in cooperation with groups in Edmonton, published qualitative phase equilibria of sodium naphthenates in aqueous solution [38] and sodium naphthenates/toluene/water system [40] and found evidence for the existence of lamellar liquid crystals in bitumen systems [41]. Horváth-Szabó gives evidence for the in situ formation of a lamellar liquid crystalline phase at the w/o interface at high pH. Obviously the occurrence of such a phase can account for the discrepancies found in these systems.

It is our opinion that the phase equilibria in the system water/sodium hexadecanoate (NaC16)/hexadecanoic acid (HC16) at 70 °C is representative also for naphthenic acid based systems. The phase diagram of this system has been published by Skurtveit et al. [42] and is given in Fig. 7.

In this system, existence of four or five isotropic phases can be observed. These are a micellar L_1-phase (with ordinary micelles), a hexagonal liquid crystalline E-phase (with long rods in an aqueous environment), a lamellar liquid crystalline D-phase (with a bilayer structure) and a reversed solution phase L_2 (with reversed micelles). It is questionable if a F-phase with a reverse hexagonal structure exists. In this diagram, the importance of the stabilization of water/oil emulsions, due to the D-phase has been documented [42].

For practical reasons, it is of importance to map the existence of the lamellar D-phase. In Fig. 7, it is noticeable that an upper limit of phase equilibria including
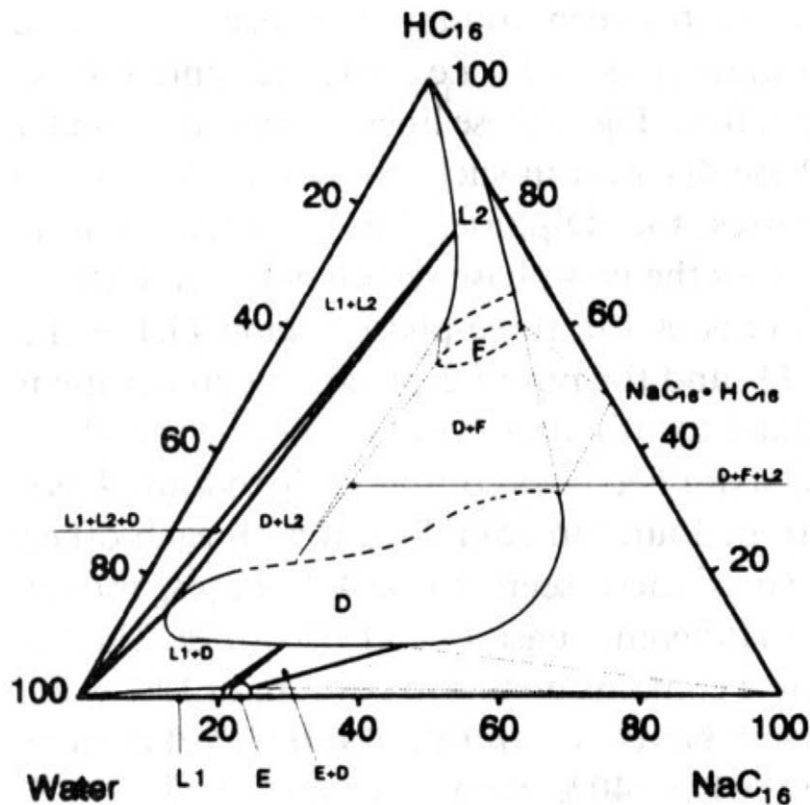
Fig. 7. Phase equillibria in the system water/hexadecanoic acid (HC16)/sodium hexadecanoate (NaC16) at 70 °C [42]. The diagram is expressed in weight percent.

the D-phase, seems to be HC16/NaC16 ≈ 85/15, and a lower limit is HC16/NaC16 ≈ 15/85. Hence it can be claimed that in an equivalent naphthenic acid-based system, a D-phase can exist for ratios of naphthenic acid to sodium naphthenate ∼0.1–6. It is enough with just 10% of a naphthenate salt to obtain the D-phase.

The stabilization mechanism behind the D-phase is the formation of a multilayer around the droplets. Especially for w/o-emulsions, this mechanism seems to be important. The existence of a multilayer around the droplets will not prevent the droplets from flocculation, but from coalescence due to the rigidity of the interface. Particle stabilization function much in the same way by modifying the mechanical properties of the droplet interface and preventing coalescence.

In order to evaluate the different levels of emulsion stability in different systems, the critical electric field technique can be applied. The experimental set-up

is explained in the Section 2. When the voltage is increased (but below the critical value) the droplets undergo a flocculation and as a result "a bridge of droplets" is formed between the electrodes. When the electric field is exceeding E_{crit}, coalescence will take place. The mechanism behind the breakdown is believed to be an ion-transport between the aqueous droplets over the protecting membrane. Hence the critical electric field will reflect the resistance towards coalescence of the interfacial structures. This is exactly what we are looking for in this approach to investigate the impact of asphaltene particles on D-phase stabilization.

In order to view the competition between D-phase stabilization and asphaltene-particle stabilization of water/oil emulsions, the following experiments were performed. A D-phase was prepared based on the equilibria in Fig. 7. A dichloromethane solution,
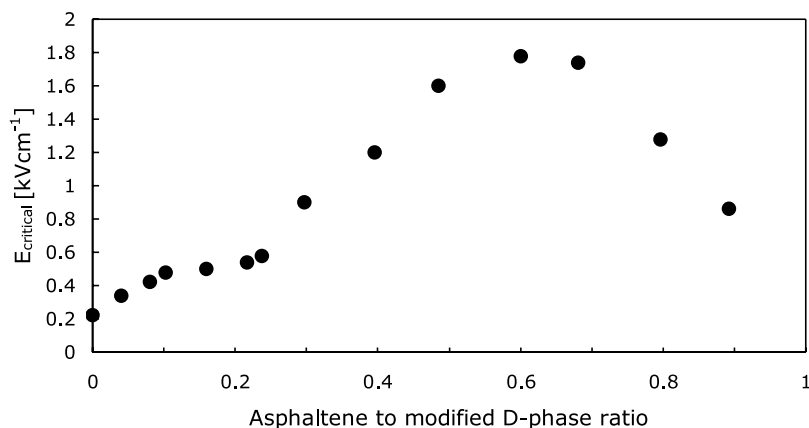
Fig. 8. Emulsion stability, represented by the critical electric field, E_{crit}, as a function of different asphaltene fractions of the modified D-phase (by weight).

containing dissolved asphaltenes, was mixed with the D-phase and the solvent was evaporated. After 24 h there was clear evidence of asphaltene particles present in the D-phase. This D-phase, modified with different amount of asphaltenes, was used to stabilize w/o-emulsions at 70 °C. The emulsions were prepared from 55.7 wt.% n-decane, 32.7 wt.% 0.5 M NaCl and 1.5 g 11.7 wt.% asphaltene modified D-phase. In order to measure the emulsion stability, the E_{crit} was determined. The result is shown in Fig. 8.

Obviously the addition of asphaltene particles can enhance the w/o-emulsion stability from the case with just a D-phase present. However, a too high amount of asphaltene particles will give a destabilization. A ratio

of 0.6, i.e. 60 wt.% particles and 40 wt.% D-phase seems to be optimal. The experiment in Fig. 8 is very important in visualizing different mechanism behind emulsion stability in crude oils with high amounts of asphaltenes and naphthenic acids. Representatives to these are heavy crudes, and bitumens.

Fig. 9 shows that naphthenic acid can take part in the HC16/NaC16LLC. In preparing the D-phase, different amounts of hexadecanoic acid was substituted with Fluka naphthenic acid, which is a commercial mixture with an average molecular weight of 250 g mol^{-1}. For naphthenic acid content in the D-phase up to about 10 wt.%, the ability of the D-phase to stabilize the emulsions is increased. This is probably due to
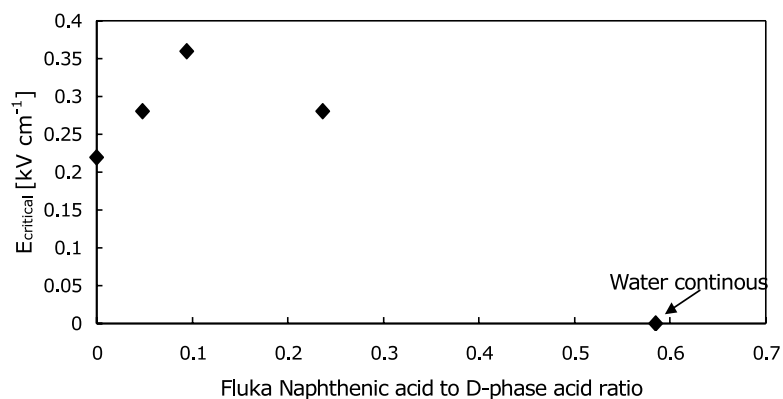

Fig. 9. Emulsion stability, represented by the critical electric field, E_{crit}, as a function of different fractions of Fluka naphthenic acid in the D-phase (by weight).

better packing conditions for a mixed multilayer structure. When the content of Fluka naphthenic acid in the D-phase becomes too high the D-phase is destroyed due to the content of oil in the commercial mixture.

The simple experiments clearly show that in acidic crude oil systems, containing naphthenic acids, there will be a tendency to form lamellar liquid crystals at w/o interfaces and theses structures will enhance the w/o emulsion stability. These observations are in line with those of Horváth-Szabó et al. [38,40,41]. However, in combination with the multiplayer stabilization, asphaltene particles can further enhance the emulsion stability. The mechanism is most likely that these nano-particles are dispersed in the surfactant multiplayer of the D-phase giving further protection towards coalescence.

4. Conclusions

Determination of the CMC for naphthenic acid salts reveals that they behave as micelle-forming surfactants at appropriate pH values.

Water-continuous emulsions, stabilized by ∼1 wt.% of different carboxylic acids were studied. As expected, pH and water-cut was important variables. High molecular weight acids seem to have a slightly better stabilizing effect on the emulsions.

It was shown that water-in-oil emulsions can be stabilized by a combined mechanism of multilayer and particle stabilization. This suggests that in many acidic crude oil systems, emulsions can be stabilized by a combination of naphthenic acids/naphthenates and asphaltenes.

Acknowledgements

References

[1] A. Goldszal, C. Hurtevent, G. Rousseau, in: SPE Oilfield Scale Symposium, Aberdeen, UK, 2002, SPE74661.

[2] G. Rousseau, H. Zhou, C. Hurtevent, in: SPE Oilfield Scale Symposium, Aberdeen, UK, 2001, SPE68307.

[3] C.S. Hsu, G.J. Dechert, W.K. Robbins, E.K. Fukuda, Energy Fuels 14 (2000) 217–223.

[4] J. Sjöblom, E.E. Johnsen, A. Westvik, L. Bergflødt, I.H. Auflem, T.E. Havre, H. Kallevik, in: The Second International Conference on Petroleum and Gas Phase Behaviour and Fouling, Copenhagen, Denmark, August 27–31, 2000.

[5] M.L.H. Márquez, March 14–18, Preprint No. 56d, p. 7, in: AICHE Spring National Meeting, Session T6005, March 14–18, 1999, Houston, Texas, 99sp 56d.

[6] S. Acevedo, G. Escobar, M.A. Ranaudo, J. Khazen, B. Borges, J.C. Pereira, B. Méndez, Energy Fuels 13 (2) (1999) 333–335.

[7] J.A. Brient, P.J. Wessner, M.N. Doyle, in: R.R Kirk, D.F. Othmer (Eds.), Encyclopedia of Chemical Technology, Wiley, New York, 1995, pp. 1017–1029.

[8] T.-P. Fan, Energy Fuels 5 (3) (1991) 371–375.

[9] L. Koike, L.M.C. Reboucas, F.d.A. Reis, A.J. Marsaioli, H.H. ichnow, W. Michaelis, Org. Geochem. 18 (6) (1992) 851–860.

[10] N.A. Tomczyk, R.E. Winans, J.H. Shinn, R.C. Robinson, Energy Fuels 15 (6) (2001) 1498–1504.

[11] K. Qian, W.K. Robbins, C.A. Hughey, H.J. Cooper, R.P. Rodgers, A.G. Marshall, Energy Fuels 15 (6) (2001) 1505–1511.

[12] W.K. Robbins, Prep. -Am. Chem. Soc. Div. Pet. Chem. 43 (1) (1998) 137–140.

[13] J. Rudin, D.T. Wasan, Colloids Surf. 68 (1992) 67–79.

[14] J. Rudin, D.T. Wasan, Colloids Surf. 68 (1992) 81–94.

[15] J.M. Pickett, K.A. Ellway, J. Pharm. Pharmacol. 28 (8) (1976) 625–628.

[16] Z. Mendez, R.E. Anton, J.-L. Salager, J. Dispersion Sci. Technol. 20 (30) (1999) 883–892.

[17] J.E. Strassner, J. Pet. Technol. 20 (3) (1968) 303–312.

[18] A.K. Pathak, T. Kumar, in: Proceedings of PETROTECH-95, Technology Trends in Oil Industry, New Delhi, 1995.

[19] A. Goldszal, M. Bourrel, C. Hurtevent, J.-L. Volle, in: The Third International Conference on Petroleum Phase Behavior and Fouling, New Orleans, USA, 2002.

[20] J.G. Speight, The Chemistry and Technology of Petroleum, Marcel Dekker, New York, 1999.

[21] J.P. Dickie, T.F. Yen, Anal. Chem. 39 (1967) 1847–1852.

[22] D.L. Mitchell, J.G. Speight, Fuel 52 (1973) 149–152.

[23] O.P. Strausz, T.W. Mojelsky, E.M. Lown, Fuel 71 (1992) 1355–1363.

[24] P.K. Kilpatrick, P.M. Spiecker, in: J. Sjöblom (Ed.), Encyclopedic Handbook of Emulsion Technology, Marcel Dekker, New York, 2001, pp. 707–730.

[25] J.D. McLean, P.K. Kilpatrick, J. Colloid Interf. Sci. 189 (1997) 242–253.

[26] J.D. McLean, P.K. Kilpatrick, J. Colloid Interf. Sci. 196 (1) (1997) 23–34.

[27] S. Friberg, L. Mandell, M. Larsson, J. Colloid Interf. Sci. 29 (1969) 155–161.

[28] S. Friberg, J. Colloid Interf. Sci. 37 (1971) 291–295.

[29] S. Friberg, P.O. Jansson, E. Cedreberg, J. Colloid Interf. Sci. 55 (1976) 614–623.

[30] S. Friberg, C. Solans, Langmuir 2 (1986) 121.

[31] N. Aske, H. Kallevik, J. Sjöblom, J. Pet. Sci. Eng. 36 (1–2) (2002) 1–17.

[32] T.E. Havre, M.-H. Ese, J. Sjöblom, A.M. Blokhus, Colloids Polym. Sci. 280 (7) (2002) 647–652.

[33] P. Mukerjee, K.J. Mysels, Critical Micelle Concentration of Aqueous Surfactant Systems, vol. 36, NSRDS-NBS, Washington, 1971.

[34] T. Gu, J. Sjöblom, Colloids Surf. 64 (1) (1992) 39–46.

[35] J. Sjöblom, R. Lindberg, S.E. Friberg, Adv. Colloid Interf. Sci. 65 (1996) 125–287.

[36] S.E. Friberg, J. Sjöblom (Eds.), Encyclopedic Handbook of Emulsion Technology, Marcel Dekker, New York, 2001, pp. 47–58.

[37] C. Ovalles, M.d.C. Carcia, D. Lujano, W. Aular, R. Barmúdez, E. Cotte, Fuel 77 (3) (1998) 121–126.

[38] G. Horváth-Szabó, J. Czarnecki, J. Masliyah, J. Colloid Interf. Sci. 236 (2001) 233–241.

[39] T.E. Havre, J. Sjöblom, J.E. Vindstad, J. Dispersion Sci. Technol. 2003, in press.

[40] G. Horváth-Szabó, J. Masliyah, J. Czarnecki, J. Colloid Interf. Sci. 242 (2001) 247–254.

[41] G. Horváth-Szabó, J. Czarnecki, J. Masliyah, J. Colloid Interf. Sci. 253 (2) (2002) 427–434.

[42] R. Skurtveit, J. Sjöblom, H. Høiland, J. Colloid Interf. Sci 133 (2) (1989) 395–403.

Paper IV

Paper IV is not included due to copyright.

Paper V

Paper V is not included due to copyright.

Paper VI

Our current understanding of water-in-crude oil emulsions.
Recent characterization techniques and high pressure performance

Johan Sjöblom[a],*, Narve Aske[a], Inge Harald Auflem[a],
Øystein Brandal[a], Trond Erik Havre[a], Øystein Sæther[a],
Arild Westvik[b], Einar Eng Johnsen[b], Harald Kallevik[b]

[a]*Norwegian University of Science and Technology (NTNU), Ugelstad Laboratory,
Department of Chemical Engineering, N-7491 Trondheim, Norway*
[b]*Statoil R&D Center, Rotvoll, N-7005 Trondheim, Norway*

Abstract

Stable water-in-oil emulsions may form during the production of crude oil, as co-produced water is mixed with the oil from reservoir to separation facilities. Such emulsions introduce technical challenges, as they must be resolved to provide the specified product quality. Asphaltenes and resins indigenous to the oil are acknowledged as the most important components in respect to stabilization of the interface against coalescence. Fine solids may also contribute to the stabilization, as may the presence of naphthenic acids. Combined, this creates a complex picture of several contributing mechanisms, and it is established that the pressure conditions will influence the behavior of active components and the properties of the interface. In order to successfully mitigate the problems of stable emulsions, a thorough

*Corresponding author. Tel.: +47-7359-5505; fax: +47-7359-5047.
E-mail address: johan.sjoblom@chemeng.ntnu.no (J. Sjöblom).

knowledge of component properties, behavior, interactions and effect on water/oil interfacial properties must be developed for pressures ranging from ambient to high. This review seeks to bring to light recent findings related to these topics.

1. Introduction

Professor Overbeek is a scientific pioneer in explaining, with mathematical stringency, the colloidal stability in aqueous systems, i.e. the DLVO theory. As we all know, this theory shows the significance of the electric double layer for aqueous colloids and remains a milestone of colloid chemistry. The importance of this theory for the whole development and the status of modern colloid chemistry cannot be overestimated [1].

The theoretical and experimental impacts to create a better understanding of oil-based systems are of a more recent date. One can say that these needs, to a significant degree, emerge from the crude oil industry where a lot of problems of practical nature are closely related to colloid chemistry. In this review we will concentrate on a description of water-in-crude oil (or model oil) emulsions and topics related to these.

The co-production of water and crude oil in the form of an emulsion is highly undesirable from a process and product quality point of view. The history of the emulsification process can start already in the reservoir where the crude oil and water is squeezed through narrow pores and the surface tension should be the driving force for spherical droplet formation. This can happen at both high pressures and temperatures. When the crude oil is processed from the well-head to the manifold, there is usually a substantial pressure reduction with a pressure gradient over chokes and valves where the mixing of oil and water can be intense. After this, the well-stream is entering the separator (usually several placed sequentially in a train), where most of the water is separated from the crude. The final treatment normally takes place in the electrocoalescer after which the level of water should be below 0.5%. The processing of oil and water offers several possibilities to vigorously mix the phases and create an emulsion. However, this does not explain the diversity of stability levels found for emulsions based on different well-streams. Obviously, indigenous components in the crude oil can cause higher or lower levels of emulsion stability. Our present view is that an interplay between asphaltenes and resins can explain most of the stability. In addition, fine solids (both organic and inorganic) will contribute to the stabilization [2,3].

According to many authors, the chemistry of asphaltenes is the clue to an understanding of the mechanisms behind the formation of resistant interfaces between oil and water. The chemistry of asphaltenes is dependent on pressure and the occurrence of organic dispersants. With a reduction in pressure, the solvency

will turn less favorable for the asphaltene monomers and an association will take place. In the absence of efficient dispersants, a large scale precipitation can occur. This phenomenon can be disastrous for the further exploration of the reservoir. The dispersants will, however, suspend the small asphaltene particles in the crude oil. When a fresh w/o interface is created (with the introduction of water) a change in the interaction pattern between the components will take place. Since the dispersant has a high affinity towards the water/oil interface, an initial monolayer might be formed. Without the protecting dispersant layer the asphaltene particles will precipitate and be accumulated at the surface of the water droplets. This is the basis for the formation of a mixed interfacial layer. In order to give high stability against coalescence the rheological properties must be correct. The layer should be more elastic than viscous. In this way, the interfacial relaxation will be much faster. This approach explains the emulsion stability of w/o emulsions based on steric and/or particle stabilization [4–8].

However, with the introduction of fatty acids (naphthenic acids) in the crude oil, the interaction pattern will undergo changes. One of the most fundamental properties in systems of fatty acid/fatty acid salt/water is the formation of a lamellar lyotropic liquid crystalline D-phase. This phase has a microstructure involving bilayers of the surfactant and intervening water layers. It has been unambiguously shown that such structures will enhance the stability of w/o emulsions. The final protection towards coalescence is believed to originate from the existence of a multilayer giving the interfacial regime a higher rigidity. The D-phase stabilization hence seems to be important for acidic crude oils [9–14].

In order to understand the complex picture behind water-in-crude oil emulsion stability, a thorough knowledge at both ambient and high pressures should involve the structure and properties of the crude oil components (mainly the heavy ones), their association tendencies and accumulation at w/o interfaces, their solubilities and sensitivity towards changes in pressure and temperature, the special features of acidic components and their association structures in water/oil systems and, above all, how these components by themselves or by an intricate interplay form highly elastic interfaces protecting the droplets against coalescence.

This review attempts to elucidate the most recent findings covering the topics above.

2. Chemistry of crude oils and asphaltenes

2.1. Chemical composition of crude oils

Crude oils are a continuum of tens of thousands of different hydrocarbon molecules. However, the proportions of the elements in crude oils vary over fairly narrow limits despite the wide variation found in properties from the lightest crude oils to highly asphaltenic crudes. The carbon content normally is in the range 83–87% and the hydrogen content varies between 10 and 14%. In addition, varying
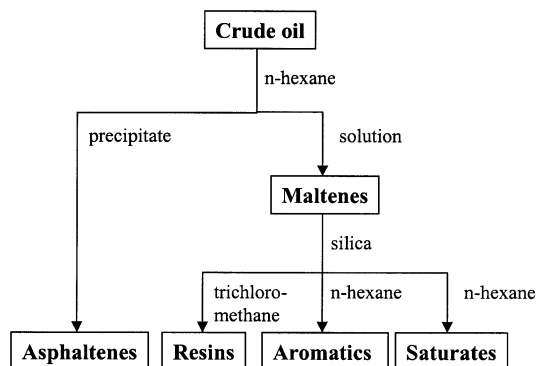
Fig. 1. SARA-separation scheme.

small amounts of nitrogen, oxygen, sulfur and metals (Ni and V) are found in crude oils [15].

Due to the complex composition of crude oils, characterization by the individual molecular types is not possible. Instead, hydrocarbon group type analysis is commonly employed [16–23]. The SARA-separation is an example of such group type analysis, separating the crude oils in four main chemical classes based on differences in solubility and polarity. Fig. 1 demonstrates the SARA-separation scheme used by Aske et al. [24]. High performance liquid chromatography (HPLC) is used in this setup due to the simplicity and low time-consumption compared to the ASTM procedures for SARA separation, which are based on liquid chromatography (LC) [25,26]. Fluorescent indicator adsorption (FIA) and thin layer chromatographic methods combined with flame ionization detection (TLC-FID) have also been used for class determination. However, the FIA method is time consuming and the results are strongly dependent on the operator. TLC-FID also requires a thorough knowledge on the limitations of the system [17].

2.1.1. Saturates and aromatics

The saturates (or aliphatics) are the non-polar compounds containing no double bonds and includes both the alkanes and the cycloalkanes. Wax is a sub-class of the saturates. The aromatics consist of all compounds with one or more benzene rings. These ring systems may be linked up with naphtene rings and/or aliphatic side chains.

2.1.2. Resins

This fraction is comprised of polar molecules often containing heteroatoms such as nitrogen, oxygen or sulfur. This fraction is operationally defined, and one common definition of resins is as the fraction soluble in light alkanes such as pentane and heptane, but insoluble in liquid propane [15,27,28]. Naphthenic acids are a part of this fraction.

2.1.3. Asphaltenes

Asphaltenes are polar molecules that can be regarded as similar to the resins, but with higher molecular weight, typically 500–1500 g/mole. The asphaltene fraction, like the resins, is defined as a solubility class, namely the fraction of the crude oil precipitating in light alkanes like pentane, hexane or heptane. The precipitate is soluble in aromatic solvents like toluene and benzene. The asphaltene fraction contains the largest percentage of heteroatoms (O, S, N) and organometallic constituents (Ni, V, Fe) in the crude oil. The structure of asphaltene molecules is believed to consist of polycyclic aromatic clusters, substituted with varying alkyl side chains [15,27].

2.2. Solubility and aggregation of asphaltenes

Asphaltenes tend to self-associate, a fact that has led to much controversy regarding asphaltene molecular weights, molecular weights from a few hundred to several million have been reported [15,29,30]. Lately, mean molecular weights of approximately 750 g/mole have been reported, which is believed to be a good estimate of the asphaltene monomer molecular weight [31]. Geographic origin is believed to influence structure, hetero-atom content and molecular weight. The self-association of asphaltenes is affected both by solvent conditions, pressure and temperature, and has been studied in detail by several authors [5,6,32–40]. Generally, increasingly aliphatic solvents and pressure reductions are the main contributors to increasing asphaltene aggregate size.

Asphaltenes are believed to be suspended as microcolloids in the crude oil consisting of ∼3 nm particles [27]. Each particle consists of one or more aromatic sheets of asphaltene monomers, with adsorbed resins acting as surfactants to stabilize the colloidal suspension. Under unfavorable solvent conditions, resins desorb from the asphaltenes, leading to an increase in asphaltene aggregate size and eventually precipitation of large asphaltene aggregates. This asphaltene aggregation model is the so-called steric stabilization model developed by Leontaritis and Mansoori [41–43] based on the earlier work by Nellensteyn and others [44–46].

An alternative view on asphaltene stabilization exists, referred to as the thermo-dynamic model, and first reported by Hirschberg et al. [47]. In this approach, the resins are not considered explicitly, but are treated as an undifferentiated part of the solvent medium. This view implies that the asphaltene monomers and aggregates are in thermodynamic equilibrium, and solvated by the surrounding medium. Thus, the critical distinction between the thermodynamic and steric stabilization models lies in the issue whether the asphaltene colloids are solvated or suspended in hydrocarbon media [27]. Asphaltene aggregation models have been reviewed by Andersen and Speight [48].

The reversibility of the asphaltene aggregation is also a subject of some controversy in the literature. Hirschberg et al. [47] assumed that the aggregation was reversible, but probably very slow. Joshi et al. [49] found the precipitation from a live crude oil to be reversible in a matter of minutes, except for a subtle irreversibility observed for the first depressurization of the crude oil. They also

discussed the different behavior of asphaltenes precipitated from crude oils with excess *n*-alkanes and by asphaltenes contained in the original crude oil. Hammami et al. [50] also found that the aggregation is generally reversible, but that the kinetics of the redissolution vary significantly depending on the physical state of the system. Peramanu et al. [51] reported differences in the reversibility of solvent- and temperature-induced aggregation.

Due to the mentioned uncertainty in asphaltene aggregation behavior, the prediction of asphaltene aggregation is a difficult task for the oil industry. Aggregation problems may be encountered both during mixing of crude oils and pressure depletion from reservoir conditions [49,50]. The aggregation and precipitation of asphaltenes may cause a large variety of problems, from formation damage, equipment plugging, catalyst deactivation etc. In addition, asphaltene aggregation has a great influence on emulsion stability of crude oil–water emulsions.

The solubility class definition of asphaltenes incorporates a broad distribution of molecular structures that can vary greatly from one crude oil to another. Recently, Spiecker and Kilpatrick [52] have investigated subfractions of asphaltenes and their influence on the stability of model emulsions. They precipitated asphaltenes from different crude oils with a heptane–toluene mixture in which approximately 35% of the asphaltenes precipitated. They found several distinct differences between the 'precipitate' and the 'soluble' fraction. The solubility of the 'precipitate' fraction was considerably less than for the 'soluble' fraction or the asphaltenes of the whole crude oil. The aggregate size of the 'precipitate' fraction was also large (500 Å) compared to the 'soluble' fraction (70–130 Å). This asphaltene aggregate size was found to have a great influence on the emulsion stability, and the most stable emulsions were always formed by asphaltenes at the limit of solubility.

2.3. Characterization of crude oils by near infrared spectroscopy

Over the last 30 years, near infrared spectroscopy has been increasingly used as an analytical tool, particularly by the food and agricultural industries, but also by the textile and polymer industries in addition to the petroleum industry [53]. The increasing popularity is due to the 4 principal advantages of the method, namely low time-consumption, simplicity, multiplicity of analysis from a single spectrum and the non-consumption of the samples. The main disadvantages of NIR spectroscopy have always been the insensitivity to minor constituents and the broad absorption bands [54]. The latter drawback however is compensated by the rapid development of advanced and user-friendly software for multivariate analysis. Near infrared spectroscopy is very central in the crude oil characterization (see also Sections 2.4 and 2.5). The main advantage of NIR for our purposes is the possibility of obtaining both chemical and physical information on the crude oils. In the following a brief introduction to near infrared spectroscopy is given. Some of the applications of near infrared spectroscopy will be demonstrated later.

The near infrared spectroscopic region lies between the visible and the mid infrared regions of the electromagnetic spectrum and is defined by ASTM as the spectral region spanning the wavelength range 780–2526 nm. In infrared spectros-

Table 1
Near infrared absorption bands

Absorption band	Wavelength region [nm]
O–H First overtone	1400–1450
O–H Combinations	1900–1975
C–H Second overtone	1125–1225
C–H Combinations first overtone	1350–1450
C–H First overtone	1625–1775
C–H Combinations	1950–2450

copy diatomic molecules will vibrate as a harmonic oscillator, and the energy will be given by [55]:

$$E_v = \left(v + \frac{1}{2}\right)hc\nu_0 \tag{1}$$

where h is Planck's constant, v is the vibrational quantum number, ν_0 is the frequency of vibration and c is the speed of light. However, vibrations in polyatomic molecules involve complex movement of their constituent atoms. In practice, such molecular vibrations tend to be anharmonic, i.e. vibrations about the equilibrium position are non-symmetric. This anharmonicity introduces overtones and combinations of the fundamental vibration bands in the mid infrared region. These absorption bands can be found in the near infrared region. The energy levels for anharmonic vibration may be written as:

$$E_v = \left(v + \frac{1}{2}\right)hc\nu_0 - \left(v + \frac{1}{2}\right)^2 hc\nu_0 x_e \tag{2}$$

where x_e is the anharmonicity constant. The intensity of the overtone and combination bands is markedly lower than for the fundamental bands. When dealing with organic compounds, as for crude oils, the most prominent NIR bands are those related to O–H, C–H and N–H groups. Main absorption bands of NIR spectra are given in Table 1.

One of the main advantages of near infrared spectroscopy when working with colloidal systems like crude oils is the ability to gain information on the state of the system. In addition to absorption, near infrared spectra will display a baseline elevation due to light scattering by aggregates or particles in solution. For slightly lossy dielectric particles in the Rayleigh limit, the scattering and absorption processes contribute separately to the extinction coefficient [56]:

$$\sigma_{tot} = \sigma_{abs} + \sigma_{sc} \tag{3}$$

where σ_{tot}, σ_{abs}, and σ_{sc} are the total, absorption, and scattering cross sections, respectively. Also, the ratio of scattering to absorption scales with r^3, indicating the importance of particle size on the total light extinction. Thus, the influence of scattering increases extensively with increasing diameter of the particles. Fig. 2
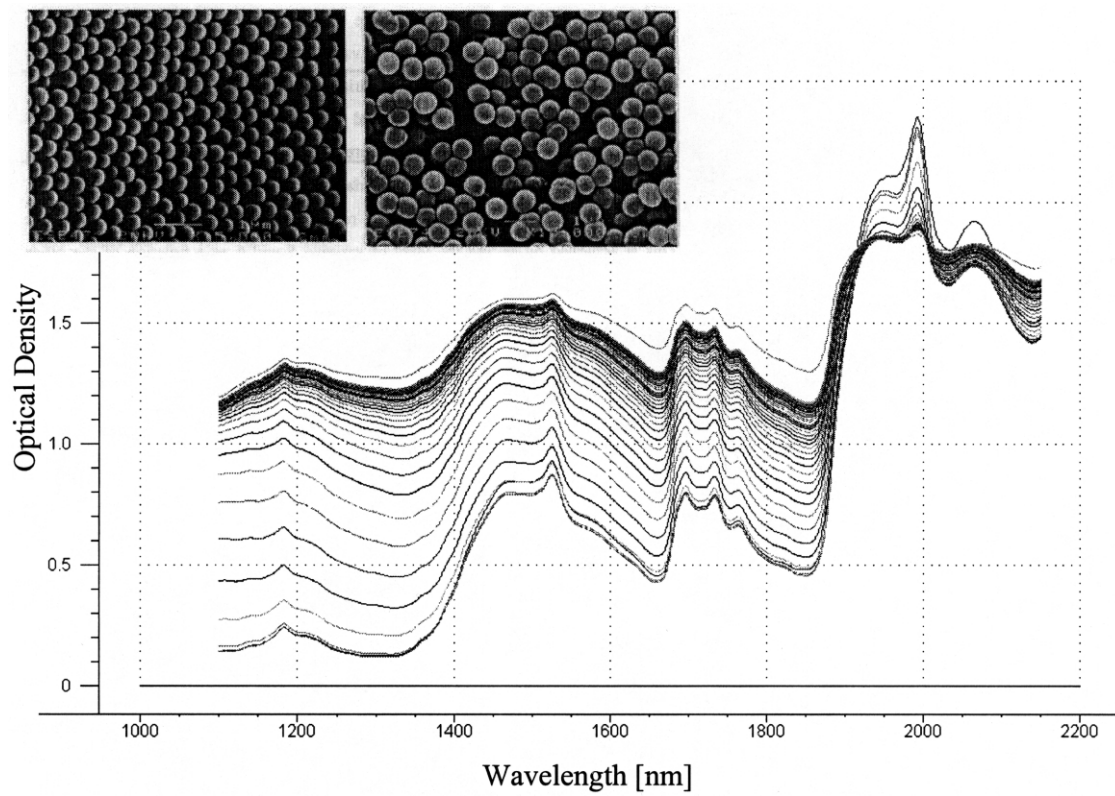
Fig. 2. NIR spectra of silica particles formed by sol–gel process. Monodisperse silica particles with $d=330$ and $d=630$ nm shown.
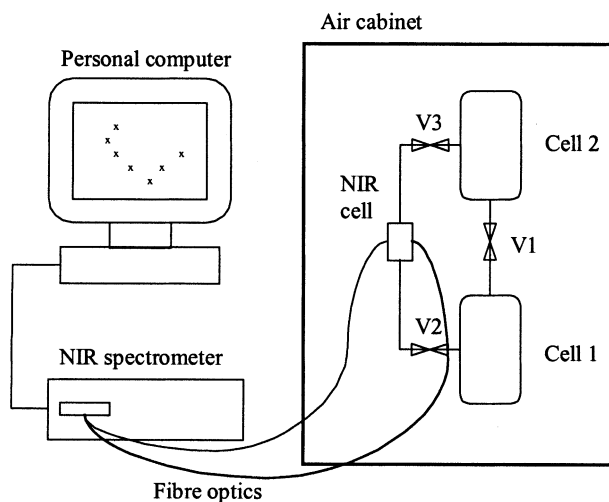
Fig. 3. High-pressure near infrared spectroscopy setup.

demonstrates the effect of particle size on NIR spectra. During a sol–gel preparation of silica particles, NIR spectra were taken at intervals, and the increasing baseline level due to increasing particle size is clearly seen.

Several authors have used NIR spectra for particle size determinations [57–60]. NIR spectroscopy has also found widespread use in the determination of both physical and chemical properties of crude oils and related materials [53,61–66].

2.4. Asphaltene aggregation studied by high-pressure NIR spectroscopy

The importance of asphaltene aggregation on several aspects of crude oil behavior has been discussed. The aggregation behavior of asphaltenes has recently been studied by use of a high-pressure NIR system shown in Fig. 3 [67]. The system combines the accurate pressure and temperature control offered by a high pressure rig in which a high-pressure transmittance NIR cell is connected. Specially designed software enables direct principal component analysis (PCA) of the spectra in order to easily detect asphaltene aggregation. By plotting principal components in so-called score plots samples are easily distinguished based on subtle changes in their respective NIR spectra. Changes caused by, for instance, compressibility or particle aggregation in the samples can also be identified by principal component analysis. A more detailed explanation of this technique is given in Section 4.4.

Both a recombined crude oil and model systems of pentane, toluene and asphaltene were studied. The model systems were constructed such as to be at the verge of asphaltene precipitation, and two systems of 1.2 wt.% asphaltene in 35 and 40 wt.% pentane-in-toluene solvents were made. The crude oil contained 0.8 wt.% asphaltene, had a reservoir bubble pressure of 155 bar and was known to be susceptible to asphaltene precipitation by pressure depletion. The systems were pressurized to 100

or 300 bar and charged to the high pressure rig at temperatures from 100 °C to 150 °C. The systems were then depressurized in steps, and the resulting NIR spectra at each pressure level were analyzed by the PCA routine. Approximately 20 min of equilibration was allowed at each pressure level. It was found that at the asphaltene aggregation onset pressure a distinct shift in the PCA score plots could be seen. Reducing the pressure even further, the bubble point was detected by NIR spectra displaying low absorbance due to gas evolution. In Fig. 4, the procedure of asphaltene onset detection for the crude oil from the NIR spectra via the PCA analysis to the impact on the phase envelope is demonstrated. At high pressures there is a decrease in optical density with pressure depletion due to the compressibility of the crude oil. A soon as aggregates start to grow, the optical density increases due to increased light scattering. Although this is difficult to see directly from the spectra it is clearly seen from the score plot. In the phase envelope the pressure depletion path is indicated along with the detected asphaltene aggregation onset pressure of 180 bar.

Performing the same type of experiments on the model systems (containing only asphaltenes in addition to solvents) produced the same type of results, thus confirming that the shift in the score plot indeed is caused by asphaltene aggregation. Depressurization of a model system without asphaltenes showed no shift in the score plot. Table 2 summarizes the experimental conditions and detected onset pressures and bubble points for the systems studied. The bubble point pressures for the low temperature model systems were too low to be detected. As expected, the onset pressure for the 40 wt.% pentane solvent is higher than for the 35 wt.% pentane system. In addition, the onset pressure at 150 °C was found to be higher than that at 100 °C.

The reversibility of the asphaltene aggregation was also studied for the crude oil and the 35 wt.% pentane system at 150 °C. This was done by repressurizing the systems stepwise from the bubble point to 100 bar and 300 bar, respectively, for the model system and the crude oil. When the original pressure was reached, the system was left to equilibrate and NIR spectra were recorded in intervals until no further spectral change was observed. In Fig. 5 the optical density at 1600 nm for both the depressurization and the repressurization for the two systems is shown.

For the crude oil, at the left hand side in the figure, considerable redissolution of the aggregates was seen when increasing the pressure from 150 to 170 bar, as seen by the decrease in optical density at 1600 nm. However, no significant redissolution was then observed until the crude oil was left at the original pressure of 300 bar (300II). After 72 h the aggregate size had practically returned to its original state. For the model system, on the other hand, the aggregates seemed to redissolve steadily during repressurizing, but the redissolution came to a stop after approximately 23 h at the original pressure of 100 bar. Thus, while the asphaltene aggregation of the crude oil was more or less completely reversible, the model system asphaltene aggregation was only partial reversible. The asphaltenes of the model system are stripped for the resin fraction when they are being prepared. The
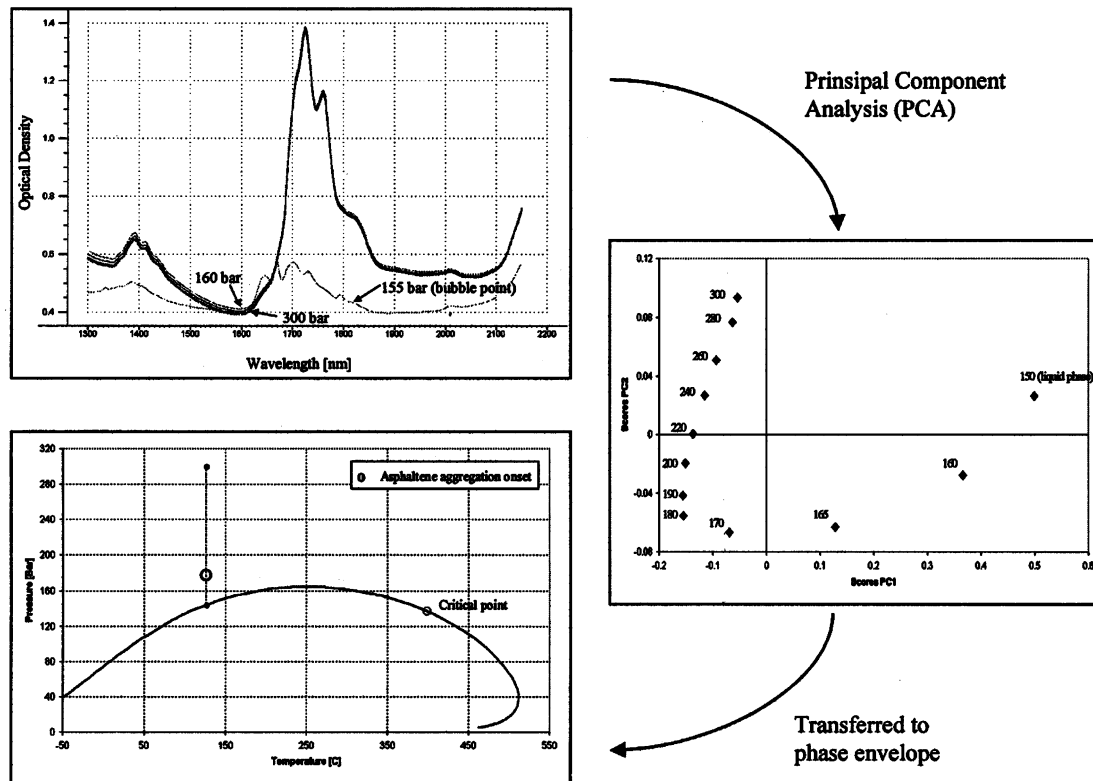
Fig. 4. Detection of asphaltene aggregation onset pressure from high-pressure NIR spectroscopy and PCA.

Table 2
Bubblepoint and asphaltene aggregation onset pressures

System	Temperature [°C]	Bubblepoint [bar]	Onset pressure [bar]
Crude oil	125	155	180
35 wt.% pentane	100	<2.5	20
35 wt.% pentane	150	10	30
40 wt.% pentane	100	<2.5	40
40 wt.% pentane, no asphaltene	150	14	–

lack of dispersing resins during the repressurization is believed to explain the different behavior of the crude oil and the model system.

Using NIR spectroscopy in combination with multivariate analytical techniques, like principal component analysis, has been shown to be a very efficient tool in studying asphaltene aggregation behavior. Very small spectral changes are detected in a score plot, enabling an accurate determination of the onset pressure. In addition bubble points are easily detected from the spectral features.

2.5. Disintegration of asphaltenes studied by NIR spectroscopy

It is currently accepted that asphaltenes consist of aromatic compounds with π–π interactions, which undergo acid–base interactions and self associate through hydrogen bonding [68,69]. The main strategy for the disintegration of asphaltene aggregates should hence, be to break these bonds and stabilize the smaller asphaltenes aggregates from precipitation. Resins are usually thought to function as a dispersant of asphaltenes in crude oil. In order to hinder asphaltene deposition, the petroleum industry injects large volumes of chemicals in to reservoirs and pipelines. These chemicals are supposed to imitate the indigenous resin function, by dispersing the asphaltenes in the hydrocarbon mixture. The size of the asphaltene aggregates will also influence the capacity to form emulsions, where the optimum size for stabilizing, will depend upon the size of the water drops. That is, changing the size of the asphaltene aggregates beyond the optimum size region, may also prevent emulsion formation. Auflem and coworkers [70] have introduced near infrared (NIR) spectroscopy as a potent tool for studying the effect of chemicals as dispersants of asphaltene aggregates. As described in Section 2.3, the NIR technique is sensitive to the size of scattering particles; thus, the change in size of the asphaltene aggregates could be probed as a function of time and additive concentration. The structures and molecular weights of the various chemicals are summarized in table 3, while and the interaction mechanisms, which are thought to take place between the asphaltenes and the chemicals are further specified as follows.
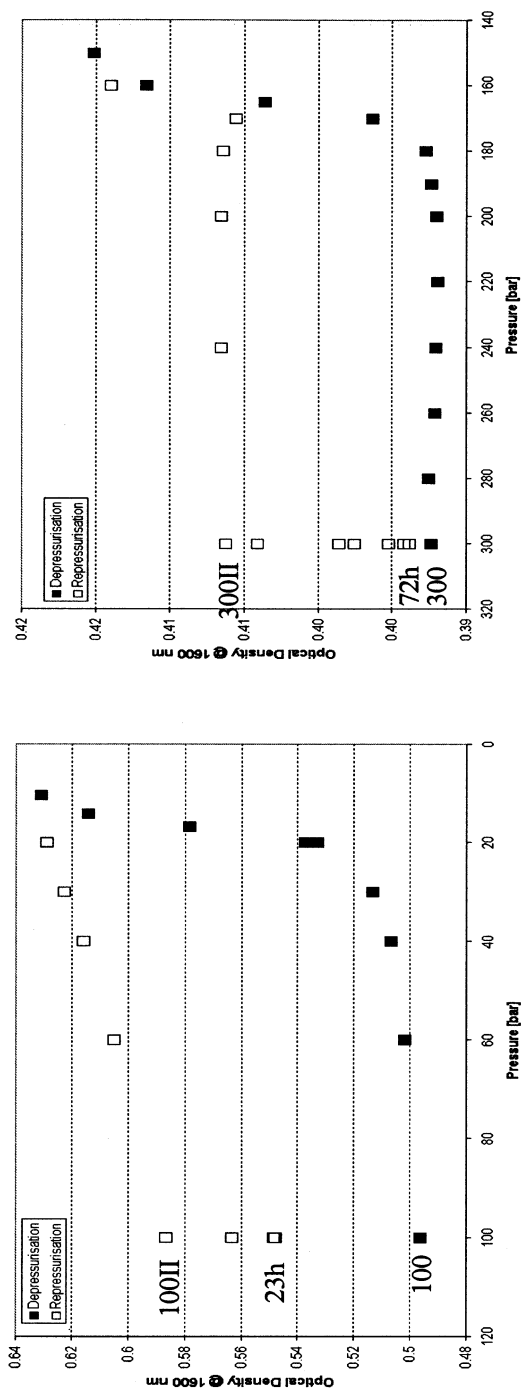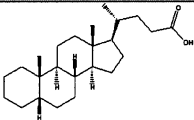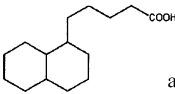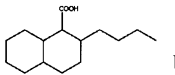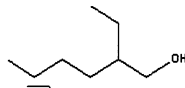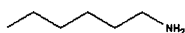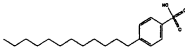
Fig. 5. Asphaltene aggregation and reversibility of model system and crude oil.

Table 3
A summary of the amphiphile and naphthenic acids used as addivies in this study.

| Name	Molecular weight	Chemical structure	Source	Purity (wt%)
5-β(H)-cholanoic acid [CHOL]	361		Chiron AS	> 95
1-Naphthalenepentanoic acid, decahydro [2C4]	238	a	Chiron AS	> 90
1-Naphthalenoic acid, decahydro-2-buthyl [C42]	238	b	Chiron AS	> 90
Crude naphthenic acid [CNA]	250	Mixture	Corn van der Locke	-
Fluka naphthenic acid [Fluka]	240	Mixture	Fluka	-
Naphthenic acid from North Sea [North Sea]	400	Mixture	Extracted	-
2-Ethyl-1-hexanol	130.23		Merck	> 99
1-Octanol	130.23		Merck	> 99
Benzyl alcohol	108.14		Fluka	> 98
Hexylamine	101.94		Merck	> 98
n-Alkylbenzenesulfonic acid, (n = C_{10}-C_{13}) [ABSA]	385.5		Alfa Aesar	96+
Inhibitor A	-	Mixture	Tros / Dyno	-
n-Heptane	100.21		Merck	> 99
Toluene	92.14		Merck	> 99

[a] Up to 30 wt% unsaturated bonds in cyclic part of molecular structure
[b] Up to 10 wt% unsaturated bonds in cyclic part of molecular structure

Fig. 6. NIR scattering measurements at 1600 nm for 0.125 wt.% asphaltenes in a 70/30 *n*-heptane/toluene mixture with crude naphthenic acid (CNA) added in various concentrations.

2.5.1. n-Alkylbenzenesulfonic acid
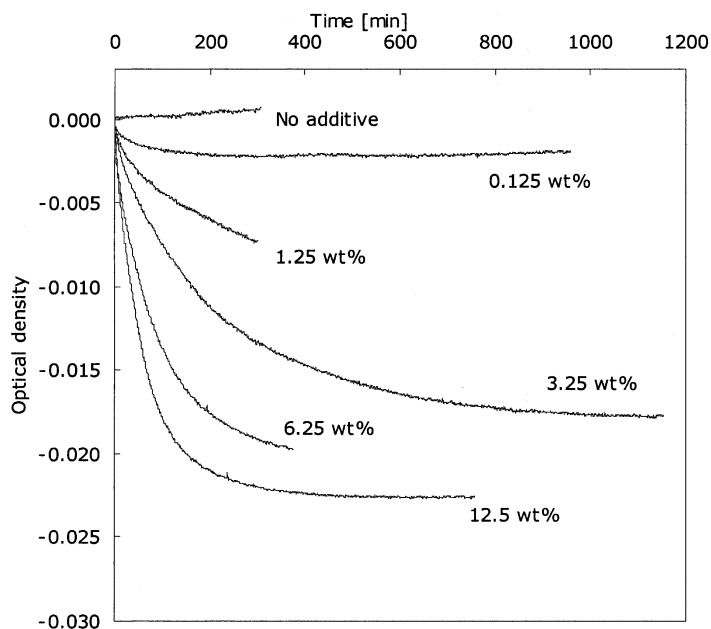
Dodecylbenzenesulfonic acid is known to efficiently disperse asphaltenes and form stable suspensions [71], and may be found in many commercial asphaltene dispersant chemicals. The mechanism behind the efficiency is assumed to be a strong acid–base interaction between the sulfonic acid headgroup and basic material in the asphaltene molecule. The alkyl chain is long enough (n-C_{10-13}) to disperse the asphaltene molecules and to give steric stabilization.

2.5.2. Naphthenic acids

In crude oils the naphthenic acids are normally incorporated in the group of resin molecules. It is generally believed that these acids, which are complex mixtures of condensed ring structures where the number of saturated and unsaturated rings and alkyl moieties, arrangement of the COOH groups and hydrophile–lipophile balance will vary, may interact with the asphaltenes. The interactions are thought to occur between the acid groups and basic components in the asphaltene molecule. Thus, the dispersing power is determined by the molecular structure, and naphthenic acid with different structures will possess different dispersing powers. In this study, we investigated the following monodisperse and polydisperse naphthenic acids: 5-β(*H*)-cholanoic acid (CHOL), 1-napthalenepentanoic acid, decahydro (2C4), 1-naphthal-

enoic acid, decahydro-2-butyl (C42), crude naphthenic acid (CNA), Fluka naphthenic acid and North Sea naphthenic acid.

2.5.3. Fatty alcohols

Fatty alcohols are normally efficient solvent molecules owing to their efficiency in breaking existing H-bonds and in forming new more favorable ones. Short-chain alcohols are believed to break down existing intermolecular hydrogen bonds between different asphaltene molecules and to replace them with alcohol–asphaltene hydrogen bonds. The alcohols used in this study were limited to 1-octanol, which is a normal paraffinic alcohol, 2-ethyl-1-hexanol, which is a branched paraffinic alcohol with the same number of carbon atoms, and benzyl alcohol, which is an aromatic derivative.

2.5.4. Fatty amines

The functionality of these is very much the same as for the fatty alcohols, i.e. the capability of replacing the hydrogen bonds with the amine group and to disperse with the alkyl moiety.

2.5.5. Inhibitor A

This is a commercial blend consisting of fatty amines and acids in polar solvents.

The experiments were performed by continuously measuring the change in scattering represented as optical density (OD) at 1600 nm wavelength, upon addition of chemicals to a solution of asphaltenes in heptane/toluene (70/30 vol.%/vol.%). At that aromatic/paraffinic ratio, the asphaltenes were expected to form rather large aggregates, and any effect on the size should be easy detectable.

Fig. 6 shows the relative OD at 1600 nm vs. time for toluene/*n*-heptane/ asphaltene mixtures with different amounts of CNA is shown. The influence of additive upon aggregate size is depicted as the decrease of scattering as a function of time. The relative OD vs. time for toluene/*n*-heptane/asphaltene mixtures with various naphthenic acids is plotted in Fig. 7. The commercial Fluka naphthenic acid and the naphthenic acids extracted from a North Sea crude seem to affect the state of the asphaltenes only to a minor extent. CNA is the most efficient of these polydisperse naphthenic acids.

A comparison between 2C4, C42 and CHOL shows these species to be somewhat more efficient than the previous group. Especially the 2C4 molecule has a very efficient breakdown to start with and also attains a low final value. It is interesting to see that the molecular structure affects the results to this extent.

The other amphiphiles, presented in Fig. 8, have a varying effect on the disintegration of the asphaltenes. The most efficient one is 1-hexylamine, which is very reminiscent of 2C4 with regard to short-term efficiency and the final state. The most efficient treatment is due to inhibitor A, the commercial mixture.

Alkylbenzenesulfonic acid is shown to associate with the asphaltenes and create aggregates of increased sizes. This is in accordance with the results obtained by Chang and Fogler [68] in an UV/vis spectroscopic study. They suggested that
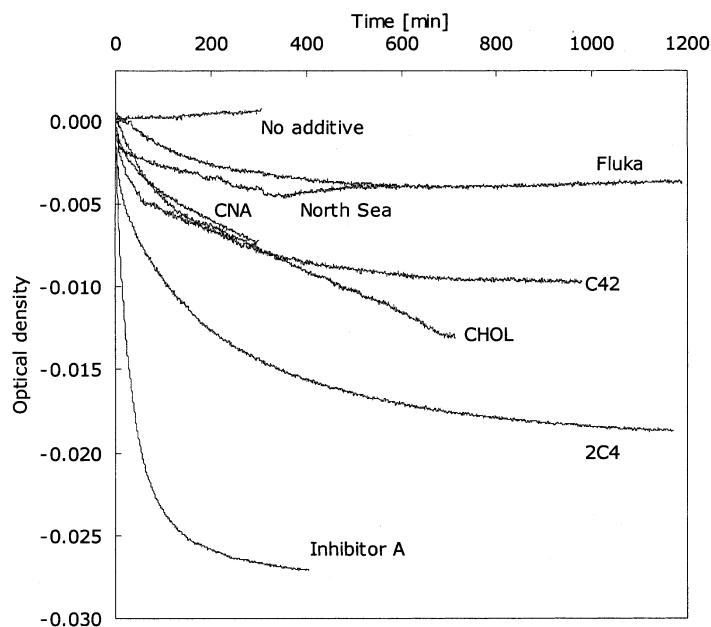
Fig. 7. NIR scattering measurements at 1600 nm for 0.125 wt.% asphaltenes in a 70/30 *n*-heptane/toluene mixture with 1.25 wt.% of various naphthenic acids added.

asphaltenes and dodecylbenzenesulfonic acid could associate into large electronic conjugated complexes.

It was shown that NIR spectroscopy is a powerful method to follow the disintegration of asphaltene aggregates upon addition of chemicals. The method is based on the scattering from preferentially large aggregates. The NIR technique, which is very fast and accurate, is a good choice for the initial screening of large numbers of chemicals for asphaltene inhibition. The results show that additives, which are efficient in replacing hydrogen bonds possess dispersive power and can serve as inhibitors. Commercial blends of active molecules gave the best results. It was also interesting to observe that the NIR technique could differentiate between the efficiency of the different naphthenic acids.

It should be mentioned that the disintegration of asphaltene aggregates had a profound influence on the corresponding emulsion stability. Prior to the addition of chemicals, the emulsions exhibited high stability, while the aggregate disintegration resulted in complete destabilization.

2.6. Asphaltene aggregation studied by NMR

Self-diffusion measurements by NMR have been utilized in numerous studies, ever since the discovery of spin echo by Hahn in 1950 [72]. Here, several new effects on spin echoes were presented, one of which was the diffusional effect on
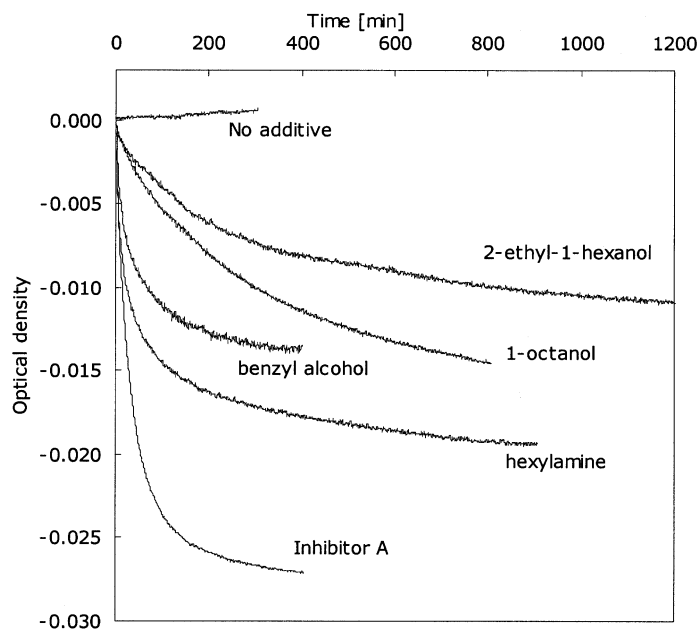
Fig. 8. NIR scattering measurements at 1600 nm for 0.125 wt.% asphaltenes in a 70/30 *n*-heptane/toluene mixture with 1.25 wt.% of various amphiphiles added.

echo amplitudes in an inhomogeneous magnetic field. The spin echo method was significantly improved in the mid-1960s with the pulsed field gradient spin-echo (PFG-SE) technique. McCall [73] is usually credited for the basic idée published in 1963, while the methodology and theory were presented later on by Stejskal and Tanner [74]. Several modifications to the technique have been made, and presently, PFG-SE NMR has evolved into a very useful approach in the studies of surface and colloid chemistry. The method is non-evasive, relatively fast, and measures the true molecular self-diffusion coefficients. It provides component resolved information concerning structural changes, bindings and associated phenomena, as well as sizes and shapes, from complex mixtures. Thus, the PFG-SE NMR technique offers an alternative way of obtaining information from, for instance, hydrocarbon mixtures, where typical light transmission techniques will struggle due to the opaqueness.

In an investigation by Östlund and coworkers [75], PFG-SE NMR (pulsed field gradient-spin echo nuclear magnetic resonance) measurements were combined with NIR (near infrared) spectroscopy, to evaluate potential interactions between asphaltenes and naphthenic acids. The NIR experiments were performed upon systems where the asphaltenes were slightly above the precipitation point, as opposed to the PFG-SE NMR experiments where the systems were below this point. The experiments were run with two types of asphaltenes, one extracted from an acidic crude (asphaltene 1) and one from a neutral crude (asphaltene 2). The naphthenic acids employed in the experiments were synthetic monodisperse acids (CHOL and 2C4).

A concentration series with asphaltenes in pure toluene was also prepared and studied, in order to obtain information about self-association of the asphaltene molecules.

The PFG-SE NMR method [76,77] measures the true molecular self-diffusion coefficients. For single diffusing species the attenuation of the spin echo is given by:

$$I = I_0 \exp(-kD_s) \tag{4}$$

where I is the integrated area of the peak of interest, I_0 the intensity of the signal at $g = 0$ and, in the case of sine-shaped pulses:

$$k = \gamma^2 g^2 \delta^2 (4\Delta - \delta)/\pi^2 \tag{5}$$

where γ is the gyromagnetic ratio of the nuclei (in this study ^{1}H), δ the gradient pulse duration and Δ the effective diffusion time. By applying a non-linear least-square fit of Eq. (4) to the experimental data the self-diffusion coefficient, D_s, can be evaluated. However, in many cases, the diffusing species is polydisperse and the echo-decay is then better represented by a function containing a distribution, $P(D)$, of diffusion coefficients:

$$I = I_0 \int_0^\infty P(D) \exp(-kD) dD \tag{6}$$

The functional form of the distribution function may vary, but in this case it was noted that a log-normal distribution described the data well:

$$P(D) = \frac{1}{D\sigma\sqrt{2\pi}} \exp\left(-\left(\frac{\ln(D) - \ln(D_m)}{\sqrt{2}\sigma} \right)^2 \right) \tag{7}$$

where D_m is the mass weighted median self-diffusion coefficient and σ is the standard deviation of the logarithm of the diffusion coefficient.

If, in addition to a continuous distribution of diffusion coefficients, a signal from one monodisperse species (such as for example a solvent) is contained in the NMR signal Eqs. (4) and (6) may be combined into:

$$I = I_0 \left(f_1 \int_0^\infty P(D) \exp(-kD) dD + f_n \exp(-kD_n) \right) \tag{8}$$

where f_1 is the fraction that is described by a distribution in diffusion coefficients and f_n the fraction that diffuse with single diffusion coefficients D_n. It was noted that Eq. (8) was sufficient to describe the echo decay in the case of asphaltenes in toluene-d_8. When studying the samples containing both naphthenic acid and asphaltenes, Eq. (8) was modified to contain one more single exponential function.

For samples studied by PFG-SE NMR, which contained both asphaltenes and naphthenic acid, the entire signal from 5-$\beta(H)$-cholanoic acid (CHOL) appeared at the same frequency (0.7–2.1 ppm), as the signal from the asphaltenes. The complete overlap of the signals complicated the evaluation of the samples containing CHOL.

1-naphthalenepentanoic acid, decahydro-, (2C4) fortunately had an additional peak at 4 ppm, hence, it was possible to study the diffusion of 2C4 without any contribution from the asphaltenes. It was observed that the echo decay of 2C4 was bi-exponential in the presence of both asphaltene 1 and asphaltene 2, which indicated that there were monomeric acid as well as associated acid in the samples. When evaluating the echo decay arising from combined signals, the fit of the experimental data using a Levenberg–Marquardt algorithm was seen to give reasonable results. The fitted results were verified by both Monte Carlo calculation of the error in each fitted parameter according to [78], and with the program CORE written by Stilbs [79,80] and designed to use the information contained in the full NMR spectrum

The PFG-SE NMR experiments were performed on a Unity Inova 500 MHz spectrometer and an Oxford magnet equipped with a diffusion probe from DOTY Sci. Inc., USA. The pulse sequence used for the diffusion measurements was a stimulated echo where the gradient pulse duration (δ) and the experimental observation time (Δ) were kept constant at 4 and 70 ms, respectively. A sine-shaped gradient was used to minimize the effect of eddy-currents. The gradient strength (g) was varied in 41 or, in the case when naphthenic acid had been added, 51 linear steps from 0 to a maximum value chosen so as to obtain a hundredfold decrease of the signal attenuation. All experiments were performed at 23 °C.

PFG-SE NMR measurements of the concentration series of asphaltenes 1 dissolved in toluene-d_8 are presented in Fig. 9. As can be seen, the median diffusion coefficient of the asphaltenes decreased as a function of increased asphaltene concentration. Östlund et al. [81] have shown that the obstruction effect in asphaltenic systems is large, due to the asphaltenes having a disc-like shaped structure. However, the decrease observed in this system was significantly larger than previously reported. It was thus likely that the asphaltenes investigated were not only subjected to obstruction, but also to self-association with an onset of flocculation at 0.1 wt.% asphaltenes.

Further, it was interesting to note from the results shown in Fig. 10 that the diffusion of asphaltene 2 decreased in all cases independently of which naphthenic acid that had been added. This indicated that both CHOL and 2C4 interacted with asphaltene 2. The diffusion coefficient of asphaltene 1, on the other hand, did not change and thus, it appeared as if there were no or only weak interactions between the naphthenic acids and asphaltenes of type 1.

The complimentary NIR measurements (Fig. 11), where the asphaltene particle size was followed as a function of time after addition of naphthenic acid, supported the NMR results. It was shown that addition of naphthenic acids to solutions with asphaltene 2 aggregates resulted in a considerable reduction in optical density. As discussed in Section 2.5, the reduction in optical density is a consequence of lower scattering from the asphaltenes, following an aggregates size reduction. This was thought to occur as a consequence of acid–base interactions between the naphthenic acids and asphaltene 1, whereby the asphaltene aggregates were dispersed into smaller sizes. The effect was more evident for asphaltene 2 than for asphaltene 1, upon addition of both CHOL and 2C4.
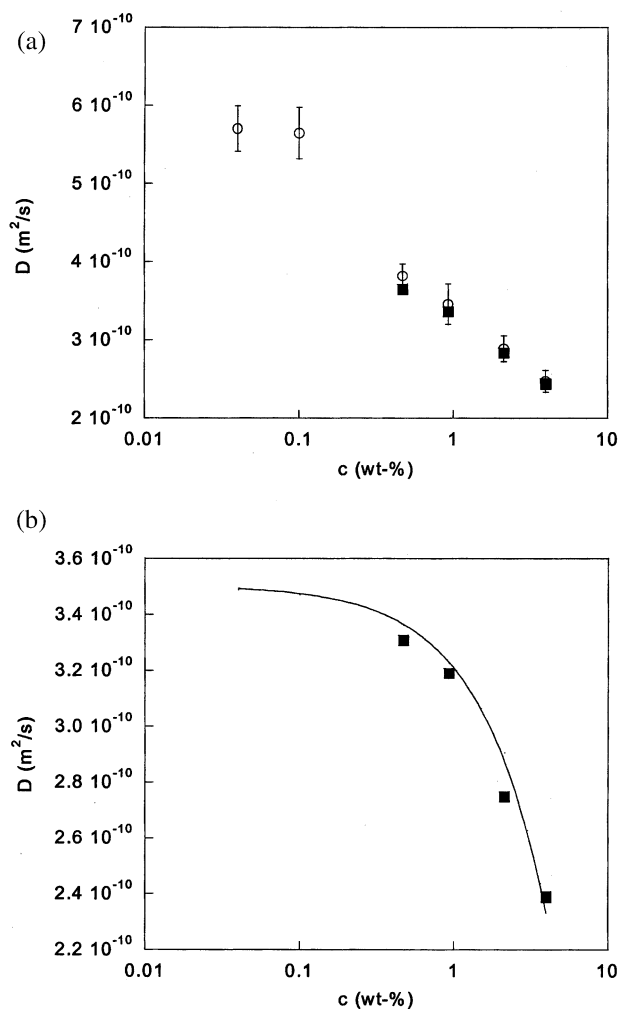
Fig. 9. The median diffusion coefficients are displayed as a function of the asphaltene concentration (O). Also included are the calculated diffusion coefficients of the asphaltene micelles (■).

2.7. Adsorption of asphaltenes and resins studied by Dissipative Quartz Crystal Microbalance (QCM-D)

The first thorough investigation of the piezoelectric effect is often attributed to Jaques and Pierre Curie, as early as 1880 [82]. However, it was not until 1917, when Langevin [83] showed that quartz crystals could be used as transducers and receivers of ultrasound in water, that a more detailed study of piezoelectricity started. In 1959, Sauerbrey [84] published a paper showing that the frequency shift of the quartz crystal was proportional to the added mass. This signified the birth of

Fig. 10. A presentation of results from samples containing naphthenic acid and asphaltenes. (■) Corresponds to the diffusion of the naphthenic acid (0.5 or 2.4 wt.% of CHOL alternatively 2C4), while (★) correspo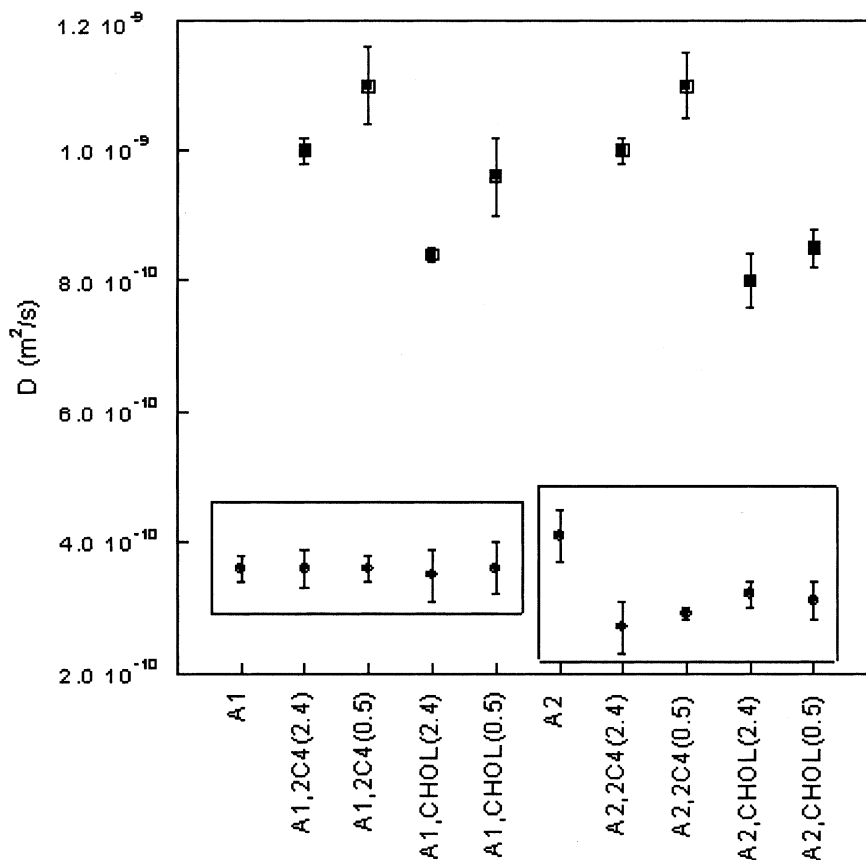nds to the diffusion of asphaltene 1 (A1) or asphaltene 2 (A2). The diffusion of only asphaltene 1 or 2 in toluene-d_8 (reference samples) has been included. Frames have been put around the diffusion coefficients from asphaltenes of the same kind (A1 or A2).

a new quantitative method for measuring very small masses, i.e. the quartz crystal microbalance. Another important step was a paper by Nomura and Okuhara [85], where QCM was proven reliable for measurements in the liquid phase. Preferably, one side of the sensor should be exposed to the liquid, and the other to a gas phase. At present, the QCM technique is in rapid expansion, and has found a wide range of applications in areas such as food, environmental and clinical analysis.

The conventional quartz crystal microbalance, QCM, consists of a thin disk of piezoelectric quartz crystal, which can be used to measure very small masses. The crystal is sandwiched between a pair of electrodes, which are hooked up to an electronic oscillator. When an AC voltage is applied over the electrodes, the crystal can be made to oscillate at its resonance frequency, f, via the piezoelectric effect.
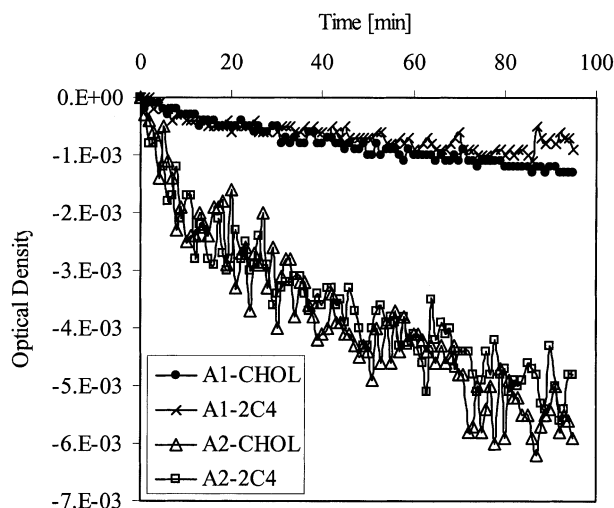
Fig. 11. The change in optical density (scattering) of asphaltene 1 (A1) and asphaltene 2 (A2) is displayed as function of time after addition of naphthenic acid (CHOL or 2C4). The spectrum at time = 0 was used as reference and has been subtracted from the subsequent spectra, thus eliminating the contribution from absorption to the optical density.

The oscillatory motion is damped due to (i) energy losses in the crystal, (ii) energy losses due to an overlayer deposited on the sensor, and (iii) energy losses to the surrounding medium. The magnitude of these losses can be measured by suddenly switching off the driving field to the sensor crystal. The oscillation will then rapidly decay in amplitude in the form of a damped sinusoidal wave, characterized by the frequency, f, and the time constant, τ, for the damping. The latter is inversely proportional to the sum of dissipative mechanisms, and termed the dissipative factor, D. The QCM-D™ technique is based on simultaneously measurements of both f and D. Changes in the conditions of the sensor crystal will induce a corresponding change in both frequency and dissipation factor. The changes are related to the deposited mass, the viscoelastic and dissipative properties of the overlayer. Thus, by continuous measurements of Δf and ΔD during deposition, information is obtained about the deposition kinetics and the amount of deposited matter (from Δf), as well as viscoelastic properties of the overlayer (from ΔD).

The adsorption of asphaltenes and resins onto a hydrophilic gold surface (a model surface for water) as a function of bulk concentration was investigated in [86]. The measurements were performed by a quartz crystal microbalance with dissipation measurements (QCM-D™), which allows for simultaneous measurements of frequency, f, and energy dissipation factor, D. The change in frequency is related to the mass adsorbed onto the surface of the sensor crystal, and from the change in dissipation factor, information about the interfacial processes can be resolved.

A schematic drawing of the measuring system is shown in Fig. 12. The key components are (i) the sensor crystal mounted in a measurement chamber with
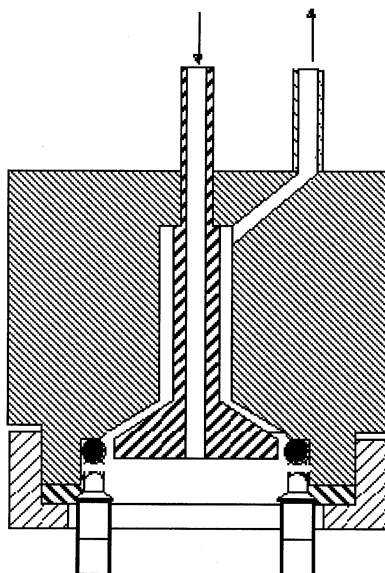
Fig. 12. A schematic of the quartz crystal microbalance cell.

facilities for batch of flow measurements in liquid or gas, (ii) the drive electronics (relay and signal generator), and (iii) the recording electronics (probe, reference frequency, filter) including data-handling and software (analog-to-digital converter and computer). In this study, AT-cut quartz crystal oscillators were used, with approximately 100-nm thick gold electrodes evaporated onto the crystal surface. To minimize the temperature flux from the system, the surrounding room was temperature controlled, and all solutions were stored in the same room. The temperature variations in the room were monitored to be in the range of $\pm$ 0.5 °C, and the temperature in the chamber was assumed to be the same.

The results showed that the resins in pure heptane adsorb onto a gold surface, and pack into a compact monolayer (see Fig. 13). However, there was no tendency of resin aggregation on the surface. With the increasing amount of aromaticity in the solvent, the adsorbed quantity decreased, and was practically zero in pure toluene. This was related to an increased solvency of the resins. The asphaltenes in heptane/toluene mixtures, or pure toluene, adsorbed to a larger extent (see Fig. 14). The adsorption was higher than observed for typical non-associating polymers indicating aggregate adsorption. At lower concentrations they formed a rigid layer. When higher concentrations were injected, it was possible to obtain further adsorption, which was related to the strong tendency of aggregation of asphaltenes in bulk solution. Desorption studies showed that resins were not able to desorb pre-adsorbed asphaltenes from the surface. Neither did they adsorb onto the asphaltene-coated surface. On the other hand, resins and asphaltenes associated in bulk liquid, and the adsorption from mixtures containing both resins and asphaltenes, was
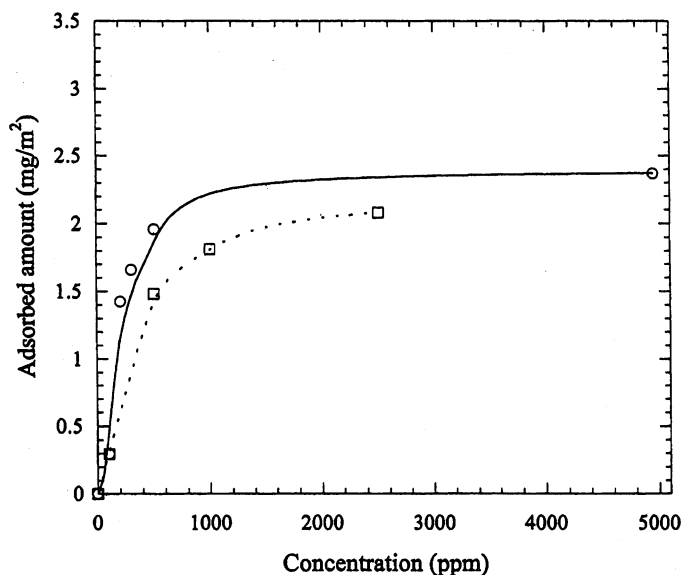
Fig. 13. Frequency and dissipation shift as a function of time for the adsorption of resins onto a hydrophilic gold surface in a *n*-heptane solution.

markedly different to that observed for the pure components. Hence, it was concluded that preformed resin-aggregates adsorb to the surface.

The irreversibly adsorbed amount for a crude oil solution was smaller than for the asphaltene and resin mixture but quite similar to that of the separate fractions. The resin and asphaltene molecules, arranged in a different way in the adsorbed layer, when the effects from other constituents like paraffin and wax were absent. These constituents could be incorporated in the adsorbed layer, or affect the interaction forces in the bulk of the crude.

The QCM technique can obviously give some insight in the adsorption behavior and affinity of different components in the crude oil. It should be mentioned that while a gold and a water surface/interface are different in nature, the driving forces for adsorption should be quite similar.

2.8. Interfacial behavior and elasticity of asphaltenes

It has been shown that different components in the crude oil have varying affinities for a fresh w/o interface. In order to understand the stability of water-in-crude oil emulsions it is imperative to understand the formation of different kinds of interfacial structures. From interfacial tension measurements (as exemplified in Fig. 15) one can draw the conclusion that it is the resin fraction that has the highest affinity towards the interface. The resins can reduce the IFT to values close to 15 mNm^{-1}. The asphaltene remained at 25 mNm^{-1} as the limiting value. The value
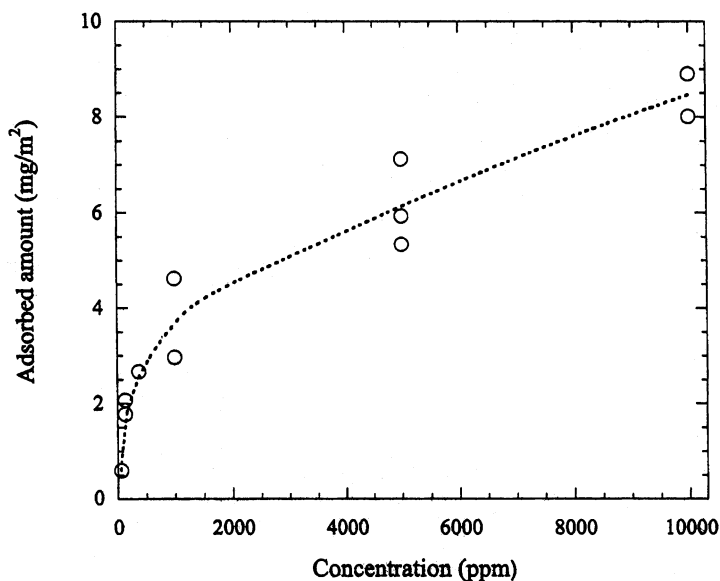
Fig. 14. Adsorption isotherm for asphaltenes onto a hydrophilic gold surface, as a function of asphaltene concentration in pure toluene.

for the entire crude oil at 30 mNm^{-1} reveals that there are other indigenous components influencing the IFT than resins and asphaltenes. There might be obstruction phenomena at the w/o interface resulting in different molecular structures in real systems and in model systems.

Generally, when an interface with adsorbed interfacially active molecules is stretched, interfacial tension gradients is generated. The tension gradients will oppose the stretching and try to restore the uniform interfacial tension state, i.e. the interface will behave elastically. This is the so-called Gibbs–Marangoni effect. The main function of interfacially active molecules is not the interfacial tension lowering they produce, but that their presence can lead to such gradients in interfacial tension able to resist tangential stresses. In practice, emulsion droplets being stretched can resist coalescence due to the elastic membrane, providing the droplet interfaces with a self-healing mechanism [87].

Interfacial rheological properties are measured through the so-called interfacial dilatational modulus. This property gives a measure of resistance to the creation of interfacial tension gradients, and the rate at which such gradients disappear after the deformation. The interfacial dilatational modulus, ε, is defined as the increase in interfacial tension for a unit of relative increase in surface area [88]:

$$\varepsilon = \frac{d\gamma}{d\ln A} \tag{9}$$

where γ is the interfacial tension and A is the interfacial area. For a small
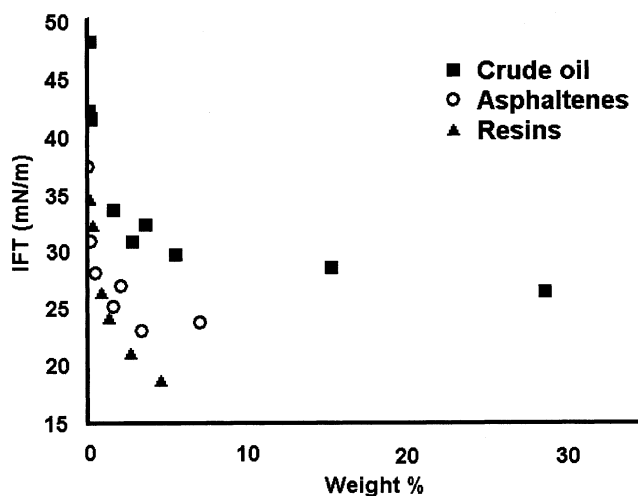
Fig. 15. Measurements of IFT at the interface between distilled water and a crude oil, extracted asphaltenes and resins dissolved in cyclohexane (redrawn from [229]).

deformation of the area, the change in interfacial tension can be written as a sum of an elastic and a viscous contribution

$$\Delta\gamma = \text{elastic} + \text{viscous} = \varepsilon_d \Delta \ln A + \eta_d \frac{d\ln A}{dt} \tag{10}$$

where ε_d and η_d is the interfacial dilatational elasticity and viscosity, respectively. The two contributions can be measured separately by subjecting the interface to small, periodic oscillations at a given frequency. In an oscillatory experiment the interfacial area is varied with time, t, according to

$$\Delta \ln A \propto \exp(i\omega t) \tag{11}$$

where ω is the frequency of the oscillations. Based on the above equations the interfacial dilatational modulus can be written as a complex number

$$\varepsilon = \varepsilon_d + i\omega\eta_d \tag{12}$$

where the first term will be equal to the elastic contribution and the second term will be proportional to the viscous contribution. Only the elastic contribution will be discussed in the following section.

2.8.1. Effect of asphaltene aggregation on interfacial elasticity

In order to measure the interfacial dilatational modulus, an oscillating pendant drop apparatus was utilized. The system is illustrated schematically in Fig. 16. It operates by oscillating an oil drop in an aqueous phase at constant frequency. Photographs are continuously taken of the drop profile, and, by knowing the densities of the two phases, the interfacial tension is calculated by use of the Laplace
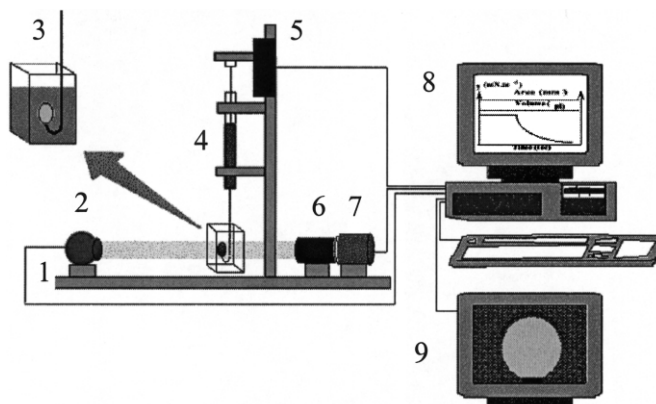
Fig. 16. The pendant drop apparatus consisting of an optical bench (1) with a halogen lamp as light source (2), a cuvette containing the oil drop in the water phase (3), a CCD camera (7) attached to a telecentric lens (6), a syringe (4), and a DC motor.

equation [89]. As both the changes in interfacial area and interfacial tension are known, the interfacial elasticity may be calculated.

For emulsion systems, the interfacial concentration of surfactants will be low due to the large interfacial area created by the small droplets formed. Therefore, in practice, the oil systems under study are diluted with some solvent in order to better simulate the interfacial concentrations encountered in real systems. The left hand side of Fig. 17 shows the measured elasticity as a function of crude oil concentration and solvent composition for a diluted crude oil [4]. The sample was diluted in heptane/toluene solutions containing 0, 50, 95 and 100 vol.% heptane (heptol(0)-heptol(100)) at concentrations of 0.002, 0.01 and 0.02 ml oil/ml solvent. In addition, all the solutions were characterized by NIR spectroscopy, and on the right hand side of the figure is shown the corresponding optical density at 1600 nm from the NIR spectra of the crude oil solutions. This value indicates the level of asphaltene aggregation in the solutions.

In poor solvents (high heptane content), the interfacial elasticity decreases with increasing oil concentration. In good solvents, the interfacial elasticity generally increases with oil concentration. From the optical density results, the formation of larger aggregates is seen to be much more dominating in poorer solvents. The lowering of the interfacial elasticity thus appears to be caused by the formation of large, weakly interfacially active asphaltene aggregates. At the lowest oil concentration, the highest elasticity values are obtained in the poorest crude oil surfactant solvents. In these solvents, the interfacial activity of resins and asphaltenes is high, and more or less no aggregation is taking place, as seen from optical density values. At higher oil concentrations, the effect of interfacial activity seems to be opposed by the formation of asphaltene aggregates.

Similar results as shown above have been found for other crude oils, and demonstrate that measuring interfacial rheological properties of crude oil systems is highly dependent both on the oil concentration and what solvent is used for dilution [4]. The effect of high interfacial activity in aliphatic solvents is quickly opposed by asphaltene aggregation when increasing the oil concentration. When comparing the interfacial rheological properties of different crude oils, both these effects have to be taken into consideration. The findings are consistent with the asphaltene aggregation model proposed by Kilpatrick and coworkers [5,6,90]. They found that precipitated asphaltenes had a lower ability to form elastic interfaces. This was attributed to lower interfacial activity of such precipitated aggregates and possibly high amounts of defects in films of precipitated material.

The emulsion stability in different crude oil-based systems is highly dependent on the rheological properties of the w/o interface. Generally, a high elasticity will increase the level of stability.

3. Chemistry of naphthenic acids

The interest in the chemical properties of naphthenic acid derivatives originates from an ever-increasing co-production of crude oils as acidic crudes [91,92]. It is well known that these naphthenic acids show a polydispersity in size and structure [93]. The smallest molecules are readily dissolved in the aqueous phase at pHs around 5, while the larger molecules are preferably oil-soluble. Most of these homologues are dissolved in an aqueous phase at pHs around 10–11 [94–96].

There are some immense crude oil production problems related to the occurrence of naphthenic acids. They cause corrosion problems at the refineries when being processed. The mechanism of this process is not clarified in detail, since it takes place in an oil environment [97]. Since the naphthenic acids and their soaps are surface/interfacially active they will accumulate at w/o interfaces and stabilize colloidal structures [93,96,98,99]. The worst scenario from an operational point of view is the stabilization of water-in-oil emulsions, which will cause problems in topside separators [100]. If Ca- or Mg- soaps are formed, the precipitation of corresponding particulate soap with low water solubility will be a consequence. The metal soaps tend to accumulate at water/oil-interfaces. The agglomeration of these particles to voluminous precipitates will cause operational problems in the separation process with shutdown periods, during which thorough cleaning must take place. The formation of naphthenate mixed scale particles in deep-offshore fields has recently been studied by Rousseau et al. [92].

In contrast, the low molecular weight and water-soluble derivatives will cause quality problems for the wastewater.

With this background, it is evident that there is a need to gain a better understanding of the chemistry of naphthenic acid and their derivatives. Although the corresponding paraffinic fatty acids are very well characterized with regard to association and micellization in water, phase equilibrium, formation of lyotropic
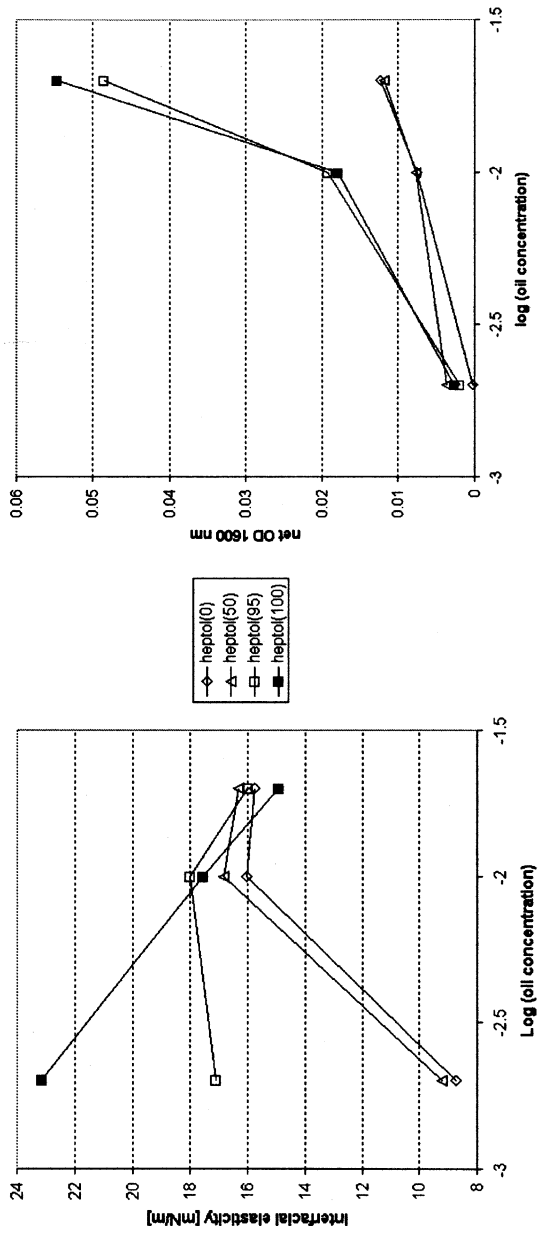
Fig. 17. Interfacial elasticity and optical density of crude oil 15.

liquid crystals and microemulsions, monomolecular film properties, etc. [101–109], little information is available for naphthenic acids.

3.1. Origin and structure

Naphthenic acids are classified as monobasic carboxylic acids of the general formula RCOOH, where R represents a cycloaliphatic structure. The term 'naphthenic acid' is often used to account for all carboxylic acids present in crude oil, including acyclic and aromatic acids. Nearly all crude oils contain some naphthenic acids. Heavy crudes from geologically young formations have the highest acid content while paraffinic crudes usually have low acid content [110]. Naphthenic acids are known to be produced during the in-reservoir biodegradation of petroleum hydrocarbons [111], and they are considered to be a class of biological marker, closely linked to the maturity and the biodegradation level of the fields [92].

The naphthenic acids are extremely complicated mixtures. Many different methods and analytical techniques have been used for analyzing these acids in the past [93,99,112–115]. An overview shows them to be C_{10}–C_{50} compounds with 0–6 fused saturated rings and with the carboxylic acid group apparently attached to a ring with a short side chain [116]. The distribution of carbon number and ring content varies with crude oil source and distillate fraction. Naphthenic acids with similar total acid number (TAN) and average molecular weight can exhibit significantly different profiles [117].

3.2. Partitioning and interfacial activity of naphthenic acids

Naphthenic acid will be distributed between the hydrocarbon and the water phase, with a partitioning constant, K_{wo}, according to Eq. (13), where $[HA_o]$ and $[HA_w]$ represents the monomeric concentration of naphthenic acid in the oil and water phase, respectively. Eq. (14) gives the acidic constant, K_a, $[A_w^-]$ is the concentration of dissociated acid and $[H^+]$ is the concentration of H^+-ions.

$$K_{wo} = \frac{[HA_w]}{[HA_o]} \tag{13}$$

$$K_a = \frac{[A_w^-] \cdot [H^+]}{[HA_w]} \tag{14}$$

By combining Eq. (13) and Eq. (14) with the appropriate mass balances, the expression for the total concentration of naphthenic acid in the water phase is obtained:

$$[HA]_{aq,tot} = [HA]_{init.oil} \frac{V_{oil}}{V_{water}} \cdot \left(1 - \frac{1}{1 + K_{wo} \dfrac{V_{water}}{V_{oil}} \cdot \left(1 + \dfrac{K_a}{[H^+]} \right)} \right) \tag{15}$$

where $[HA]_{init.oil}$ is the initial concentration of the naphthenic acid in the oil phase

and V_{oil} and V_{water} is the volume of the oil and water phase, respectively. Other equilibria, such as micellization and dimerization will influence the net distribution of acids between water and oil.

A crude oil from the Norwegian continental shelf, with a naphthenic acid content of 2 wt.%, has been used to study the partitioning and acidic constants of the naphthenic acids [118]. The crude oil samples were mixed with an equal amount of water with different pH-values. After an equilibration time of at least 24 h, the concentrations of the naphthenic acids were determined with GCMS. The technique gives information about the content of some of the naphthenic acid structures defined by size and number of rings. The naphthenic acids in the crude oil were extracted by an ion exchange method and then analyzed by GCMS. The partitioning and acidic constants were then obtained by fitting Eq. (15) to the experimental points as shown in Fig. 18 for naphthenic acids with 12 carbons and two rings.

pK_a–values for C10–C16 naphthenic acids with one, two, or three rings were determined to 4.9 ± 0.1 at 25 °C. The partitioning constants for these naphthenic acids are shown in Fig. 19. The logarithm of the partition coefficients varies linearly vs. the number of carbons in the naphthenic acid molecules. This is in accordance with findings of Reinsel et al. [119] who have studied the partitioning of acetic, propionic and butyric acids between crude oil and water. The naphthenic acids with three rings are apparently more hydrophilic than acids with one or two rings.

3.2.1. Interfacial activity of naphthenic acids

The presence of amphiphilic carboxylic acids in a water/hydrocarbon system will result in a reduction in interfacial tension. The dissociated and associated form of the acid molecules will have different interfacial properties. Several studies have been performed in assessing the pH dependence on interfacial tension in oil/water/carboxylic acid-systems [104,105,120–126]. The interfacial activity for surfactants in crude oil has also been studied by several authors [98,100,127,128]. A marked decrease is generally observed in interfacial tension as the pH of the water phase increases and the concentration of dissociated acid molecules becomes significant. Danielli [122] explained why the interfacial tension continued to decrease after complete ionization by use of the Donnan equilibrium. The reduction in interfacial tension occurs at the same pH as when the naphthenic acids shift from oil-soluble to water-soluble due to dissociation.

Rudin and Wasan [94,95] have studied the mechanism for lowering of interfacial tension in alkali and acidic oil systems. In addition, to relate lowering of interfacial tension to dissociation of acid molecules, they also considered the presence of un-ionized acids at the interface. They argue that the interfacial tension vs. pH goes through an ultra low minimum due to simultaneous adsorption of ionized and un-ionized acids. They also consider the influence of micelles formed by both ionized and un-ionized molecules.

The fact that interfacial tension decreases at high pH for acidic crude oils is used in enhanced oil recovery. Alkaline solutions can be injected into the reservoir in order to lowering capillary forces and facilitating oil recovery [94].
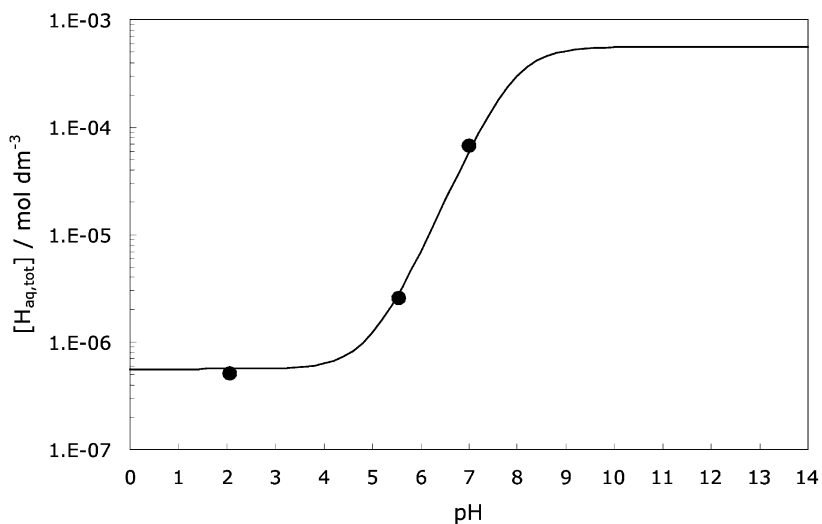
Fig. 18. pH vs. total concentration of naphthenic acids, with 12 carbons and two rings, in the water phase. Equation (15) (line) is fitted to the experimental points.

The interfacial tension between a hydrocarbon phase consisting of cyclohexane and a water-phase with different pH has been investigated for various concentration of a commercial naphthenic acid mixture (Fluka). The results are presented in Fig. 20. It is seen that the undissociated form, dominating at low pH, causes a decrease in the interfacial tension. As the pH increases, a marked decrease in the interfacial tension is seen. One might expect this decrease to set in around the pK_a of the naphthenic acids. However, it is the total amount of dissociated acid, in both water and hydrocarbon phase, that must be considered. At $pH > pK_a$ the dissociated forms

Fig. 19. Partitioning constants, K_{wo}, for naphthenic acids with one, two and three rings and different numbers of carbons.

Fig. 20. Interfacial tension between cyclohexane and water as a function of pH for various concentration of a commercial naphthenic acid mixture (Fluka).
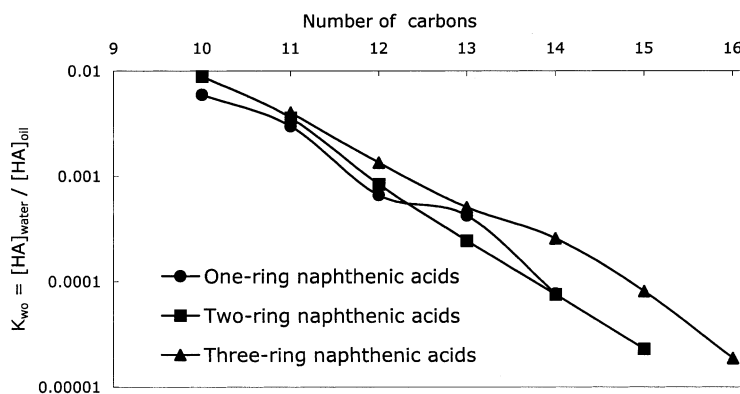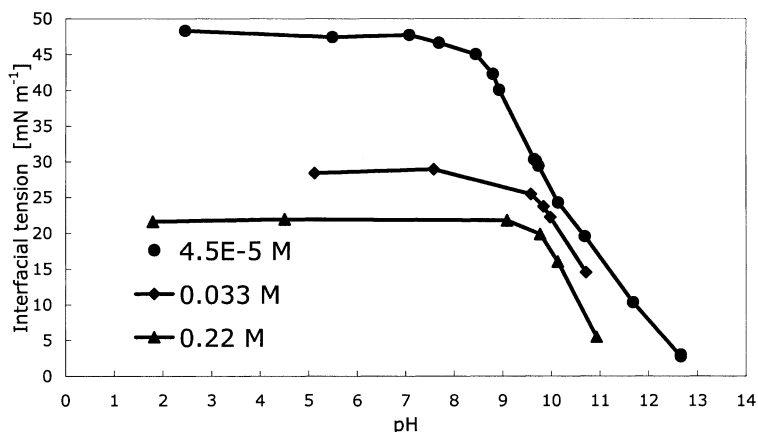
of the naphthenic acids dominate the undissociated forms in the water phase. In the overall system, the amount of dissociated acids will still be small at pH $\sim$ pK_a. If K_{wo} (Eq. (13)) has a value of 10^5, the amount of dissociated and undissociated naphthenic acids will be equal at pH-value approximately 5 pH-units above pK_a [118].

3.2.2. CMC determination at high pH

Normally, a determination of CMC gives a first basis in understanding the intermolecular interactions in aqueous solutions of surfactants. For paraffinic fatty acid salts with sufficiently long alkyl chains a distinct CMC is normally observed. The driving force is normally considered to be a strong attractive hydrophobic interaction between the hydrocarbon chains. At the same time, the paraffinic alkyl chains do not have any severe packing constraint. On the other hand, pharmaceutical surfactants with condensed ring structures are known to have a step-wise association in water and a weak CMC is resulting. Obviously, these molecules have restrictions in their packing, and ordinary spherical micellar structures do not emerge. The difference in the molecular packing is also reflected in the aggregation numbers. For the paraffinic fatty acid salts, the micelles can contain up to 100 monomers, which is considerably higher than for the monomers with large condensed ring structures. The interesting thing with naphthenates is to compare the structures and see to what extent they follow an association tendency as ordinary paraffinic homologues, or when a stacking of monomers will set in.

The critical micelle concentration (CMC) has been determined for some naphthenic acids. The area/molecule is determined from Gibbs' adsorption equation. The results are given in Table 4. The CMC-curve for Fluka naphthenic acid is shown in Fig. 21. These results have recently been published [129].

Table 4
Critical micelle concentration (CMC) and area per molecule for the naphthenic acids at high pH

	pH	CMC [mol dm^{-3}]	Area/molecule [Å^2]
1-naphthalenepentanoic acid, decahydro (9CI)	11.0	2E-4	52
Fluka naphthenic acid	11.3	8E-4	61

The CMC for the polydisperse Fluka naphthenic acid is rather distinct. The plot of surface tension vs. log concentration for 1-naphthalenepentanoic acid, decahydro- indicates possible contamination. The reason may be due to presence of aromatic forms of the naphthenic acid, i.e. incomplete hydrogenation in the synthesis.

$5\beta(H)$-cholanoic acid does not have a distinct CMC. The time necessary for achieving an equilibrium value increases for decreased acid concentration. For a concentration of 0.01 g dm^{-3}, 3 h is required to reach equilibrium. It is uncertain whether this is due to contamination by other surfactants in the chemicals.

The area per molecule for 1-naphthalenepentanoic acid, decahydro- and Fluka naphthenic acid is 52 and 61 Å^2/molecule, respectively. Ovalles et al. [128] have reported values for area/molecule for natural occurring naphthenic acids at an interface between water and toluene. They found 113–152 Å^2/molecule for different fractions.

The CMC-measurements reveal that the naphthenic acid salts behave as micelle-forming surfactants at appropriate pH values. For this kind of surfactants, the molecular packing parameter, MPP, can be applied.
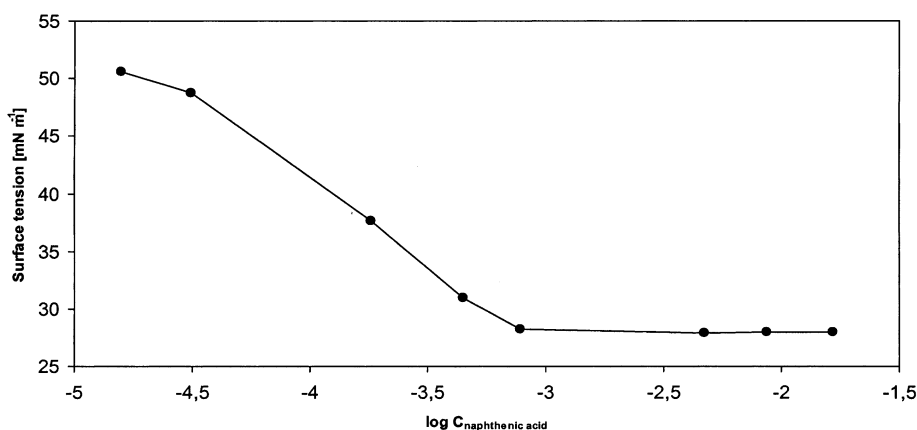
$$MPP = \frac{V}{a \cdot l} \tag{16}$$

Fig. 21. CMC-curve for Fluka naphthenic acid at pH 11.3. Surface tension vs. log concentration [mol dm^{-3}].

Here, V is the volume of the surfactant, a is the head-group area (topological) and l is the length of the almost extended hydrocarbon chain. For micelle-forming surfactant (spherical aggregates) in water, the MPP is approximately $1/3$. For lamellar aggregates (and microemulsions) MPP obtains a value of approximately 1, while oil-continuous structures, like reversed micelles, have a MPP > 1 [130].

In a system consisting of a naphthenic acid, NA and a naphthenic salt, N^-, the ratio, N^-/NA, will determine what kind of structure to occur. Normally by varying N^-/NA (in water), at high enough pH, one will have micelles, liquid crystals and reversed structures [131]. For emulsion stabilization, the occurrence of a lamellar liquid crystal D-phase will be most crucial.

3.3. Film formation

A central property for emulsion stabilization is the formation of a w/o film that is stable against coalescence. Film formation of naphthenic acids can be studied by Langmuir technique. The technique is used in order to characterize monolayer properties of surface-active materials. The objective is to get information about how the molecules pack in a monolayer, i.e. how much area each molecule requires and how the molecules interact with each other. The stability of the monolayer and how the pH and electrolyte concentration affects this stability is also discovered. A stable monolayer indicates the ability of the surfactant to stabilize emulsions.

Fluka naphthenic acid, $5\beta(H)$-cholanoic acid (1) and 1-naphthalenepentanoic acid, decahydro- (9CI) (2) (Chiron AS) (see table 3) have been used in a Langmuir study [129].

1-naphthalenepentanoic acid, decahydro- rapidly dissolves into the bulk phase and, hence, no stable films are formed. Acidifying the subphase or addition of cations does not influence this situation.

$5\beta(H)$-cholanoic acid and Fluka naphthenic acid form stable films when cations are present in the aqueous sub phase. The stability isotherm for $5\beta(H)$-cholanoic acid is given in Fig. 22. The results are expressed as A/A_0 vs. time, t, where A_0 is the area of the monolayer after compression to constant surface pressure (10 mN/m) and A is the area of the monolayer at time t. At lower pH, the addition of metal ions will have less effect since the naphthenic acid is not protolyzed and naphthenates will not be formed. The divalent calcium ions have a more stabilizing effect on the film than the sodium ions.

Pressure–area isotherms for different pH values, at a fixed sodium ion concentration of 0.1 M, are given in Fig. 23. As the pH increases, the film tends to tolerate a higher pressure before collapse. This is an indication of more stable films owing to naphthenate formation. The figure shows that the pressure increase sets in at different areas per molecule at the different pH values. At pH 3.0 the film properties are dominated by the fact that this film has a low long-term stability (Fig. 22, curve c). The reason for this is that the molecules are in an undissociated form and will not be stabilized by Na^+ ions.

Joos [132,133] has suggested that the collapse pressure, $\pi_{c,m}$, of a mixed miscible
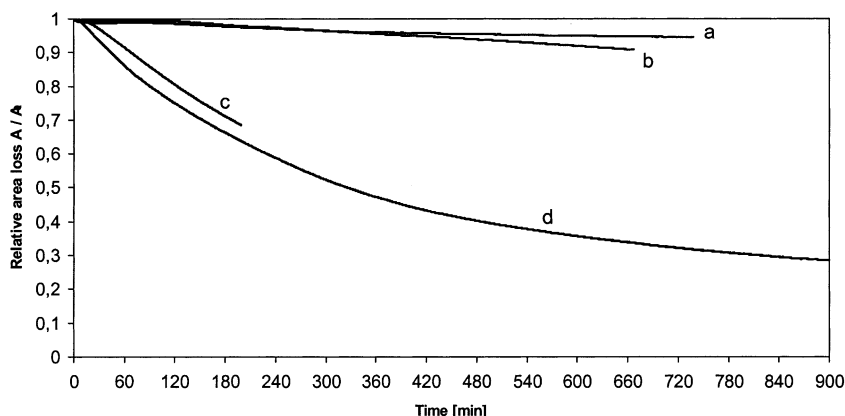
Fig. 22. Stability isotherms (surface pressure of 10 mN/m) for 5 (*H*)-cholanoic acid at (a) pH 5.6, $[Ca^{2+}] = 0.01$ M, (b) pH 7.0, $[Na^+] = 0.1$ M, (c) pH 3.1, $[Na^+] = 0.1$ M and (d) pH 5.6, pure water.

monolayer may be evaluated from the collapse pressures, $\pi_{c,1}$ and $\pi_{c,2}$, of the separate components according to Eq. (17):

$$X_1 \exp\left[\frac{(\pi_{c,m} - \pi_{c,1})\omega_1}{kT}\right] + X_2 \exp\left[\frac{(\pi_{c,m} - \pi_{c,2})\omega_2}{kT}\right] = 1 \qquad (17)$$

Wherein X_1 and X_2 are the mole fractions in the monolayer of component 1 and 2, respectively and ω_1 and ω_2 are their partial molecular area. The activity coefficients are neglected, and it is assumed that equilibrium exist between the molecules in the monolayer and in the collapsed phase.

The acidity constant, K_a^s, in the monolayer can be defined according to Eq. (18):

$$K_a^s = \frac{X_{ZH}}{X_{ZNa}[H^+]} \qquad (18)$$

Here X_{ZH} and X_{ZNa} represent the mole fractions in the monolayer of naphthenic acid and sodium naphthenate, respectively. $[H^+]$ refers to the bulk concentration of H^+ ions. Due to the electrical double layer, the concentration of H^+ at the surface will be higher than in the bulk. The pK_a^s-value will thus be higher than an ordinary pK_a.

If it is assumed that the partial molecular area of the undissociated and the soap form of the acid is the same ($\omega_{ZH} = \omega_{ZNa} = \omega$), Eq. (17) and Eq. (18) can be rewritten as

$$\pi_{c,m} = -\frac{kT}{\omega} \ln\left[\frac{[H^+]}{K_a^s + [H^+]} \exp\left(\frac{-\pi_{c,ZH}\omega}{kT}\right) + \frac{K_a^s}{K_a^s + [H^+]} \exp\left(\frac{-\pi_{c,ZNa}\omega}{kT}\right)\right]. \qquad (19)$$

This equation relates the collapse pressure of the monolayer as a function of the H^+ concentration or the pH of the bulk phase, provided the collapse pressures of
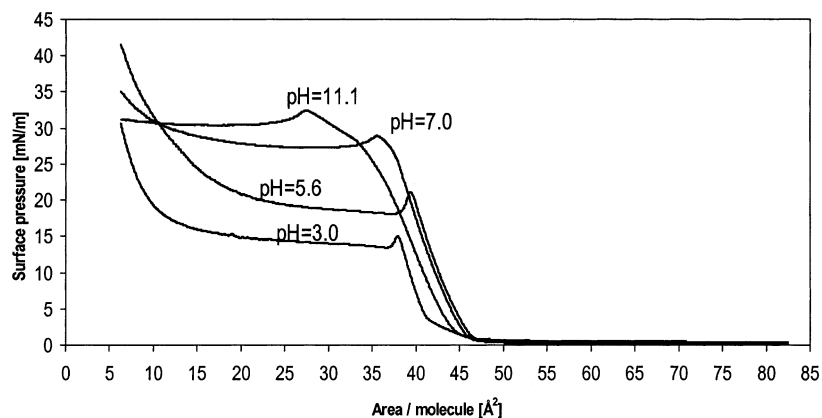
Fig. 23. Pressure-area isotherms for 5 (*H*)-cholanoic acid at $[Na^+] = 0.1$ M and pH 11.1, 7.0, 5.6 and 3.0.

the acid form and the soap form are known. It is seen that the surface dissociation constant, K_a^s, can be evaluated from such experiments.

A plot of a curve according to Eq. (19) and the experimental points from Fig. 23 are shown in Fig. 24. The fitting of the theoretical curve to the experimental values gives a pK_a^s of 5.65 for 5(*H*)-cholanoic acid. Joos obtained p$K_a^s = 7.5$ for cholic acid. The barrier speed and the composition of the subphase will probably influence the determination of pK_a^s.
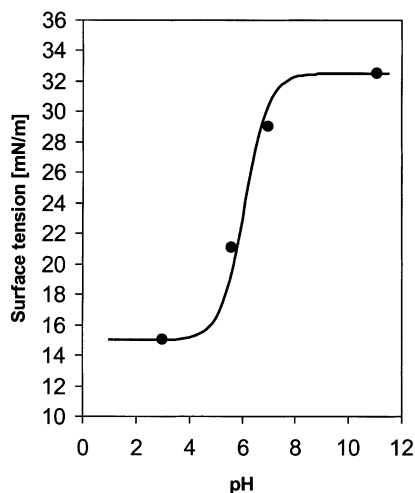
Fig. 24. Collapse pressure of a 5 (*H*)-cholanoic acid monolayer as a function of pH. *Points*: experiment; *full line*: calculated according to Eq. (19). $\omega = 46$ Å^2, $T = 293$ K, p$K_a^s = 5.65$, $\pi c,ZH = 15$, $\pi c,ZNa = 32.5$.

3.4. Phase equilibria

Professor Stig E. Friberg was a pioneer in linking the importance of phase equilibria in water/oil/stabilizer systems with emulsion stability. He documented very clearly the importance of the existence of a lamellar liquid crystal (a so-called D-phase) and a corresponding increase in emulsion stability [9–12].

The basic idea is to cover the emulsion droplets with a multiple layer of surfactant/water to enhance the rigidity of the interfacial w/o-layer. In this way, a barrier against coalescence is built up. Per today, no detailed and complete phase equilibria of a naphthenic acid (different pH)/water/oil or sodium naphthenate/naphthenic acid/water/oil has been published. Horváth-Szabó has, in cooperation with groups in Edmonton, published qualitative phase equilibria of sodium naphthenates in aqueous solution [131] and sodium naphthenates/toluene/water system [134] and found evidence for the existence of lamellar liquid crystals.

It is our opinion that the phase equilibria in the system water/sodium hexadecanoate (NaC16)/hexadecanoic acid (HC16) at 70 °C is representative also for naphthenic acid-based systems. The phase diagram of this system has been published by Skurtveit et al. [101] and is given in Fig. 25.

In this system, existence of 4 or 5 isotropic phases can be observed. These are a micellar L_1-phase (with ordinary micelles), a hexagonal liquid crystalline E-phase (with long rods in an aqueous environment), a lamellar liquid crystalline D-phase (with a bilayer structure) and a reversed solution phase L_2 (with reversed micelles). It is questionable if an F-phase with a reverse hexagonal structure exists. In this diagram, the importance of the stabilization of water/oil emulsions, due to the D-phase has been documented [101].

For practical reasons, it is of importance to map the existence of the lamellar D-phase. In Fig. 25, it is noticeable that an upper limit of phase equilibria including the D-phase, seems to be HC16/NaC16 ≈ 85/15, and a lower limit is HC16/NaC16 ≈ 15/85. Hence, it can be claimed that in an equivalent naphthenic acid-based system, a D-phase can exist for ratios of naphthenic acid to sodium naphthenate ∼ 0.1–6. It is sufficient to have just 10% of a naphthenate salt to obtain the D-phase.

In order to view the competition between D-phase stabilization and asphaltene-particle stabilization of water/oil emulsions, the following experiment has been performed [14]. A D-phase was prepared based on the equilibria in Fig. 25. A dichloromethane solution, containing dissolved asphaltenes, was mixed with the D-phase and the solvent was evaporated. After 24 h there was clear evidence of asphaltene particles present in the D-phase. This D-phase, modified with different amount of asphaltenes, was used to stabilize w/o-emulsions. In order to measure the emulsion stability, the $E_{critical}$ was determined. The result is shown in Fig. 26.

Obviously, the addition of asphaltene particles can enhance the w/o-emulsion stability from the case with just a D-phase present. But too high an amount of asphaltenes particle will give destabilization. A ratio of 0.6, i.e. 60 wt.% particles and 40 wt.% D-phase seems to be optimal. The experiment in Fig. 26 is very important in visualizing different mechanisms behind emulsion stability in crude
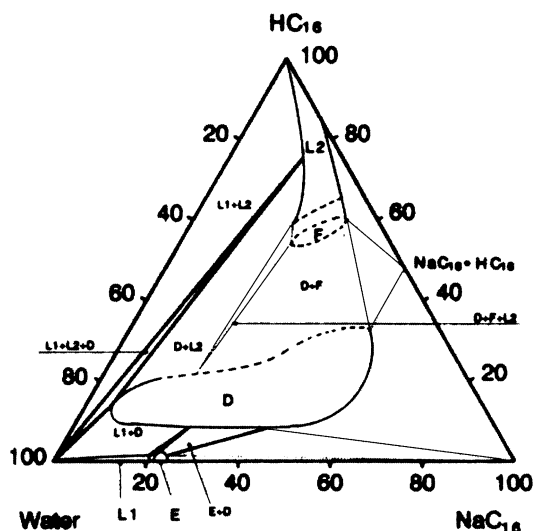
Fig. 25. Phase equillibria in the system water/hexadecanoic acid (HC16)/sodium hexadecanoate (NaC16) at 70 °C [101]. The diagram is expressed in weight percent.

oils with high amounts of asphaltenes and naphthenic acids. Representatives to these are heavy crudes, and bitumens.

4. Water-in-crude oil emulsions

4.1. Stability mechanisms

An emulsifying agent must be present to form stable water-in-crude oil emulsions. Such agents include scale and clay particles, added chemicals or indigenous crude oil components like asphaltenes, resins, waxes and naphthenic acids [8]. Asphaltenes are believed to be the main contributor to emulsion stability, and McLean and Kilpatrick [5,6] have postulated that the dominating mechanism whereby crude oil emulsions are stabilized is through the formation of a viscoelastic, physically cross-linked network of asphaltenic aggregates at the oil–water interface. The ability of asphaltenes and resins to form elastic crude oil–water interfaces have been emphasized by several other authors as an important factor with regard to emulsion stability [127,135–137]. The aggregation state of the asphaltenes in the crude oil is very decisive with regard to the emulsion stability properties. Several authors have pointed out that emulsions are to a small extent stabilized by individual asphaltene molecules as compared to emulsions stabilized by colloidal asphalthene aggregates [5,138–141].
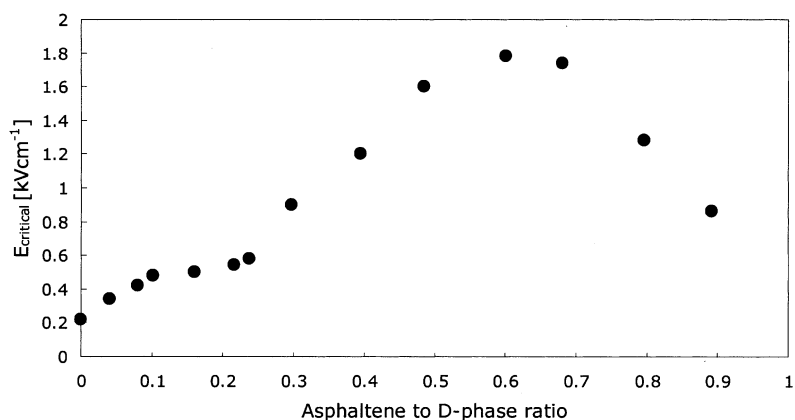
Fig. 26. $E_{critical}$ as a function of asphaltene to D-phase ratio for water in *n*-decane emulsions [14].

4.2. Droplet size measurements

A great number of techniques based on widely different scientific principles have found use in the measurement of droplet size. Visual techniques (microscopy, video, photographic), light scattering, nuclear magnetic resonance, acoustic techniques—the list is comprehensive, and the choice of method is often a function of the properties of the emulsion (or, more generally, the dispersion) under scrutiny. Different methods will measure different size ranges, all demand some form of contrast in the measured parameter between the droplets and the surrounding medium, some are direct (measuring the size droplet by droplet), other indirect (fitting a distribution function to the measured signal). All techniques have virtues, all have faults.

But first, why this interest in the droplet size/size distribution (DSD) in emulsions? From the perspective of emulsion stability, the droplet size occurs in equations describing important processes that lead to droplet collision (which is, of course, the first step towards separation)—gravity-induced sedimentation/creaming (Stokes law) and diffusion (Einstein's diffusion equation). An emulsion with broader distribution where large droplets are present will experience enhanced sedimentation of small droplets as well, as the large droplets moving through the continuum cover a greater area and catch up with the slower moving, smaller droplets. An analogous effect is seen in flowing emulsions, with different droplet sizes flow at different speeds. These examples show that droplet size must be taken into account when designing processing equipment, in order to control the evolution of the DSD. The DSD is also in itself an indicator of emulsion stability, when measured as a function of time.

In the following, some currently popular techniques are described, with comments on *pro et contra* features. Special emphasis is given to video microscopy (VM)

based methods. A section is devoted to the description of experiments with a novel VM method for droplet size distribution studies in emulsions at elevated pressures, and its applications within crude oil emulsion research (see Section 4.5.2).

4.2.1. Near-infrared spectroscopy

Near infrared spectroscopy (NIR) [57,60,142] utilizes the ability of different chemical functionalities to absorb and scatter light in the near infrared spectrum (700–2500 nm). A separate section treats the basic features of the NIR technique (see Sections 2.3 and 2.4 for fundamental NIR theory). The application of NIR in the measurement of particle size is related to the measurement of scattered light, detected as intensity shifts in the spectra. If a water-in-oil emulsion is illuminated by NIR radiation the water droplets will scatter parts of the incoming light with an intensity proportional to the droplet radius to the power of 6 [143]:

$$\frac{I_d}{I_0} \propto \frac{r^6}{x^2 \lambda^4} \tag{20}$$

r is the droplet radius, x is the sample thickness and λ is the wavelength. I_d/I_0 is the ratio between scattered and incoming light intensity. This can be used in the determination of droplet size [142]. In two w/o emulsions, with same water content but different DSDs, the emulsion with the larger droplets will scatter light with a greater total intensity than the emulsion with the smaller droplets. The difference is manifested by a shift in the baseline of the spectra. The spectra are otherwise identical, due to equal chemical composition (Fig. 34 can serve as an example of NIR spectrum response to an increase in the number of scattering particles; the spectrum remains largely the same, while the baseline is shifted).

The use of NIR has expanded tremendously over the last decade, manifested in the number of scientific publications rising from a handful during the 1950s and 1960s to several 100 by the start of the 1990s [142]. Much of the increase can be attributed to advances in equipment, especially the introduction of fiber optics. The methods are quick, with modest demands on sample preparation. NIR probes are versatile and offer great opportunities for online sampling.

Since the information from a NIR measurement does not provide quantified DSDs directly, careful calibration is necessary. The creation of calibration curves is a work-intensive process that is absolutely crucial for the achievement of precise data. It is common to introduce several variables (e.g. amount dispersed phase), due to the broadness of absorption bands making separation of sample points somewhat demanding. Thus, DSD measurements by NIR is often coupled with multivariate data analysis techniques.

4.2.2. Electron microscopy

The resolution power of the electron microscopy (EM) is far better than that of the usual optical microscopy, due to the use of electron beam illumination with wavelengths down to ~ 0.1 nm [144–146]. The beams are focused by electric/magnetic fields replacing the conventional lenses. This gives the electron microscope

a resolution of approximately 0.5 nm and the technique can be used for studies of very small structures. An imaging technique, the image is created through focusing on a fluorescent screen or a photographic slide. Usually, a sample is coated (replication) with a heavy metal (e.g. Pt) or carbon layer or fixated by reaction with OsO_4. The preparate is thus a solid, low vapor pressure surface.

Electron microscopes have been developed to a multitude of different technical configurations for different applications, e.g. the scanning electron microscope (SEM) and the transmission electron microscope (TEM). In SEM, a narrow electron beam is used to scan the preparate line-wise to create the image. For measurement of particle size a technique called secondary electron emission (SEE) has been used.

The fine resolution makes EM useful for measurements of droplet size in microemulsions (D < 0.2 μm). However, electrons can only move unhindered at very low vapor pressures, which puts demands on the pressures of the sample chamber. This means that samples are usually dried or frozen prior to measurement. A preparative technique called freeze-fracture has been used for the study of emulsions. Freezing is often performed with the use of liquid nitrogen, propane or freon. This introduces the risk for structural changes in the sample [146]. In some cases the electron beam itself may affect the sample properties. The preparative challenges and high cost of purchase and operation of EM instruments make EM based techniques less used for droplet size measurements.

4.2.3. Microscopy/video microscopy

Microscopy [147–151], photomicrography [152–163] and video microscopy [164–184] have combined a long history in the determination of particle and droplet size. A number of studies have been performed comparing the microscopy methods to alternative methods, such as light scattering [154,167,185], Coulter counting [148,151,160,167,185], turbidimetry [149,153,162], NMR [168,180,181], and other [159,163]. Generally, the comparison is favorable and objections often relate to the labor-intensity of the derived methods. Amongst many applications reported in literature, are the study of vesicles (size and shape) [186,187], particle trajectories [188] and emulsion (suspension) kinetics [161,173,176,183,189–196], measurement of pair potentials [197], film studies and interfacial tension measurements [198,199], and emulsions in electric fields [149,157,200,201], to name but a few to illustrate the versatility of such techniques.

Video-enhanced microscopy (VEM, or video microscopy, VM) is a technique which combines the magnification power of a microscope with the image acquisition capability of a video camera. The resulting data matrix from which information about the sample can be extracted, is an image or a series of images. This intimately relates VM to image analysis techniques, now frequently with the assistance of a computer. Current image analysis software provides a wide range of analytical features, in addition to image enhancement (the improvement of image quality prior to analysis), which is only briefly treated here. It is obvious that image analysis is not restricted to video microscopy, but finds application within any technique where

the data takes the form of an image, e.g. electron microscopy, other video or photographic techniques.

Typical information that can be found in images is sample state, geometry, dispersity and so on. For emulsions, this generally means droplet size and concentration, which are important properties of any emulsion. Fig. 27 shows a coarse and a fine emulsion, the behavior of which can be expected to differ strongly due to droplet size and concentration. Further, the state of flocculation will indicate droplet/droplet interactions. Series of images or continuous video provide information about droplet interactions and the kinetics of important processes within the emulsion, like flocculation and coalescence. All the above parameters are central to the understanding of emulsion behavior and emulsion stability.

Fig. 28 shows a schematic of a typical VEM setup. A video camera (digital or analogue) is attached to the photo-tube of a microscope. The image is transferred to the image captureboard installed onto the computer motherboard (digitization). Image enhancement and analysis is accomplished with image analysis software.

It is natural at this point to define the factors limiting the applicability of video microscopy. First, the sample must have certain optical properties, since the technique relies on the reflection, refraction, scattering and absorption of radiation, for instance visible light, as is the case for optical microscopy. For emulsions, this means that the sample must be transparent and that the continuous liquid and the droplets must have different refractive indices, different color, i.e. properties which make them optically distinguishable. Second, the *resolution limit*, and hence, the operational size domain, is governed by the wavelength of the illumination. This feature is known as the Rayleigh limit [202] [Eq. (21)] and results in a physical limit of approximately 0.2 μm (half the illumination wavelength) [203]. The practical limit tends to be slightly higher, because of rapidly increasing measurement error with decreasing particle dimensions (p. 47 in [143]). This is caused by diffraction; the image of a particle is actually a diffraction pattern, and the overlapping patterns of closely spaced particles result in image blurring. Regarding *magnification*, there is no theoretical upper limit. Still, increasing the magnification only renders larger, blurred images of the particles. Recent innovations in optics have, however, proven the diffraction-imposed barrier not to be absolute [204].

The Rayleigh criterion [202]:

$$R = \frac{0.61\lambda}{N.A.} \tag{21}$$

λ is the illumination wavelength and $N.A.$ is the numerical aperture.

Video-enhanced microscopy, and in particular when coupled with phase contrast (PC) and differential interference contrast (DIC) optics, enables some bending of the Rayleigh criterion. Jokela et al. [167] experienced a VEM resolution limit that was about half that stated by the criterion (0.1 μm). As described above, the absence of a magnification limit enables observation of particles smaller than the resolution limit, but the images will appear blurred with lack of detail. However, the contrast enhancing ability of VEM, PC and DIC can help clarify minute features
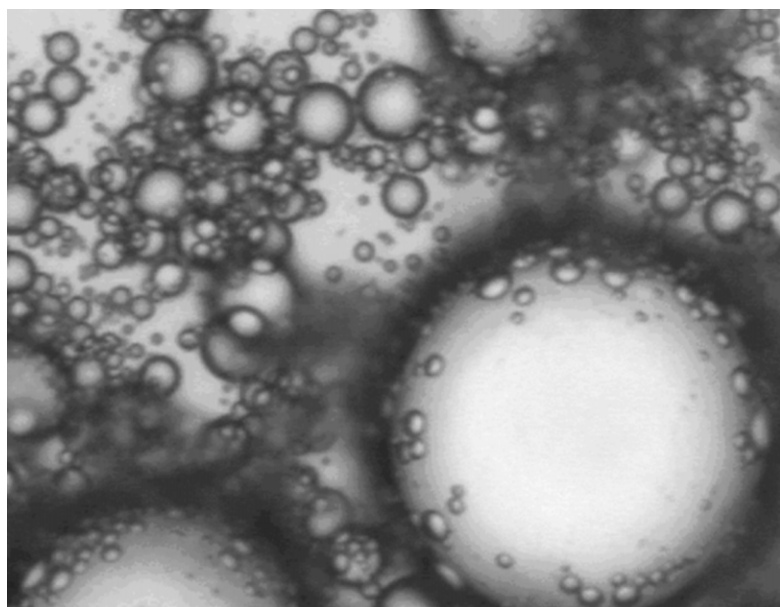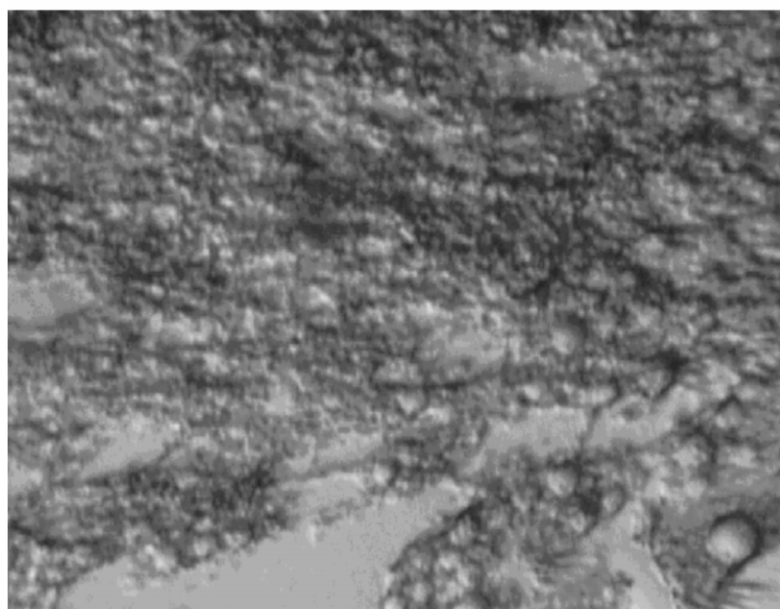
Fig. 27. Microscopy images of a course and a fine emulsion (from [230]).

Fig. 28. Schematic of a video microscope. (a) A compound microscope—can be replaced with a single microscope objective; (b) video camera; (c) computer with framegrabber card and image analysis software (from [230]).

normally lost due to the blurring diffraction patterns; e.g. Allen [205] observed the behavior of individual 25-nm diameter microtubules.

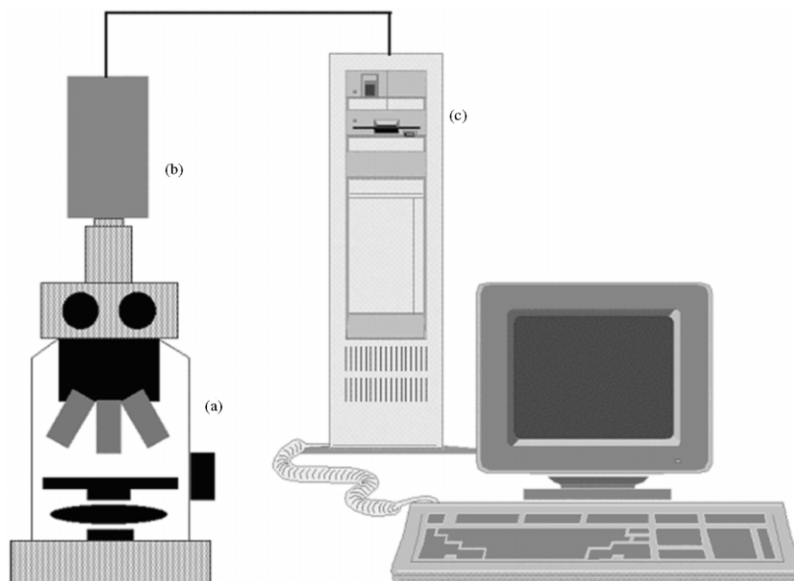As with most techniques, proper sampling is critical. An emulsion is three-dimensional, while an image is two-dimensional (a depth of field of some magnitude provides information of droplets within a certain volume). Emulsions can be prepared in several ways, according to which parameters one seeks to observe and measure. The most common way of studying a sample droplet deployed between an object slide and a cover slide is prone to pollution and distortion (evaporation, shear). Often, some form of sample cell may be used with advantage. Hollow, flat microcapillaries are one example. Within such a cell, the sample can remain protected against the surrounding working environment, which makes them ideal for long-term observation.

Well stabilized emulsions are not so prone to changes through immediate coalescence. This can be utilized by letting droplets cream or sediment to the upper or lower cell wall, forming a slightly concentrated layer within a narrow focal zone. This simplifies the accumulation of data. However, if the droplets tend to coalesce rapidly upon collision, or it is desirable to retain the three-dimensional structure of the sample, one may increase the viscosity of the continuous phase (e.g. glycerin) or solidify the sample altogether (freezing). For kinetic studies, a cell preparation technique must be used [164,165,173,176,183,190,191].

Jokela et al. [167] developed a flow cell system for VEM-assisted DSD measurements. Images of non-sedimented droplets were analyzed, and the method performed favorably compared to light scattering and Coulter counting. It occurs that such a technique would work better with less well stabilized droplets than would the microslide technique, as droplet contact (with each other or the cell walls) could be reduced. Jokela et al. [167] discuss central features of VM DSD determination.

Image enhancement signifies any process, which applied to the image improves its quality, hereunder clarifying the features of interest for the subsequent analysis and measurements. Before the arrival of the digital age, simple but valuable enhancement operations were performed with the aid of specialized equipment. Now, image enhancement software enables the same and more to be done digitally, increasing method versatility tremendously. The different processes vary greatly in complexity and, hence, the computational power required. However, currently available computers provide this in affluence at minimal cost, leaving the main issue to be the flexibility of the software (often three times as expensive as the machinery on which it is runs).

An image contains a lot of information that in different ways can be useful when attempting to describe the sample. However, when the task at hand is that of determining droplet size and the size distribution, the procedure of measurement uses only a small amount of this information. In its purest sense, the procedure seeks to distinguish the droplets from their surroundings (the background) and from each other, and then to perform the measurement on each of the defined droplets. The most primitive way is, of course, when the operator performs both the defining and measurements manually, a course which does not really need the assistance of a computer (although this may somewhat ease the tedious work). For complex systems this may be the only way to go, because the decision process of defining separate droplets is too complicated for a practical and reliable use of automated procedures that may be found within the software. For simpler systems, such procedures may tremendously simplify the generation of statistically sufficient amounts of reliable data, making the method a competitive alternative. Readily analyzable samples are typically dilute and non-flocculated, with a rather narrow distribution of droplet sizes.

The general procedure is simple: first, define the parameters distinguishing the droplets from the background. This is typically accomplished by performing a thresholding on the basis of grayscale (or color) pixel values characteristic to the droplets. The second step is based on shape criteria; a droplet has a monotonous curvature, and a break in the monotony represents a droplet–droplet contact.

4.2.4. NMR and emulsions

Nuclear magnetic resonance (NMR) occurs when the nuclei of some atoms (those that possess *spin*, e.g. ^1H, ^2H, ^{13}C, ^{19}F and ^{31}P) are immersed in a static magnetic field and exposed to a second oscillating magnetic field [206]. NMR spectroscopy is applied to the study of the interaction of electromagnetic radiation with matter, and it can for example be used to determine the structure of molecules or diffusion

coefficients. Individual and unpaired protons, electrons, and neutrons each possesses a spin of $1/2$. Spin has the value and can be positive or negative. If a nucleus consists of, say, two or more particles that possess spin of opposite sign they may in sum pair up to eliminate observable spin. If the particles of a nucleus in sum do not add up to a net spin of zero, which is true for selected isotopes of almost every element, such nuclei can be used in NMR spectroscopy. A particle possessing spin can be viewed as a magnetic moment vector which will cause the particle to behave like a magnet. When the particle is immersed in an external magnetic field, its spin vector is aligned with the external field. There exists two energy states now, depending on whether the particle is aligned or anti-aligned with the field, and the particle can shift from the low to the high energy state by absorption of a photon of energy matching the energy difference between the two states. The energy of a photon is related to its frequency, which is called the resonance frequency. When leaving the exited state, the particle will emit energy (through the course of a relaxation time) which can be detected. This gives rise to characteristic spectra that can be interpreted for the purposes mentioned above. The form of the spectrum is a function of several factors, e.g. type of nucleus, the chemical surroundings of the nucleus (enabling the determination molecular structure), dynamic properties, etc. NMR is a versatile tool and new applications are following a steady development of the technique.

In NMR studies of emulsions [168,207–209] dynamic properties of the systems are examined. In a water-in-oil emulsion the water diffusion is low due to the dispersed state and almost equals the diffusion of droplets. Water diffusion is detected by the pulsed field gradient spin echo (PFG-SE) method (see Section 2.6 for more NMR theory in relation to PFG-SE NMR determination of particle size). In short, the emulsion sample is exposed to two identical RF pulses at 90° and 180° at intervals $t=\tau$. After $t=2\tau$ an echo is detected. Self-diffusion is measured by applying to equal magnetic gradients of magnitude g and duration δ with an interval Δ, one on each side of the 180° pulse (see Fig. 29). The echo signal depends on the observed restricted diffusion; if droplets diffuse during Δ the echo will decrease compared to the situation where no diffusion has taken place. From this, the droplet size can be calculated. ^{1}H-NMR is most commonly used for such studies.

For homogeneous systems with unrestricted diffusion, Eqs. (4) and (5) can be used.

In contrast, for heterogeneous systems, like emulsions, diffusion barriers are present. The equation usually applied to such systems builds on a model initially developed by Douglas and McCall. Its basis is that diffusion following the gradient pulses is Gauss phase distributed. For spherical geometry, Murday and Cotts have developed the following relation between the measured echo intensity I and the droplet radius r:

$$I(r)=I_0 \ \exp\left[\left(-\frac{2\gamma^2 g^2}{D}\right)\sum_{m=1}^{\infty}\frac{\alpha_m^{-4}}{\alpha_m^2 r^2-2}\right.$$

$$\left.\times\left(2\delta-\frac{\begin{subarray}{c}2+\exp(-\alpha_m^2 D(\Delta-\delta))-2\exp(-\alpha_m^2 D\delta)\\-2\exp(-\alpha_m^2 D\Delta)+\exp(-\alpha_m^2 D(\Delta+\delta))\end{subarray}}{\alpha_m^2 D}\right)\right] \qquad (22)$$
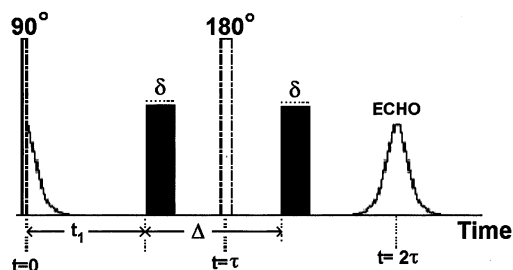
Fig. 29. Illustration of the PFG-SE NMR technique.

where α_m is the m'th root of the Bessel function (), while D is the bulk diffusion coefficient for the dispersed phase. By measuring I at varying duration δ of the RF pulses one can determine the droplet radius. The pulse duration can vary from milliseconds to several seconds.

In most cases emulsion droplet size distributions are polydisperse. The radius of Eq. (22) is thus a median value for the population. The typical shape of the DSD is log-normal, which gives Eq. (7). By writing the observed intensity signal I as:

$$I_{\mathrm{poly}} = \frac{\displaystyle\int_0^\infty r^3 P(r) I(r) \, dr}{\displaystyle\int_0^\infty r^3 P(r) \, dr} \tag{23}$$

one can get numerical values for D (diameter mean) and σ (width of distribution) in Eq. (7).

The technique proscribes diluted emulsions with little water/water contact between droplets during the time of observation. Otherwise, diffusion between droplets may occur. For high droplet concentrations, expressions have been developed [168,207–209].

Pulsed field gradient spin echo PFG-SE NMR has proven a simple technique for DSD determination in w/o emulsions and it has been compared (favorably) to microscopy techniques [207]. With moderate gradient field strengths (1 T/m, [208]) it can measure droplet sizes in the range of 1 to 50 μm. A great advantage of PFG-SE NMR to Coulter counting and laser diffraction is that presence of solid particles does not severely affect the measurements, since the relaxation times of solid matter is generally too short for measurement [210]. It is also non-destructive, and several measurements can be done on the same (low volume) sample [208,209]. Sample preparation is also simple.

However, it is stated in literature [168,207] that the quality of the result from Eq. (7) depends on all size classes being represented in the measurements. This can be done by varying g and Δ, that is, measuring diffusion for long times at strong enough gradient fields. Sedimentation and creaming can be a problem, as the spin

number changes during the measurement. This can be accounted for by reference measurements at no gradient field prior to and after the measurement.

A weakness of the technique is the function fitting. One may argue that most emulsions have a single mode log-normal distribution, but this is not always the case. There will thus always be some reservations connected to the validity of the derived distribution function.

4.2.5. Acoustic and electroacoustic measurements

The principle for techniques measuring particle (droplet) size by acoustics is simple [211]. The instrument, called an acoustic spectrometer, generates sound pulses that move through the dispersion. When traversing the sample, the pulses change in intensity and phase. The resulting sound is detected by a receiver, and the energy losses (called attenuation) and the speed of the sound is measured. Attenuation is due to interaction of sound with particles in the dispersion, and the determination of particle properties (e.g. size) is done by fitting attenuation data to theoretical models for acoustic loss mechanisms. This introduces some level of complexity into the DSD determination, however, this is also the case for other techniques that are currently more commonly applied and which cover much the same size regimes.

Six mechanisms are known for ultrasound interaction with a dispersed system [211]: (1) Viscous loss due to shear waves generated by particles oscillating in the sound field. This is the most important mechanism for small solid particles; (2) Thermal loss due to temperature gradients near the particle surface. This is important for soft particles, e.g. emulsion droplets; (3) Scattering loss due to scattering of the sound by the particles. This is especially important for larger particles; (4) Intrinsic loss due to molecular level interaction between sound wave and medium; (5) Structural loss due to oscillations of interconnected particles. This can be used to characterize structures within systems; (6) Electrokinetic loss due to oscillation of charged particles, transforming acoustic energy into electrical energy and eventually, heat.

Of these, the first four are usually the most important. Acoustic spectra are not dependent on the electrokinetic loss, which represents the distinction between acoustic and electroacoustic spectroscopy.

The gap between transmitter and receiver is an important instrument feature. In highly attenuating liquid, the ultrasonic signal (1–100 MHz for particle sizes below 10 μm, [211]) cannot penetrate the liquid to reach the receiver. Water has a very low attenuation. In water-rich dispersions, a wide gap must be used. When water is dispersed in a liquid with a high thermal expansion coefficient, attenuation increases drastically, and only a small gap will prove applicable. It is important to be able to vary the gap size, to enable measurement over a range of system attenuations.

It is a notable advantage that the technique can be applied to a rather wide range of dispersed concentrations, from below 0.1% to more than 40% [211] (ESA electroacoustic spectroscopy, 60% [212], see below). This can, in many cases, eliminate the need for (possibly destructive) dilution.

Electroacoustics can generate information on the DSD of a dispersion (when measurements are made over a range of frequencies), and can also provide zeta potential measurements [212]. There are two different approaches based on different fields to generate driving force. In the first, sound energy is applied to the dispersion and an electric field (current) results from the vibrations of the electric double layers of particles (colloid vibration current, CVC, or potential, CVP). In the second, the application of an electric field to the sample causes the generation of sound energy (electrokinetic sound amplitude, ESA). In principle, spectra from these two approaches contain the same information regarding zeta potential and particle size. The more complicated deduction of the size distribution is due to the added complexity of the electric field.

From the ESA response the dynamic mobility can be determined. This complex quantity has a magnitude and a phase angle. While the magnitude yields information about the zeta potential, it is in the phase angle that one can find information of particle size. The lag between the applied electric field and the resulting sound signal will vary with the frequency. The phase angle is zero for small particles and increases to approximately 45° with larger particle size (and higher frequency). This collective dependence on frequency of both magnitude and phase angle for a certain particle size enables particle size and zeta potential determination from measurements over some frequency range.

Although the principles that found the basis for acoustic and electroacoustic spectroscopy have been long established, the techniques have yet found only limited application for determination of droplet size. The promise of these techniques is however apparent, and further theoretical development should secure their firm establishment among the most useful techniques available.

4.3. Characterization by critical electric fields

Demulsification by electrocoalescence is common in the oil industry. Water is separated from the emulsion by applying a high electric field of 1–10 kV/cm to cause flocculation and coalescence of water droplets in the oil phase [213]. The principle behind the electrically-induced coalescence is that the electric field acts to enlarge the droplets of the dispersed phase by inducing coalescence. After this initial step, the water phase settles out under gravity at an increased rate. There is a variety of factors influencing the electrically-induced coalescence, such as the dielectric properties of the dispersed and the continuous phase, the volume fraction of the dispersed phase, conductivity, size distribution of the dispersed droplets, electrode geometry, electric field intensity, the nature of the electric field (AC or DC), etc. [214].

The electric field strength needed to cause such coalescence can be used as a measure of the emulsion stability. In low electric fields, water droplets surrounded by a rigid interfacial film will attain a chain-like configuration. Increasing the field strength the droplets will bridge the gap between the electrodes. Ultimately, an irreversible rupture of the interfacial films between the droplets will increase the conductivity through the emulsion sample [139,213]. This may then be defined as
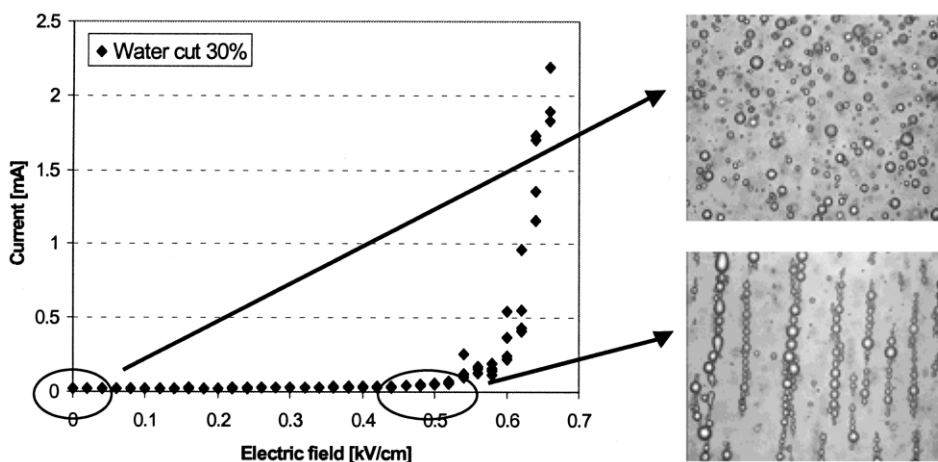
Fig. 30. Emulsion droplets in an increasing electric field.

a measure of the emulsion stability, the so-called $E_{critical}$. Fig. 30 demonstrates the effect of increasing the electric field strength over an emulsion.

An electric field cell has recently been developed for the determination of emulsion stability [215]. The method is similar to the one employed by Kallevik et al. [216]. The cell is depicted schematically in Fig. 31. It consists of a Teflon plate with a 10-mm diameter hole in the center, with a brass plate on each side. The distance between the plates is 0.5 mm, and the upper brass plate has two small holes for sample injection. The brass plates are connected to a power supply, which can increase the applied voltage in user-defined steps. The system is held together with isolating plexiglass plates. The power supply delivers a maximum of 100 V DC, corresponding to a maximum electric field of 2.0 kV/cm. Emulsions are injected into the cell volume, and the electric field over the emulsion sample is increased until $E_{critical}$ is reached, as seen by increased conductivity.

4.4. Multivariate analysis and emulsion stability

Principal component analysis (PCA) is a projection method that helps visualize the most important information contained in a data set. PCA finds combinations of variables that describe major trends in the data set. Mathematically, PCA is based on an eigenvector decomposition of the covariance matrix of the variables in a data set. Given a data matrix $\mathbf{X}$ with m rows of samples and n columns of variables, the covariance matrix of $\mathbf{X}$ is defined as

$$\mathrm{cov}(\mathbf{X}) = \frac{\mathbf{X}^{\mathrm{T}}\mathbf{X}}{m-1} \tag{24}$$
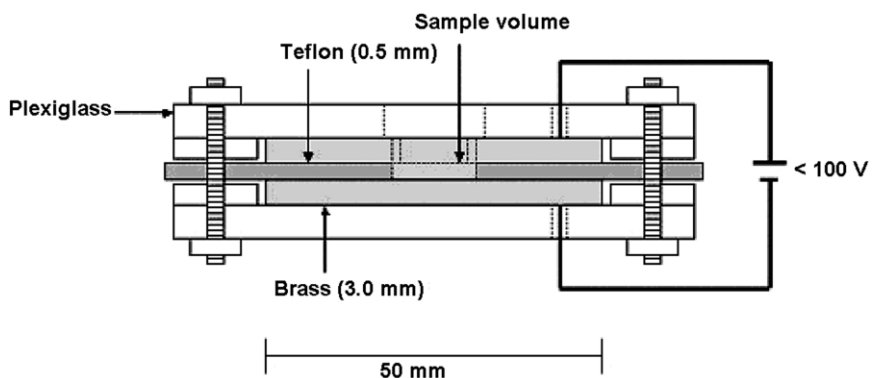
Fig. 31. Electric field cell for emulsion stability measurements.

The result of the PCA procedure is a decomposition of the data matrix $\mathbf{X}$ into principal components called score and loading vectors

$$\mathbf{X}_{n \times m} = \mathbf{t}_1 \mathbf{p}_1^T + \mathbf{t}_2 \mathbf{p}_2^T + \mathbf{t}_i \mathbf{p}_i^T + \cdots + \mathbf{t}_k \mathbf{p}_k^T + \mathbf{E}_{n \times m} \qquad (25)$$

Here $\mathbf{t}_i$ is the score vector, $\mathbf{p}_i$ is the loading vector and $\mathbf{E}$ is the residual matrix. The score and loading vectors contain information on how the samples and variables, respectively, relate to each other. The direction of the first principal component ($\mathbf{t}_1$, $\mathbf{p}_1$) is the line in the variable space that best describes the variation in the data matrix $\mathbf{X}$. The direction of the second principal component is given by the straight line that best describes the variation not described by the first principal component and so on. Thus, the original data set can be adequately described using a few orthogonal principal components instead of the original variables, with no significant loss of information. When plotting principal components against each other, relations between samples are easily detected [217].

Regression is used to fit a model to observed data in order to quantify the relationship between two groups of variables. The regression model may then be used to predict properties of new samples. Regression between the $\mathbf{X}$ data and the response $\mathbf{y}$ is often impossible by ordinary least squares methods due to strongly correlated and redundant information in the data set. This problem is especially prominent for spectral data sets. One solution to this is to decompose the $\mathbf{X}$ matrix as shown in Eq. (2), and perform the regression between the resulting score vectors and the response. PCA decomposition followed by regression is called principal component regression (PCR). The partial least squares (PLS) technique is another alternative. In PCA the scores and loadings are the vectors that best describes the variance of the $\mathbf{X}$ matrix. In PLS the scores and loadings (called latent variables) are the vectors that have the highest covariance with the response vector $\mathbf{y}$. The decomposition is followed by a regression between the latent variables and the response.

Due to the risk of overfitting the regression model, the optimum number of latent variables to be used is determined. One way of doing this is the cross validation technique. Cross validation checks a model by repeatedly taking out different subsets of calibration samples from the model estimation, and instead using them as temporary, local sets of secret test samples. If the model parameter estimates are stable against these repeated perturbations, this indicates that the model is reliable [218]. In the simplest case, each subset contains only one sample, which is called full cross validation, and is the technique employed in the regression modeling in this study.

Data may be transformed prior to multivariate analysis in order to make them more suitable for a powerful analysis. xy-transformations, thus including logarithmic transformations, are especially useful to make the distribution of skewed variables more symmetrical.

The critical electric field cell above was developed to measure the emulsion stability of a set of characterized crude oils and condensates. By multivariate analysis the emulsion stability was then correlated to the physico-chemical properties of the samples. In addition to SARA-data and interfacial elasticity, properties like density, interfacial tension, molecular weight, total acid number and viscosity of the samples were known. The aim of this study was to gain insight into which parameters govern the emulsion stability properties of the crude oils. In addition, NIR spectra of the crude oils were also used as input data. Table 5 shows the data matrix, including E_{critical} values for water cuts of 20% and 30%. **t**1 and **t**2 are the first and second score vectors from a principal component analysis of the NIR spectra. These two variables illustrate, in a condensed form, large parts of the variation between the samples found in the NIR spectra.

A PLS regression model was built using the average E_{critical} values at water cuts of 20% and 30% as response. Due to a skewed distribution the E_{critical} values were logarithmically transformed before modeling. This excluded the condensates from the model since their E_{critical} values were zero. Fig. 32 shows the regression coefficients and the predicted vs. measured plot for the resulting model. The R^2 value of the model is 0.93. From the regression coefficients the amount of asphaltenes and interfacial elasticity are seen to be main contributors to emulsion stability. In addition, the NIR spectra (through the scores **t**1) seem to contain much information with regard to emulsion stability properties. On the opposite, high values of aromatics and the relation resins/(resins+asphaltenes) seem to be the two main variables decreasing emulsion stability.

Based on the full model, a reduced model, containing only a few of the most important variables, was built. Five parameters from the full model were preserved, the four SARA-parameters and the interfacial elasticity. All four SARA-parameters were kept since they are determined in the same experiment. This model produced an R^2 value of 0.82. This means that data from only two experimental procedures, the SARA-separation and the interfacial elasticity determination, are able to give a reasonable estimate of the emulsion stability properties of a crude oil. Earlier attempts to correlate the emulsion stability to SARA-data and some of the other

Table 5
Data matrix on crude oils and condensates

	Origin	WC20 [KV/cm]	WC30 [KV/cm]	S [wt.%]	A [wt.%]	R [wt.%]	Asph. [wt.%]	$(S+\text{Asph})/(R+A)$	$R/(R+\text{Asph})$
1	West Africa	0.58	0.47	47.9	36.5	15.2	0.4	0.93	0.97
2	North Sea	0.87	0.61	48.0	37.5	14.2	0.3	0.93	0.98
3	West Africa	2.00	0.68	41.2	36.4	20.4	2.1	0.76	0.91
4	North Sea	0.00	0.00	82.7	13.4	3.9	0.0	4.78	1.00
5	North Sea	1.00	0.64	62.7	23.6	12.2	1.5	1.79	0.89
6	North Sea	0.91	1.03	45.5	37.1	16.0	1.4	0.88	0.92
7	North Sea	2.00	1.50	35.3	36.8	24.5	3.5	0.63	0.88
8	North Sea	0.55	0.45	56.0	29.6	14.1	0.3	1.29	0.98
9	North Sea	0.84	0.59	41.8	38.8	18.7	0.6	0.74	0.97
10	North Sea	0.53	0.33	50.9	34.6	14.0	0.5	1.06	0.97
11	West Africa	2.00	1.85	40.6	32.1	20.6	6.6	0.90	0.76
12	North Sea	0.00	0.00	79.8	16.5	3.6	0.1	3.98	0.97
13	West Africa	0.61	0.45	57.3	27.9	13.5	1.3	1.42	0.91
14	North Sea	0.59	0.08	60.6	30.0	9.2	0.2	1.55	0.98
15	West Africa	0.85	0.40	42.4	36.1	20.5	1.0	0.77	0.95
16	North Sea	0.00	0.00	65.0	30.7	4.3	0.0	1.86	1.00
17	North Sea	0.47	0.42	44.1	41.6	13.8	0.5	0.81	0.97
18	North Sea	0.93	0.43	50.3	31.4	17.5	0.7	1.04	0.96
19	North Sea	2.00	2.00	54.5	28.8	14.9	1.8	1.29	0.89
20	West Africa	0.91	0.72	55.4	28.3	12.9	3.4	1.43	0.79
21	France	2.00	1.70	24.4	43.4	19.9	12.4	0.58	0.62

	Origin	t1	t2	OD, 1600 nm	Elasticity [mN/m]	Density [g/cm³]	IFT [mN/m]	Mw [g/mole]	Visc., 25 °C [kg/ms]	TAN
1	West Africa	−5.45	0.11	0.168	11.5	0.914	20.5	234	18.7	1.10
2	North Sea	−3.16	0.26	0.240	7.3	0.916	24.8	279	57.4	3.10
3	West Africa	8.91	0.16	0.659	7.8	0.916	26.4	310	143.0	1.50
4	North Sea	−7.42	0.17	0.107	−1.1	0.839	37.1	166	1.8	0.69
5	North Sea	−3.62	−0.43	0.236	16.5	0.844	12.8	201	5.4	0.18
6	North Sea	−0.39	0.52	0.332	3.7	0.862	31.9	244	14.5	0.02
7	North Sea	5.99	0.81	0.544	11.7	0.945	27.4	333	386.6	2.30
8	North Sea	−5.02	−0.10	0.185	6.7	0.850	24.7	216	6.6	0.17
9	North Sea	−3.53	0.28	0.229	8.4	0.914	11.8	284	51.0	3.10
10	North Sea	−4.54	0.12	0.197	5.0	0.885	22.8	234	11.6	2.70
11	West Africa	17.50	−0.49	0.991	10.6	0.888	29.0	260	27.8	0.49
12	North Sea	−5.84	−0.60	0.165	−1.4	0.796	34.2	157	1.7	0.01
13	West Africa	−2.87	−0.05	0.257	–	0.873	24.6	235	17.7	0.50
14	North Sea	−5.11	−0.39	0.186	0.2	0.857	22.9	227	10.5	0.04
15	West Africa	1.33	−0.02	0.395	9.2	0.921	16.2	295	105.8	3.60
16	North Sea	−7.36	0.18	0.107	−0.6	0.796	27.6	142	1.2	0.02
17	North Sea	−4.94	−0.37	0.192	8.1	0.847	19.9	223	11.7	0.15
18	North Sea	−4.24	0.14	0.206	14.8	0.898	19.5	249	19.1	1.20
19	North Sea	9.54	0.11	0.684	24.9	0.840	27.4	298	63.1	0.36
20	West Africa	4.91	−0.41	0.525	5.6	0.873	19.0	248	15.3	0.44
21	France	15.31	0.00	0.893	12.9	0.939	13.4	303	278.9	0.20

variables in the data matrix were not successful, underlining the importance of knowing the interfacial properties of crude oils when discussing emulsion stabilization/destabilization. Crude oil 19 may serve as an example by forming very stable emulsions despite its relatively low asphaltene content (1.8 wt.%). However, from the data table this crude oil is seen to produce by far the highest values of interfacial elasticity.

The NIR spectra appeared to contain information on the emulsion stabilizing properties of the crude oils due to the high value of the t1 regression coefficient. Based on this, a third PLS model using NIR spectra of the crude oils as X-data was
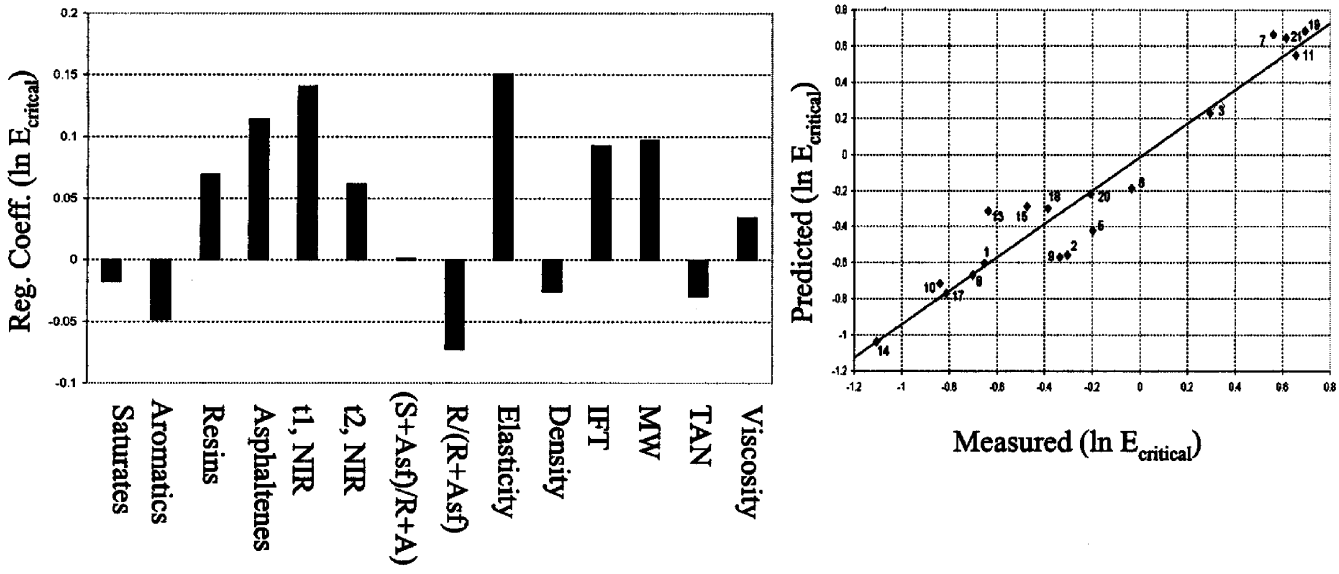
Fig. 32. Regression coefficients and predicted vs. measured plot for the emulsion stability model (from [215]).

constructed. Wavelengths from 1300–2200 nm were used to predict the same $E_{critical}$ values as in the other two models. Fig. 33 shows NIR spectra and the predicted vs. measured plot of the resulting model. The model produced an R^2 value as high as 0.95, confirming that near infrared spectroscopy is a very good source of information for crude oil properties. We have earlier demonstrated that SARA-parameters could be predicted from NIR spectra [24], and in addition NIR spectra have been shown to contain information on the aggregation state of the asphaltenes in the crude oils [67]. These are all factors contributing to emulsion stability, and explain some of the good predictive power of near infrared spectroscopy.

One of the problems associated with the prediction of emulsion stability from single parameters like SARA, elasticity, viscosity etc. is that detecting the effect of constituents of very low concentration in the crude oil may be difficult. However, such constituents may have a dramatic effect on the emulsion stability properties. One example is chemical demulsifiers added during crude oil production at ppm-levels. A SARA-determination will not be able to distinguish between a crude oil sample with and without such additives. An indirect analytical procedure like near infrared spectroscopy, on the other hand, can be able to detect such additives by measuring the effect they have on the crude oil, i.e. their functionality. Fig. 34 shows two NIR spectra of the same North Sea crude oil, the only difference being the addition of 10–15 ppm of demulsifier. It is seen that this has an adverse effect on the NIR spectra, a difference that a SARA-analysis would not have revealed. The emulsion stability of the crude oil with no added demulsifier (as measured by $E_{critical}$) is twice as high as for the sample with addition.

4.5. High pressure performance of w/o emulsions

4.5.1. High pressure rig for emulsion stability studies

In order to study separation of emulsions under realistic conditions, a high pressure separation rig has been constructed at Statoil's R&D Center. The rig can be used to prepare emulsions and monitor the separation of oil and water, as well as any stable foam formation, in a horizontal batch separation cell. The separator cell is made from sapphire, assuring full visibility of the separation processes, it has a volume of 0.5 l and can stand pressures up to 200 bar. A schematic drawing of the rig is presented in Fig. 35. The rig includes four 600 cc high pressure sample cylinders. With the aid of four motor driven high capacity piston pumps, water and oil are pumped from the sample cylinders, through the choke valves and into the separator. The four pumps can be controlled independently, however, the total flow rate is usually kept constant. Pressure drops through the choke valves are back-pressure controlled. In order to control the separation pressure, the separation cell is pressurized with gas, inert or natural gas, and the pressure is regulated by another back-pressure controlled valve. To ensure temperature control of the system, a thermostatted cabinet encloses the separation cell and provides temperatures in the range of -7 to 175 °C.

The principle of the rig is that two flows of pressurized fluids meet and stream through a choke valve (VD1) and into the batch separator. As the fluid mixture
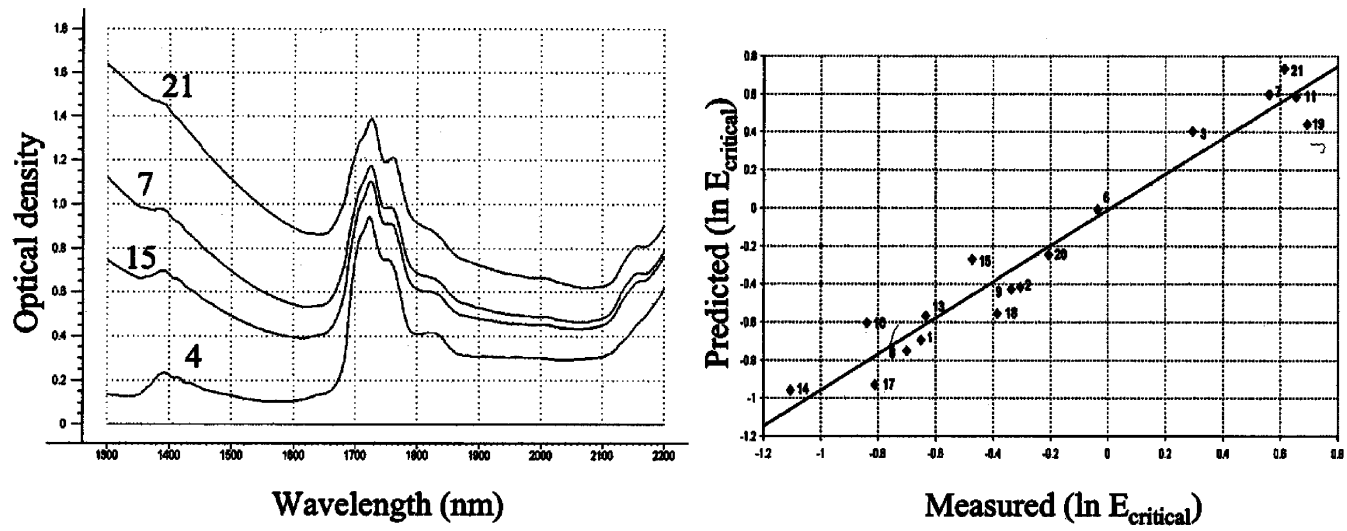
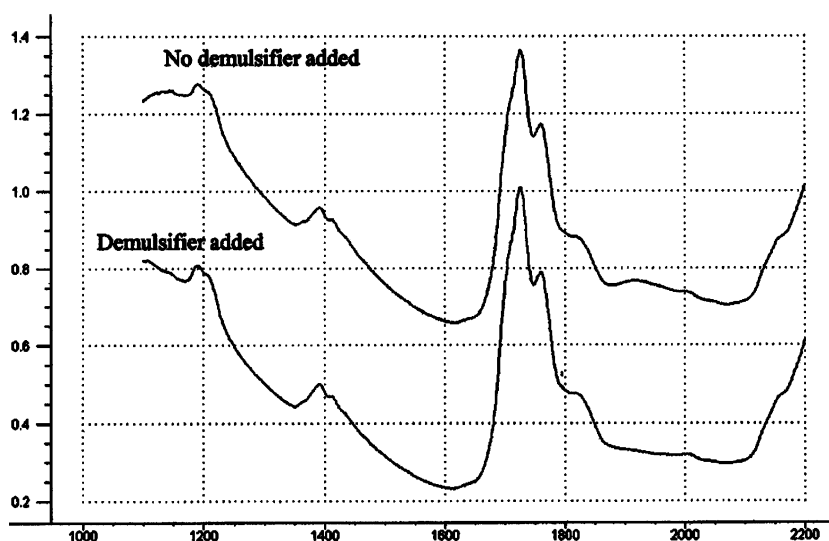Fig. 33. Example NIR spectra and predicted vs. measured plot for the NIR model (from [215]).

Fig. 34. Effect on NIR spectra of crude oil with addition of demulsifier.

passes through the choke valve it undergoes a pressure drop, which provides the shear force necessary to create more interface between the oil and water phases, and water droplets are formed and dispersed into the oil. If the pressure drops below the bubble point pressure, a gaseous phase appears. The gas evolved may form a foam layer, as well as influence the sedimentation and coalescence processes, which the water droplets go through. The quantity of the different phases, foam, oil, emulsion/dispersion and water, can thereafter be recorded as a function of time. To aid in the monitoring process, video cameras are connected to the rig. After a given separation time, oil, water and emulsion layers are sampled and analyzed. Upstream of the choke valve VD1 there is two other choke valves, one on each separate line (VD2 and VD3). Through these choke valves the same processes take place as described for VD1, and dispersions of oil and water can be prepared. To study the effect of emulsion and foam inhibitors or demulsifiers, the rig is equipped with two independent high precision pumps, pump 5 and 6, which delivers volumes down to 0.03 cc/h. In this way, low concentration chemicals can be injected in to any of the flow lines. Injections can also be made in the bottom of the cell, where a stirrer can be used to distribute the chemicals.

The high pressure separation rig is a batch separator, and the results will, therefore, not apply exactly for a field separation process where the separation is continuous. Nevertheless, the results will show trends for temperature, pressure, pressure drop, and mixing with other oils, etc. It will also indicate whether there is a need for chemical treatments (demulsifier, foam inhibitor, etc.).

4.5.2. Video microscopy measurement of the DSD in emulsions at high pressures

When crude oil is produced from offshore oil fields water and oil can be co-transported from reservoir to downstream separation facilities on the production
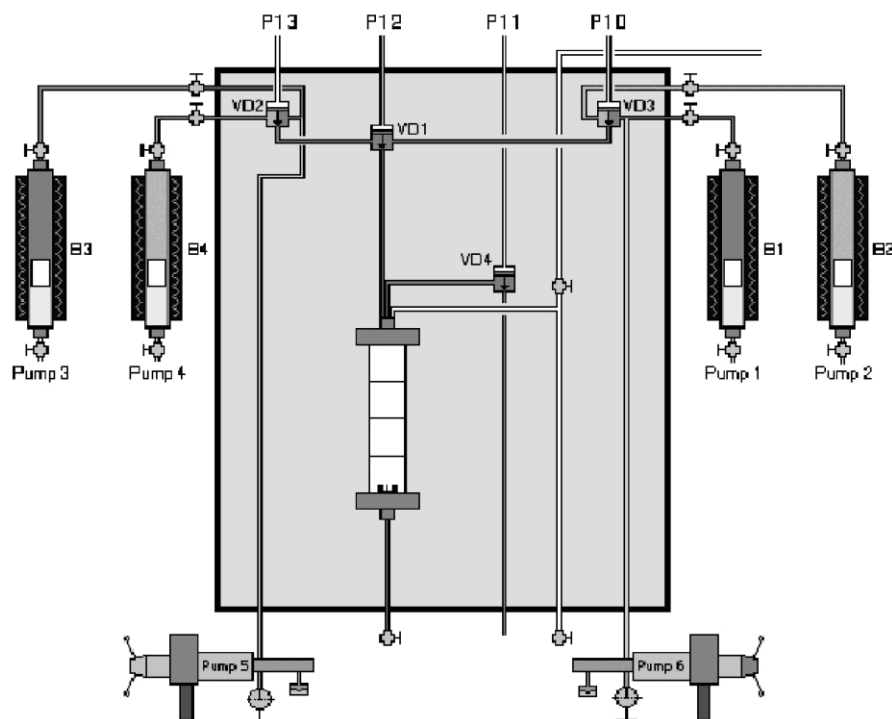
Fig. 35. Schematic drawing of the high pressure separation rig.

platforms. The reservoir pressures vary greatly, and as production at very deep waters and from very deep reservoirs is initiated, emulsions form at pressures far from what ordinary lab facilities are designed to handle. It is a fact that system pressure does affect the asphaltene (the most important crude oil components in relation to emulsion stabilization) state, e.g. aggregate size. Asphaltene aggregates and particles are coadsorbed into the interfacial film, giving rise to high droplet stability against coalescence. Too large particles will not coadsorb, and very small aggregates and monomers give weaker, less stabilizing films. By the development of the HP separation facilities (see section Section 4.5.1), it is now possible to sample emulsions at HP that have been created under realistic process conditions and measure the DSD at the same pressure, the advantage of which is that one avoids possible re-agitation during pressure release (and subsequent changes in the DSD). The VM has been equipped with a flow-cell which can withstand pressures up to 600 bar which enables image capture from the flowing emulsion. The image analysis is of course the same as for ambient pressure studies.

The HP/VM system has been used for studying the effect of system pressure changes on DSD related to changes in asphaltene aggregate formation (see also section Section 2.4). Studies have been performed on separation behavior as function of mixing of oils from different fields, in order to predict possible separation
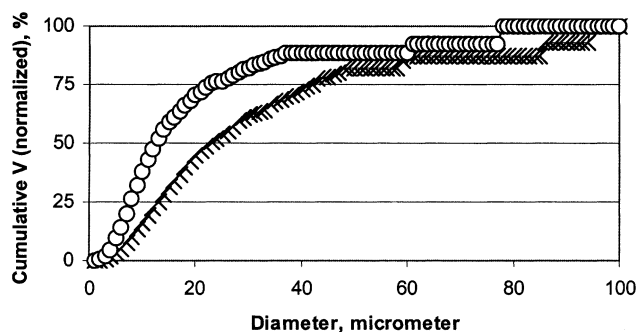
Fig. 36. When the pressure drop ($\Delta p_{total}=20$ bar) is distributed equally across two consecutive valves (open circles) the droplet size is smaller than when the entire pressure drop is located at one valve only (%). The emulsion is 30% water-in-crude oil and the initial system pressure is 31 bar.

problems in co-processed streams. DSD measurements have also been used for determining changes in droplet size arising from mixing at valves (and series of valves) due to variations in the pressure drop across the valves. Further, the effects of variations in pipe length and flow distance after mixing have been examined. All under genuine processing conditions.

Fig. 36 shows how the distribution of a pressure drop across two consecutive valves shifts the DSD towards smaller droplet sizes than is the case when the entire pressure drop is located at one valve only. It is natural to assume that this is due to the fact that at the second valve what is mixed is an emulsion created at the first valve, rather than separate phases. Fig. 37 illustrates how the increasing relative amount of dispersed phase under equal pressure drop (mixing energy) shifts the distribution towards larger droplet sizes, when the energy is distributed over a larger volume of (eventually) external phase liquid. In Fig. 38 a crude oil was pressurized mechanically above the bubble point (b_p), and emulsions were mixed at 45 bar and 5 bar above the b_p. As the system pressure approaches the b_p, more large droplets are formed due to the accompanying growth in the size of asphaltene aggregates.

The VM set above is the first attempt to measure droplet sizes under true pressures. The experimental setup has shown clear evidence of how sampling, emulsion processing and pressure release will influence the DSD. These factors are very important when designing large scale process facilities.

4.5.3. Recombination of crude oils at high pressure

When designing new fields and exploration processes, the fluid properties are crucial for a correct design and dimensioning of the process unit. It is normal that crude oil samples are delivered as 'dead' (degassed) samples, since true bottom hole samples are expensive and difficult to obtain in large quantities. In most cases, the crude oil has also been exposed to air and has therefore aged, a process that changes the crude oil properties drastically, as shown earlier by Rønningsen et al. [219] and Sjöblom et al. [220]. It is, therefore, highly motivated to question how
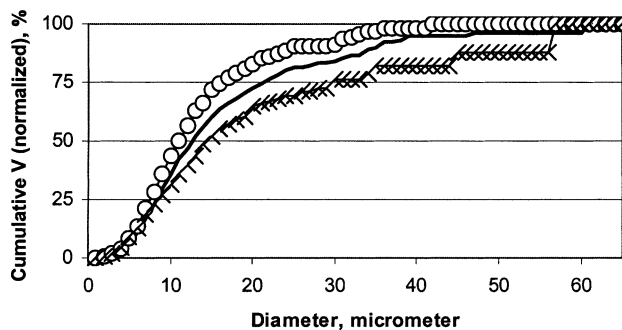
Fig. 37. A constant mixing energy (20 bar pressure drop) is applied to various ratios of water-in-crude oil, causing variations in the DSD of the water droplets remaining dispersed in the oil as free water separates; 10% w/o (open circle), 30% w/o (solid line) and 70% w/o (%).

representative such samples are as candidates for the true fluid streams. Test procedures that are performed to evaluate emulsion stability have traditionally been based on bottle tests. However, one severe drawback of carrying out bottle tests is the lack of pressure dependence. One way to introduce more realistic testing conditions is the rig presented in section Section 4.5.1. Nevertheless, the problem with a realistic recombination of dead oil samples still remains to be solved. As a consequence, one must, in order to study oil and emulsion properties at elevated pressures, undertake a recombination with a gas mixture to the relevant pressure. The resulting emulsion stability at that pressure is very dependent on how the recombination has taken place.

In Auflem et al. [221] the emulsion stability for a 'live' crude oil was compared to the emulsions stability of the same crude oil recombined with, N_2, CO_2, CH_4, C_2H_6 or a natural gas mixture. Emulsion stability experiments, where varying amounts of the lighter molecules in the live crude oil had been removed, were also
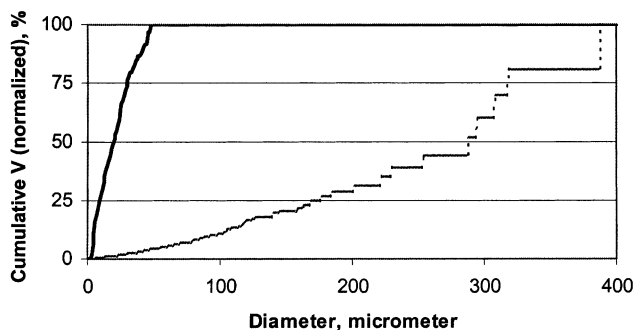

Fig. 38. As the system pressure is reduced from 200 bar (solid bold line, left) to 160 bar (dotted line, right) asphaltene aggregates grow to sizes where they do not contribute to the stabilization of the w/o interface, resulting in the formation of larger droplets. The crude oil is saturated with natural gas at 155 bar—the bubble point under which gas is released.

performed. The experiments were thus comprised from the following three types of oil samples: (1) 'Live' crude oil samples with a bubble point of 15 bar; (2) Samples where the gas phase had been removed from 'live' samples by depressurizing to 1 bar while allowing the gas to evaporate (degassing), and thereafter repressurized to 15 bar with either N_2, CO_2, CH_4, C_2H_6 or the natural gas mixture; and (3) Samples that were degassed in the recombination cell to 10 or 1 bar, respectively, and thereafter mechanically repressurized to 15 bar by use of a piston pump and no addition of gas.

The oil samples were then transferred into the sample cylinder on the high pressure/high temperature rig, described in section Section 4.5.1, and further pressurized to 20 bar by use of a piston pump. To create emulsions, the oil samples were streamed together with synthetic formation water through a choke valve, while varying the pressure drop and separation pressure. The decomposition of the resulting emulsion and foam layer could thereby be monitored visually in the vertical high-pressure separation cell. Thus, the separation properties of the water-in-crude oil emulsions from the different recombined samples and the 'live' crude oil could be compared.

The results from experiments performed on oil type 1 and 2 showed the following trends: Water-in-oil emulsions produced from 'live' North Sea crude oil, generally separated faster and more complete, than emulsions based on recombined samples of the same crude oil. An example of such a water resolution map is shown in Fig. 39. Increased water content or smaller pressure drop into the separator, resulted in faster and more complete separation of the emulsions for both 'live' and recombined samples. It was also observed that the height of the foam layer increased when reducing the water content from 60 to 40 vol.%, probably due to the increased ratio of oil to water.

Experiments performed on oil type 3, i.e. oil samples with varying content of light molecules, can be concluded as follows: As expected, the 'live' (15 bar) sample gave the highest amount of foam for water content of both 60 and 40 vol.%. A smaller amount was obtained for the 10 bar sample and none for the sample degassed to 1 bar. The emulsion stability for the mechanically recombined crude oil samples seemed to depend on the degassing pressure of the 'live' sample, i.e. the content of gas present in the oil phase. Samples with the lowest gas content gave, probably as a result of the higher viscosities, a less complete emulsification. This would, in turn, create a higher number of relatively large droplets, which separated within the first few minutes, while the rest emulsion maintained the same stability as for the samples with higher amount of gas remaining. As for the other oil samples, the amount of water influenced the emulsion stability together with the pressure gradient over the choke. Smaller water content (40%) and large ΔP over the choke (19 bar) gave higher emulsion stability in comparison with 60% of water and 5 bar pressure drop. Most likely, the drop size distribution was quite different for these samples with much smaller droplets for 40 vol.% of water and high ΔP.

4.5.4. High pressure experiments on w/o emulsions

The objective of this chapter is to present studies of the effects of separation pressure, pressure drop, and solvency as well as release of gas bubbles on the
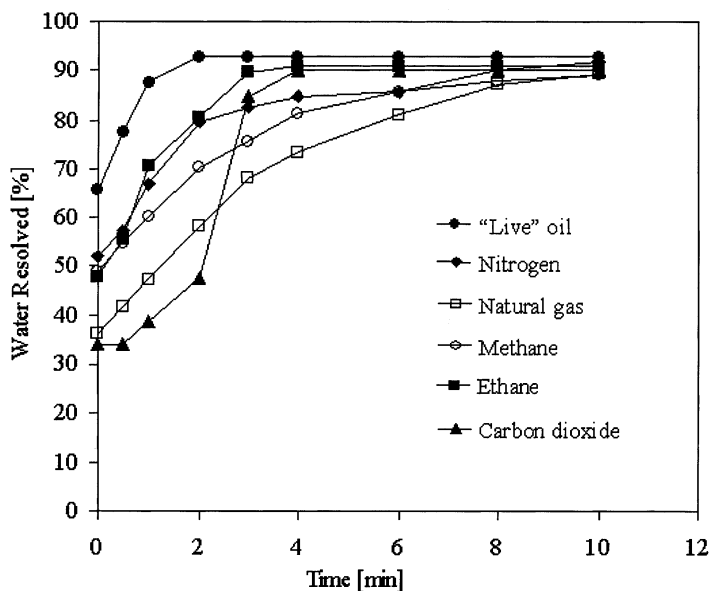
Fig. 39. Percentage water separated vs. time for 'live' and recombined oil samples. Separation pressure, pressure drop and water content were 15 bar, 5 bar and 60 vol.%, respectively.

stability of crude oil emulsions. In the next section (Section 4.5.5), the conclusions are summarized.

Auflem et al. [222] give experiments where a North Sea crude oil was recombined with dry natural gas to a separator pressure of 11 bar. The sample was thereafter mechanically pressurized further to 100 bar, or in some cases 182 bar, by a piston pump connected to the sample cylinder. The experiments were performed in a high pressure separation rig, which is described in section Section 4.5.1. In the rig, water and oil can be mixed (choke valve mixing) under conditions similar to manifold/ upstream separator conditions, and then pumped across another choke valve into a vertical batch separator cell.

In the experiments, several effects on the separation were observed: (1) an increased separation with increasing pressure drop below the bubble pressure; (2) a increased pressure drop gave more stable emulsions for separation above the bubble pressure; and (3) toluene dilution of the crude oil resulted in less stable emulsions.

The results in (1) and (2) were accounted for by a flotation effect from gas bubble on the stabilizing material. As the oil phase is depressurized, the solubility of light end molecules decreases, and a gas phase evolves. The gas phase will then rise through the solution in the form of small bubbles, which rip off surface-active material from the water–oil interface.

A higher energy input, due to a larger pressure drop, resulted in smaller water droplets and consequently a slower separation process, at separation pressures above the bubble point. The relation between energy input and droplet size has been

shown before by several authors [223–227] and thus came as no surprise. Also, a destabilizing effect from diluting the crude with toluene, was expected. McLean and Kilpatrick showed in 1996 [5] (and also Førdedal [140]) that as the aromaticity of the oil phase increased, the asphaltene aggregates were dissolved, and the stability of the emulsions was reduced. Further, the foamability was also affected by the toluene addition. For increasing content of toluene in the oil phase, the capacity of the system to form foam decreased as a result of dissolution of stabilizing material. More interesting was a comparison of experiments performed on (1) a recombined oil phase, and (2) a recombined oil phase that had been degassed and repressurized mechanically. That is, the recombined oil phase was depressurized to atmospheric pressure, while allowing the gas phase to evaporate. The degassed sample was, thereafter, repressurized mechanically by use of a piston pump to the original pressure (100 bar). Thereafter, the two types of oil samples were put through an identical emulsification procedure as follows. The oil was mixed with the pressurized formation water, 35 vol.%, by pressure drops through two succeeding choke valves: From 100 to 11 bar and from 11 to the separation pressure in the separator of 7 or 1 bar. For the recombined samples there were a significant foam formation and relatively fast separation for both separation at 7 and 1 bar. Interesting to notice was that the experiment with the largest pressure drop over the second choke valve, separated fastest. For the degassed samples there were no foam formation, and both the separation at 7 and 1 bar were equally poor, as shown in Fig. 40.

In order to further investigate the influence of flotation upon separation of particle stabilized water-in-oil emulsions, a series of experiments on different crude oil and model oil systems were performed. Results from two different North Sea crudes, A and B, are shown. Both of these have been known to give very stable water in crude oil emulsions although the stabilizing mechanisms can be different. Crude A is a heavy crude with a high content of asphaltenes, while crude B is a very acidic crude with a high amount of naphthenic acids. In addition, a model system consisting of crude A (1% of A in Exxsol D80) was tested. The dispersed aqueous phase was either pure water or water saturated with CO_2. Essential for the discussion is that these samples were run through pressure reductions where the initial pressure (100 bar) was reduced to the separator pressure 65 bar.

The emulsions were placed in the vertical separator for 5 min, before the final pressure was adjusted as a gas release from 65 bar to 1 bar. Under this period of time, the emulsion will undergo a sedimentation process if the droplet size is large enough. The effect of propagating gas bubbles should be increased if the major part of the water droplets is assembled in a dense packed region. Fig. 41 shows the separation of water for emulsions made up from crude oil A. The model system, where 1% of crude oil A was diluted into Exxsol D80 and combined with 40% water with and without CO_2, is presented in Fig. 42. The separation level of the model emulsions was much lower, but also in this case an acceleration of the gas release upon the separation of water, was clearly seen.

Without CO_2, the pressure gradient (20 or 5 bar) seemed to have minor influence on the separation process. The emulsions were stable and only 20–25% of water
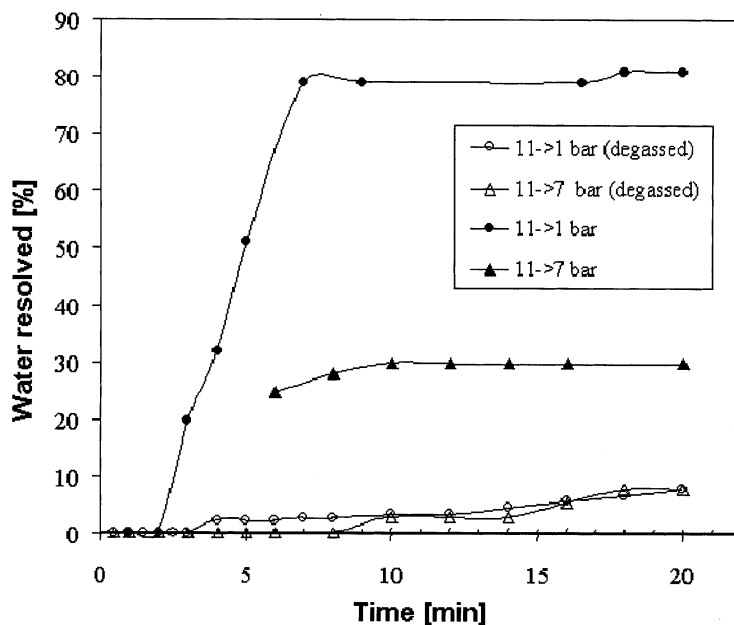
Fig. 40. Resolution of water from water-in-oil emulsions made from recombined samples and degassed recombined samples at 7 and 1 bar separation pressure.

was separated after 20 min. However, in most of the cases, the separation was accelerated by the release of CO_2 after 5 min. With a 5 bar pressure gradient there was no significant difference to the samples without CO_2. However, the large effect was seen for the emulsion with a $\Delta P = 20$ bar and an aqueous phase saturated with CO_2. For the first 5 min, the separator pressure was kept at 65 bar, and the level of separation was low or almost negligible. Then, as the pressure reduction took place, between 50 and 60% of the water phase would separate within 1–2 min. After 15 min, 90% of the emulsion had broken and separated into the original components. This was a significant result for a crude oil, which has proven to give very stable emulsions that are resistant to both chemical and mechanical treatment.

Fig. 43 shows the separation sequence for emulsions based on crude oil B. Characteristic for this system was that some separation, approximately 10%, would take place already at 65 bar. However, when the gas was released after 5 min the separation profile changed dramatically. All curves, independent of pressure drops over the chokes and content of CO_2 in the water phase, showed an accelerated resolution of water. Thus, the selectivity between the different emulsions was lost. Large effects were seen both with and without CO_2 in the aqueous phase, and with small and larger pressure gradients over the choke. In these cases, one could not with certainty relate the increased separability to carbon dioxide release.

The results from the experiments above have lead to the development of a patent [228] for the use of a polar gas as separation promoter for breaking of water-in-oil
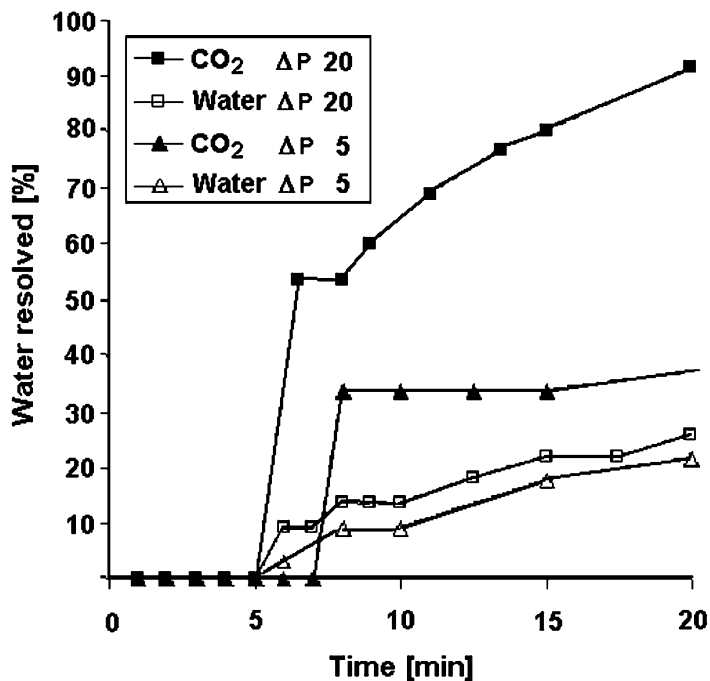
Fig. 41. Water separated vs. time for the dead crude oil A system. The pressure in the separation cell was reduced from 65 to 1 bar after 5 min.

emulsions. The mechanisms that are thought to occur in the water–oil mixture during pressure release are described in more detail in the next section.

4.5.5. New destabilization mechanisms

The basic idea is that CO_2 (g) or some other polar gas should be mixed with the water phase at an early stage in the separation process. In this way the emulsification would take place with an aqueous phase enriched with dissolved CO_2 (g). By the pressure lowering in a separator tank, there would be a release of the gaseous CO_2 (g) in the form of bubbles, which could enhance the breaking of oil-continuous emulsions.

Proposed mechanisms for breaking of oil-continuous emulsions (Fig. 44).

4.5.5.1. The droplet rupturing effect.

The polar gas dissolved into the aqueous phase (the droplets) will rapidly coalesce and form small bubbles upon a pressure reduction to below the bubble point. Due to gravity reasons, these bubbles will propagate through the emulsified system. When the bubbles leave the water droplet they have to pass the interfacial film built up by indigenous polar components (asphaltenes, resins and waxes). As a consequence, the interface will be ruptured. If the CO_2 (g) bubbles carry with them surface active material from the interface
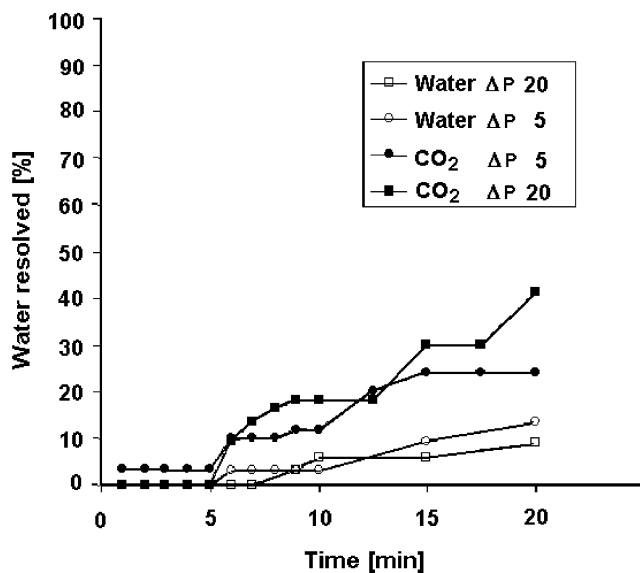
Fig. 42. Water separated vs. time for a model system consisting of 1% crude oil A in Exxsol D-80. The pressure in the separation cell was reduced from 65 to 1 bar after 5 min.
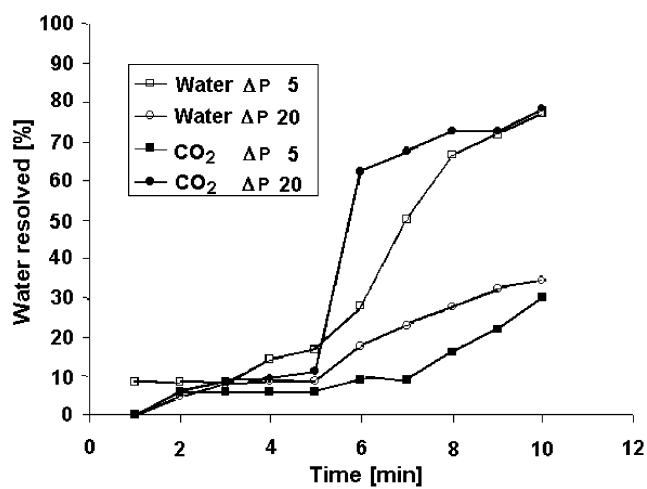

Fig. 43. Water separated vs. time for crude oil B. The pressure in the separation cell was reduced from 65 to 1 bar after 5 min.
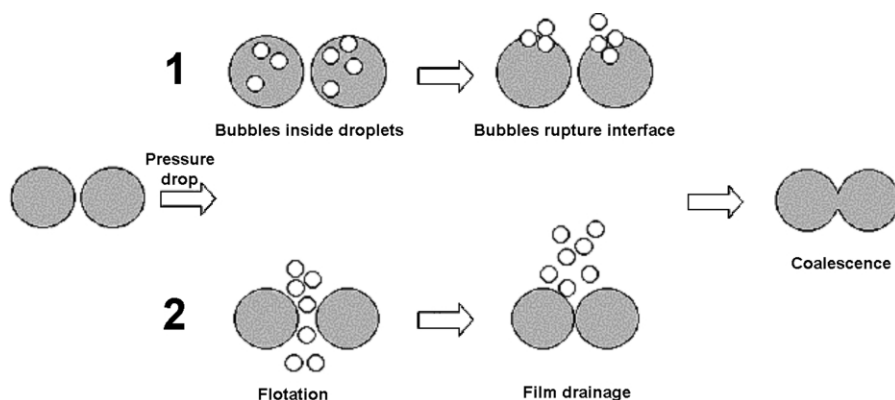
Fig. 44. Illustration of the proposed effects from CO_2 gas bubbles on water droplets in an oil-continuous phase.

(flotation effect) the time for the interface to reform will, most likely, be much longer than the coalescence time. Hence, the system will break and water and oil phases should appear. Application pressures could be approximately 60 bar depending on the chemical system and the whole process design.

4.5.5.2. The film drainage effect. The gas dissolved in the oil phase (the continuous phase) will also rapidly coalesce and form bubbles upon a pressure reduction below the bubble point. The buoyancy forces will cause the bubbles to propagate through the emulsified system. In doing so, they will tear off surface-active material from the o/w interface described as a flotation effect. This effect should be common for all oil soluble gases below the bubble point.

It was experimentally shown in section Section 4.5.4 that a polar gas, such as CO_2, could accelerate the breaking of crude oil based emulsions. However, this was not possible for all types of crude oil emulsions. Presumably it is most feasible for those types of crude oil emulsions which are particle stabilized. Also, the use of CO_2 will be effective in a gravitational separator and most effective in a separator of batch type. The emulsion will be held for a few minutes in the separator and settle before the gas pressure in the separator is reduced. However, in a continuous process, the effect will be much less.

Acknowledgments

References

[1] E.J.W. Verwey, J.T.h.G. Overbeek, Theory of the Stability of Lyophobic Sols, Elsevier, 1948.
[2] J. Sjöblom (Ed.), Emulsions and Emulsion Stability, Marcel Dekker, New York, 1996.
[3] J. Sjöblom (Ed.), Encyclopedic Handbook of Emulsion Technology, Marcel Dekker, New York, 2001.
[4] N. Aske, R. Orr, J. Sjöblom, Interfacial properties of water-crude oil systems using the oscillating pendant drop. Correlations to asphaltene solubility by near infrared spectroscopy, submitted Colloid Polym. Sci. (2002).
[5] J.D. McLean, P.K. Kilpatrick, J. Colloid Interface Sci. 189 (1997) 242.
[6] J.D. McLean, P.K. Kilpatrick, J. Colloid Interface Sci. 196 (1997) 23.
[7] J. Sjöblom, Ø. Sæther, Ø. Midttun, M.-H. Ese, O. Urdahl, H. Førdedal, in: E. Sheu, O.C. Mullins (Eds.), Structures and Dynamics of Asphaltenes, Chapter 11, Plenum Press, New York, 1998.
[8] J. Sjöblom, E.E. Johnsen, A. Westvik, et al., in: J. Sjöblom (Ed.), Encyclopedic Handbook of Emulsion Technology, Marcel Dekker, New York, 2001, p. 595.
[9] S. Friberg, L. Mandell, M. Larsson, J. Colloid Interface Sci. 29 (1969) 155.
[10] S. Friberg, J. Colloid Interface Sci. 37 (1971) 291.
[11] S. Friberg, P.O. Jansson, E. Cederberg, J. Colloid Interface Sci. 55 (1976) 614.
[12] S. Friberg, C. Solans, Langmuir 2 (1986) 121.
[13] J. Sjöblom, O. Urdahl, K.G.N. Børve, L. Mingyuan, J.O. Sæten, A.A. Christy, T. Gu, Adv. Colloid Interface Sci. 41 (1992) 241.
[14] T. Havre, J. Sjöblom, Emulsion Stabilization by means of Combined Surfactant Multilayer (D-phase) and Asphaltene Particles, Colloids Surf. A (2002) in press
[15] J.G. Speight, The Chemistry and Technology of Petroleum, Marcel Dekker, New York, 1999.
[16] K.J. Leontaritis, SPE International Symposium on Oilfield Chemistry, Houston, Texas, 1997, p. 421.
[17] E. Lundanes, T. Greibrokk, J. High Resolution Chromatogr. 17 (1994) 197.
[18] J.C. Suatoni, R.E. Swab, J. Chromatogr. Sci. 13 (1975) 361.
[19] C. Bollet, J.-C. Escalier, C. Souteyrand, M. Caude, R. Rosset, J. Chromatogr. 206 (1981) 289.
[20] W.A. Dark, J. Liq. Chromatogr. 5 (1982) 1645.
[21] M.A. Ali, W.A. Nofal, Fuel Sci. Technol. Intl. 12 (1994) 21.
[22] M. Radke, H. Willsch, D.H. Welte, Am. Chem. Soc. 52 (1980) 406.
[23] P.L. Grizzle, D.M. Sablotny, Anal. Chem. 58 (1986) 2389.
[24] N. Aske, H. Kallevik, J. Sjöblom, Energy Fuels 15 (2001) 1304.
[25] ASTM Method D4124, 1991.
[26] ASTM Method D2007, 1993.
[27] E.Y. Sheu, O.C. Mullins, Asphaltenes: Fundamentals and Applications, Plenum Press, New York, 1995.
[28] S.I. Andersen, J.G. Speight, Pet. Sci. Technol. 19 (2001) 1.
[29] B. Dabir, M. Nematy, A.R. Mehrabi, H. Rassamdana, M. Sahimi, Fuel 75 (1996) 1633.
[30] S. Peramanu, B.B. Pruden, P. Rahimi, Ind. Eng. Chem. Res. 38 (1999) 3121.
[31] H. Groenzin, O.C. Mullins, Energy Fuels 14 (2000) 677.
[32] E. Rogel, O. Leon, G. Torres, J. Espidel, Fuel 79 (2000) 1389.
[33] W. Loh, R.S. Mohamed, A.C.S. Ramos, Pet. Sci. Technol. 17 (1999) 147.
[34] O. Leon, E. Rogel, J. Espidel, G. Torres, Energy Fuels 14 (2000) 6.

[35] S.I. Andersen, K.S. Birdi, J. Colloid Interface Sci. 142 (1991) 497.
[36] S.I. Andersen, E.H. Stenby, Fuel Sci. Technol. Intl. 14 (1996) 261.
[37] S.J. Park, G.A. Mansoori, Energy Sources 10 (1988) 109.
[38] I.K. Yudin, G.L. Nikolaenko, E.E. Gorodetskii, et al., J. Pet. Sci. Eng. 20 (1998) 297.
[39] M.A. Anisimov, I.K. Yudin, V. Nikitin, et al., J. Phys. Chem. 99 (1995) 9576.
[40] J. Castillo, A. Fernandez, M.A. Ranaudo, S. Acevedo, Pet. Sci. Eng. 19 (2001) 75.
[41] K.J. Leontaritis, G.A. Mansoori, SPE International Symposium on Oilfield Chem., Richardson, Texas, 1987.
[42] K.J. Leontaritis, SPE Production Operations Symposium, Oklahoma City, Oklahoma, 1989.
[43] G.A. Mansoori, J. Pet. Sci. Eng. 17 (1997) 101.
[44] F.J. Nellensteyn, Chem. Weekblad 36 (1939) 362.
[45] J. Swanson, J. Phys. Chem. 46 (1942) 141.
[46] J.P. Pfeiffer, R.N. Saal, Phys. Chem. 24 (1940) 139.
[47] A. Hirschberg, L.N.J. deJong, B.A. Schipper, J.G. Meijer, Soc. Pet. Eng. J. (1984) 283.
[48] S.I. Andersen, J.G. Speight, J. Pet. Sci. Eng. 22 (1999) 53.
[49] N.B. Joshi, O.C. Mullins, A. Jamaluddin, J. Creek, J. McFadden, Energy Fuels 15 (2001) 979.
[50] A. Hammami, C.H. Phelps, T. Monger-McClure, T.M. Little, Energy Fuels 14 (2000) 14.
[51] S. Peramanu, C. Singh, M. Agrawala, H.W. Yarranton, Energy Fuels 15 (2001) 910.
[52] P.M. Spiecker and P.K. Kilpatrick, 3rd International Conference on Petroleum Phase Behavior & Fouling, New Orleans, LA, 2002.
[53] M. Blanco, S. Maspoch, I. Villarroya, X. Peralta, J.M. Gonzalez, J. Torres, Anal. Chimica Acta 434 (2001) 133.
[54] W.F. McClure, Anal. Chem. 66 (1994) A43.
[55] K.J. Laidler, J.H. Meiser, Physical Chemistry, Benjamin/Cummings Publishing Company, Menlo Park, 1982.
[56] O.C. Mullins, Anal. Chem. 62 (1990) 508.
[57] P.D. Gossen, J.F. MacGregor, R.H. Pelton, Appl. Spectrosc 47 (1993) 1852.
[58] P. Frake, I. Gill, C.N. Luscombe, D.R. Rudd, J. Waterhousea, U.A. Jayasorriya, Analyst 123 (1998) 2043.
[59] M.C. Pasikatan, J.L. Steele, C.K. Spillman, E. Haque, J. Near Infrared Spectrosc. 9 (2001) 153.
[60] A.F. Santos, E.L. Lima, J.C. Pinto, J. Appl. Polym. Sci. 70 (1998) 1737.
[61] A.F. Parisi, L. Nogueiras, H. Prieto, Anal. Chimica Acta 238 (1990) 95.
[62] J.J. Kelly, J.B. Callis, Am. Chem. Society 62 (1990) 1444.
[63] K. Hidajat, S.M. Chong, J. Near Infrared Spectrosc. 8 (2000) 53.
[64] H. Chung, M.-S. Ku, Appl. Spectrosc. 54 (2000) 239.
[65] M.-S. Ku, H. Chung, Appl. Spectrosc. 53 (1999) 557.
[66] M. Kim, Y.-H. Lee, C. Han, Comput. Chem. Eng. 24 (2000) 513.
[67] N. Aske, H. Kallevik, E.E. Johnsen, J. Sjöblom, Asphaltene Aggregation from Crude Oils and Model Systems Studied by High Pressure NIR Spectroscopy, submitted Energy & Fuels (2002).
[68] C.-L. Chang, S.H. Fogler, Langmuir 10 (1994) 1758.
[69] C.-L. Chang, S.H. Fogler, Langmuir 10 (1994) 1749.
[70] I.H. Auflem, T.E. Havre, J. Sjöblom, Near Infrared Study on the Dispersive Effects of Amphiphiles and Naphthenic Acids on Asphaltenes in Model Heptane-Toluene Mixtures, Colloid Polym. Sci. 280 (8) (2002) 695.
[71] M.E. Newberry, K.M. Barker, U.S. Patent No. 4414035, 1983.
[72] E.L. Hahn, Phys. Rev. 80 (1950) 580.
[73] D.W. McCall, D.C. Douglas, E.W. Anderson, Ber. Bunsenges. Phys. Chem 67 (1963) 366.
[74] E.O. Stejskal, J.E. Tanner, J. Chem. Phys. 42 (1965) 288.
[75] J.-A. Östlund, M. Nydén, I.H. Auflem, J. Sjöblom, Interactions between asphaltenes and naphthenic acids, submitted Energy & Fuel (2002).
[76] P. Stilbs, Prog. NMR Spectrosc. 19 (1987) 1.
[77] P.T. Callaghan, Aust. J. Phys 37 (1984) 359.

[78] J.S. Alper, R.I.J. Gelb, J. Phys. Chem 94 (1990) 4747.
[79] P. Stilbs, K. Paulsen, P.C. Griffiths, J. Phys. Chem. 100 (1996) 8180.
[80] P. Stilbs, J. Magn. Reson. 135 (1998) 236.
[81] J.-A. Östlund, S.-I. Andersson, M. Nydén, Fuel 80 (2001) 1529.
[82] J. Curie, P. Curie, Rendu 91 (1885) 294.
[83] W.G. Cady, Piezoelectricity, 2nd ed, Dover, New York, 1964.
[84] G. Sauerbrey, Zeitschrift fur Physik 155 (1959) 206.
[85] T. Nomura, M. Okuhara, Anal. Chim. Acta. 142 (1982) 281.
[86] P. Ekholm, E. Blomberg, P. Claesson, I.H. Auflem, J. Sjöblom, A. Kornfeldt, J. Colloid Interface Sci. 247 (2002) 342.
[87] E.H. Lucassen-Reynders, in: P. Becher (Ed.), Encyclopedia of Emulsion Technology, 4, Marcel Dekker, New York, 1996, p. 63.
[88] E.H. Lucassen-Reynders, Food Struct. 12 (1993) 1.
[89] J. Benjamins, A. Cagna, E.H. Lucassen-Reynders, Colloids Surf. 114 (1996) 245.
[90] P.K. Kilpatrick, P.M. Spiecker, in: J. Sjöblom (Ed.), Encyclopedic Handbook of Emulsion Technology, Marcel Dekker, New York, 2001, p. 707.
[91] A.Goldszal, C. Hurtevent, G. Rousseau, Scale and Naphthenate Inhibition in Deep-Offshore Fields, SPE Oilfield Scale Symposium, Aberdeen, UK, 2002.
[92] G. Rousseau, H. Zhou, C. Hurtevent, Calcium carbonate and naphthenate mixed scale in deep-offshore fields, SPE Oilfield Scale Symposium, Aberdeen, UK, 2001.
[93] C.S. Hsu, G.J. Dechert, W.K. Robbins, E.K. Fukuda, Energy Fuels 14 (2000) 217.
[94] J. Rudin, D.T. Wasan, Colloids Surf. 68 (1992) 67.
[95] J. Rudin, D.T. Wasan, Colloids Surf. 68 (1992) 81.
[96] J. Sjöblom, E.E. Johnsen, A. Westvik, L. Bergflødt, I.H. Auflem, T.E. Havre, H. Kallevik, Colloid Chemistry in Sub Sea Petroleum and Gas Processing, Second International Conference on Petroleum and Gas Phase Behaviour and Fouling, Copenhagen, Denmark, 2000.
[97] E. Slavcheva, B. Shone, A. Turnbull, Br. Corros. J. 34 (2) (1999) 125.
[98] M.L.H. Márquez, Interfacial activity of of native acids in heavy crude oil, AICHE Spring National Meeting Session T6005, Houston, Texas, 1999.
[99] S. Acevedo, G. Escobar, M.A. Ranaudo, et al., Energy Fuels 13 (2) (1999) 333.
[100] A.K. Pathak, T. Kumar, Study of Indigenous Crude Oil Emulsions and their Stability, Proceedings of PETROTECH-95, Technology trends in oil industry, New Dehli, 1995.
[101] R. Skurtveit, J. Sjöblom, H. Høiland, J. Colloid Interface Sci. 133 (2) (1989) 395.
[102] J. Sjöblom, R. Lindberg, S.E. Friberg, Adv. Colloid Interface Sci. 95 (1996) 125.
[103] G. Gillberg, H. Lehtinen, S.E. Friberg, J. Colloid Interface Sci. 33 (1) (1970) 40.
[104] S.E. Friberg, L. Mandell, P. Ekwall, Kolloid-Z. Z. Polym. 233 (1-2) (1969) 955.
[105] B. Lindman, H. Wennerstroem, Top. Curr. Chem. 87 (1980) 1.
[106] H. Wennerström, B. Lindman, Phys. Rev. 52 (1979) 1.
[107] P. Ekwall, I. Danielsson, P. Stenius, in: M. Kenken (Ed.), MTP Rev. Sci. Phys. Chem. Ser. 1, 7, Butterworths, London, 1972, p. 97.
[108] P. Ekwall, in: G.H. Brown (Ed.), Advances in Liquid Crystals, 1, Academic Press, New York, 1975, p. 1.
[109] P. Ekwall, L. Mandell, K. Fontell, Mol. Cryst. Liq. Cryst. 8 (1969) 157.
[110] J.A. Brient, P.J. Wessner, M.N. Doyle, in: K. Othmer (Ed.), Encyclopedia of Chemical Technology, John Wiley & Sons, New York, 1995, p. 1017.
[111] W. Meredith, S.-J. Kelland, D.M. Jones, Org. Geochem. 31 (11) (2000) 1059.
[112] T.-P. Fan, Energy Fuels 5 (3) (1991) 371.
[113] L. Koike, L.M.C. Reboucas, F.D.A. Reis, A.J. Marsaioli, H.H. Ichnow, W. Michaelis, Org. Geochem. 18 (6) (1992) 851.
[114] N.A. Tomczyk, R.E. Winans, J.H. Shinn, R.C. Robinson, Energy Fuels 15 (6) (2001) 1498.
[115] K. Qian, W.K. Robbins, C.A. Hughey, H.J. Cooper, R.P. Rodgers, A.G. Marshall, Energy Fuels 15 (6) (2001) 1505.

[116] W.K. Robbins, Prepr-Am. Chem. Soc. Div. Pet. Chem. 43 (1) (1998) 137.
[117] J.A. Brient, Prepr – Am. Chem. Soc. Div. Pet. Chem. 43 (1) (1998) 131.
[118] T. Havre, J. Sjöblom, J.E. Vindstad, Partitioning and Interfacial Behavior of Naphthenic Acids, in preparation.
[119] M.A. Reinsel, J.J. Borkowski, J.T. Sears, J. Chem. Eng. Data 39 (3) (1994) 513.
[120] H. Hartridge, R.A. Peters, Proc. R. Soc. A 101 (1922) 348.
[121] R.A. Peters, Proc. R. Soc. A 131 (1931) 140.
[122] J.F. Danielli, Proc. R. Soc. A 122 (1937) 155.
[123] P.D. Cratin, J. Disp. Sci. Technol. 14 (5) (1993) 559.
[124] P.D. Cratin, Colloids Surf. 89 (2/3) (1994) 103.
[125] S.H. Standal, A.M. Blokhus, J. Haavik, A. Skauge, T. Barth, J. Colloid Interface Sci. 212 (1999) 33.
[126] K. Spildo, H. Høiland, J. Colloid Interface Sci. 209 (1999) 99.
[127] J.E. Strassner, J. Pet. Technol. 20 (3) (1968) 303.
[128] C. Ovalles, M.D.C. Carcia, D. Lujano, W. Aular, R. Barmúdez, E. Cotte, Fuel 77 (3) (1998) 121.
[129] T.E. Havre, M.-H. Ese, J. Sjöblom, A.M. Blokhus, Colloid Polym. Sci. 280 (7) (2002) 647.
[130] S.E. Friberg, in: J. Sjöblom (Ed.), Encyclopedic Handbook of Emulsion Technology, Marcel Dekker, New York, 2001, p. 47.
[131] G. Horváth-Szabó, J. Czarnecki, J. Masliyah, J. Colloid Interface Sci. 236 (2001) 233.
[132] P. Joos, Bull. Soc. Chim. Belg. 78 (3-4) (1969) 207.
[133] P. Joos, Bull. Soc. Chim. Belg. 80 (3-4) (1971) 277.
[134] G. Horváth-Szabó, J. Masliyah, J. Czarnecki, J. Colloid Interface Sci. 242 (2001) 247.
[135] D.D. Eley, M.J. Hey, M.A. Lee, Colloids Surf. 24 (1987) 173.
[136] R.A. Mohammed, A.I. Bailey, P.F. Luckham, S.E. Taylor, Colloids Surf. 80 (1993) 223.
[137] R.A. Mohammed, A.I. Bailey, P.F. Luckham, S.E. Taylor, Colloids Surf. 80 (1993) 237.
[138] H. Førdedal, E. Nodland, J. Sjöblom, O.M. Kvalheim, J. Colloid Interface Sci. 173 (1995) 396.
[139] H. Førdedal, Y. Schildberg, J. Sjöblom, J.-L. Volle, Colloids Surf. 106 (1996) 33.
[140] H. Førdedal, Ø. Midttun, J. Sjöblom, O.M. Kvalheim, Y. Schildberg, J.-L. Volle, J. Colloid Interface Sci. 182 (1996) 117.
[141] J. Djuve, X. Yang, I.J. Fjellanger, J. Sjöblom, E. Pelizzetti, Colloid Polym. Sci. 279 (2001) 232.
[142] H. Kallevik, S.B. Hansen, Ø. Sæther, O.M. Kvalheim, J. Sjöblom, J. Disp. Sci. Technol. 21 (2000) 245.
[143] D.J. Shaw, Introduction to Colloid and Surface Chemistry, 4th ed, Butterworth Heinemann, Oxford, 1996.
[144] P.C. Mørk, Overflate og kolloidkjemi, grunnleggende prinsipper og teorier (Surface and Colloid Chemistry, Fundamental Principles and Theory, 5th Ed.), Department of Industrial Chemistry, Norwegian University of Science and Technology, Trondheim, 1997.
[145] R.J. Mikula, in: L.L. Schramm (Ed.), Emulsion Characterization in Emulsions, Fundamentals and Applications in the Petroleum Industry, American Chemical Society, Washington DC, 1992.
[146] D.J. Stokes, B.L. Thiel, A.M. Donald, Langmuir 14 (1998) 4402.
[147] S. Bradbury, Microsc. Anal. May (1990) 7.
[148] P. Walstra, H. Oortwijn, J. Colloid Interface Sci. 29 (1969) 424.
[149] A. Takamura, S. Noro, S. Ando, M. Koishi, Chem. Pharm. Bull. 25 (1977) 2644.
[150] J. Drelich, G. Bryll, J. Kapczynski, J. Hupka, J.D. Miller, F.V. Hanson, Fuel Process. Technol. 31 (1992) 105.
[151] K. Eberth, J. Merry, Int. J. Pharm. 14 (1983) 349.
[152] C. Orr, in: P. Becher (Ed.), Encyclopedia of Emulsion Technology, 3, Marcel Dekker, New York, 1988.
[153] S. Friberg, J. Colloid Interface Sci. 37 (1971) 2617.
[154] R.H. Müller, S. Heinemann, Clin. Nutr. 11 (1992) 223.
[155] T. Kubo, S. Tsukiyama, A. Takamura, I. Takashima, Yakugaku Zasshi (Japan) 91 (1971) 518.

[156] S.L. Mason, K. May, S. Hartland, Colloids Surf. A 96 (1995) 85.
[157] C.-J. Lee, S.-S. Wang, C.-C. Chan, J. Chin. Inst. Chem. Eng. 26 (1995) 263.
[158] A. Bhardwaj, S. Hartland, J. Disp. Sci. Technol. 15 (1994) 133.
[159] E.E. Isaacs, H. Huang, A.J. Babchin, R.S. Chow, Colloids Surf. A 46 (1990) 177.
[160] N. Garti, Colloids Surf. A 123-124 (1997) 233.
[161] P.J. Halling, CRC Crit. Rev. Food Sci. Nutr. 15 (1981) 155.
[162] M. Britten, H.J. Giroux, J. Food Sci. 56 (1991) 792.
[163] G.J. Hanna, K.M. Larson, Ind. Eng. Chem. Prod. Res. Dev. 24 (1985) 269.
[164] Ø. Sæther, S.S. Dukhin, J. Sjöblom, Ø. Holt, Colloid J. 57 (1995) 793.
[165] Ø. Holt, Ø. Sæther, J. Sjöblom, S.S. Dukhin, N.A. Mishchuk, Colloids Surf. A 141 (1998) 269.
[166] B. Balinov, O. Urdahl, O. Söderman, J. Sjöblom, Colloids Surf. A 82 (1994) 173.
[167] P. Jokela, P.D.I. Fletcher, R. Aveyard, J.R. Lu, J. Colloid Interface Sci. 134 (1990) 417.
[168] I. Fourel, J.P. Guillement, D. Le Botlan, J. Colloid Interface Sci. 169 (1995) 119.
[169] C. Solans, R. Pons, S. Zhu, et al., Langmuir 9 (1993) 1479.
[170] A.W. Pacek, I.P.T. Moore, R.V. Calabrese, A.W. Nienow, Trans. Inst. Chem. Eng. A: Chem. Eng. Res. Des. 71 (1993) 340.
[171] A.W. Pacek, A.W. Nienow, I.P.T. Moore, Chem. Eng. Sci. 49 (1994) 3485.
[172] A.W. Pacek, A.W. Nienow, Trans. Inst. Chem. Eng. A: Chem. Eng. Res. Des. 73 (1995) 512.
[173] N.A. Mishchuk, S.V. Verbich, S.S. Dukhin, Ø. Holt, J. Sjöblom, J. Disp. Sci. Technol. 18 (1997) 517.
[174] T.C. Scott, W.G. Sisson, Sep. Sci. Technol. 23 (1988) 1541.
[175] A.W. Pacek, I.P.T. Moore, A.W. Nienow, R.V. Calabrese, AIChE J. 40 (1994) 1940.
[176] Ø. Holt, Ø. Sæther, J. Sjöblom, S.S. Dukhin, N.A. Mishchuk, Colloids Surf. A 123-124 (1997) 195.
[177] S.I. Pather, S.H. Neau, S. Pather, J. Pharm. Biomed. Anal. 13 (1985) 1283.
[178] A.H. Kamel, S.A. Akashah, F.A. Leeri, M.A. Fahim, Comput. Chem. Eng. 11 (1987) 435.
[179] R.D. Hazlett, R.S. Schechter, J.K. Aggarwal, Ind. Eng. Chem. Fundam. 24 (1985) 101.
[180] B. Balinov, O. Söderman, T. Wärnheim, J. Am. Oil. Chem. Soc. 71 (1994) 513.
[181] X. Li, J.C. Cox, R.W. Flumerfelt, AIChE J. 38 (1992) 1671.
[182] Y. Wang, S. Bian, D. Wu, Pestic. Sci. 44 (1995) 201.
[183] Ø. Sæther, J. Sjöblom, S.V. Verbich, N.A. Mishchuk, S.S. Dukhin, Colloids Surf. A 142 (1998) 189.
[184] U.T. Lashmar, J.P. Richardson, A. Erbod, Int. J. Pharm. 125 (1995) 315.
[185] W.L. Lammers, H.J. van der Stege, P. Walstra, Neth. Milk Diary J. 41 (1987) 147.
[186] B. Kachar, D.F. Evans, B.W. Ninham, J. Colloid Interface Sci. 100 (1984) 287.
[187] K. Florine-Casteel, Biophys. J. 57 (1990) 1199.
[188] J.C. Crocker, D.G. Grier, J. Colloid Interface Sci. 179 (1996) 298.
[189] Ø. Holt, Ø. Sæther, J. Sjöblom, S.S. Dukhin, N.A. Mishchuk, Colloids Surf. A 141 (1998) 269.
[190] Ø. Sæther, J. Sjöblom, S.V. Verbich, S.S. Dukhin, J. Disp. Sci. Technol. 20 (1999) 295.
[191] S.V. Verbich, S.S. Dukhin, A. Tarovski, Ø. Holt, Ø. Sæther, J. Sjöblom, Colloids Surf. A 123-124 (1997) 209.
[192] H. Matsumura, K. Watanabe, K. Furusawa, Colloids Surf. A 108 (1995) 175.
[193] P.T. Spicer, W. Keller, S.E. Pratsinis, J. Colloid Interface Sci. 184 (1996) 112.
[194] S.R. Deshiikan, K.D. Papadopoulos, J. Colloid Interface Sci. 174 (1995) 302.
[195] W. Bartok, S.G. Mason, J. Colloid Sci. 14 (1959) 13.
[196] J. Bongers, H. Manteufel, K. Vondermassen, H. Versmold, Colloids Surf. A 142 (1998) 381.
[197] J.C. Crocker, D.G. Grier, Phys. Rev. Lett. 73 (1994) 352.
[198] A. Bhardwaj, S. Hartland, Ind. Eng. Chem. Res. 33 (1994) 1271.
[199] K.L. Alexander, D. Li, Colloids Surf. A 106 (1996) 191.
[200] S.E. Taylor, Colloids Surf. A 29 (1988) 29.
[201] R. Isherwood, B.R. Jennings, M. Stankiewicz, Chem. Eng. Sci. 42 (1987) 913.
[202] M. Spencer, Fundamentals of light microscopy, Cambridge University Press, New York, 1982.

[203] E.M. Chamot, Elementary Chemical Microscopy, John Wiley & Sons, New York, 1915.

[204] P.M. Cooke, Anal. Chem. 64 (1992) R219.

[205] R.D. Allen, Annu. Rev. Biophys. Biophys. Chem. 14 (1985) 265.

[206] B.E. Christensen, H. Grasdalen, NMR spektroskopi (NMR spectroscopy), Department of Biotechnology, Norwegian University of Science and Technology, Trondheim, 1999.

[207] B. Balinov, O. Söderman, in: J. Sjöblom (Ed.), Encyclopedic Handbook of Emulsion Technology, Marcel Dekker, New York, 2001.

[208] L. Ambrosone, A. Ceglie, G. Colafemmina, G. Palazzo, J. Chem. Phys. 107 (1997) 10756.

[209] K.J. Packer, C. Rees, J. Colloid Interface Sci. 40 (1972) 207.

[210] J.G. Seland, Diffusion in heterogeneous polymer systems, A nuclear magnetic resonance study, Thesis, Department of Chemistry, Norwegian University of Science and Technology, Trondheim, 2000.

[211] A.S. Dukhin, P.J. Goetz, T.H. Wines, P. Somasundaran, in: J. Sjöblom (Ed.), Encyclopedic Handbook of Emulsion Technology, Marcel Dekker, New York, 2001, p. 185.

[212] R.J. Hunter, in: J. Sjöblom (Ed.), Encyclopedic Handbook of Emulsion Technology, Marcel Dekker, New York, 2001, p. 169.

[213] T.Y. Chen, R.A. Mohammed, A.I. Bailey, P.F. Luckham, S.E. Taylor, Colloids Surf. 83 (1994) 273.

[214] H. Førdedal, W/O Emulsions in High Electric Fields as Studied by Means of Time Domain Dielectric Spectroscopy, Ph.D. thesis, University of Bergen, Norway, 1995.

[215] N. Aske, H. Kallevik, J. Sjöblom, submitted Journal of Petroleum Science and Engineering (2001).

[216] H. Kallevik, O.M. Kvalheim, J. Sjöblom, J. Colloid Interface Sci. 225 (2000) 494.

[217] B.M. Wise, N.B. Gallagher, J. Proc. Cont. 6 (1996) 329.

[218] H. Martens, M. Martens, Multivariate Analysis of Quality. An Introduction, John Wiley & Sons, Chichester, 2001.

[219] H.P. Rønningsen, J. Sjöblom, L. Mingyuan, Colloids Surf. 97 (1995) 119.

[220] J. Sjöblom, L. Mingyuan, A.A. Christy, H.P. Rønningsen, Colloids Surf. 96 (1995) 261.

[221] I.H. Auflem, A. Westvik, J. Sjöblom, Destabilisation of water-in-crude oil emulsions based on recombined oil samples at various pressures, submitted Journal of Dispersion Science and Technology.

[222] I.H. Auflem, H. Kallevik, A. Westvik, J. Sjöblom, J. Pet. Sci. Eng. 31 (1) (2001) 1.

[223] J.O. Hinze, AIChE J. 1 (3) (1955) 289.

[224] A.J. Karabelas, AIChE J. 24 (2) (1978) 170.

[225] J.T. Davies, Chem. Eng. Sci. 40 (5) (1985) 839.

[226] C.A.J. Sleicher, AIChE J. 8 (4) (1962) 471.

[227] F.H. Meijs, R.W. Mitchell, J. Petroleum Technology May (1974) 563.

[228] H. Kallevik, J. Sjöblom, A. Westvik and I.H. Auflem, Patent P 4202-1, ONSAGERS AS, Norway, 2002.

[229] May Britt Eiken, M.Sc. thesis, Norwegian University of Science and Technology, Trondheim, 1999.

[230] Ø. Sæther, in: J. Sjöblom (Ed.), Encyclopedia of Emulsion Technology, Marcel Dekker, New York, 2001.